UBFC
UNIVERSITÉ
BOURGOGNE FRANCHE-COMTÉ

UFC
UNIVERSITÉ
DE FRANCHE-COMTÉ

PH.D. THESIS OF THE UNIVERSITY BOURGOGNE FRANCHE-COMTÉ

PREPARED AT THE UNIVERSITY OF FRANCHE-COMTÉ

Doctoral school n°37

Engineering Sciences and Microtechnologies

Ph.D. in Automatic

by

MEILING YUE

Contribution of developing a prognostics-based energy management strategy for fuel cell hybrid system - application to a fuel cell/battery hybrid electric vehicle

Thesis presented and defended in Belfort on October 7, 2019

Composition du Jury :

KHATIR ZOUBIR	Research director of IFSTTAR, HDR	President
OULD BOUAMAMA BELKACEM	Professor of University of Lille	Reviewer
OSSART FLORENCE	Professor of Sorbonne University	Reviewer
HISSEL DANIEL	Professor of University Bourgogne Franche-Comté	Examiner
CHEN ZHENG	Professor of Queen Mary University of London	Examiner
JEMEI SAMIR	Professor of University Bourgogne Franche-Comté	Supervisor
ZERHOUNI NOUREDDINE	Professor of University Bourgogne Franche-Comté	Co-Supervisor

N° | X | X | X |

UBFC
UNIVERSITÉ
BOURGOGNE FRANCHE-COMTÉ

UFC
UNIVERSITÉ
DE FRANCHE-COMTÉ

THÈSE DE DOCTORAT DE L'ÉTABLISSEMENT UNIVERSITÉ BOURGOGNE FRANCHE-COMTÉ

PRÉPARÉE À L'UNIVERSITÉ DE FRANCHE-COMTÉ

Ecole doctorale n°37

Sciences Pour l'Ingénieur et Microtechniques

Doctorat d'Automatique

par

MEILING YUE

Contribution au développement d'une stratégie de gestion de l'énergie basée sur pronostics pour des systèmes hybrides à pile à combustible - application à un véhicule électrique hybride à pile à combustible et batterie

Thèse présentée et soutenue à Belfort, le 07 Octobre 2019

Composition du Jury :

KHATIR ZOUBIR	Directeur de recherche à l'IFSTTAR, HDR	Président
OULD BOUAMAMA BELKACEM	Professeur à l'Université de Lille	Rapporteur
OSSART FLORENCE	Professeure à Sorbonne Université	Rapporteur
HISSEL DANIEL	Professeur à l'Université Bourgogne Franche-Comté	Examinateur
CHEN ZHENG	Professeur à Queen Mary Université de Londres	Examinateur
JEMEI SAMIR	Professeur à l'Université Bourgogne Franche-Comté	Directeur de thèse
ZERHOUNI NOUREDDINE	Professeur à l'Université Bourgogne Franche-Comté	Co-directeur de thèse

N° | X | X | X |

école doctorale **sciences pour l'ingénieur et microtechniques**

Titre : Contribution of developing a prognostics-based energy management strategy for fuel cell hybrid system - application to a fuel cell/battery hybrid electric vehicle

Mots-clés : pronostic et gestion de la santé, système hybride à pile à combustible, filtrage particulaire, prise de décision basée sur le pronostic

Résumé :

Le système de propulsion hybride à pile à combustible (PàC) gagne du terrain sur le marché automobile actuel et offre une solution durable au changement climatique mondial dans le secteur des transports. Cependant, la durabilité et la fiabilité des sources d'énergie utilisées dans le système hybride sont les obstacles inévitables à sa commercialisation massive. Pour optimiser et maximiser la durée de vie du système hybride, une approche de pronostic et gestion de la santé (PHM) est mise en œuvre pour gérer et atténuer le comportement de dégradation des sources d'énergie et appliquée à un véhicule électrique hybride à pile à combustible.

Dans ce contexte, deux contributions principales sont apportées. La première consiste à déployer une méthode de pronostic pouvant être utilisée dans le système hybride. Le filtrage de particules, en tant que méthode d'estimation d'état communément utilisée, est adapté aux fins de pronostic dans cette thèse. Il est utilisé pour traiter les données de dégradation imprécises et incertaines et pour estimer la durée de vie utile restante. La méthode est validée par les ensembles de données historiques de PàC et de batterie et les résultats sont évalués par les métriques de pronostic conçues.

Ensuite, une deuxième étape sur l'aspect gestion de la santé du PHM est proposée. Comme la répartition de la puissance demandée dans un système hybride est gérée par une stratégie de gestion de l'énergie (EMS), l'orientation de cette étape est de développer une EMS conscient de sa santé dans le contexte du PHM. Une grande quantité de recherches sur les pronostics avec des données expérimentales finies ont été trouvées dans la littérature, alors que la manière d'utiliser les résultats de pronostics pour réaliser des actions de contrôle correctives est rarement discutée. Afin de pallier cette lacune dans les applications de système hybride, un processus de prise de décision basé sur le pronostic est conçu. Les performances sont évaluées en quantifiant la dégradation et la durée de vie du système dans un environnement simulé et une discussion sur l'occurrence des pronostics est lancée pour des investigations ultérieures sur la maintenance.

Title: Contribution of developing a prognostics-based energy management strategy for fuel cell hybrid system - application to a fuel cell/battery hybrid electric vehicle

Keywords: prognostics and health management, fuel cell hybrid system, particle filtering, prognostics-enabled decision-making

Abstract:

Fuel cell hybrid propulsion system is gaining momentum in today's automotive market and offers a sustainable solution for the world climate change in the transport sector. However, the durability and reliability of the power sources used in the hybrid system are the inevitable obstacles for its massive commercialization. To optimize and maximize the lifespan of the hybrid system, a prognostics and health management (PHM) approach is deployed to manage and mitigate the power source degradation behaviour and applied to a fuel cell hybrid electric vehicle.

In this context, two main contributions are made. The first stage is to deploy a prognostics method that can be used in the hybrid system. Particle filtering, as a commonly used state estimation method, is adapted for prognostics purpose in this thesis. It is used to handle the imprecise and uncertain degradation data and estimate the remaining useful life. The method is validated by the historical fuel cell and battery datasets and the results are evaluated by the designed prognostics metrics.

Subsequently, a second stage on the health management aspect of PHM is proposed. As the split of demanded power in a hybrid system is managed by an energy management strategy (EMS), the orientation of this stage is to develop a health-conscious EMS in the context of PHM. A great number of researches on prognostics with finished experimental data have been found in the literature, while how to use the results of prognostics to make corrective control actions is rarely discussed. To help against this vacancy in hybrid system applications, a prognostics-enabled decision-making process is designed. The performance is evaluated by quantifying the degradation and the lifetime of the system in a simulated environment and a discussion on prognostics occurrence is launched for further investigations on maintenance.

UBFC UNIVERSITÉ BOURGOGNE FRANCHE-COMTÉ

Université Bourgogne Franche-Comté
32, avenue de l'Observatoire
25000 Besanon, France

ACKNOWLEDGEMENTS

This work of thesis is supported by the French region Bourgogne Franche Comté as a part of the regional project PHyTie. The preparation of the thesis started in the university year of 2016/2017 and lasted three years : the first 16 months of the thesis have been realized in the "Prognostics and Health Management" (PHM) team of the department "Automatic Control and Mechatronic Systems" (AS2M) in the research institute "Franche-Comté Electronics Mechanics Thermal Science and Optics – Sciences and Technologies" (FEMTO-ST Institute), which is located in Besançon, France. Then, the next 20 months of the thesis have been done in the "Systèmes Electriques Hybrides, Actionneurs Electriques, Systèmes Piles à Combustible" (SHARPAC) team of the department ENERGIE, which also belongs to the research institute FEMTO-ST but is situated in Belfort, France. Most works have been realized in the research federation FCLAB, which is a laboratory attached with Centre National de la Recherche Scientifique (CNRS), Université de Bourgogne Franche-Comté (UBFC), Université Techonologique de Belfort-Monbéliard (UTBM) and Ecole National Supérieure de Micromécanique et Microtechnologie (ENSMM).

I would like to give the most sincere thanks to all the persons that have contributed to the accomplishment of this thesis. In the first place, I would like to thank Professor Rafael GOURIVEAU for starting this project and giving me the chance to be involved and I would like also to express my deepest gratitude and respect to Professor Samir JEMEI and Professor Noureddine ZERHOUNI, who have supervised this thesis with continuous guidance and support. I appreciate a lot their encouragement, trust and responsibility, as well as their insightful advice and constructive comments all along with the research work.

Special thanks go to Professor Belkacem OULD BOUAMAMA and Professor Florence OSSART for their review of the manuscript and the precious suggestions that they have made to help me improve the work. Profuse thanks go equally to Professor Zoubir KHATIR, Professor Daniel HISSEL, Professor Zheng CHEN for their being members of my thesis jury and for their profound insights and comments.

I would also thank the personnel in FEMTO-ST and FCLAB for their support and help in my study and in my life, with whom I have spent all the unforgettable moments in the last three years. I give my special thanks to my colleagues and my friends for their company and regards, whose presence and encouragements were never missing. I am extremely grateful to them.

In the end, I wouldn't forget my family, my parents and all my relatives, who have always been standing in my back and supporting my dreams over the years. I would like to give the thesis as a special gift for all of you.

CONTENTS

General Introduction

During the period where energy transition has become not only an environmental priority but also an economic and political issue, fuel cell appears to be a promising alternative energy source and fuel cell hybrid system has been widely considered in industrial applications. However, despite considerable research efforts on fuel cell hybrid system have been made for several decades, its transfer to massive production is still struggling. According to the U.S. Department of Energy, improvements on the cost and durability of the fuel cell system are the two primary challenges in its commercialization, while durability can highly influence its cost-effectiveness.

To optimize and maximize the lifespan of fuel cell hybrid systems, it is necessary to understand the power sources degradation behaviour and act at their best to slow down the degradation process before failure. In the state of the art, various health-conscious energy management strategies (EMSs) for fuel cell hybrid systems have been developed by taking the power source degradation into consideration. However, in most works, the degradation is roughly considered by setting operation limits or by designing pre-defined models based on finished experimental data. Online health states have rarely been involved in the EMS design. At this point, prognostics and health management (PHM) is positioning itself as an interesting discipline. It allows to follow and to continuously estimate the state of health of a system, to predict its remaining useful life, and to make the decisions to preserve it as long as possible. PHM works of fuel cell hybrid systems have been investigated mostly in the stage of prognostics, while the health management decision support has rarely been involved. To go further from the prognostics to the health management of fuel cell hybrid systems, a French regional project PHyTie has been launched, in which this thesis is inscribed. This project aims to develop online prognostic approaches offering remaining useful life estimates with controlled uncertainty and also to transfer these results to further decision-making phase where an energy management strategy is expected to be developed to implement auto-corrective control for the fuel cell hybrid system.

To be specific, this thesis will focus on completing the two aspects of PHM, namely, the prognostics and the health management, for a fuel cell hybrid electric vehicle (HEV) application, by developing an online prognostic approach and designing a prognostics-enabled EMS. The hybrid electric vehicle will be constructed in a simulated environment and the power source degradation will be simulated based on historical data. The manuscript is structured in four chapters. They are organized as follows :

Chapter 1 starts by explaining the key elements for understanding the problem. The context of fuel cell hybrid system and its durability challenge are discussed. A brief state of the art on health-conscious EMSs is analyzed, highlighting the motivations of practizing energy management with PHM. A framework of implementing on-board prognostics-based health-conscious EMS is proposed.

Chapter 2 describes the general context of the lithium-ion battery and the PEM fuel cell that are used in the studied hybrid system. Their degradation mechanisms are studied

and methods of estimating their degradation in the literature are reviewed including their pros and cons, which provide the basis for selecting a powerful prognostics approach used in PHM cycle.

Chapter 3 develops the prognostics method for the hybrid system based on particle filtering algorithm**.** Particle filtering is a recursive state estimation method and it is adapted for prognostics purpose through propagating the particles with estimated parameters. Performance metrics are evaluated to justify the effectiveness of the method and the possibility of combining it to the EMS design of the studied fuel cell HEV.

Chapter 4 proposes an online health-conscious EMS based on prognostics for the fuel cell HEV. A prognostics-enabled decision-making process is developed based on a series of classification and decision fusion methods**.** A closed loop is formulated with the developed EMS to evaluate the performance of the developed EMS. Results of durability improvement and degradation economic cost are compared and possible future works are discussed as perspectives.

The manuscript ends with the conclusions and perspectives of this research work, together with the appendices of figures and tables**. Appendix A** is the genetic algorithm optimization results under difference degradation states and **Appendix B** is the simulation results of the developed EMS with different prognostics occurrence. These two appendices are the complementary parts for **Chapter 4. Appendix C** lists the scientific publications that have been realized during this thesis.

I

Context and State of the art

1

TOWARDS A PROGNOSTICS-BASED HEALTH-CONSCIOUS EMS

1.1/ INTRODUCTION

In an era of accelerating change, the imperative to limit climate change and achieve sustainable growth is strengthening the momentum of the global energy transformation. The rapid decline in renewable energy costs, improving energy efficiency, widespread electrification, increasingly smart technologies, continual technological breakthroughs and well-informed policymaking all drive this shift, bringing a sustainable energy future within reach. While the transformation is gaining momentum, it must happen faster. Around two-thirds of global greenhouse gas emissions stem from energy production and use, which are at the core of efforts to combat climate change. To meet the climate goals, progress in the energy transition needs to be further accelerated, while the de-carbonization of the transport sector must pick up steam.

Thanks to the reliable use of hydrogen energy, fuel cell propulsion has seen a promising future, which offers a similar recharge time to that of the current gasoline solution and a comparable autonomy. However, a central issue holding back the critical achievement and massive use of fuel cell systems is the durability of the power sources used in the powertrains, e.g., fuel cells and batteries, typically studied in this thesis. U.S. Department of Energy (DOE) has reported the technical durability targets for integrated hydrogen-fueled polymer electrolyte membrane (PEM) fuel cell power systems and fuel cell stacks operating on direct hydrogen as 8000 hours for transportation applications [188], while the target level of performance for electric vehicle lithium-ion batteries is namely 1000 cycles or 15-year lifetime with adequate pulse power [5]. Efforts have been made to prolong their lifetime and in the automation field, a delicately designed energy management strategy for the hybrid system has drawn increasing attention. To be health-conscious, existing researches have considered the degradation of the power sources by setting constraints or using fitting degradation models, which are less accurate and cannot signify the real health states of the power sources. Without an exact understanding of the current health state, the actions taken by the controller may not be adequate and may even cause more damages to the power sources, shortening their lifetime.

To assess the health state and estimate remaining useful life, the fuel cell research federation FCLAB (FR CNRS 3539) has been making efforts towards the prognostics and health management (PHM) of fuel cell systems. The aim of this axis is to propose intelligent PHM methods in order to assess the health state of a fuel cell system, to predict its

remaining useful life (RUL) and to decide the corresponding mitigation/control actions for mission achievement. To this spirit, an application of fuel cell hybrid electric vehicle (HEV) is studied specifically in this thesis and an energy management strategy (EMS) under the guide of PHM is proposed, which is believed to be one of the promising solutions to the durability problems for fuel cell hybrid systems. A prognostics-enabled decision-making (PDM) process is developed to formulate the EMS and to the author's knowledge, it is a first trial of completing the health management aspect of PHM in HEV applications.

In this chapter, motivations and objectives of the thesis are explained and then, the possibility of combining PHM with EMS is detailed based on the literature review of health-conscious EMSs of fuel cell HEVs. At last, the framework of developing an on-board prognostics-based health-conscious EMS is proposed.

1.2/ MOTIVATIONS AND OBJECTIVES

1.2.1/ CONTEXT

According to the International Energy Agency (IEA)'s first Global Energy and CO_2 Status Report released in March 2018, global energy-related CO_2 emissions rose by 1.4% in 2017, an increase of 460 million tones (Mt), and reached a historic high of 32.5 Gt (Figure 1.1). The growth came after three years of flat emissions and contrasted with the sharp reduction needed to meet the goals of the Paris Agreement on climate change [3]. The growth in energy-related CO_2 emissions in 2017 is a strong warning for global efforts to combat climate change and demonstrates that current efforts are insufficient to meet the well below 2°C climate objective, and even further from attaining the aspirational target of limiting warming to 1.5°C [179].

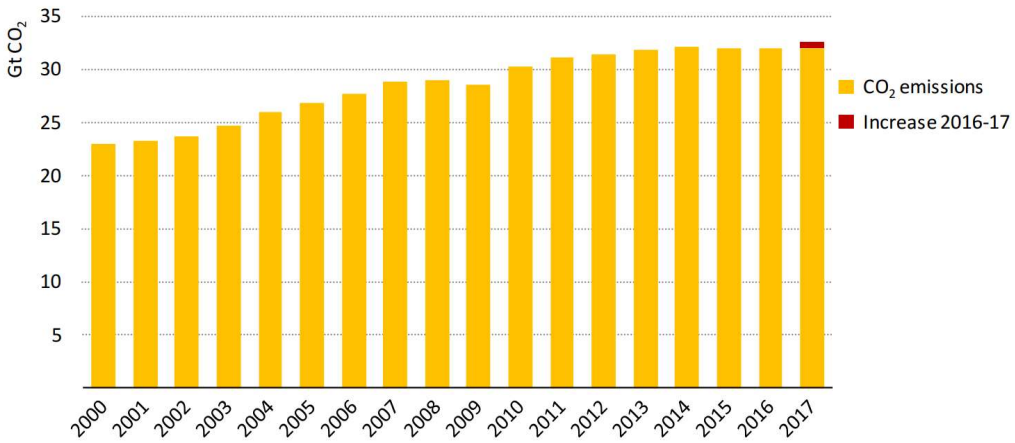

FIGURE 1.1 – Global energy-related CO_2 emissions, 2000-2017 [3]

Although many approaches can reduce energy-related carbon emissions, there is a universal agreement that working towards the energy transition is of considerable significance. Efforts are demanding to execute a transition from consuming non-renewable energy to renewable energy. However, according to International Renewable Energy Agency (IRENA), the transport sector has lagged behind in the energy transition scenario, which shared a very small part of just 4% of renewable energy consumption of

the year 2015 (Figure 1.2) [179]. Electrification, one of the technologies that can help to decarbonize the sector if associated with renewable power generation, is also extremely limited : it has a share of just above 1%.

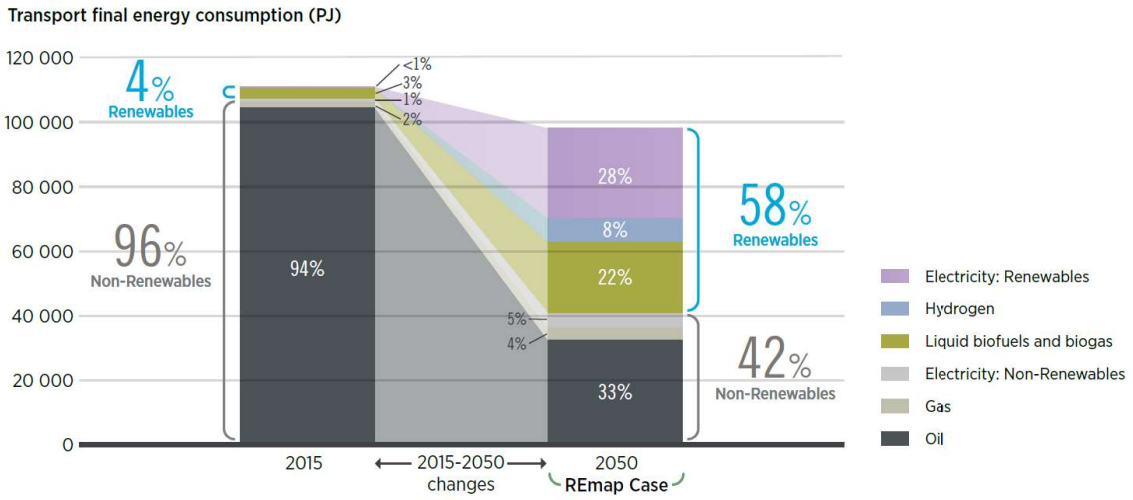

FIGURE 1.2 – Energy transition in transport sector [179]

Given adequate policies and developing orientations, the electricity consumption in the transport sector has shown a steady increase according to the analysis of IRENA's Renewable Energy Roadmaps (REmap) programme, as shown in Figure 1.2. Through thirty year's changing period, it shows the potential for the world to scale up renewable energy in 2050. Such development is driven mostly by the penetration of electric vehicles in the road transport sector. According to the EU Reference Scenario 2016, car manufacturers are expected to comply with the CO_2 standards by marketing vehicles equipped with a hybrid system on their powertrain (see Figure 1.3) [139]. The sales of plug-in hybrid electric vehicles (PHEVs) hold a significantly larger share in total sales of electrically chargeable vehicles in the mid-term. PHEVs, equipped with an internal combustion engine, do not pose range limitations to the travellers and are relatively less capital intensive than battery electric vehicles (BEVs), resulting in their increased sales compared to BEVs especially over the period 2020-2025. However, since the PHEV combines a short-range electric powertrain with a combustion engine, the level of PHEV emissions strongly depends on the use cases. PHEVs operated in the regional distribution or local drop-and-drive environments have the potential to run on very low CO_2 emissions, as they employ the battery often. However, as soon as users demand longer driving ranges or higher payloads, PHEVs act as a conventional ICE-powered vehicle and emit as much CO_2. In Figure 1.3, pure electric vehicles present higher levels of maturity, in particular, beyond 2025. The developments of the battery costs also allow a decrease in capital costs of BEVs and enable their penetration, especially in the urban zones [139]. However, BEVs have lengthy charging time and limited charging infrastructure. Even with superchargers, it will still require about 20 minutes to charge the vehicle to 80% full. Moreover, the battery pack for BEVs has lower energy density compared to fossil fuel resulting in a shorter driving range compared to a conventional vehicle of the same weight. To improve this situation, manufacturers tend to enlarge the size of batteries to increase the energy storage capacity and hence to allow longer driving ranges, however, these large batteries bring a higher cost. A more promising solution in the current energy context is demanding.

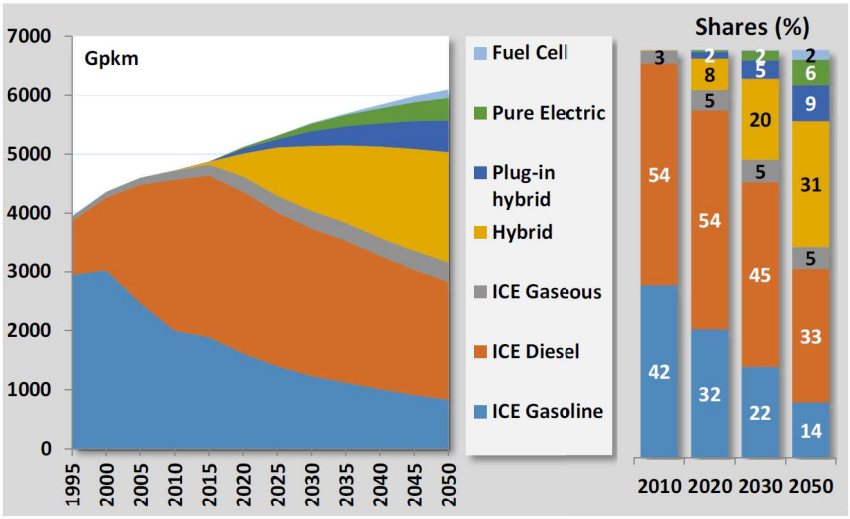

FIGURE 1.3 – Evolution of activity of passenger cars and vans by type and fuel [139]

Hydrogen is an essential element in the energy transition and can account for 24% of final energy demand and 5.4 million jobs by 2050, says the new study by the FCH JU, "Hydrogen Roadmap Europe : A sustainable pathway for the European Energy Transition" [4]. According to their study, hydrogen is the most promising decarbonization option for trucks, buses, ships, trains, large cars, and commercial vehicles, where the lower energy density (hence lower range), high initial costs, and slow recharging performance of batteries are major disadvantages of BEVs. A fuel cell electric vehicle can drive further and transport more payload than a BEV thanks to its significantly higher energy density than batteries, both in terms of volume and weight. Although fuel cell might represent a niche market by 2050 due to its relatively higher, albeit decreasing, cost, the REmap programme have explored that the use of hydrogen in vehicles powered by fuel cells is particularly relevant because variable renewable electricity generation is expanding and the production of hydrogen from renewable power may provide an important option in efforts to meet demand flexibility and expand renewable power generation [179]. Although the technology is not yet ready for widespread commercialization, compared to batteries and combustion engines, fuel cells require significantly less raw materials. In addition, hydrogen refuelling infrastructure has significant advantages : it requires only about one-tenth of the space in cities and along highways compared to fast battery charging. Likewise, suppliers can provide hydrogen flexibly, while at-scale fast-charging infrastructure would require significant grid upgrades [4].

As it could be seen from the Figure 1.3, the share of activity of total electric chargeable light-duty vehicles in the total activity of light-duty vehicles reaches 17% in 2050 [139], which has seen a dramatically increase and is making a change to the dominant place of the internal combustion engine in vehicle's propulsion system. Among them, the fuel cell exists as a brand new hydrogen-based electrical solution, which offers a similar recharge time to that of the current gasoline solution and a comparable autonomy. Compared to BEVs, fuel cell electric vehicles, whether or not in a hybridized way, are assumed to be a more promising solution for the future's automotive market. Researches oriented on their massive production are worth being taken place both in the scientific and technical way. This thesis will focus on its durability limits and a solution based on EMS is proposed for fuel cell HEV applications, which is detailed in the following sections.

1.2.2/ DURABILITY AND ENERGY MANAGEMENT

1.2.2.1/ POWER SOURCE DURABILITY : AN IMPORTANT ISSUE

According to DOE, fuel cell system status and targets in different concerning performances are plotted in a radar diagram, as shown in Figure 1.4 [188]. From Figure 1.4, one can conclude that the two primary challenges for the current fuel cell system commercialization are the cost and the durability. The challenge of reducing the cost of a fuel cell system nowadays is mainly linked to the industrial deployment, while the challenge of durability remains as a technological issue to be solved and the unsatisfied durability can highly influence the cost-effectiveness of the system.

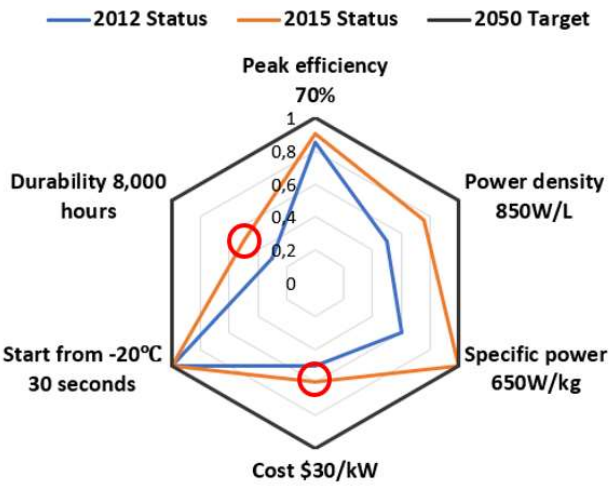

FIGURE 1.4 – Fuel cell system performance status and targets

Concerning the fuel cell HEV application in this thesis, the electrochemical components, namely, lithium-ion battery packs and hydrogen-fueled PEM fuel cells, by their very nature, prone to irreversible degradation phenomena during storage and operation mode, leading to accelerated performance losses and shortened lifetime. Neglecting the degradation could result in misunderstanding of the components' available lifetime and overconfidence of the vehicle's condition, which would cause serious consequence. Degradation of the power sources may be caused by different storage and driving conditions and the degradation degree becomes especially high when they are submitted to harsh operating conditions aboard HEVs. Analysis of the on-road fuel cell electric vehicles data provided by NREL has shown that the maximum projected durability, which is the projected time to 10% voltage degradation for the fleet that displays the best average durability, has more than quadrupled over the last ten years, increasing from 950 hours in 2006 to 2,500 hours in 2009 and reaching 4,100 hours in 2016 [189]. In 2016, the DOE Fuel Cell Technologies Office made the decision, based on industry feedback, to increase the ultimate target for fuel cell durability from 5,000 hours to 8,000 hours. The 5,000-hour target was initially set to correspond with an expected lifetime of 150,000 miles driven within a particular range of speeds. Increasing the target to 8,000 hours effectively expands the metric so that vehicles can achieve 150,000 miles in slower-speed driving conditions (e.g. city driving) [193].

Besides the fuel cell, the lifespan of batteries can also be influenced by the use. If the lithium-ion batteries are fully charged and depleted every day, known as deep cycles, they

might only last a few years, while partial charge/discharge cycles help to save the battery's life [183]. Also, if the battery temperature exceeds 40 °C, they can suffer a permanent loss of up to 20% of storage capacity within two years [102]. To allow for the expansion of the electrification of vehicles, batteries must store more energy per unit volume and weight, and they must be capable of undergoing many thousands of charge-discharge cycles [2].

Therefore, there is an increasing demand for improving the durability of power sources in vehicle applications. Various efforts have been made : working on the materials, reducing the causes of degradation, improving the structural design, implementing new supervision and management designs, etc. The last solution appears to be of great interest in our field and numerous studies have proved that it is possible to exercise active control over the operating conditions, and in turn to mitigate the deleterious effects of the degradation [45, 91].

1.2.2.2/ IMPROVE DURABILITY THANKS TO ENERGY MANAGEMENT

When more than one power sources are used to supply a certain load, an efficient EMS is needed to guide the flow of energy in the hybrid system. It controls the power distribution among different power sources in HEVs and the performance of a hybrid system can be highly affected by the designing of EMSs [131]. Based on non-exhausted bibliography research, for fuel cell/battery HEVs, various EMSs have been developed to take power sources' degradation into consideration and therefore, to prolong the lifetime of the HEVs. To be health-conscious, most researchers tend to develop degradation models to quantify performance degradation and to get the optimal solutions by designing rule-based and optimization-based EMSs. A detailed literature review on the existed health-conscious EMSs that consider the energy source degradation using different approaches is given in the following Section 1.3 where the idea of developing an EMS based on prognostics is proposed and believed to be a meaningful and promising solution to the health management of the hybrid system.

1.3/ LITERATURE REVIEW ON HEALTH-CONSCIOUS EMS

1.3.1/ MULTI-OBJECTIVE PROBLEM

Since the degradation of energy sources in HEVs is inevitable and highly influences the durability of the system, a health-conscious EMS aiming at prolonging the lifetime of the energy sources is demanding. Developing a health-conscious EMS is generally regarded as a multi-objective problem since the objectives of such an EMS may consist of not only minimizing the economic cost of the system but also prolonging its lifetime. Some others may also have the objectives of maximizing the efficiency and minimizing the energy source degradation. The multi-objective optimization problem is also known as Pareto optimization problem, which has more than one objective function to be maximized/minimized simultaneously. Since the objectives are often conflicting with each other, optimal decisions need to be taken with trade-offs between the conflicting objectives. A solution is said to be Pareto optimal or non-dominated if none of the objectives can be improved without degrading some of the other objectives [66]. For example, a multi-objective problem can be stated as follows :

$$\begin{cases} Objective\ function: & F(x) = [f_1(x)f_2(x)f_3(x)...f_m(x)] \\ Constraints: & g_j(x) <= 0, \text{ for } j = 1, 2, ..., k \end{cases} \quad (1.1)$$

where $x = [x_1 x_2 x_3 ... x_n] \in S$ is an n-dimensional vector of solutions which could be dominated or non-dominated. The set of all non-dominated solutions is called the Pareto front, which is supposed to be the final result of a multi-objective problem [66].

Therefore, how to find a solution that makes at least one objective better off without making others worse off remains discussing in the energy management field. The following part of this section has reviewed the existing health-conscious EMSs for fuel cell HEVs in the literature. They are classified into two categories : rule-based health-conscious EMSs and optimization-based health-conscious EMSs.

1.3.2/ RULE-BASED HEALTH-CONSCIOUS EMSS

Rule-based health-conscious EMS is usually a set of rules that are designed based on human expertise and the aim is to find efficient operation points that can mitigate the energy source degradation. This kind of EMS is less sensitive to real-time driving conditions and easy to implement. However, the rules and the thresholds used to formulate the strategy are hard to define and one cannot declare whether they are the optimal or not. Based on the techniques to formulate the rules, rule-based EMSs are then classified into two categories : the deterministic rule-based strategies and the fuzzy ones, as shown in Figure 1.5. Some representative works using rule-based EMSs to solve the health management problem are reviewed in the following part of this section.

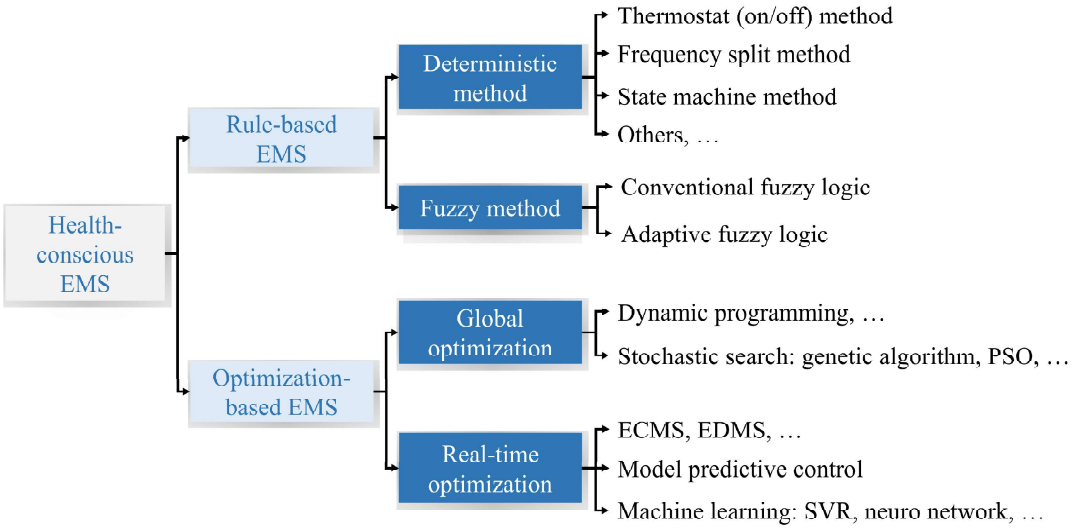

FIGURE 1.5 – Category of health-conscious EMSs

1.3.2.1/ DETERMINISTIC RULE-BASED STRATEGIES

Deterministic rule-based strategies are mainly developed through look-up tables and among which, thermostat strategy, frequency split strategy and state machine strategy

are mostly used [46]. Thanks to the simple and straightforward way of designing rules, deterministic rule-based strategies are regarded as the most practical way to achieve multiple objectives.

For example, in order to reduce system's degradation and fuel consumption at the same time, Marx et al. [157] designed the sizing strategy based on expertise knowledge : reducing degradation by starting as few fuel cells as possible, operating the fuel cell under its open-circuited voltage, limiting the depth-of-discharge of the battery, and reducing consumption by operating at maximum efficiency as much as possible. State machine method is therefore used to decide how many fuel cells should be turned on and a set of rules are made to decide the power level of the fuel cells. However, the rules are defined based on human expertise and the optimality hasn't been discussed.

To optimize the rules in an intelligent way, researchers have started to combine some optimization techniques with deterministic rules. For example, in [29], the boundaries of state-of-charge (SOC) and desired torque of the rule-based controller are dynamically calculated by the minimizing the real-time consumption. Also, in [94], the optimal parameters for the rule-based EMS are calculated offline, which allow the vehicle to achieve lower fuel consumption and higher autonomy.

Furthermore, a frequency split EMS has been proposed in [116] which decomposed the power demand into different frequency bands by wavelet transform, and to be health-conscious, the frequencies of the decomposed signals are in the range of acceptable frequencies of the battery and the fuel cell. Therefore, both energy sources are operating in their health modes. However, the auto-regressive integrated moving average model used for the prediction of the time series in this work is highly dependent on the available data and researchers' expertise, which causes generality problem.

1.3.2.2/ FUZZY RULE-BASED STRATEGIES

Fuzzy rule-based strategies use fuzzy inference systems to transfer the deterministic inputs and outputs into linguistic ones. The fuzzy outputs are then defuzzied into precise control signals for the system. The fuzzy inference system solves the multi-objective problem by adding multiple inputs and designing proper rules.

For example, a multi-input fuzzy logic controller has been proposed in [150], in which a set of rules are designed to determine the power split for battery/ultracapacitor storage system. At the same time, some other rules are developed to reduce battery degradation by sacrificing the operation time of the ultracapacitor. Besides, to manage the fuel cell degradation, Ravey et al. have used the degradation index of the fuel cell as an input of fuzzy logic controller and the reference current of the fuel cell as the output [129]. When degradation or failure happens, the fuel cell can be operated over its efficiency point in order to maintain the battery's SOC. In [105], the C-rate of the battery has been used as an auxiliary input of the fuzzy logic controller in addition to the voltage and the demanded power. C-rate is only functioned in part of the rules which are used to suppress the battery power when the value of C-rate is high. This consideration is responsible for protecting the battery. However, similar to deterministic rule-based strategies, fuzzy rule-based strategies are easy to implement but can hardly reach the optimal if the rules are designed without combining any optimization methods.

A general way to improve the optimality of fuzzy rule-based strategies is to tune the mem-

bership functions of the fuzzy logic controller using intelligent methods. For example, Wang et al. have proposed to use the genetic algorithm for fine-tuning the parameters of membership functions [21] and Chrendo et al. have referred that neural network algorithm can also be used to improve the conventional fuzzy logic, which is the so-called adaptive neuro fuzzy inference system [112]. However, these algorithms are developed highly dependent on the driving profiles and the parameters derived for certain driving conditions may be not applicable to other conditions. Martinez et al. have proposed to design a survey-based fuzzy logic controller to combine different expertise and use the type-2 fuzzy system to handle the uncertainty in the rules [64, 79]. In the application of a fuel cell HEV, the reference fuel cell current has been controlled to satisfy the power demand and maintain the SOC of the battery to avoid further degradation.

1.3.2.3/ Synthesis on rule-based EMSs

According to the literature, rule-based strategies are easy to design and implement in real time for HEV applications when designing health-conscious EMSs. However, the optimality of rule-based strategies is hard to achieve. Although some offline optimization techniques can be combined with the rules to reach better management results, the real-time capability is weakened. On the other hand, the above mentioned rule-based strategies in the literature have performed health management by designing rules on SOC values, degradation models, C-rate, etc. It should be noticed that the rules could only be correctly designed once the degradation models are well defined.

1.3.3/ Optimization-based health-conscious EMSs

Optimization-based strategies are often classified into two categories : global optimization strategies and real-time optimization strategies, as shown in Figure 1.5. The idea of developing a health-conscious global optimization strategy is to get the global optimal solution by solving a health-conscious cost function. However, global optimization strategies are carried out based on the overall driving cycle information, which cannot be applied in real time applications unless the driving cycle could be predicted. On the contrary, real-time optimization strategies solve the optimization problem by defining an instantaneous cost function, which is updated along with the time. Therefore, real-time strategies are preferred to be as simple as possible due to the heavy computation cost. Various optimization-based EMSs used to solve the health management problem for HEVs are reviewed in the following part of this section.

1.3.3.1/ Global optimization strategies

Dynamic programming Dynamic programming can divide the optimization problem into a series of sub-problems by discretization and the cost function is calculated for each discrete time step. Consequently, a path with the minimum cost at each step is obtained [133].

For example, a cost function for minimizing the overall battery degradation has been formulated in [101] and the power splitting to the battery was determined according to the minimization results. Another optimization problem has been proposed in [125], where

the cost function considered battery degradation, hydrogen consumption, as well as grid recharge expenses. The cost function has been used to evaluate each decision made by the dynamic programming algorithm. Other dynamic programming algorithm applications considering both battery and fuel cell degradation could be found in [76, 124, 156].

However, dynamic programming algorithm is sensitive to driving cycles and the computation load is heavy. To overcome these constraints, stochastic dynamic programming (SDP) method has been proposed that applies a Markov process to represent the power demand and allows real-time application. For example, Fletcher et al. have defined the driving cycle using a Markov decision process, which was subsequently solved by SDP algorithm aiming at minimizing the total cost of hydrogen consumption and fuel cell degradation [142]. Besides, SDP has been proposed in [162] to optimize the energy consumption by integrating the battery lifetime wear model into the cost function and obtaining a single-objective problem. Moura et al. have formulated a multi-objective problem aiming at finding a trade-off between energy consumption and battery's health. Two battery degradation models, solid-electrolyte interphase (SEI) film layer model and ampere-hour processed model, have been evaluated and the problem was solved by a shortest-path SDP [83].

Moreover, dynamic programming can be used as evaluation, comparison and analysis tools [133]. For example, it can derive the optimal performance condition for a given driving profile and help to formulate rules for real-time management. Carla et al. have used dynamic programming to produce a dataset which is large enough to train an artificial neural network [169]. The cost function of dynamic programming consisted of both fuel consumption and battery degradation. With the results of dynamic programming, an artificial neural network has been implemented with the SOC of the battery and the forecast power demand as two inputs and the fuel cell power as the output and has achieved near-optimal results in real time.

Stochastic search method Stochastic search methods are commonly used in HEV applications, which are the most effective methods to solve multi-objective problems. According to [133], frequently used stochastic search methods consist of genetic algorithm, particle swarm optimization (PSO), extreme algorithm, etc. They are able to solve the optimization problem by iterative approach.

For example, a multi-objective fitness function including battery cost, capacity cost and total energy cost is formulated in [146]. In each generation of genetic algorithm, the population generates a set of Pareto-optimal solutions and at the end, the most feasible solution with respect to all objective functions is selected. Besides, authors in [45] and [38] have proposed to use a non-dominated sort genetic algorithm (NSGA-II) to solve the optimization problem of two conflicting objectives. With the formation of a Pareto front, the opposite effects of energy minimization and battery health on the cost function are traded off optimally. In [144], three objective functions have been proposed including operation cost, efficiency and system lifetime, which were integrated into a single function through weight aggregation approach. The optimization problem was subsequently solved by the PSO algorithm. Furthermore, Chen et al. have proposed a novel EMS which used quadratic equations to find a relationship between fuel rate and battery power and applied simulated annealing method to determine the battery power input when taking into account the state-of-health (SOH) of the battery [111].

However, similar to dynamic programming algorithm, stochastic search methods are sen-

sitive to driving cycles and are usually implemented based on specific pre-defined driving conditions. Therefore, unless combining with driving cycle identification, stochastic search methods still lack the generality in HEV applications.

1.3.3.2/ REAL-TIME OPTIMIZATION STRATEGIES

ECMS and EDMS Equivalent cost minimization strategy (ECMS) and equivalent degradation minimization strategy (EDMS) are widely used for real-time optimization in HEV applications. Generally, an equivalent cost function is established to transfer the global optimization problem into a local optimization problem by minimizing the cost function in real time [133].

For example, an instantaneous optimization process based on ECMS has been proposed in [168] for a multi-mode power-split HEV. In this work, the battery degradation has been modelled by SEI film growth and integrated into the cost function. Instead of minimizing the total cost, Hissel et al. [171] have proposed to minimize the battery degradation in the hybrid energy storage system. The cost function was formed by an equivalent factor which represented the marginal degradation caused by the power demanded from the capacitor.

Besides, Pontryagin's minimum principle (PMP) is one of the most commonly used optimal approaches in ECMS and EDMS, which works effectively with constrained optimization problems. For example, in order to prolong the battery's lifetime, Liu et al. have minimized the fuel consumption with the constraints of battery's SOC and current, solving by PMP optimal control [121]. To better demonstrate the degradation of the battery, a severity factor map has been built based on the battery ageing model and combined into the cost function in [160]. The problem was then solved by PMP to reach a trade-off between battery ageing minimization and fuel consumption minimization. However, Ettihir et al. claimed that some cost function minimization method can only be used to minimize the fuel consumption over a global level and the real performance of the fuel cell has been ignored. In order to track the best performance of the fuel cell, they have applied an adaptive recursive least square algorithm to seek the optimal performance of the fuel cell when considering ageing effects and integrated it with PMP to form an adaptive management strategy, A-PMP [141].

Model predictive control (MPC) MPC is another real-time optimization-based approach which assumes that the current state is the initial condition and solves the optimization problem at each sampling instant. It is implemented in three steps : (1) calculate optimal control sequence in a prediction horizon that minimizes the cost function subject to constraints ; (2) implement the first part of derived optimal control sequence to physical plant ; and (3) move entire prediction horizon one step forward and repeat step (1) [133]. Therefore, it is interesting to use MPC in a multi-objective health-conscious EMS since it can involve several constraints into the control actions.

For example, Arce et al. have used MPC to track the power demand of an HEV and set constraints to battery's SOC to avoid degradation [34]. On the other hand, the fuel cell degradation is limited by setting the threshold of fuel cell power and the time limit between its start-ups and shut-downs. Due to MPC's receding horizon nature, it is possible to reduce the computation cost when comparing to PMP and dynamic programming results

after multiple trials to different driving cycles. However, by dividing the problem into several time steps, the solutions of MPC are usually suboptimal.

Machine learning methods Machine learning methods are known as intelligent control strategies, which are suitable to solve complex nonlinear problems. Therefore, they are widely used in developing EMSs. Various machine learning strategies exist in the literature including neural network, support vector regression (SVR), etc.

For example, to be health-conscious, Caihao et al. have used SVR to monitor the SOH of battery in HEV applications, which realized the real-time analysis of battery ageing based on partially charging data [86]. Besides, neural network has been used in [159] to perform power split between two storage system - battery and ultracapacitor. The instantaneous battery current has been considered to have an impact on its degradation and the power delivered by the ultracapacitor could help to handle the peak current demand in the battery, and therefore to reduce the degradation of the battery during operation. These methods have shown some improvements in robustness but the solution is not an optimal one. To improve the optimality, Chen et al. have proposed to train two neural network modules for known and unknown trips separately based on the optimization results of offline dynamic programming method and improved the optimality to some extent [90]. However, machine learning methods are not that practical since the computation load of training datasets is considerably heavy.

1.3.3.3/ SYNTHESIS ON OPTIMIZATION-BASED EMSS

Optimization-based strategies are widely used in developing health-conscious EMSs and various health-conscious objectives can be achieved through formulating health-conscious cost functions with proper constraints. Global optimization-based strategies are able to find an optimal solution to the cost function and they could also work as an evaluation and analysis tool. However, they cannot be applied directly to a real-time application unless the driving cycle can be identified or predicted by other identification or prediction approaches. When it comes to instantaneous applications, real-time optimization-based strategies are used but they are not supposed to be designed in a complicated way due to the computational burden and memory limits. Therefore, one has to reduce the complexity of the problem in order to make it implementable. Another weak point of real-time EMSs is low optimality since they lack the global understanding of the problem.

1.3.4/ OPEN ISSUES AND REMAINING CHALLENGES

1.3.4.1/ OPEN ISSUE 1 : OPTIMALITY OF EMSS

Optimality of multi-objective health-conscious EMSs is always regarded as a tough issue and generates many discussions. As discussed above, the optimality of rule-based strategy can hardly be assured if the rules are designed based on human expertise. One possibility is to use other optimization techniques to tune the rules or the membership functions of the fuzzy logic controller offline. However, the control effects of all existing offline optimizations are affected by different driving cycles and in vehicle applications, the operation condition of the vehicle is changing all the time so that the offline tuning is

rarely convinced. Although real-time optimization strategies can adjust the control strategies according to the current state of the vehicle, the computation burden is too high and the calculation speed is limited. The existing approaches usually choose to reduce computation load at the expense of optimization performance or using rather simple models. Besides, without a global understanding of the driving condition, their optimality can be also weakened.

1.3.4.2/ OPEN ISSUE 2 : DEGRADATION QUANTIFICATION IN EMSS

For the moment, most of the existing health-conscious EMSs just set boundaries to battery's SOC or limit the upper or lower voltage to protect the fuel cell, which can hardly quantify the degradation or the lifetime of the energy sources. Other studies quantify the ageing phenomenon by degradation rate derived from pre-defined degradation models, which are highly dependent on the driving conditions (acceleration, idling, etc.). With different driving cycles and different vehicle configurations, the effectiveness of the model cannot be guaranteed. Although some prognostics and health management works have been done to predict the RULs of the battery and the fuel cell, they are implemented with finished experimental datasets. The prognostics results have neither been used in the design of EMSs nor applied in the realization of vehicle applications yet.

1.3.4.3/ FACING THE CHALLENGES

In light of quantitative and qualitative literature survey on developing a health-conscious EMS for fuel cell HEVs, the following challenges are pointed out and a possible solution based on prognostics is proposed. The synthesis scheme is shown in Figure 1.6.

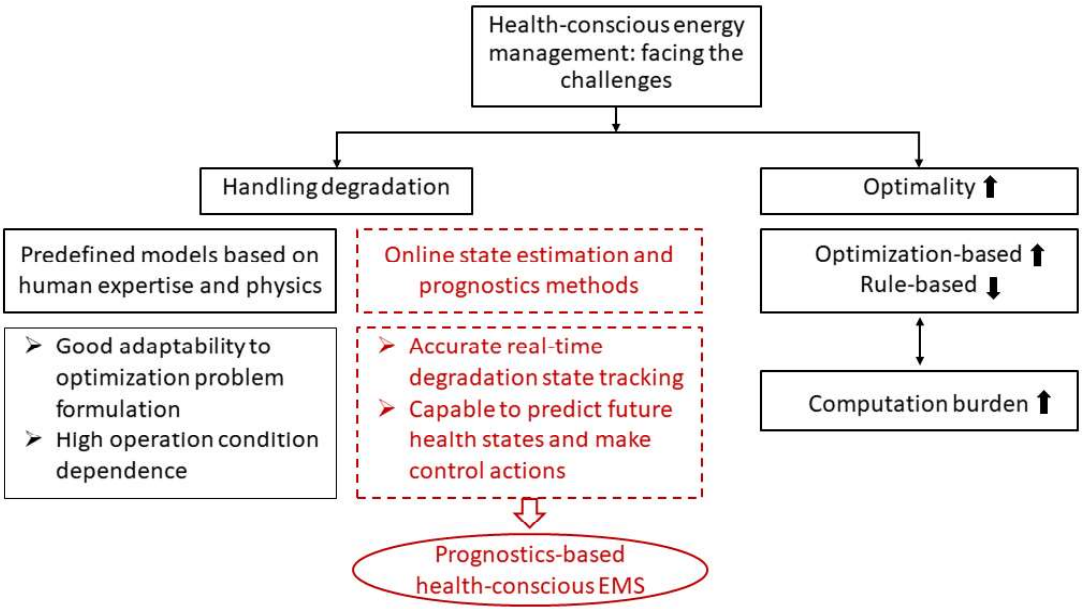

FIGURE 1.6 – Facing the challenges in energy management of fuel cell HEVs

To face the afore-mentioned issues, a way to improve the optimality of the EMSs and a method to quantifying the power source degradation are demanding. The difficulty of

solving the optimality problem does not only come from its multiple objectives but also come from the various operation conditions in real time. Solutions depend on which kind of strategy is going to be used. The optimality of rule-based EMSs can be achieved by designing the rules delicately and combining intelligent algorithm, while for optimization-based EMSs, possible perspectives could be placed on the prediction of driving cycles to improve global strategies or reducing computation burden of real-time strategies and improving its optimality.

Furthermore, works have been done to exhaustively search for the accurate power source degradation models but due to the variable operation conditions, the existing degradation models are far from satisfaction. In this case, state estimation and prognostics techniques are believed to be one of the possible solutions to provide real-time health state information as a guide for taking automatic corrective actions along with the vehicle's operation. PDM is a newly emerging research area that aims to integrate prognostic health information and knowledge about the future operating conditions into the process of selecting subsequent actions for the system, namely, the management aspect of PHM. It is of great interest in the health assessment and life prediction field of power sources, with which one can incorporate the current SOH into the health management.

Due to the fact that the prognostics study of battery and fuel cell has remained on component level and has not yet been combined in the control part of the system, a proposition of health-conscious EMS based on prognostics aiming at preserving the system and improving its durability is expected to be highlighted in the near future and has been enforced in this thesis as a beginning step.

1.4/ RESEARCH ORIENTATION - PROGNOSTICS-BASED EMS

1.4.1/ WHAT IS PROGNOSTICS ?

Predicting the future health states of the system and estimating its RUL could be regarded as a prognostic process. Various definitions of prognostics have been proposed in the literature and according to the international organization for standardization (ISO) committee, prognostics can be defined as [15] :

> Standard ISO 13381 (2004). *The aim of prognostics is the "estimation of time to failure and risk for one or more existing and future failure modes".*

We can highlight from the definition that prognostics implies not only that we should be able to project into the future the behaviour of a system, but also that we should be capable of identifying the health state at each instant, taking into account the chosen mission criteria. Prognostics appears to be a key process which makes the current industrials think more about "predict to prevent" rather than "fail to fix". As the main goal of prognostics is to provide information that helps in taking corrective decisions, therefore, to evaluate prognostics, one of the metrics to quantify is the RUL - it is defined as the time between the current instant t_c and the instant where the degradation will reach the failure threshold t_f - end of life (EOL) [77]. The EOL threshold is usually set as a certain percentage of the original value. It also needs to construct a confidence measure in order to indicate the degree of uncertainty of the RUL, as shown in Figure 1.7. In Figure 1.7, Y

axis could be any health indicator that degrades along with time. The green dots denote the available measurement data and the dotted line denotes the predicted trajectory. RUL can be calculated as :

$$RUL = t_f - t_c \tag{1.2}$$

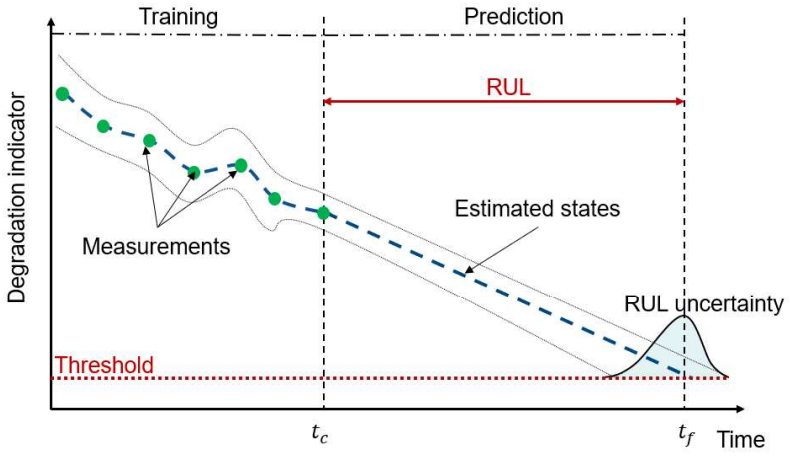

FIGURE 1.7 – Definition of RUL and its uncertainty

Prognostic methods usually differ in the type of considered applications, while the implemented tools depend mainly on the nature of available data and knowledge. In the scope of our study, prognostics used in the applications of predicting battery capacity loss and fuel cell performance degradation are discussed. The approaches exist in three manners : data-driven approach, model-based approach and the hybrid one, shown as the ***Cluster I*** in the bibliography map (Figure 1.8). For battery prognostics, support vector machine [84], neural network [47] and Gaussian process [27] have been used as data-driven methods to simply capture the inherent trends without knowing the exact ageing mechanisms, while some filter algorithms like extended Kalman filter [26], unscented Kalman filter [134] and particle filter [80] have existed as hybrid methods to perform prognostics with state-space models. Moreover, the equivalent circuit model makes it possible to develop a model-based method which uses the knowledge of battery's physical failing mechanism to estimate the RUL [20]. For fuel cell's prognostics, two of the three approaches exist in the literature : echo-state networks [82] and adaptive neuro fuzzy inference system (ANFIS) [104] as data-driven approaches and unscented Kalman filter [70] and particle filter [77] as hybrid approaches. However, these prognostics methods are investigated based on finished experimental degradation data. Although these methods contribute to estimating the RUL, post-prognostics decisions are lacking, let alone the mitigation actions in HEV control. Therefore, developing an integrated PHM cycle to benefit from not only from the results of the prognostics but also the corrective control actions is demanding.

1.4.2/ TOWARDS PHM OF FUEL CELL/BATTERY HYBRID SYSTEM

To complete the bibliography map, previous discussed health-conscious EMSs are mapping as ***Cluster II*** in Figure 1.8. As indicated in the map, existed health-conscious EMSs

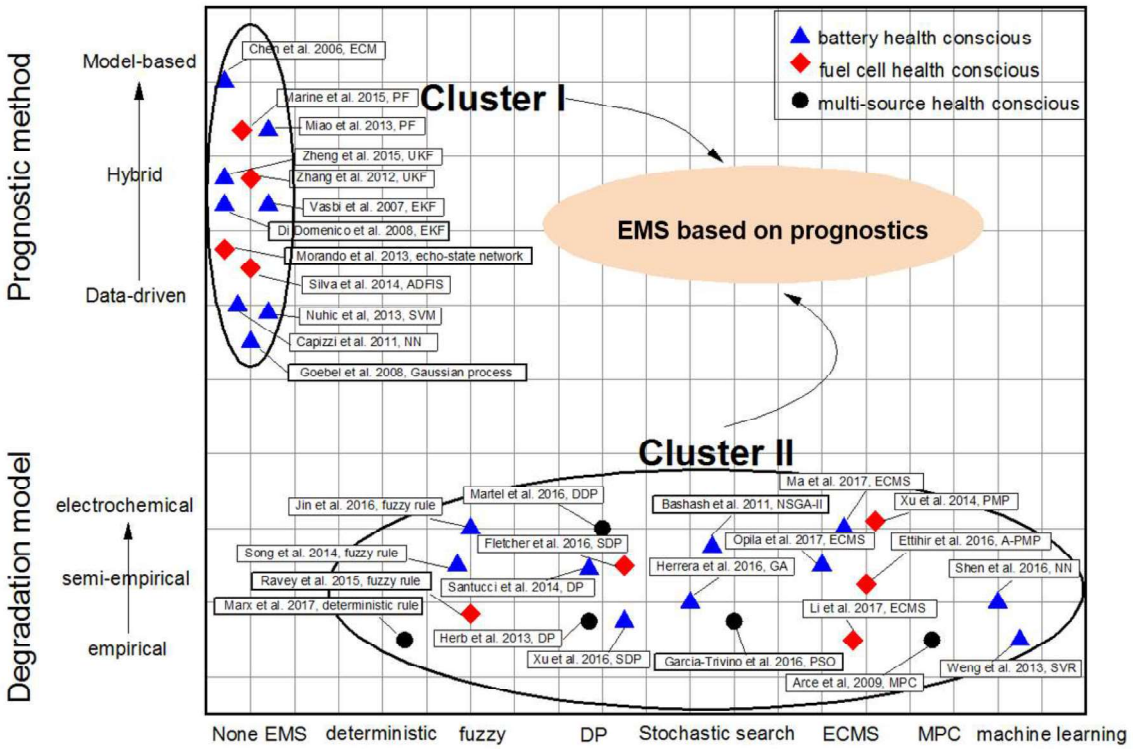

FIGURE 1.8 – Bibliography mapping

are based on pre-developed degradation models and no prognostics work is combined to EMSs, which means there is a lack of knowledge of knowing the current health state of the system and the corrective actions taken by the EMSs maybe not suitable to the current health state. Therefore, health-conscious EMSs are still poorly developed. Indeed, the predictive nature of prognostics does give a chance to develop a new health-conscious EMS, which performs energy management through automatic corrective actions with the help of the awareness of the power sources' health states. The whole can be summarized as a PHM system.

According to the definition made by the Center for Advanced Life Cycle Engineering (CALCE), PHM is a discipline developed originally from condition-based maintenance, which is defined as the means to predict and protect the integrity of equipment and complex systems, and avoid unanticipated operational problems leading to mission performance deficiencies, degradation, and adverse effects to mission safety [77]. The entire PHM procedure contains a set of activities that permits the evaluation of a system's reliability in its actual life-cycle conditions and aims to enhance the effective reliability and availability of the system by detecting its current and approaching failures. Three phases and seven layers of a general PHM architecture are shown in Figure 1.9 and described in the following paragraphs :

Layer 1 : Data acquisition In this layer, analogue data from sensors or transducers are acquired as digital data and provided to the system. Physical quantities like voltage, current, power, etc. in the electrical domain and force, displacement, speed, etc. in the mechanical domain are observed.

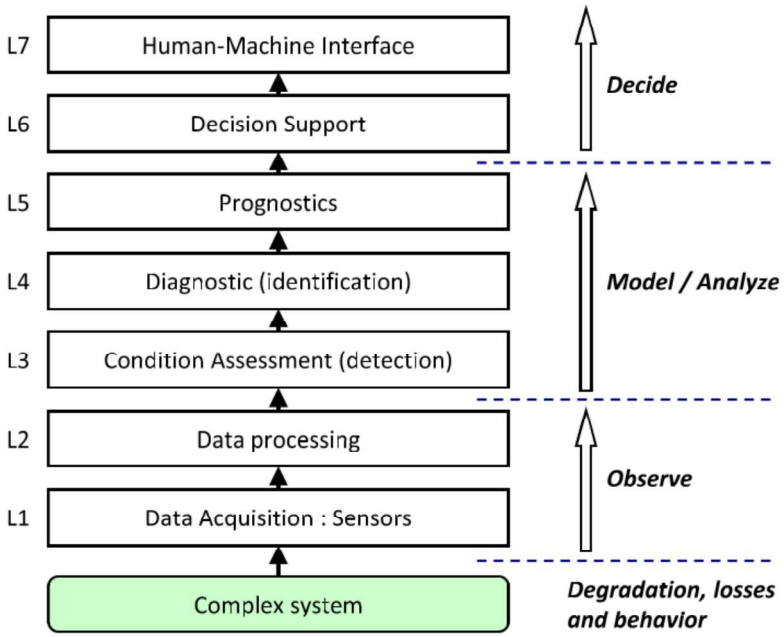

FIGURE 1.9 – PHM architecture [77]

Layer 2 : Data processing This layer aims at filtering noise and extracting/selecting features that enable to characterize the functioning of the system. Data acquired for sensors are processed, which normally undergoes feature extraction, reduction and selection procedures.

Layer 1 and **Layer 2** are known as the "**Observe**" phase, which deal with the problems of data. The main challenge of this phase is firstly to find reliable, non-intrusive and non-damaging observation techniques. Besides, easily implementable technology concerning cost, volume and online operation is another challenging aspect.

Layer 3 : Condition assessment The extracted features are compared with the expected values to get the current health state of the system. This layer is also able to give alerts when the performance loss exceeding the pre-defined thresholds.

Layer 4 : Diagnostic The diagnostic layer performs the identification and localization of the system's fault and failure. It is launched when the system has already ceased and is used to propagate back to the causes according to the effects.

Layer 5 : Prognostics Prognostics performs the estimation of remaining useful life and the estimation of the probability of a system to fail at a given time, which based on the current state of the system. Opposite to diagnostic, prognostics propagate from causes to effects, which gives the possibility of improving the reliability of the system and reducing the cost at the same time.

Layer 3, **Layer 4** and **Layer 5** are indicated as "**Model/Analyse**" phase, which gives users the reference of whether the current mission could be fulfilled and also whether the

future mission could be completed. An extended framework for detection and diagnostics approaches and advance prognostics models are expected in the future development.

Layer 6 : Decision support The function of this layer is to take actions based on the previous modules, which has the objectives of ensuring mission achievement, prolonging useful life, reducing cost and optimizing maintenance strategy. It aims to improve the quality of services and help operators perform their duties faster, more accurately and more efficiently by providing a decision aid.

Layer 7 : Human-machine interface This presentation layer is necessary in the industrial application which should be developed more user-friendly in order to ensure communication between modules.

Layer 6 and **Layer 7** are known as the "**Decide**" phase, which is a post-prognostics phase mainly to give maintenance decisions. Different to passive decision support systems, which depend on pre-defined strategies and models leading to sub-optimal solutions in most cases, this phase of the PHM cycle gives system maintenance decisions or control actions based on the dynamic system knowledge. However, for the moment, this phase hasn't seen its full development yet and a fault-tolerant, self-adaptive and reconfigurable control system is demanding. Besides, verification and validation procedures are needed to verify the effectiveness of the control.

In fact, one of the research areas of our lab (Federation FCLAB) is towards the PHM of fuel cell systems. In the PHM axis, the health states of the power sources are assessed and the RULs are estimated. However, RUL estimation is not the objective of PHM : predicting the remaining life should enable the degradation mitigation actions in order to improve the durability of the system (Layer 6 : decision support). To accomplish this work, PDM has emerged as a newly emerging research area that aims to integrate prognostic health information and knowledge about the future operating conditions into the process of selecting subsequent actions for the system. It is of great interest in health assessment and life prediction of the power sources, with which one can incorporate the prognostics aspect of PHM with the health management aspect.

As the prognostics aspect of PHM enables the estimation of RUL of a system, which indicates whether it is necessary to implement preventive maintenance in order to avoid further degradation, PDM is then defined as the process of selecting system actions informed by prognostics results, which is actually the management aspect of PHM [71]. Speaking about PDM in HEV applications, the decision-making process turns out to be a part of EMS, which is regarded as the high-level control loop to distribute the power between multiple power sources. However, the immediate characteristics of control actions may cause problems when considering the granularity of decisions : how to make immediate controls to avoid or to mitigate the degradation that appears as a long-term phenomenon ? This question turns out to be the main issue to be solved in this thesis. The framework of developing an on-board prognostics-based health-conscious EMS is introduced in the next section, which is a first trial of completing the health management aspect of PHM in HEV applications.

1.4.3/ ON-BOARD PROGNOSTICS-BASED HEALTH-CONSCIOUS EMS

To combine PHM in the energy management of fuel cell HEV, a system-level block diagram is proposed in Figure 1.10. In this process, when the mission is initiated, the system collects the raw data and a data processing module is used to clean and select the data. Then, state estimation is performed based on the preprocessed data and when a threshold is reached, the prognoser is triggered to perform the prognostics and get the RULs. According to the results of the prognostics, EMS is modified based on a PDM process with the objective to improve the durability of the system. By tuning the current EMS, the demanded power (Pdem) is redistributed to the fuel cell and the battery by a current-based control scheme as shown in the action module of Figure 1.10.

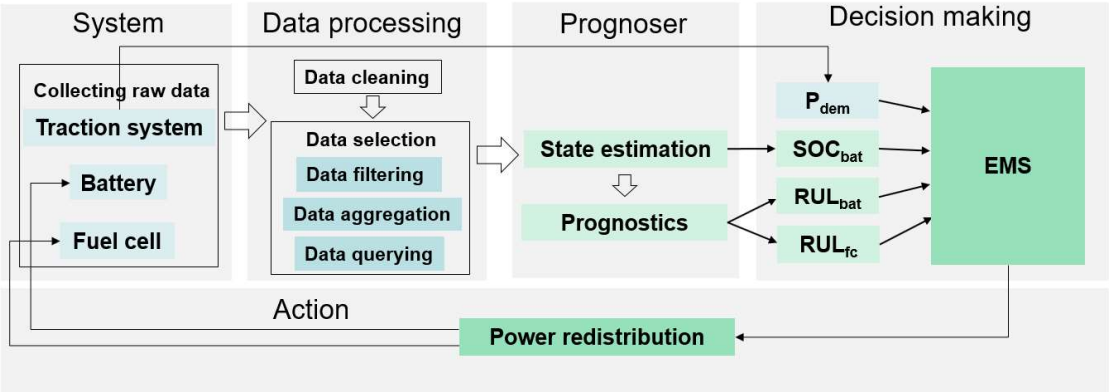

FIGURE 1.10 – System-level block diagram of PHM process in fuel cell HEV

As mentioned above, to implement PDM in fuel cell HEVs, it is important to determine when prognostics should be performed. According to [151], setting a threshold on the SOH to capture a performance drop is one of the possible solutions. The PDM process based on this idea is illustrated in Figure 1.11. The thresholds are chosen based on the historical datasets and the RUL estimate and its confidence interval could be obtained by prognostics algorithm [184]. Each time a threshold is reached, the prognostics is triggered and the power is redistributed based on the proper decision-making process, which is adaptable to the current health state of the system by making full use of the results of prognostics. By setting the prognostics triggering thresholds, this process will be repeated and the power will be redistributed again and again until the mission is completed and the lifetime of the system is expected to be prolonged.

1.5/ SYNTHESIS

This chapter has presented an overview of the current energy context and it has been justified that the fuel cell system applied in transport sector still has a long way to browse before it fully entering the automotive market. The main obstacles are concerning about the cost and the durability, while the durability highly influences the cost-effectiveness. Therefore, this research work positioned itself on enhancing the durability and prolonging the lifetime of fuel cell systems for automotive applications.

A framework of developing on-board health-conscious EMS for the hybrid system based

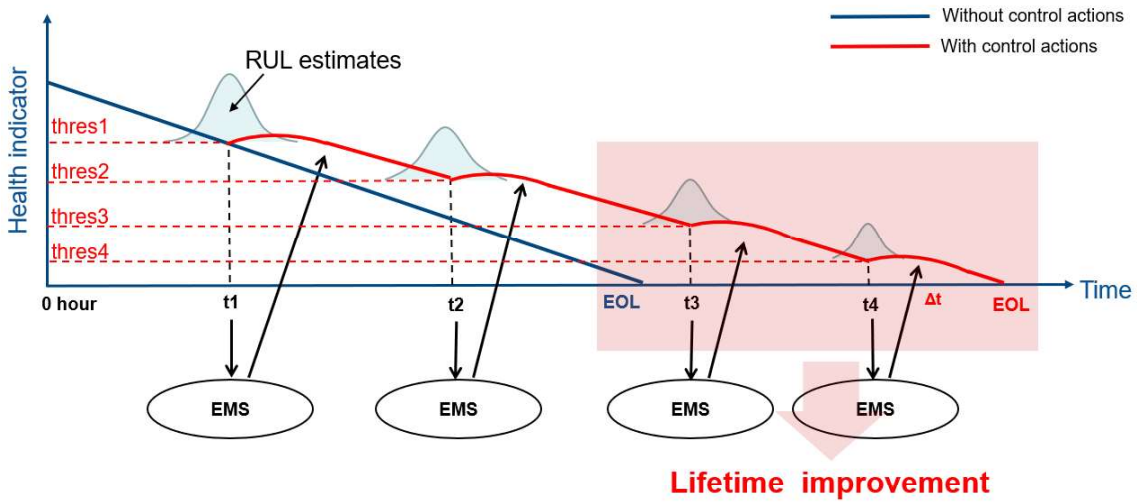

FIGURE 1.11 – PDM process

on PHM cycle is proposed in this chapter. First, the context of the energy market worldwide has been described and a hydrogen solution based on fuel cell propulsion has been justified as the momentum of today's sustainable development. Then, the durability limits of the energy sources have been pointed out for the automotive applications, which are believed to be the principal obstacles for the massive commercialization of fuel cell vehicles. Next, the state of the art oriented towards solving the durability issue based on EMS design has been reviewed according to the literature research. Challenges have been analyzed and a PHM solution has been proposed.

Due to the fact that the prognostics study of battery and fuel cell has remained on component level and has not yet been combined in the control part of the system, a health-conscious EMS based on prognostics aiming at preserving the system and improving its durability is going to be developed and enforced in this thesis as a beginning step.

In the next chapter, some generalities concerning about the durability of the studied energy sources, i.e., lithium-ion battery and PEM fuel cell, are going to be explained and the possibility of building a fuel cell hybrid system is going to be addressed.

2

GENERALITIES ON LITHIUM-ION BATTERY AND PEM FUEL CELL

2.1/ INTRODUCTION

This chapter is started by justifying the necessity of hybridizing the fuel cell with other energy storage devices, e.g. batteries, for high-qualified performance in the vehicle propulsion system. Hybridization is proposed based on the fact that the fuel cell itself cannot provide satisfying driving conditions as it suffers from worse performance during starting-on and acceleration due to its low power density. On the contrary, lithium-ion batteries have relatively high power density and energy density, which allow them to operate as energy storage systems and provide fast dynamics. Therefore, a fuel cell hybrid propulsion system together with lithium-ion batteries has gained more popularity in today's automotive market. In the vehicle applications, compared to battery-only electric vehicles, fuel cell HEVs benefit not only the high power density of the battery but also improve the limited driving distance and the long charging time.

However, a central issue holding back the critical achievement of fuel cell hybrid propulsion is the durability of the power sources. Both batteries and fuel cells in the hybrid system are operated through complicated electrochemical reactions, which bring more difficulties to quantify their degradation. Concerning this issue, this chapter assumes that the interaction between them in a hybrid system is neglectable and then analyses the lithium-ion batteries and PEM fuel cells separately, starting by describing their characteristics and then discovering their degradation mechanisms and modelling methods. During battery's lifetime, both calendar ageing and cycle ageing damage its available capacity. The ageing phenomenon happens on anode and cathode due to various chemical reactions, resulting in its capacity fade and impedance rise. Besides, PEM fuel cell, as the main power source of fuel cell HEVs, suffers from the degradation from different components of the stack : electrolyte, electrodes, membrane, bipolar plates and sealing gaskets. To assess their degradation, various degradation modelling and estimation methods are reviewed from the literature. In fact, this part is not only a literature review but also the basis of selecting possible PHM solutions to implement the energy management for the hybrid system.

This chapter is arranged as follows : first, a description of building fuel cell hybrid systems is given, in which the battery is used as the energy storage system. Next, the ageing phenomenon and degradation modelling and estimation methods of the lithium-ion battery are studied, and then those of PEM fuel cell are discussed with the same structure. The

advantages and disadvantages of different methods are also analyzed and summarized with comparison tables.

2.2/ FUEL CELL/BATTERY HYBRID SYSTEMS

2.2.1/ FUEL CELL/BATTERY HYBRID PROPULSION

As shown in Figure 2.1, a Ragone plot is used for performance comparison of various energy storing devices. On such a chart the values of specific energy (in $W \cdot h/kg$) are plotted versus specific power (in W/kg). Both axes are logarithmic, which allows comparing the performance of very different devices (for example, extremely high and extremely low power) [12]. According to the Ragone plot, fuel cell serves a significantly higher energy density than batteries (40,000 $W \cdot h/kg$ compared to 278 $W \cdot h/kg$ of the lithium-ion battery according to the literature). This implies that given limitations in the weight and size of the energy storage in the vehicle, a fuel cell electric vehicle can drive further and transport more payload than a BEV. However, due to fuel cell's relatively low power density, one favourable way to deal with the start-ups and acceleration for electric vehicles is by hybridizing fuel cell with another energy storage devices with high power density, e.g., lithium-ion batteries. Therefore, a fuel cell/battery hybrid propulsion system is considered when developing fuel cell electric vehicles where the fuel cell provides the most power required for cruising and the battery deals with the transient power demand.

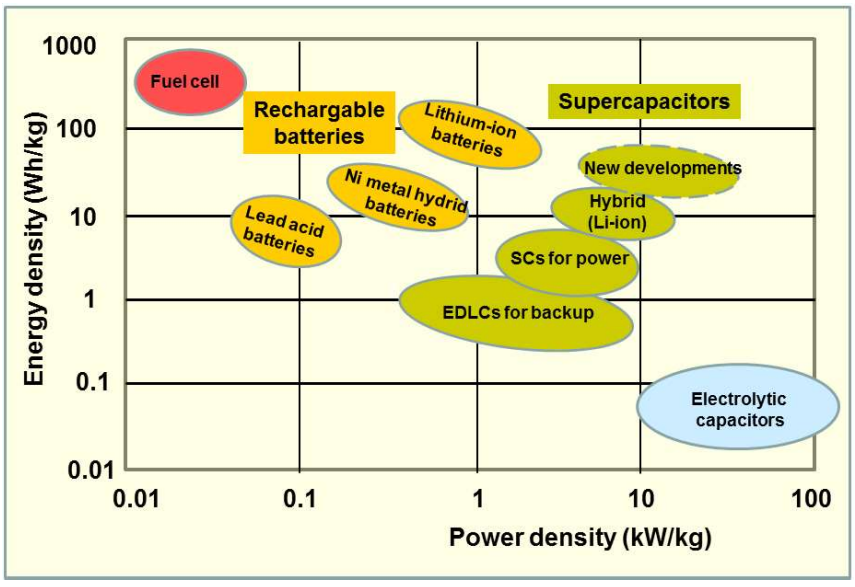

FIGURE 2.1 – Ragone plot : power density vs. energy density

The development of fuel cell vehicles has been a polarizing topic for years. At its core, a hydrogen-fueled fuel cell pulls the stored hydrogen gas, mixes it with oxygen from the atmosphere, and runs it through a proton exchange membrane to release electricity along the way, namely, a PEM fuel cell. Compared to the BEVs, the on-board battery in this hybrid configuration can be reduced in size, decreasing the overall weight of the propulsion system. Since there is no need to plug in the vehicle to recharge the batteries, the total cost of the vehicle is then reduced. Besides, hydrogen refuelling takes one-tenth to one-

fifteenth of the time battery fast charging requires. That means the hydrogen refuelling station infrastructure requires about 10 to 15 times less space to fuel the same number of vehicles [4]. And as a further benefit, the by-product heat of the electricity production reaction is useful as a source of energy for heating system, such that as little energy as possible is lost in the process.

In fact, there are more than 4000 fuel cell vehicles on the road today and numerous vehicle enterprises are devoted to developing fuel cell powertrains to deliver the quality, reliability and dependability to accelerate their commercialization in the vehicle market. For example, Mirai fuel cell vehicles developed by Toyota have used mass-production PEM fuel cells with a 3.1 kM/L volume power density and a 144 kW (155 DIN hp) maximum power output, where a 1.6 kWh nickel-metal hydride battery is connected in parallel to deal with the regenerative braking and also assist during high-power demands like accelerating. A high-capacity fuel cell boost converter is developed to boost the fuel cell voltage to a maximum output of 650 V. Its operation principle is shown in Figure 2.2.

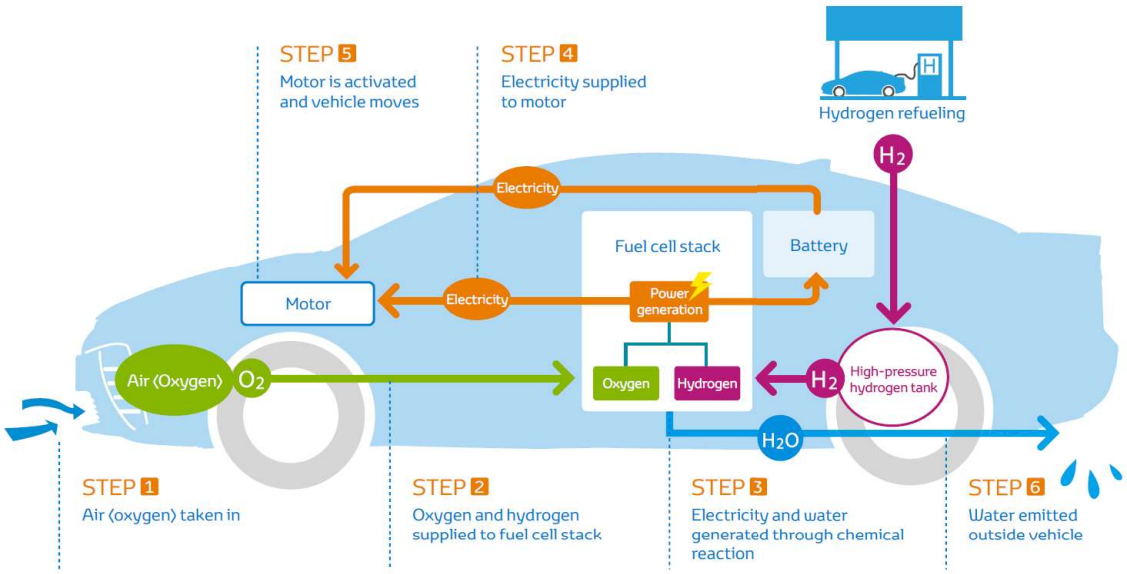

FIGURE 2.2 – Operation principle of Toyota Mirai fuel cell vehicle

This parallel configuration is also favourable to other commercial fuel cell vehicles, e.g., Honda's Clarity fuel cell vehicle, Hyundai's NEXO fuel cell vehicle, etc. Their characteristics and performance are listed in Table 2.1. Despite this kind of parallel structure, other alternatives of powertrains also exist in the literature varying on the physical arrangement of the power sources, selection of the energy storage devices, and the control strategy for splitting power between the fuel cell and the energy storage unit [40, 44, 49, 78, 88, 141], as shown in Figure 2.3. Figure 2.3 (a) uses a fuel cell only powertrain where the bus voltage equals the output voltage of the fuel cell. Figure 2.3 (b) uses an ultra-capacitor as the energy storage system to recover the braking energy. Figure 2.3 (c) is the one discussed above which uses the fuel cell as the principal power source and the battery as a secondary source. Figure 2.3 (d) uses the fuel cell as a range extender while the battery used in this structure is larger than the one used in Figure 2.3 (c). Next, the roles of fuel cell and battery used in the hybrid propulsion system are discussed separately.

TABLE 2.1 – Examples of commercial fuel cell vehicles

Vehicle type	Fuel economy	Engine
Toyota Mirai (2019)	67 MPGe city / 67 MPGe highway	113 kW electric motor + 245 V Nickel-Metal hydride battery
Honda Clarity (2018)	69 MPGe city / 67 MPGe highway	130 kW electric motor + 346 V lithium-ion battery
Hyundai NEXO (2019)	59 MPGe city / 54 MPGe highway	95 kW electric motor + 240 V lithium-ion battery

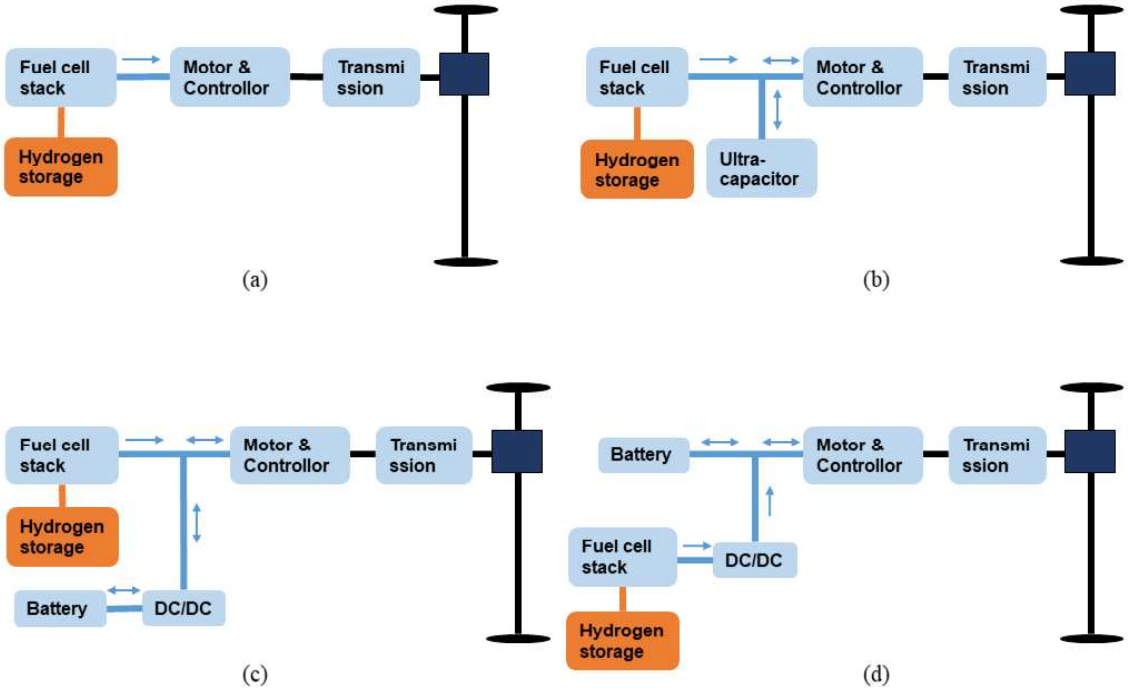

FIGURE 2.3 – Some alternatives of powertrains for fuel cell vehicles

2.2.2/ USE OF FUEL CELLS IN ELECTRIC VEHICLES

Fuel cell is an electrochemical device that converts the chemical energy into electrical energy with high energy density. Among various types of fuel cells, PEM fuel cell is the one most widely used in vehicle applications due to the fact that they can be operated at low temperature (-20-80°C), therefore a fast starting from idle to full load operation can be achieved. PEM fuel cells use a solid polymer as an electrolyte and porous carbon electrodes with a platinum catalyst, however, the use of platinum makes PEM cells highly sensitive to carbon monoxide and Sulphur pollutants. As a result, they need to be fuelled by very pure hydrogen. Hydrogen produced from natural gas, for instance, is likely to require purification before being used by PEM fuel cells.

Besides, fuel cell can rarely be the mono-source in fuel cell electric vehicles due to the following considerations : firstly, as we know, electric vehicles are well suited to recover the energy dissipated in braking since their electric motors can be reversed to act as ge-

nerators. Fuel cell can provide a direct current/voltage to power the electric motors, while it cannot absorb energy reversibly ; secondly, fuel cells usually achieve their maximum efficiency at partial loads. Both of the facts suggest that fuel cells are particularly well adapted to be hybridized with other energy storage systems (e.g., batteries). The introduced energy storage systems can be used to store recovered braking energy and help provide the peak power demand. Hybridization in this way can also help reduce costs if the energy storage system has higher specific power and lower cost than the fuel cell stack. Given these considerations, most fuel cell electric vehicles are preferred to be hybrid ones. The technology of hybridizing fuel cell with energy storage systems is in an earlier stage of development than the technologies of mono-source electric vehicles and few models are currently commercially available. Further technological developments are needed to improve their durability and lower the costs.

Concerning the durability issues of both battery and fuel cell, their characteristics and degradation mechanisms, together with degradation modelling and estimation methods are discussed in the following sections.

2.2.3/ BATTERIES AS ENERGY STORAGE SYSTEM

Batteries are essential energy storage devices that facilitate the conversion from chemical energy into electrical energy, and vice versa. Being used in a hybrid propulsion system, the batteries could have a much longer life in shallow depths of discharge since they will be charged either by the fuel cells or through regenerative braking during cruising and will rarely be over-discharged. Lithium-ion batteries serve as supplemental power sources for propelling the electric vehicles in most of the present work. This is because that they have a higher energy density than most other types of rechargeable batteries, i.e., for the same size or weight, they can store more energy than others, as derived from Figure 2.1. In addition, lithium-ion batteries have a lower self-discharge rate than other types of batteries, which means that once they are charged, they will retain their charge for a longer time. Besides, lithium-ion batteries can offer good dynamic performance with high charge/discharge current. Charging/discharging tests performed in [57] on fuel cell vehicle equipped with lithium-ion batteries and lead-acid batteries suggest that for high discharge currents ($\leq 40\ A$), the nominal capacity of lithium-ion batteries was almost completely maintained, while the actual capacity of lead-acid batteries was reduced by about 50%. The good performance for dynamic driving conditions allows the lithium-ion battery to offer major flexibility in the design and energy management of hybrid powertrains.

2.3/ LITHIUM-ION BATTERY AND ITS DEGRADATION

2.3.1/ INTRODUCTION TO LITHIUM-ION BATTERY

2.3.1.1/ LITHIUM-ION BATTERY CHARACTERISTICS

Batteries are essentially energy storage devices that facilitate the conversion from chemical energy into electrical energy and vice versa. Lithium-ion batteries are widely used as energy storage systems in fuel cell HEVs in most of the present work. The charge and discharge mechanism of a lithium-ion battery is shown in Figure 2.4. The lithium-ion

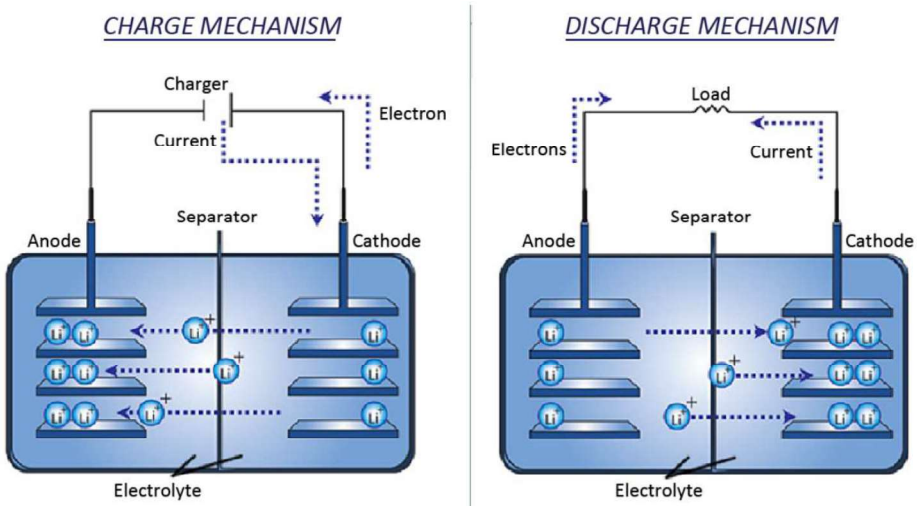

FIGURE 2.4 – Lithium-ion battery charge and discharge mechanisms

battery consists of a pair of electrodes (anode and cathode), which are immersed in an electrolyte and sometimes separated by a separator. The main role of the separator in a battery is to isolate the positive and negative electrodes, while allowing the transport of ions. Recently, a microporous membrane of polyethylene or polypropylene has been used commercially as a separator [118]. Considering lithium manganese oxide batteries as an example, during charging the Li^+ escapes from the LiMn2O4 at the cathode, under the electromotive force, the Li^+ passes through the electrolyte and embeds into the carbon interlayer of the graphite. Thus, lithium and carbon interlayer are combined internally. When discharging, the Li^+ escapes from the carbon interlayer of the anode, through an opposite process under the electromotive force, and embeds into the anode LiMn2O4. The charging reactions of the batteries are as follows, which the discharging process is in the opposite direction.

$$LiMn_2O_4 \rightarrow Li_{1-x}Mn_2O_4 + xLi^+ + xe^- \tag{2.1}$$

$$C + xLi^+ + xe^- \rightarrow Li_xC \tag{2.2}$$

The overall reaction is written as :

$$LiMn_2O_4 + C \rightarrow Li_{1-x}Mn_2O_4 + Li_xC \tag{2.3}$$

The chemical driving force across the cell is due to the difference in the chemical potentials of its two electrodes, which is determined by the difference of the standard Gibbs free energies between the products of the reaction and the reactants. The theoretical open circuit voltage, E_0, of a battery is measured when all reactants are at 25°C and at 1 atm pressure. However, this voltage is not available during use. When a cell or battery is discharged, its voltage is lower than the theoretical voltage, as illustrated in Figure 2.5. Under actual conditions, the initial voltage of the cell under a discharge load is lower than the theoretical value due to the internal cell resistance and the resultant ohmic drop as well as polarization effects at both electrodes [35].

The voltage drop due to the above-mentioned factors are detailed as follows :

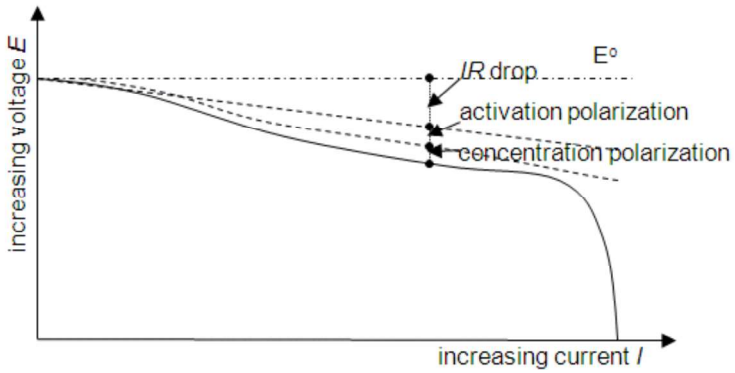

FIGURE 2.5 – Typical polarization curve of a battery [35]

Ohmic Drop refers to the diffusion process through which Li-ions migrate to the cathode via the electrolytic medium. The internal resistance to this ionic diffusion process is also referred to elsewhere as the IR drop. For a given load current, this drop usually decreases with time due to the increase in internal temperature that results in the increased ion mobility.

Activation Polarization refers to a self-discharge process, which is caused by the residual ionic and electronic flow through a cell even when there is no external current being drawn. The resulting drop in voltage has been modelled to represent the activation polarization of the battery.

Concentration Polarization represents the voltage loss due to spatial variations in reactant concentration at the electrodes. This is mainly caused when the reactants are consumed by the electrochemical reaction faster than they can diffuse into the porous electrode, as well as due to variations in bulk flow composition. The consumption of Li-ions causes a drop in their concentration along with the cell, between the electrodes, which causes a drop in the local potential near the cathode.

Since these factors are current-dependent, i.e., they come into play only when some current is drawn from the battery, the voltage drop caused by them usually increases with increasing output current. The term most often used to indicate the rate at which a battery is discharged is the $C - Rate$. The discharge rate of a battery is expressed as C/r, where r is the number of hours required to completely discharge its nominal capacity. So, a 2 Ah battery discharging at a rate of $C/10$ or 0.2 A would last for 10 hours. The terminal voltage of a battery, as also the charge delivered, can vary appreciably with changes in the $C - Rate$. Furthermore, the amount of energy supplied, related to the area under the discharge curve, is also strongly $C - Rate$ dependent. Besides, along with battery's cycling, they exhibit a gradual decrease in discharge capacity which is manifested as a loss of autonomy for the powered device, i.e., they cannot provide as much energy as its initial state even at the same $C - Rate$. This is due to the ageing phenomenon of lithium-ion batteries. An ageing lithium-ion battery is demonstrated in Figure 2.6. There are three zones : an empty zone that can be refilled by charging, an available energy zone and a dead zone which cannot be usable any more. To understand the ageing mechanisms of lithium-ion batteries is not easy since they are such complex systems and their ageing

are even more complicated. According to the use condition of the battery, there are two types of ageing : calendar ageing and cycle ageing, which are introduced in the following part of this section.

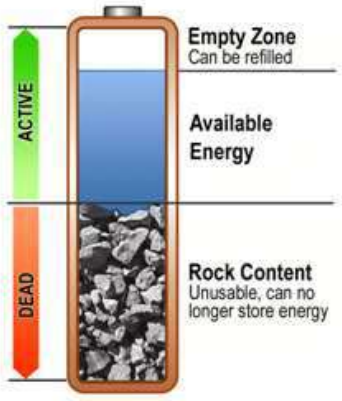

FIGURE 2.6 – An ageing battery

2.3.1.2/ CALENDAR AGEING AND CYCLE AGEING

Ageing of the lithium-ion battery can be dissociated into two categories : the calendar ageing and the cycle ageing. Each term defines the alterations caused by different uses of the battery. Calendar ageing is the irreversible proportion of the lost capacity during storage taking into account the fact that, a personal vehicle spends about 90-95% of its lifetime in storage mode when parked [102]. Self-discharge rate varies highly according to storage conditions. Hence, effects occurring within the battery can be accelerated or slowed depending on the storage conditions. The first factor affecting battery's calendar ageing and its self-discharge is the storage temperature. When the temperature is high, secondary reactions such as corrosion are facilitated and the lithium loss is more important than in moderate temperature conditions, which induces capacity fade. Low temperatures enable to limit the development of these phenomena but these conditions engender some problems due to the loss of material diffusion and alter the battery chemistry. Another variable of calendar ageing is the level of SOC during storage. One can observe a higher battery degradation for elevated SOC. This is because, for high SOC, there is a huge potential disequilibrium on the electrode/electrolyte interface causing electrochemical instability on electrolyte material. Intercalated lithium in lithiated graphite tends to diffuse to the edges where it may interact with solvent components [73, 102].

Cycle ageing happens when the battery is being charged or discharged. It is a direct consequence of the discharge level, the utilization mode, the temperature conditions and the current solicitations of the battery. Consequently, an immense number of factors are involved in this kind of ageing. All previously described factors that affect the calendar ageing are also included in the cycle ageing because the previously cited ageing phenomenons may appear whether the battery is used or not. Apart from these factors, cycling ageing is also a function of the battery utilization mode. A recurrent factor existing in literature is the ΔSOC, which represents the state of charge variation during a cycle. This is an important factor considering the amount of charge taken from or given to the battery during a discharge or charge cycle. Deep cycling considerably reduces the cycle life

of the battery due to the volume changes in materials (impact on the mechanical stability) [130]. Another variable impacting the lithium-ion battery ageing and function of the utilization mode is the charging/discharging voltage during its life. Thus, high charging voltage implies accelerated ageing phenomenon [73].

Calendar ageing and cycle ageing are the two origins of lithium-ion battery's degradation. However, when considering the ageing phenomenon, capacity loss and power fading do not originate from one single cause, but from a number of various processes and their interactions. Moreover, most of these processes cannot be studied independently due to different time scales, complicating the investigation of ageing mechanisms. In the next section, the ageing mechanisms are discussed in detailed on anodes and cathodes, separately.

2.3.2/ DEGRADATION MECHANISMS

Lithium-ion batteries are competitive in vehicle applications thanks to their high energy density and high power density. They have also shown good lifespan attributes without memory effects like nickel-cadmium and nickel-metal-hydride batteries, which will gradually lose usable capacity owing to a reduced working voltage after being only partially discharged. However, the health of lithium-ion batteries can be affected by other various effects, resulting in capacity fade and impedance rise [172]. Figure 2.7 shows the operation principle of a lithium-ion battery and its ageing phenomenon. The change happening at the electrode/electrolyte interface is the most dominant ageing phenomenon of the lithium-ion battery where solid electrolyte interface (SEI) is formed, shown in the zooming part of Figure 2.7. The continuous growth of SEI leads to the change of surface porosity, the decrease of active surface and the deposition of metallic lithium, resulting in the loss of capacity and power capability. However, the processes occurring at the anode and cathode are significantly different but they can rarely be considered independent since reaction products formed on one side which are at least partially soluble in the electrolyte can diffuse to the other electrode and result in additional reactions [181]. Details of degradation mechanisms on both anode and cathode are described in the following part of this section.

2.3.2.1/ AGEING MECHANISMS ON ANODE

Carbon, in particular, graphite, is the most important anode material in lithium-ion batteries and the changes at the electrode/electrolyte interface are believed to be responsible for the ageing on carbon anode, known as SEI instability and lithium metal plating [181]. However, changes of the active material and the contactless of the composite electrode may also have an influence on the ageing process [19], which will be discussed here by a short summary.

Changes at the electrode/electrolyte interface : The most dominant ageing mechanism on the anode is caused by SEI formation, as shown in Figure 2.8. This solid interphase is naturally created during the first charge at the beginning of its life cycle. Its role is to protect the negative electrode from possible corrosions and the electrolyte from reductions [73]. However, SEI is permeable to the lithium ions and also to other charged

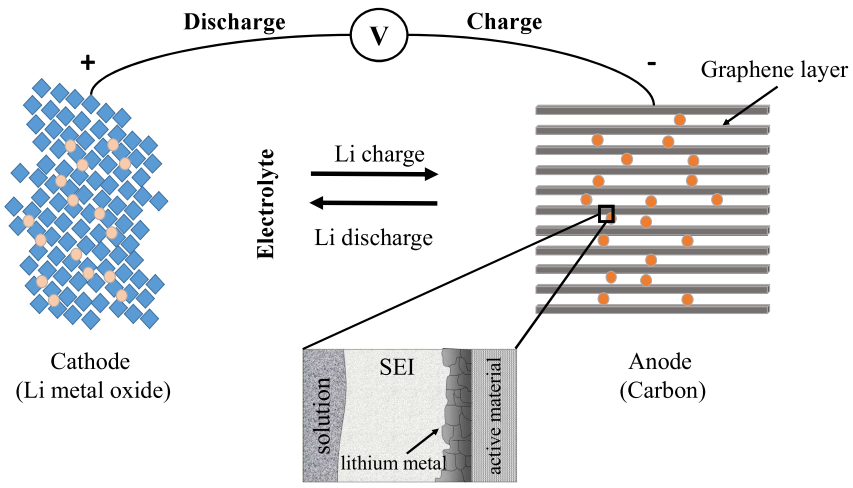

FIGURE 2.7 – Ageing phenomenon of the lithium-ion battery

elements (anion, electrons) or neutral elements (solvent). Therefore, the solvent interacts with the graphite after diffusion through the SEI resulting in graphite ex-foliation. Together with the crack formation in the SEI due to mechanical stress, an additional SEI grows consuming the electrolyte and leading to an impedance rise at the anode due to the ex-

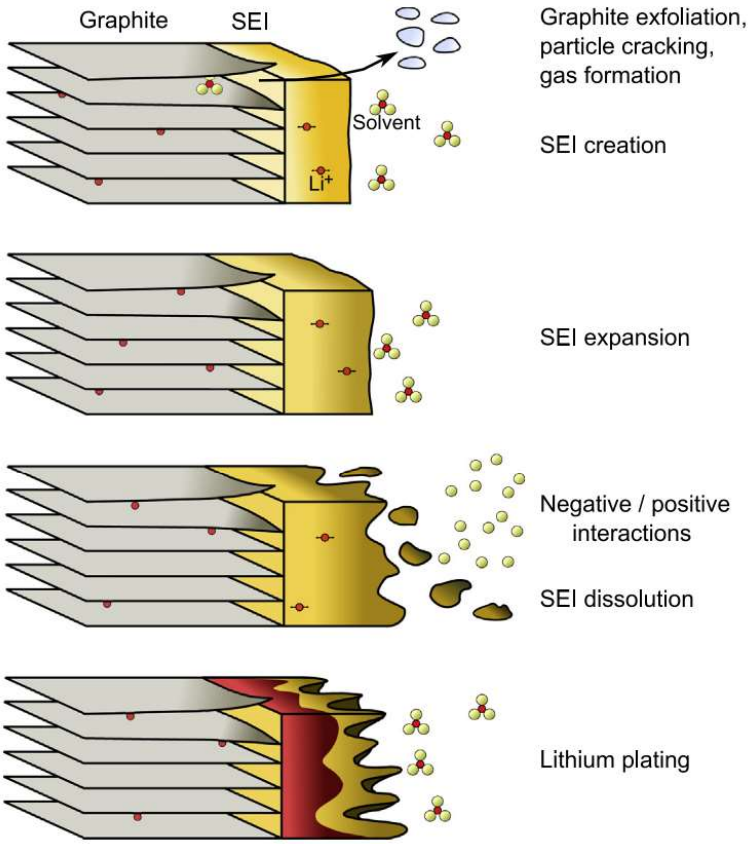

FIGURE 2.8 – Ageing mechanism on anode/electrolyte interface of lithium-ion battery [73]

posure of fresh naked graphite surfaces to the electrolyte [181]. Normally, SEI formation takes place mainly at the beginning of cycling, while SEI growth proceeds during cycling and storage and is favoured by elevated temperatures. On a long time scale, the SEI penetrates pores of the electrode and in addition may also penetrate the pores of the separator. This may result in a decrease in the accessible active surface area of the electrode [19]. A high SOC will accelerate these phenomena as it enlarges the potential difference between electrode interfaces and electrolyte. Moreover, inadequate conditions can also accelerate the process, such as high temperature, overcharge, short circuit, etc [73].

Lithium metal plating might occur at low temperatures and high charge rates. At low temperatures, the diffusion of Li^+ ions inside the graphite structure becomes slow. The deposited lithium reacts to form its SEI, consuming the electrolyte. At high charge rates, high cell polarization can enable reaching the lithium metal deposition potential, where the Li metal reacts with the electrolyte leading to accelerated ageing [181]. Besides, inhomogeneous current and potential distributions may also contribute to the lithium metal plating [19].

Changes of the active material : Graphite ex-foliation and cracking due to solvent co-intercalation, electrolyte reduction inside graphite, and gas formation inside graphite will certainly lead to rapid degradation of the electrodes due to the SEI's penetration. These reactions lead to the loss of active material, which contribute to cell ageing. Besides, at the surface of the active material, ion exchange at surface groups with lithium ions and redox reactions of surface groups are possible but should also have only a minor impact on cell ageing [19].

Contact loss within the composite electrode : Obviously, the loss of active material on the anode will lead to the volume changes, which is an inevitable source for contact loss resulting in the mechanical disintegration within the composite electrode. Contact loss may happen (i) between the carbon particles, (ii) between current collector and carbon, (iii) between the binder and carbon, and (iv) between binder and current collector [19]. Also, the electrode porosity is affected by the volume changes of the active material since it allows the electrolyte to penetrate the bulk of the electrode.

2.3.2.2/ AGEING MECHANISMS ON CATHODE

The cathode of the battery is subject to a low alteration within time, depending on the chosen material. There is also an SEI creation on the positive electrode/electrolyte interface causing electrolyte decomposition, especially at high potentials [181]. Figure 2.9 gives a schematic overview of the ageing mechanisms for lithium-ion cathode materials. In addition to the SEI formulation, another two main degradation processes on cathode materials are transition metal dissolution and catalytic reduction. The dissolution of transition metal involves net loss of transition ions from the cathode through the acid attack, which may be related to specific operation conditions (i.e. high temperature) [164, 185]. According to [19], following changes on the cathode will result in the decrease of the lifetime of a lithium-ion cell :

1. Ageing of active material ;

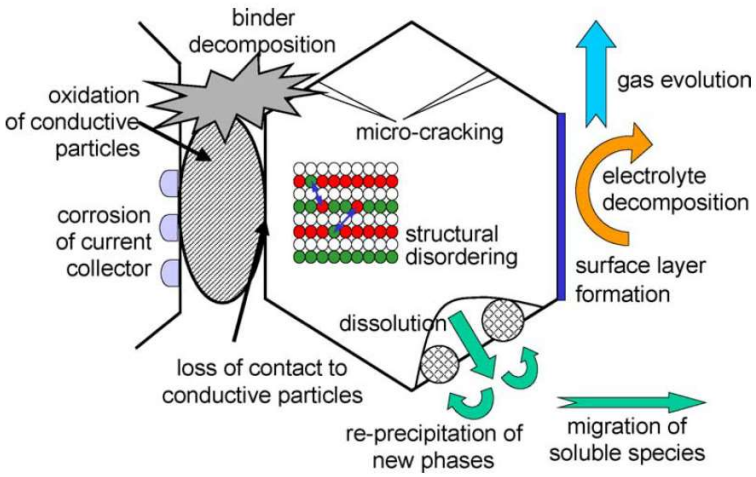

FIGURE 2.9 – Ageing mechanism on the cathode of lithium-ion battery [19]

2. Degradation or changes of electrode components like conducting agents, binder, corrosion of current collector ;
3. Oxidation of electrolyte components and surface film formation ;
4. Interaction of ageing products with the negative electrode.

Based on the literature investigation, a summary of the ageing phenomenons regarding the anode and the cathode of lithium-ion battery has been listed in Table 2.2. As discussed above, two principal effects of battery ageing can be identified : capacity fade and impedance rise. In vehicle application, the capacity loss induces an autonomy reduction while the impedance raise reduces the maximum power available. As indicated in Table 2.2, the causes of ageing are related to temperature, SOC, DOD, current, etc., therefore, how to use the battery in an adequate way to avoid its performance degradation is widely concerned by the researchers. As a priority, knowing the current health state of the battery is necessary before exercising an active control over the battery system. Numerous battery degradation modelling and estimation methods in the literature are reviewed and compared in the next section, which has taken an important place in developing health-conscious EMS.

2.3.3/ LITHIUM-ION BATTERY DEGRADATION MODELLING AND ESTIMATION

Since a lithium-ion battery is such a complex system that its ageing process is even more complicated, accurately modelling and estimating its degradation is of great significance before developing a health-conscious EMS. Based on the analysis of battery's ageing mechanisms above, different degradation modelling and estimation methods that can be used on-board are studied in this section. Some of them are electrochemical models which are closely related to the chemical reactions happening inside the battery. This kind of model is accurate but complicated and difficult to apply in practice. Others are empirical models which can be obtained by fitting experimental data. They are used to estimate the health state of the battery and predict RULs. However, it is inevitable that empirical models have problems of inaccuracy and huge dataset. Therefore, researchers start to place more attention on finding a semi-empirical model, which combines the theoretical aspects

TABLE 2.2 – Summary of the ageing phenomenon of lithium-ion battery (Source [19, 73, 120, 164, 181, 185])

Components	Causes	Phenomenon	Results
Anode	Overcharging ; very high state of charge (SOC) ;	Intercalation of solvent/ peeling of graphite/ crack ;	Loss of capacity (loss of active material, loss of lithium) ;
Anode	High temperature ; high SOC ;	Dissolution of electrolyte (cathodic oxidation/ anodic reduction) ; dissolution of binder ;	Loss of capacity ; loss of power capability ;
Anode	High current rate ; high depth of discharge (DOD) ;	Growth of SEI/ change of surface porosity ;	Growth of impedance ; loss of power capability ;
Anode	High temperature ; high SOC ;	Decrease of active surface because of continuous growth of SEI ;	Growth of impedance ; loss of power capability ;
Anode	Low temperature ; high current rates ; bad design of cells ;	Deposition of metallic lithium/ formation of SEI ;	Loss of capacity ; loss of power capability (loss of lithium) ;
Anode	High current rates ; high DOD ;	Contact loss because of volume changes ;	Loss of capacity ;
Anode	Low SOC ; high DOD ;	Corrosion of conductor ;	Loss of power capability (overvoltage) ; growth of impedance ;
Cathode	Storage condition ;	Structural disordering ;	Loss of storage places for lithium ;
Cathode	High temperature ; high SOC ;	Migration of soluble species ;	Loss of capacity by firm formation on anode ;
Cathode	High temperature ; high potential ;	Electrolyte decomposition ;	Loss of power capability ;
Cathode	Low SOC ; deep discharge ;	Corrosion of conductor ;	Loss of power capability (overvoltage) ; growth of impedance ;

with data fitting. This kind of model is more implementable compared to electrochemical ones and at the same time, more accurate than empirical ones [172]. The following part of this section has roughly reviewed these modelling methods according to the output of the models. This work may not be a complete one with an exhaustive survey on all existing battery degradation models but it is committed to finding practical ones that can be used in the energy management of HEVs.

2.3.3.1/ SEI FILM THICKNESS MODEL

From an electrochemical point of view, the cell degradation of the battery is, to a large extent, due to the loss of lithium on the SEI. Therefore, researchers have proposed to use the SEI film formation model to symbolize the degradation degree of the battery [83, 168]. The change of the film thickness is written as :

$$\frac{\partial \delta_{film}(x,t)}{\partial t} = -\frac{M_p}{a_n \rho_p F} J_S(x,t) \tag{2.4}$$

where δ_{film} is the film thickness, M_p is the average molecular weight of the SEI layer's compounds, a_n is the specific surface area, ρ_p is the average density of the compounds, F is Faraday's constant and J_S is the side reaction current density calculated by Tafel equation [83] :

$$J_S(x,t) = -i_{0,s} a_n e^{\frac{-0.5F}{R_{gas}T}\eta_S(x,t)} \tag{2.5}$$

where $i_{0,s}$ denotes the exchange current density for the side reaction, R_{gas} is the universal gas constant and T is the temperature. η_S represents the side reaction over potential, calculated by :

$$\eta_S(x,t) = \phi_1(x,t) - \phi_2(x,t) - U_{ref,s} - \frac{J_{tot}(x,t)}{a_n} R_{film}(x,t) \tag{2.6}$$

where ϕ_1 and ϕ_2 represent solid and electrolyte potentials, $U_{ref,s}$ denotes the equilibrium potential of the solvent reduction reaction, J_{tot} is the total intercalation current calculated as a sum of intercalation current in anode and R_{film} is the resistance of the film.

However, this model consists of a large number of state variables and a large set of nonlinear algebraic constraints, which brings a heavy burden for calculation [38]. To simplify the calculation, Forman et al. have proposed to linearize the constraints by a quasi-linearization method and a family of analytic Padé approximations has been used to reduce the number of state variables [41]. The implementation of this simplification enables real-time operations without a trade-off on the system accuracy.

2.3.3.2/ INTERNAL RESISTANCE MODEL

Rather than using an electrochemical model, the internal resistance of the battery can be estimated by equivalent circuit models. As shown in Figure 2.10, the model with one ohmic resistance and two RC brunches is commonly used. For example, Remmlinger et al. have proposed to use this equivalent circuit to estimate the internal resistance and derive a temperature-related degradation index calculated from the increase of battery's internal resistance [54]. The index k_d is solved by the equation :

$$R_{i,actual} = k_d R_{i,new}(T) \tag{2.7}$$

where i is the time step, R denotes the internal resistance and the actual resistance is calculated by the identification method using terminal voltage and the measured current. The idea is to calculate the proportion factor between the theoretical resistance of a new battery cell under actual temperature and the actual internal resistance [54]. An exponential expression is used to calculate the theoretical resistance value related to the temperature :

$$R_{i,new}(T) = ae^{-bT} + c \tag{2.8}$$

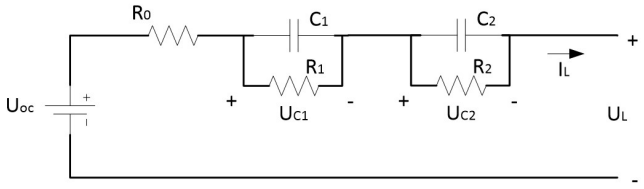

FIGURE 2.10 – Battery equivalent circuit model (two RC branches)

Besides, Stroe et al. have found the dependence of the battery's internal resistance on its storage time, SOC level and temperature [173]. They used a two-step fitting procedure to develop the model for 2.5 Ah LFP/graphite battery cells with all the three aspects :

$$R = (a \cdot e^{\alpha \cdot T}) \cdot (b \cdot SOC^{\beta}) \cdot t \tag{2.9}$$

where a, b, α and β are the fitting results.

In fact, the internal resistance of the battery can also be estimated through the filtering algorithm with the help of the equivalent circuit. A broad variety of state estimation methods were proposed and dual extended Kalman filter (EKF) is one of the key scenarios [16–18]. Instead of observing only the state variables, the internal resistance is regarded as a parameter, which can also be estimated through tracking the system performance [18]. However, the effectiveness and adaptability of this method are highly dependent on the credibility and robustness of the prescribed battery models [115].

2.3.3.3/ CAPACITY DEGRADATION MODEL

The capacity of a battery refers to how much electrical charge that the battery can hold in its fully charged state. When the capacity fades to the threshold, usually 20%-30% of its original value, batteries are believed to be not able to operate their normal mode and should be replaced [35].

As battery's capacity is the most widely used indicator of battery's SOH, numerous prognostics approaches based on capacity estimation and prediction have been proposed in the literature. He et al. have experimentally found that the sum of two exponential functions can well describe the capacity degradation trends of several different batteries, which is frequently used in the studies of battery prognostics [50]. He et al's model is expressed as :

$$Q = a \cdot exp(b \cdot k) + c \cdot exp(d \cdot k) \tag{2.10}$$

where Q denotes the battery capacity and k denotes the full charge-discharge cycle number.

Xing et al. have compared He et al.'s model with another capacity degradation model in the form of polynomial regression. Particle filter estimation results have shown that the exponential model had better predictive performance [69]. Base on that, the authors have developed another model that has shown an even better regression characteristic over the whole battery life. The model is expressed as [87],

$$Q = \gamma_1 \cdot exp(\gamma_2 \cdot k) + \gamma_3 \cdot k^2 + \gamma_4 \tag{2.11}$$

However, models in prognostics works are usually verified through the degradation data with regular charge/discharge cycles. When it comes to vehicle applications, randomized charge and discharge process should be considered due to uncertain driving conditions. In order to quantify this kind of capacity fade, semi-empirical models are then proposed in the literature to take more physical parameters into consideration, such as SOC, DOD, Ah throughput, current rate, etc. For example, Wang et al. have carried out the battery ageing tests under different DODs (10%-90%), temperatures (-30°C-60°C) and discharge rates (C/2-10C) [58]. To demonstrate the capacity loss, a power-law equation has been adopted with related to time, charge throughput and an Arrhenius correlation of temperature, which is expressed as :

$$Q_{loss} = B \cdot exp(-(\frac{E_a + m \cdot C_{rate}}{RT}))(Ah)^z \tag{2.12}$$

where B is a pre-exponential factor, E_a is the activation energy, m is the compensation factor for C-rate and Ah is the total charge throughput. This model can also be used to estimate the SOH of the battery [62] and as a battery life indicator to study the degradation issues in vehicle applications [105, 138, 166]. To further improve the accuracy, the parameter B in the above equation has been introduced as a function of SOC in [160], which extends the model to be SOC-related. Similarly, using self-organizing maps, Fernandez et al. have yielded another semi-empirical capacity fade model, in which both temperature and DOD are identified to be the most related aspects of degradation [75]. In order to study its ageing phenomenon under a realistic vehicle driving cycle, Cordoba-Arenas et al. add another parameter into this model, which is the ratio of charge depleting time to total driving time, $\frac{t_{CD}}{t_{CD}+t_{CS}}$ [113].

However, Baghdadi et al. pointed out that Ah-throughput could lead to mistakes in separating calendar ageing and cycle ageing [136]. Therefore, a total ageing expression with only one ageing rate based on Dakin's degradation approach was proposed and tested over three different temperatures (30°C, 45°C and 60°C) with three different SOC levels (30%, 65% and 100%) for calendar ageing and four ageing factors including current, charge throughput, temperature and DOD for cycle ageing. The ageing rate k is express as :

$$k = e^{(a(T)\times I)} \times e^{\frac{cSOC}{a}} \times e^{\frac{d}{a}} \times e^{\frac{-b}{aT}} \tag{2.13}$$

The capacity is calculated by :

$$Q = Q_0 \cdot exp^{(\pm kt^z)} \tag{2.14}$$

where the time-dependent parameter z is determined by fitting the logarithm of battery capacity fade according to (2.14) and it varies with different kinds of batteries. Similarly, Schmalstieg et al. have considered the calendar ageing and cycle ageing separately with different parameters [103]. The normalized capacity is expressed as :

$$Q = 1 - \alpha(T, V) \cdot t^z - \beta(SOC, I, V) \cdot \sqrt{Ah} \tag{2.15}$$

where α is the calendar ageing coefficient related to the temperature and voltage, while β is the cycle ageing coefficient related to SOC, current, I and voltage, V.

Although semi-empirical models complete the problem by adding physical interpretations of the ageing sources, the drawback is that they are highly dependent on the design of ageing experiments [136].

2.3.3.4/ RESIDUAL LIFETIME MODEL

Estimating the residual lifetime of the battery is another approach to indicate the degradation degree if the same conditions were maintained during its lifetime [172]. Some researchers have proposed to use *rainflow counting technique* to estimate the lifespan of the battery [145, 146]. The model is established based on cycle numbers and DOD. The battery degradation is accumulated by counting the swapping SOCs. For example, the effect of cycling is considered in [146] where the rainbow algorithm records the number of charge/discharge cycles with different values of DOD until the end of life. The battery lifetime (L) is calculated by :

$$L(year) = min\Big[L_{nom} \cdot \frac{1}{\sum_{j=1}^{9}(k \cdot 365/L_j)}\Big] \tag{2.16}$$

where L_{nom} is the nominal value of battery's cycle life with no degradation, k is the counted charge/discharge cycle number according to the rainbow algorithm and L_j is the predefined number of life cycles for nine different values of DOD.

Besides, an empirical lifetime prediction model have been proposed in [51] takes into consideration the influence of temperature, SOC as well as DOD, written as :

$$\frac{\Delta L_1}{L} = \int \frac{1}{8760 \cdot L(T + R \cdot \mid P(t) \mid)} dt + \frac{t_{max} - t_{ch}}{8760 \cdot L \cdot T} - \frac{t_{max}}{8760 \cdot L(P_{min} \cdot R + T)} \tag{2.17}$$

$$\frac{\Delta L_2}{L} = \frac{m \cdot SOC_{avg} - d}{CF_{max} \cdot 15 \cdot 8760} \tag{2.18}$$

$$\frac{\Delta L_3}{L} = \frac{E_{T,used} - E_{T,base}}{E_{TL}} \tag{2.19}$$

Equation (2.17) denotes the temperature-related degradation where P is the charging power. L denotes either the power lifetime or the capacity lifetime which is inversely proportional to the Arrhenius relationship ($r = A \cdot e^{-E/kT}$). The second term and the third term indicate the life expense of no charging plugging in and slow charging, respectively.

Equation (2.18) suggests the SOC-related degradation where CF_{max} is the maximum capacity fade at the end of life and m and d are tuned parameters. Equation (2.19) is the DOD-related degradation where E_{TL} is defined as the lifetime energy throughput, $E_{T,used}$ is the total change in the remaining energy throughput, and $E_{T,base}$ is the minimum energy throughput required to recharge the battery [51]. This modelling method has also been used in [150] as an analysis tool to demonstrate the effectiveness of the designed EMS.

2.3.3.5/ PARTIAL SYNTHESIS

Since batteries in HEVs usually have a limited life, health monitoring of battery is of considerable importance. Numerous studies have been done to evaluate the health state of the battery and to quantify the degradation in order to implement health management, as summarized in Table 2.3. Nevertheless, battery's ageing models on an experimental scale or a simulation scale are insufficient to describe the battery in actual use because the power profiles in automotive applications are completely random. Well-designed ageing tests are helpful in developing models and saving time and costs. However, they can hardly cover all operating conditions. Therefore, in order to develop an effective health-conscious EMS, modelling and estimating battery's ageing performance is one of the most crucial problems to solve. Using the same structure of this section, the next section gives an introduction to PEM fuel cell as well as its degradation modelling methods.

TABLE 2.3 – Summary of various battery degradation modelling methods

Model output	Modelling method	Advantages	Disadvantages
SEI film thickness model [41, 83, 168]	Electrochemical model	Accurate with theoretical interpretations ;	Complicated ; difficult to determine the parameters and their ranges ;
Internal resistance model [54, 173]	Electrochemical model/ Equivalent circuit model	Calculated by the instantaneous behaviour of the battery ;	Less accurate than the electrochemical models ;
Capacity degradation model [27, 50, 58, 62, 69, 75, 87, 103, 105, 113, 136, 138, 160, 166]	Empirical/ Semi-empirical model	Easy to implement ; online and close-loop ; able to perform prognostics ;	Need of large experimental dataset ; parameters need to be tuned each time with the changing of operating conditions ; heavy computational burden ;
Residual life model [51, 145, 146, 150]	Semi-empirical model	Easy to implement ; moderate complexity ;	Sensitive to operating conditions ; least accurate ;

2.4/ PEM FUEL CELL AND ITS DEGRADATION

2.4.1/ INTRODUCTION TO PEM FUEL CELL

2.4.1.1/ FUEL CELL OPERATION PRINCIPLE

Figure 2.11 shows the fuel cell operation principle, where the cell is fed with the fuel (hydrogen) and air at the anode and cathode respectively. Hydrogen gas, with the help

of a catalyst, separates into electrons and hydrogen ions. These ions flow to the cathode through the electrolyte while the electrons flow through an external circuit (electricity is generated). At the cathode, the hydrogen ions combine with oxygen (from the air) to form water.

The reactions involved at the electrodes are :

$$2H_2 \rightarrow 4H^+ + 4e^- \tag{2.20}$$

$$O_2 + 4H^+ + 4e^- \rightarrow 2H_2O \tag{2.21}$$

The general reaction equation of the system is :

$$2H_2 + O_2 \rightarrow 2H_2O + electricity + heat \tag{2.22}$$

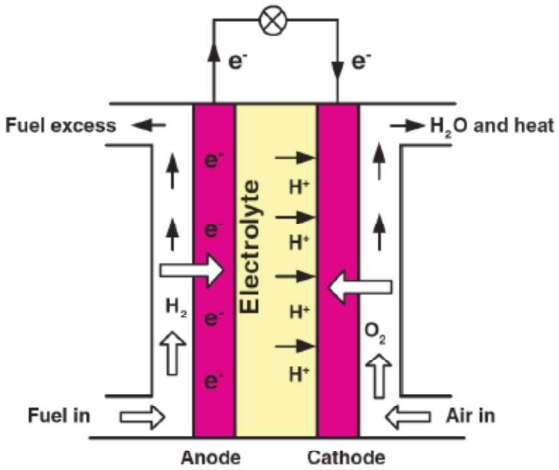

FIGURE 2.11 – Fuel cell operation principle

2.4.1.2/ STACK STRUCTURE

PEM fuel cell is widely used in vehicle applications since it has shown high power density, relatively lower operating temperature (60-80 °C) and low corrosion compared to other types of fuel cells [165]. According to Jouin et al., ”PEM fuel cell system” refers to a PEM fuel cell stack and all its auxiliaries (reactant storages, pumps, power electronics, thermal management system, etc.), while the stack is the part which converts the energy and is referred as the fuel cell [152]. The stack contains several cells and one cell contains different components, namely, electrodes, membrane, gas diffusion layer (GDL) and bipolar plate, as shown in Figure 2.12. All of these components may suffer from different processes of degradation during usage, which is going to be discussed in the next section.

The stack is an energy converter. It cannot work alone but requires auxiliaries to supply reactants, monitor the operating conditions and collect the electricity produced. The study of this multi-physics system (stack + auxiliaries) can be very complex because of the number of elements and their failures. Therefore, in this thesis, we suppose that this study is limited to the stack and its subcomponents. The degradation mechanisms of different components are described one by one in the next section.

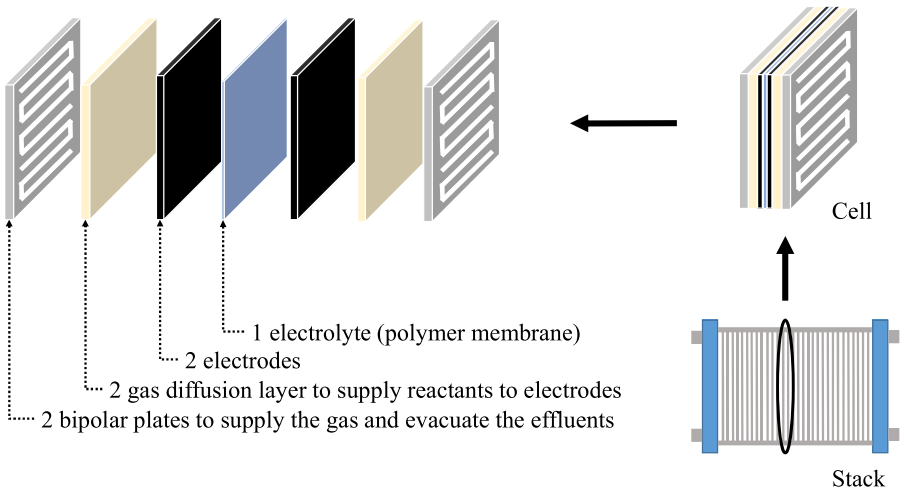

FIGURE 2.12 – Components in a PEM fuel cell stack

2.4.2/ DEGRADATION MECHANISMS

2.4.2.1/ BIPOLAR PLATES

The bipolar plates are the skeleton of the stack. They isolate the individual cells, conduct the current between the cells, help in water and thermal managements but also provide flow fields for incoming reactants and outgoing products. Three degradation mechanisms intervene in bipolar plates : (1) corrosion leading to the production of multivalent cations that impact seriously the durability of the membrane and the catalyst layers ; (2) appearance of a resistive surface layer on the plates leading to a higher ohmic resistance ; and (3) fractures or deformation of the plates accentuated by operational factors such as thermal cycles, bad temperature distributions or non-uniform currents [152].

2.4.2.2/ GAS DIFFUSION LAYERS (GDL)

The GDL, with its porous nature, plays an essential role for assisting the reactions of hydrogen oxidation and oxygen reduction in the catalyst layers by allowing the reactant to diffuse from the flow fields to the active sites. It facilitates water management in the catalyst layer and the membrane by ensuring the diffusion of vapour water mixed with the reactants and by evacuating liquid water out of the stack. The GDLs are electrically conductive to ensure the electrons transfer from the catalyst layer to the bipolar plates. Because of the major difficulty of separating the degradation of the GDL from that of the membrane-electrodes assembly, most of the ageing studies on GDL are ex-situ. Three main changes can be observed when the GDL degrades : (1) behaviour modifications regarding water due to the loss of hydrophobicity and changing of the carbon surface ; (2) changes in the GDL structure due to the carbon corrosion and the mechanical constraints ; and (3) changes in the electrical and thermal resistance combined with a loss of porosity [152].

2.4.2.3/ ELECTRODES

The electrodes are composed of two layers : a catalyst layer and a support for that layer, the carbon support. A conventional catalyst layer is made with platinum (Pt) nanoparticles supported by a surface of black carbon in close contact with a controlled quantity of ionomer (membrane material). The carbon support allows the nanoparticles to have a high dispersion (2-3 nm) and provides a porous structure electronically conductive. Two main families of phenomena are responsible for the loss of performance with the electrodes : the catalyst layer degradation and the carbon support degradation. Together these phenomena lead to a loss of active area of the electrode and its consequent loss of electrochemical activity. Among them, we can find : (1) the dissolution and diffusion of Pt through the ionomer, re-deposit on other particles forming bigger particles or diffusion through the membrane to create a band ; (2) the carbon corrosion into dioxide and consequent disintegration of the catalytic layer leading to Pt agglomeration and to the formation of oxides on the carbon surface ; (3) the generation of reactive species as the hydrogen peroxide (H_2O_2), radicals of hydroperoxyl ($\bullet OOH$) and radicals $\bullet OH$ causing the degradation of the membrane ; and (4) reversible and irreversible adsorption of contaminants from air, reactants or products from other components degradation. It should be noticed that the impact of the degradation is not the same for both electrodes (anode at the hydrogen input or cathode at the oxygen side). The anode remains almost unaffected by the dissolution, oxidation and agglomeration of Pt, whatever the conditions. By contrast, the cathode is very impacted and this results in a loss of active area in time. It is aggravated by potential and temperature cycles [152].

2.4.2.4/ MEMBRANE

The membrane has several roles in the cell. First, it allows the protons transport from the anode to the cathode thanks to its hydrophilic and hydrophobic domains. Then, it acts as a separation between the fuel and the air. A good membrane must have excellent proton conductivity, thermal and chemical stability, good mechanical resistance, flexibility, low permeability to gases and low water drag. To consider the membrane's degradation, [63] proposes three categories : (1) Chemical degradation : direct attacks of the polymer by radical species leading to the decomposition of the membrane ; (2) Mechanical degradation : membrane fracture caused by cycled constrains or fatigue imposed by varying temperature or humidity ; (3) Shorting : an electronic current goes through the membrane because of an over-compression of the cell or topographical irregularities of the neighbouring components leading to local over-compression and creep. In addition, the membrane also suffers from thermal degradation characterized by the decrease of proton conductivity at high temperatures, and gas crossover, which will lead rapidly to the death of the stack due to a combustion reaction when a great quantity of hydrogen crosses and meets oxygen [152].

2.4.2.5/ SEALING GASKETS

The assembly of the membrane and electrodes includes sealing components to prevent hydrogen and air to mix but also to leak out of the stack. All the components should be perfectly aligned to maintain the appropriate closing pressure. This is important to reduce the contact resistances but also to avoid an over-compression of the GDLs.

To summarize, the degradation mechanisms on each component are listed in Table 2.4.

2.4.3/ PEM FUEL CELL DEGRADATION MODELLING AND ESTIMATION

As we know, degradation happening on each area of the fuel cell stack cannot reach the same degree, for example, cells near the edges tend to degrade faster [151]. Besides, if we consider degradation on the component level, the degradation between component and auxiliaries cannot be covered and the parameters are hard to obtain. Therefore, fuel cell degradation is generally modelled on the stack level. Various modelling methods have existed in the literature based on its ageing mechanisms.

Similar to the modelling of battery's degradation, there are data-driven methods and physical model-based methods to estimate the degradation of PEM fuel cell. Data-driven methods depend on the features extracted from the data but once the operating condition changes, the parameters need to be adjusted from time to time [149, 176]. Physical models consider the internal reactions of fuel cell's performance degradation, such as the decline of the carbon support, the surface area loss of Pt, etc. However, the degradation process in vehicle applications is much more complex and hard to be expressed by a theoretical model and the identification of the inner parameters is difficult to realize [53, 132]. The following part of this section reviews several modelling methods that have been applied in vehicle applications. The purpose is to find the most effective and implementable methods that could be used to develop an EMS to improve the health management of the fuel cell.

2.4.3.1/ STACK VOLTAGE DEGRADATION MODEL

The stack voltage drop of the fuel cell is the most principle change so that the output voltage is widely used to demonstrate the degradation phenomenon [167]. Pei et al. have proposed to use the cycle information to calculate the stack voltage degradation, expressed as [30] :

$$V_{stack} = V_{rate} \cdot D_{fc} \tag{2.23}$$

$$D_{fc} = k_p(P_1 n_1 + P_2 n_2 + P_3 t_1 + P_4 t_2) \tag{2.24}$$

where D_{fc} is the degradation rate, k_p is the accelerating coefficient, P_1-P_4 are the degradation rates resulting from load change, start/stop, idling and high power demand, respectively, and n_1, n_2, t_1, t_2 denotes the times of load change, the times of start/stop switches, the time for idling and the time of high power demand, respectively. This model tries to contain the driving conditions in the modelling of fuel cell degradation process. For example, on the electrodes, low current may cause degradation in the catalyst layer while the frequent transition of start-up and shut-down and fuel starvation may cause carbon corrosion on the carbon support layer. Chen et al. and Xu et al. have used this model with the real running data of a PEM fuel cell vehicle to analyse the fuel cell's degradation under different driving conditions [107, 110]. However, once tuning of the parameters of this model only works for a specific driving cycle so that it is hardly applicable to general cases.

TABLE 2.4 – Major failure modes of different components in the PEM fuel cell (Source [33, 152])

Component	Functions	Failure mode	Causes
Membrane	Allow the protons transport from the anode to the cathode ; separating the fuel from the air ;	Mechanical degradation	Mechanical stress due to non-uniform press pressure ; inadequate humidification or penetration of the catalyst and seal material traces ;
		Thermal degradation	Thermal stress ; thermal cycles ;
		Chemical/ electrochemical degradation	Contamination ; radical attack ;
Electrodes	An electrical conductor used to make contact with the nonmetallic part where electrons leave and enter ; the carbon support allows the nanoparticles to have a high dispersion and provides a porous structure electronically conductive ;	Loss of activation	Sintering or dealloying of electrocatalyst ;
		Conductivity loss	Corrosion of electrocatalyst support ;
		Decrease in mass transport rate of reactants	Mechanical stress ;
		Loss of reformate tolerance	Contamination ;
		Decrease in water management ability	Change in hydrophobicity of materials due to Nafion or PTFE dissolution ;
GDL	Allow the reactant to diffuse from the flow fields to the active sites ;	Decrease in GDL structure	Degradation of backing material ; carbon corrosion ;
		Decrease in water management ability	Mechanical stress ; change in the hydrophobicity of materials ;
		Conductivity loss	Corrosion ;
Bipolar plate	Isolate cells and conduct current between cells ;	Conductivity loss	Corrosion ; appearance of a resistive surface layer ;
		Fracture/ deformation	Mechanical stress ; thermal cycles ;
Sealing gasket	Separate the hydrogen from the air ; avoid leaking out of the gas ;	Mechanical failure	Corrosion ; mechanical stress ;

Fletcher et al. have specified the influence of demanded power on degradation causes and calculated the degradation rate which penalized stack voltage according to the change of power demand [143]. For example, following equations have represented the proportion of fuel cell's performance drop :

$$D_1 = \begin{cases} \frac{1}{n_{max}} & \text{,if } P_{FC,t+1} > 0 \bigwedge P_{FC,t} < 0 \\ 0 & \text{,otherwise} \end{cases} \tag{2.25}$$

$$D_2 = \begin{cases} \frac{1}{t_{max}} \times \frac{P_{FC} - 0.8P_{max}}{0.2P_{max}} & \text{,if } P_{FC} > 80\%P_{max} \\ 0 & \text{,otherwise} \end{cases} \tag{2.26}$$

where n_{max} denotes the maximum start/stop switches estimated by the manufacturer, P_{max} denotes the rated power and t_{max} is the maximum lifetime of the fuel cell under P_{max}. D_1 have penalized stack voltage whenever the demanded power drops below $0W$, which represents the degradation causing by non-uniform fuel distribution due to fuel cell's start-up/shut-down cycling. Another penalty D_2 happens when the demanded power is over 80% of the rated value and is assumed to be linear. This degradation rate represents the reactant starvation and thermal degradation of membrane causing by successive high power demand [142].

Besides, Ettihir et al. have proposed to use a semi-empirical model to present the degradation of the stack voltage by measuring both the current and the voltage of the fuel cell [14, 141]. The model is represented as :

$$V_{stack} = V_0 - b\log(i_{fc}) - ri_{fc} + \alpha i_{fc}^{\sigma}\log(1 - \beta i_{fc}) \tag{2.27}$$

where V_0 denotes the open circuit voltage, b denotes the Tafel slope, r denotes the ohmic resistance and β denotes the inverse of the limiting current. α is a parameter related to the diffusion mechanism while σ is related to the water flooding phenomena. Since the identified model is a semi-empirical one, a trade-off is made between its physical meaning and calculation cost.

2.4.3.2/ IMPEDANCE ESTIMATION BASED ON EIS

Electrochemical impedance spectrometry (EIS) is a powerful tool to characterize the phenomenon inside the fuel cell and evaluate the fuel cell degradation [85]. EIS is carried out by adding a small sinusoidal perturbation on the nominal current and the impedance is calculated as a ratio between the response and the perturbation. Compared to polarization, the total energy and experimental duration of EIS measurement are significantly reduced, which makes it a promising tool for estimating the performance of the fuel cell without invasion [89]. Different operation conditions or different degrees of system ageing will lead to the change of spectrum shape. To demonstrate that change, Nyquist plots are widely used to indicate the degradation by the derivation of the arcs. Using EIS together with Nyquist plots has made it possible to characterize PEM fuel cell and to study its static and dynamic behaviours regarding performance losses. Figure 2.13 gives an example of a group of impedance plots, which are recorded during the ageing tests on a fuel cell stack. Using the extracted feature from the EIS plots, one can estimate the operation time of the fuel cell stack, which could be regarded as the indicator of its health state [53].

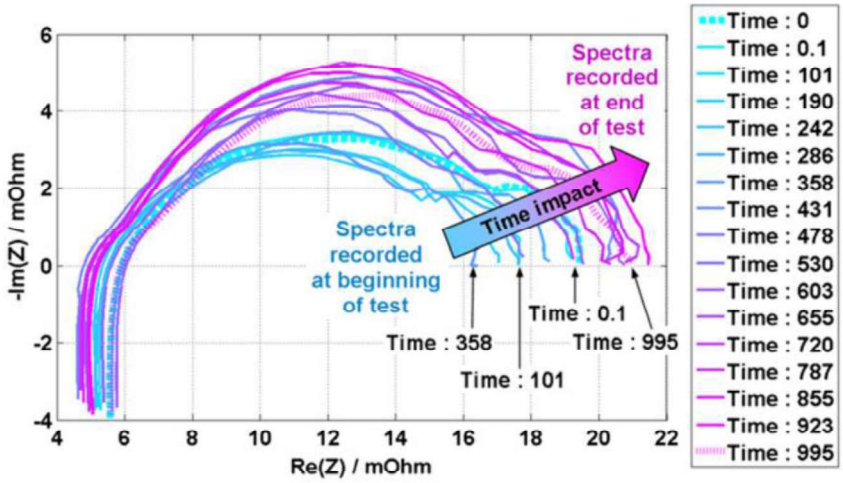

FIGURE 2.13 – Evolution of the impedance spectra [53]

Cadet et al. [89] have proposed the guidelines of using EIS as a diagnostic tool regarding flooding and drying faults of fuel cells and to analyse experimental data with Bayesian networks. Moreover, using EIS with Nyquist evolution plots, Hissel et al. have selected two values (the difference between polarization resistance and internal resistance of the considered fuel cell stack and the maximal absolute phase value of the Nyquist plot) from the Nyquist plots to indicate the fuel cell degradation [23].

2.4.3.3/ REMAINING USEFUL LIFE ESTIMATION

Unlike battery capacity, fuel cell health in prognostics field is usually defined by its voltage or power performance, which means it suffers from more dynamics. Therefore, various efforts have been made to estimate the RULs of the fuel cell through state estimation and prognostics approaches, instead of estimating the voltage directly. For example, Xian et al. have proposed to use an unscented Kalman filter to estimate the degradation rate of the electrochemical surface area and the RUL of the stack [70]. Besides, when considering characterization disturbances and voltage recovery, Jouin et al. have used a particle filter framework to estimate the fuel cell's power degradation and the RULs based on a logarithmic expression [97]. Bressel et al. have proposed to use a degradation factor to represent the degradation phenomenon in the fuel cell voltage. Thanks to this degradation factor, fuel cell degradation could be estimated and tracked whatever the operation conditions are [137]. Furthermore, echo-state networks [82] and adaptive neuro fuzzy inference system (ANFIS) [104] are another two data-driven prognostics methods that have been used to estimate the health state of the fuel cell. However, these data-driven methods have not yet been combined to the energy management of hybrid vehicles due to the large calculation cost and low generality for different road conditions.

Another RUL estimation method proposed in [25] has used a surrogate model to present the Pt catalyst diffusion degradation rate. Response surface methodology (RSM) has been used to develop such a surrogate life model in a statistical framework. With the analysis through Pareto plots and scatter plot matrix, the upper potential limit of the fuel cell is found to be the most controllable variable to the Pt catalyst diffusion, following by cycle numbers. This work has indicated that the durability of the fuel cell system can be

improved by operating at a relatively low potential with limits number of start/stop cycles.

2.4.3.4/ PARTIAL SYNTHESIS

The degradation of the PEM fuel cell in HEVs is inevitable which has a significant influence on the durability of the system. The above-mentioned methods of degradation modelling, together with their advantages and disadvantages, are compared in Table 2.5. However, in the literature, when it comes to design a health-conscious EMS, the degradation of the fuel cell is usually considered using a rough model which is not accurate and cannot be generalized to all driving conditions [107, 127, 149]. This is mainly due to the complex structures and reactions of the fuel cell and the difficulties in the modelling. Although some prognostics works have been done to evaluate the health state of the fuel cell but post-prognostics decisions, or in other words, the part of the control configuration is lacking. Therefore, it gives us the possibility to design a health-conscious EMS based on state estimation and prognostics, which could not only solve the modelling problems but also realize the automatically corrective control.

TABLE 2.5 – Summary of various fuel cell degradation modelling methods

Model output	Modelling method	Advantages	Disadvantages
Stack voltage degradation model [30, 107, 110, 142, 143]	Model-based/ hybrid method	Easy to implement ; disclosure of the influences of related factors the health state ;	Less accurate ; strongly dependent on experiment data (low generality) ;
EIS impedance estimation [53, 85, 89]	Data-driven/ model-based method	Non-invasive ; easy to implement ; good performance in diagnostics field ;	Incapable of directly solving SOH estimation issues ;
RUL estimation [25, 70, 82, 97, 104, 137]	Data-driven/ Hybrid method	Robust to uncertainties and operation conditions ; able to perform prognostics ;	Large experimental datasets ;

2.5/ SYNTHESIS

This chapter has firstly justified that fuel cell hybridization is necessary for automotive applications to benefit from the high power density and braking energy recovery ability of battery-like energy storage system. Then, lithium-ion battery and PEM fuel cell have been discussed separately towards the degradation and durability issues based on the hypothesis that the interaction between them in a hybrid system is neglectable. Operation principles and ageing mechanisms of the lithium-ion battery and PEM fuel cell are discussed in Section 2.3 and Section 2.4. Then various degradation modelling and estimation methods are reviewed based on the literature. They are summarized according to the outputs of the model.

Lithium-ion battery degradation model includes :

— SEI film thickness model
— Internal resistance model

— Capacity degradation model
— Residual lifetime model

while PEM fuel cell degradation modelling method includes :

— Stack voltage degradation model
— Impedance estimation based on EIS
— Remaining useful life estimation

Advantages and disadvantages of each model are analyzed and it can be seen that models built based on electrochemical characteristics are complicated and highly dependent on the type of batteries and fuel cells. They are not suitable to be used in developing health-conscious EMSs. State estimation is a promising way in diagnostics and prognostics field, which is easy to implement without complicated models. There are some prognostics works that have been done to evaluate the health states of the power sources and achieved good results both for the battery and the fuel cell. This gives a chance for the researchers to consider combining the prognostics results when developing EMSs. From a PHM point of view, post-prognostics decisions, i.e., the management aspect of PHM is about to draw attention. Following that, various activities, ranging from data collection through the recommendation of specific control actions, must be carried out.

In the next chapter, the prognostics of both lithium-ion batteries and PEM fuel cells in the hybrid system are studied. State estimation and prognostics based on particle filtering algorithms are going to be presented based on various datasets. Results are analyzed to verify the possibility of developing a health-conscious EMS based on prognostics.

II

CONTRIBUTION

3

HYBRID SYSTEM PROGNOSTICS BASED ON PARTICLE FILTERING

3.1/ INTRODUCTION

PHM has been a recent dynamic discipline to master the lifespan of industrial systems. To improve the durability of fuel cell hybrid electric vehicles, PHM has been proposed to be combined with EMS in hybrid systems in order to complete the decision-making process. Before developing the EMS, a prognostics phase must be achieved, which can enable predictive maintenance by predicting the future RUL based on the information obtained in the first four layers of PHM. Different from the diagnostics layer, which deals with fault detection, isolation and identification when the fault has already occurred, prognostics must be able to estimate how soon the fault will occur. Based on this knowledge, sequence actions could be taken to save the system, or al least slow down the failure process.

Based on the degradation knowledge described in the last chapter for the hybrid system, this chapter introduces a particle filtering based prognostics method to estimate and predict future health state for fuel cell and battery. First, some generalities of prognostics are explained. Implementing prognostics on an HEV is different from other applications because the vehicle operation conditions are random and dynamic. Therefore, it is of great significance to adapt the essential prognostics requirements to this application. Although no one knows the real failure time of an operating system, offline evaluation metrics are necessary for the design phase of an algorithm, which are used to assess the prognostics results. Then, to estimate the RULs, particle filtering-based approach is chosen as the methodology in our context of prognostics. Particle filtering is a powerful recursive state estimation approach to solve nonlinear and non-Gaussian problems by allocating weights to the particles. It could be adapted for prognostics purpose by propagating the particles to the future unknown states even without measurements and it is widely used in the prognostics applications for predicting the health state of batteries and fuel cells.

To verify the effectiveness of the prognostics method in vehicle applications, historical datasets from different degradation experiments are chosen to imitate the dynamic operation of batteries and fuel cells in hybrid systems and an assumption is made that the interaction between them is neglectable. Particle filtering is implemented on these datasets and adapted with empirical models for the degradation path estimation and prediction. Besides, the influence of data quality and volume are believed to be interesting aspects for online prognostics applications. They are investigated by changing the prognostics horizon and raw data sampling time in this study.

The contents of this chapter are arranged as follows : Section 3.2 introduces the generalities of prognostics including prognostics requirements, offline performance evaluation metrics and a short review of various prognostics methods. A particle filtering framework adapted for prognostics purposed is presented in Section 3.3 and the degradation data of the fuel cell and the battery are prepared in Section 3.4, which is used to represent the dynamic operations of the hybrid electric vehicle. Prognostics results by particle filtering method are demonstrated and evaluated in Section 3.5 and a multi-time scale analysis is presented at the last of this chapter.

3.2/ GENERALITIES ON PROGNOSTICS

3.2.1/ REQUIREMENTS ON PROGNOSTICS

3.2.1.1/ ADEQUATE PROGNOSTICS HORIZON

Prognostics horizon quantifies how much in advance an algorithm can predict before a failure occurs. As shown in Figure 3.1, the prognostics horizon is calculated by the difference between the time index t_λ when the predictions first meet the specified performance criteria (within the acceptable error margins) and the time index for EOL :

$$Prognostics\ horizon = EOL - t_\lambda \tag{3.1}$$

As discussed earlier, the prognostics approaches developed here are intended for decision-making related to the re-planning of power distribution of the hybrid system. As a system approaches a failure threshold, the prognostic horizon to take a corrective action becomes shorter, and consequently, the accuracy of predictions becomes more critical for decision-making. Therefore, a longer prognostics horizon is preferred as more time is then available for preventive or corrective actions. But how to define this "longer prognostics horizon"? It should be defined that how much time we need to predict the RUL and perform the following management actions. According to [151], the planning of the operations, the delay to obtain spare parts and the maintenance realization are taken into consideration. For example, it gives a total duration between 12 and 29 days, which gives the prognostics horizon with a duration between 300 and 700 hours to be considered as a good performance for the fuel cell system.

3.2.1.2/ ACCEPTABLE ERROR MARGINS

The error margin of a width of 2α shrinks with the prediction time index t_λ, which creates an accuracy zone covering the true residual life RUL^*, as shown in Figure 3.1. The upper bound of the accuracy zone α^+ is calculated by

$$\alpha^+ = RUL^*_\lambda * (1 + \alpha) \tag{3.2}$$

while the lower bound of the accuracy zone α^- is calculated by

$$\alpha^- = RUL^*_\lambda * (1 - \alpha) \tag{3.3}$$

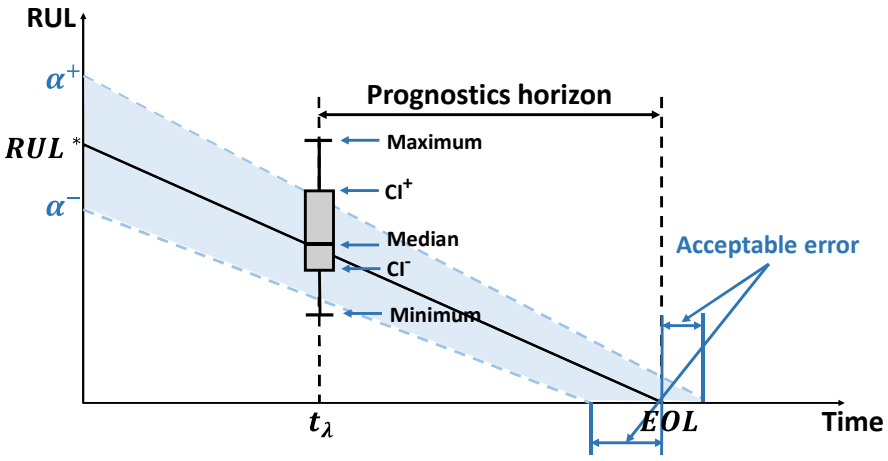

FIGURE 3.1 – Time vs. RUL plot with the accuracy zone

where RUL^*_λ is the median value of predicted RULs at the prediction time t_λ.

Regarding the RUL estimates ($\hat{RUL}$), there are two cases : (1) the estimate is smaller than the actual RUL ($\hat{RUL} < RUL^*$), it is an early prediction, or (2) the estimate is greater ($\hat{RUL} > RUL^*$), it is a late prediction. The acceptable error is the same in each case. Indeed, by validating a prediction with a consequent delay, one may risk a complete shutdown of its power source. Therefore, one may propose to allow a maximum error of 8%. The case of the early prediction allows more flexibility. It is proposed to set the early prediction limit at 16% of the actual RUL [151].

3.2.1.3/ ALLOWABLE UNCERTAINTY

The uncertainties are represented by the probability density function (PDF). The estimation uncertainty is represented by a confidence interval (CI) and the median value of the PDF is commonly chosen to represent the estimated point values in PHM. As shown in Figure 3.1, the upper bound and lower bound of the boxplot represent the upper and lower confidence interval, respectively. According to Jouin et al. [151], to ensure that the prognostics results are reliable, the uncertainty on the RUL estimates should be constrained in a 5% interval. Nevertheless, a confidence interval of 10% allows asserting that the predictions are quite satisfying but can be improved.

3.2.2/ OFFLINE PROGNOSTICS PERFORMANCE EVALUATION

Prognostics performance evaluation is a tricky issue since it is an acausal problem, which requires the inputs from what is expected to happen in the future, while in real cases no one knows the real end of life of the system [36]. However, to help the development of the prognostics algorithm, it is important to propose a series of evaluation metrics by providing a way to measure the performance and obtaining feedback. Once these metrics are fined tuned, one can extend these concepts to the online evaluation.

3.2.2.1/ PROGNOSTICS HORIZON

Prognostics horizon (PH) is used to evaluate whether a prognostics algorithm is good to leave enough duration for the future corresponding operation based on the prognostics results. Figure 3.2 is an illustration of the prognostics horizon while comparing two algorithms based on point estimates [43]. The prognostics horizon for an algorithm is declared as soon as the corresponding prediction enters the accuracy zone. As is evident from the illustration, the second algorithm has a longer prognostics horizon (PH^2). This metric indicates whether the prognostics results are within specified limits around the actual RULs so that the predictions are considered trustworthy. Therefore, when comparing algorithms, an algorithm with a longer prediction horizon would be preferred.

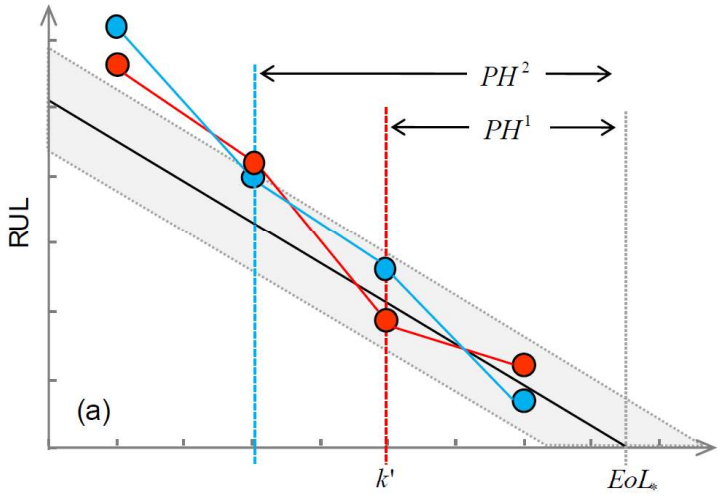

FIGURE 3.2 – Illustration of prognostics horizon while comparing two algorithms based on point estimates [43]

3.2.2.2/ $\alpha - \lambda$ ACCURACY

This metric quantifies prediction quality by determining whether the prediction falls within specified limits at particular times. It further tightens the desired accuracy levels using a shrinking cone of the desired accuracy as EOL approaches. $\alpha - \lambda$ accuracy is defined as a binary metric that evaluates whether the prediction accuracy at specific time instance t_λ falls within specified α– bounds ($[\alpha^+, \alpha^-]$) :

$$\alpha - \lambda\ accuracy_\lambda = \begin{cases} 1, & if\ \alpha^+ \leq \hat{RUL} \leq \alpha^- \\ 0, & otherwise \end{cases} \tag{3.4}$$

where α^+ and α^- are calculated by (3.2) and (3.3).

3.2.2.3/ RELATIVE ACCURACY

Relative accuracy, denoted as $ReAcc$ is defined as a measure of error in RUL prediction relative to the actual RUL at a specific time index t_λ :

$$ReAcc_\lambda = 1 - \frac{|RUL^*_\lambda - \hat{RUL}_\lambda|}{RUL^*_\lambda} \tag{3.5}$$

Different to the $\alpha - \lambda$ accuracy indicating only the estimates falling into the accuracy zone or not, the relative accuracy indicates quantitatively the accuracy level. A large value of relative accuracy represents better accuracy.

3.2.2.4/ PRECISION

To indicate the precision of the RUL estimates, a precision index is defined based on the relative width of the prediction interval, written as :

$$Precision_\lambda = \frac{\hat{RUL}^{CI+}_\lambda - \hat{RUL}^{CI-}_\lambda}{RUL^*_\lambda} \tag{3.6}$$

where $\hat{RUL}^{CI+}_\lambda$ and $\hat{RUL}^{CI-}_\lambda$ are the upper and lower bounds of the confidence interval of the estimated RULs distribution. Obviously, smaller values of $Precision_\lambda$ indicate more precise predictions.

3.2.3/ PROGNOSTICS METHODS

Different approaches to implement the prognostic process can be distinguished in the literature. In most of the recent works, the prognostic approaches are commonly categorized into three major types : 1) Model-based methods ; 2) Data-driven methods and 3) Hybrid methods [109, 174].

3.2.3.1/ MODEL-BASED METHOD

Model-based prognostics method is to develop mathematical equations that include many physical parameters to predict the physics governing failures. Many researchers have used precise electrochemical models to predict the power sources' health states [20, 26, 41, 85]. An accurate mathematical model can benefit the prognostics process, where the difference between the output from a mathematical model and the real output of the system can be used to find the anomalies, malfunctions, disturbances, etc [174]. A diagram of a typical model-based method is shown in Figure 3.3.

Lechartier et al. have proposed a PEM fuel cell model for prognostics purpose, which composed of a static part and a dynamic part. The static part is developed based on the Butler-Volmer law that takes into account the activation loss at the cathode and the anode. The parameters in the static model can be identified by fitting it to the polarization curves, while the dynamic model is developed according to the impedance of an equivalent circuit model and its parameters can be identified by fitting it to the EIS spectrum [119]. This approach is therefore dedicated to the specific applications that were developed and rely on the assumption that the behaviour of the system can be described analytically while remaining accurate. However, the lithium-ion batteries, as well as the PEM fuel cells are dynamic, time-varying and nonlinear electrochemical systems, the internal reactions and

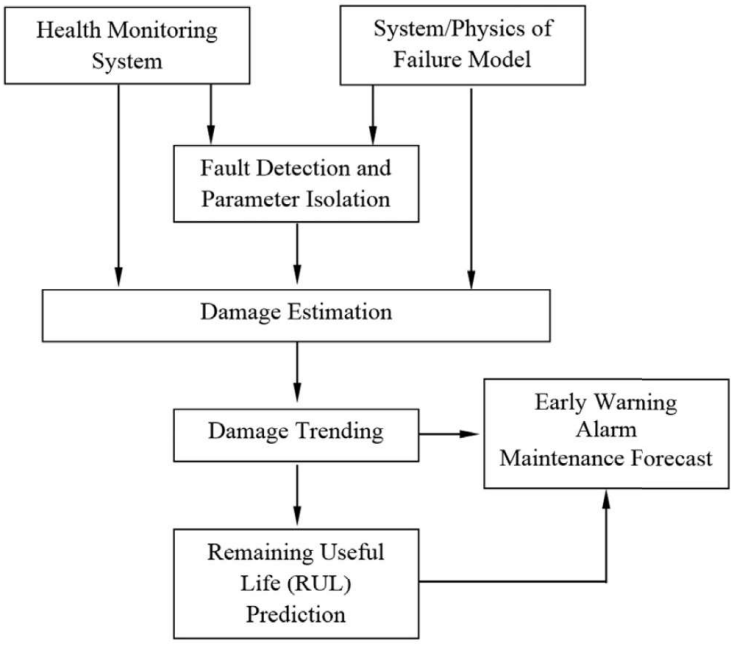

FIGURE 3.3 – Typical process of model-based prognostics method [174]

failure modes are very complicated, which may change under different operation conditions. Therefore, physical models or mathematical models are difficult to be built to precisely describe the mechanism of the system degradation and failure modes [122]. Even if the physical model is available, under most situations, for a real system, it is difficult (even impossible) to obtain the dynamic model in the analytic form to integrate the degradation phenomenon. Besides, the model built for one application cannot be transferred to another application.

3.2.3.2/ DATA-DRIVEN METHOD

Data-driven models rely only on previously observed data to predict the projection of a system's state or to match similar patterns in the history to infer the RULs [99]. Using data-driven prognostics methods, the system is considered as a black box. No precise physical model is required. Different from model-based methods, data-driven methods can reflect the inherent relationships by learning the historical and monitoring data and then predict the future trend. Thus, this approach gradually becomes the main methodology for battery and fuel cell prognostics due to the easy-to-use and flexible modelling properties [122]. Methods used for battery prognostics mainly include support vector machine [84], neural network [47], gaussian process [27], etc. For fuel cell prognostics, echo-state networks [82] and adaptive neuro fuzzy inference system (ANFIS) [104] have been used to predict fuel cell's RULs. Besides, Javed et al. have used a constraint-based summation wavelet-extreme learning machine to learn the system behaviour directly from the data and to train a single layer feedforward neural network [117]. The structure of this data-driven method is shown in Figure 3.4. One of the limitations of data-driven method lies in the confidence level of the training data. Data-driven approaches highly depend on historical data to determine correlations, establish patterns and evaluate data trends leading to failure [161, 174]. Besides, results of data-driven methods are not easy to explain since

there is no physical meaning, therefore, in prognostics applications, there will be some challenges in determining thresholds and solving the over-fitting issues [99].

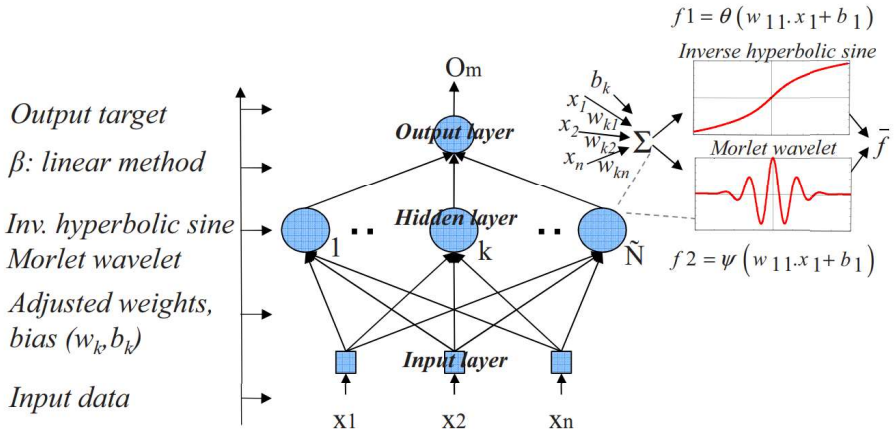

FIGURE 3.4 – Summation wavelet-extreme learning machine algorithm [117]

3.2.3.3/ HYBRID METHOD

The hybrid methods are the combination of the two previous types. This method involves the knowledge of a system's failure mechanisms to build a mathematical description of the system's degradation process to estimate the RULs, while the parameters changing over time are estimated by learning approaches. For example, the lithium-ion battery is commonly modelled by equivalent circuit model, while the prognostics of lithium-ion battery is executed by solving state space models through some filtering algorithms : extend Kalman filter, unscented Kalman filter, particle filter, etc [48,80,100,109,114,134]. In [48], the data-driven part has been accomplished by a Gaussian process regression using an exponential degradation model with two parameters estimated online. Then, RULs are predicted by an extended Kalman filter and a particle filter, while the particle filter method has shown the best performance. Besides, unscented Kalman filter and particle filter are also found to be used to perform prognostics on PEM fuel cells in [70,135,153]. A prognostics process based on particle filter is shown in Figure 3.5. The hybrid prognostics method based on particle filter uses a set of available measurements to learn the state or the behaviour of the system and then predicts its future state of health and remaining useful life. The learning could be model-based, data-driven or a combination of both because both physical models and data can be incorporated into the framework with a state vector model [155]. The aim of the hybrid method is to overcome the limitations of model-based and data-driven methods to estimate the RULs. However, the drawbacks of both methods are also accumulated : it is necessary to have both a precise model description and a sufficient database. Thus, the costs of implementation are getting heavier.

Indeed, the ageing processes of the lithium-ion battery and PEM fuel cell are nonlinear and non-Gaussian, which are preferably represented by state space models. In this study, the particle filter is then chosen as a prognostics tool to predict the RULs of the power sources as the recursive Bayesian algorithm are well suited to solve the real-time estimation and the Monte-Carlo method could generate a probabilistic output which is conve-

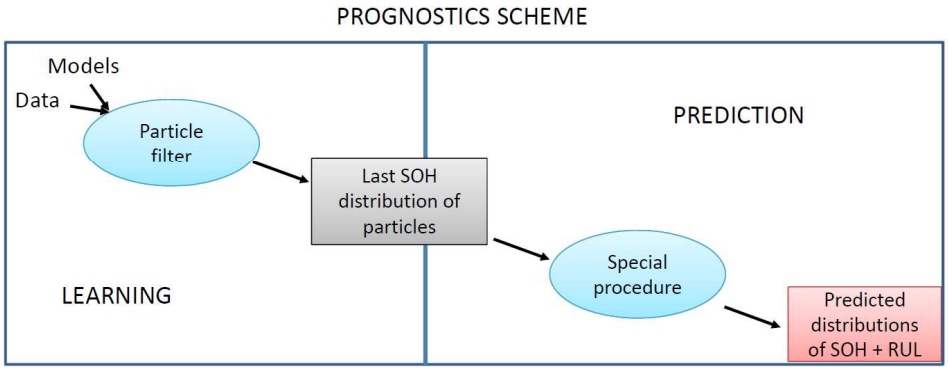

FIGURE 3.5 – Particle filtering-based prognostics method [155]

nient to represent the uncertainty of the outputs. The prognostics procedure through particle filtering is going to be described in details and demonstrated by historical datasets.

3.3/ PROGNOSTICS IN A PARTICLE FILTERING FRAMEWORK

3.3.1/ NONLINEAR BAYESIAN TRACKING

Particle filtering is a recursive state estimation technique for nonlinear and non-Gaussian problems. As unknown states from noisy observations are going to be estimated with available prior knowledge, nonlinear Bayesian tracking approach is described before looking into the depth of the particle filtering prognostics.

3.3.1.1/ MODEL FORMULATION AND SELECTION

The Bayesian tracking approach provides a framework which can estimate the parameters or the state of a nonlinear stochastic system using noisy measurements as observations. At least two models are required for describing the system : first, a model describing the evolution of the state with time (the system model) and, second, a model relating the noisy measurements to the state (the measurement model) [13].

The state model describes the transition of the states, noted as $\mathbf{x}_k, \mathbf{x}_k \in N$. The states are modelled by a Markov process with a initial distribution $p(\mathbf{x}_0)$ and a probabilistic model $p(\mathbf{x}_k|\mathbf{x}_{k-1})$. It has to be noticed that a Markov process is a stochastic process with the Markov property, i.e. the conditional probability distribution of future states only depends from the current state. The commonly used discrete representation of the state model is written as :

$$\mathbf{x}_k = f(\mathbf{x}_{k-1}, \mathbf{u}_k, \mathbf{w}_k) \leftrightarrow p(\mathbf{x}_k|\mathbf{x}_{k-1}) \tag{3.7}$$

where $\mathbf{u}_k$ is the command input of the system and $\mathbf{w}_k$ is process white noise, non-necessarily Gaussian.

The measurement model relates the noisy measurements to the states. The sequence of measurement is written as $\mathbf{z}_k, \mathbf{z}_k \in N$. $\mathbf{z}_k$ is assumed to be conditionally independent to

the process and of marginal distribution $p(\mathbf{z}_k|\mathbf{x}_k)$ [155]. To be used in a Bayesian tracking problem, the measurement model is written as :

$$\mathbf{z}_k = h(\mathbf{x}_{k-1}, \mathbf{v}_k) \leftrightarrow p(\mathbf{z}_k|\mathbf{x}_k) \tag{3.8}$$

where $\mathbf{v}_k$ is the measurement white noise, non-necessarily Gaussian.

According to the literature, the degradation of a lithium-ion battery is characterized by the decrease of the capacity over repeated charge/discharge cycles. As the battery ages, the maximum available capacity will decrease. Based on the regression analysis of the experimental data, several models are usually deployed to approximate battery's capacity degradation path. Goebel et al. have used a sum of two exponential functions to model the increase of internal impedance due to solid electrolyte interface thickening with time [27]. As battery capacity degradation is closely related to the internal impedance increase, potential models for capacity degradation can also be exponential models. Following up Goebel et al.'s work, He et al. have experimentally demonstrated that the sum of two exponential functions can well describe the capacity degradation trend of many different batteries, which is frequently used in the studies of prognostics on batteries [50, 80, 134]. It is composed of a sum of exponential functions of discharge cycles, which can well describe the capacity fade trend of different batteries :

$$Q(k) = \alpha_1 \cdot exp(\alpha_2 \cdot k) + \alpha_3 \cdot exp(\alpha_4 \cdot k) \tag{3.9}$$

A second-order polynomial regression model has been used in [52] to describe the capacity degradation, written as :

$$Q(k) = \beta_1 \cdot k^2 + \beta_2 \cdot k + \beta_3 \tag{3.10}$$

Xing et al. have developed another ensemble model based on He et al's exponential model and the polynomial model, which has a better regression characteristic over the whole battery life than the existing empirical models [87]. It is expressed as,

$$Q(k) = \gamma_1 \cdot exp(\gamma_2 \cdot k) + \gamma_3 \cdot k^2 + \gamma_4 \tag{3.11}$$

Moreover, as the capacity noisy measurements are available, there is no need to construct a particular measurement function and no need to add additional noise. Similarly, the voltage drop of the fuel cell is usually chosen as an indicator of its degrading states. Consequently, the state model represents the voltage evolution through time. Commonly used regression models are one or two order polynomial model and exponential model, logarithmic model, etc. [70, 96, 97] :

$$V(t) = a_1 \cdot t^2 + a_2 \cdot t + a_3 \quad or \quad a_1 \cdot t + a_2 \tag{3.12}$$

$$V(t) = b_1 \cdot exp(b_2 \cdot t) + b_3 \cdot exp(b_4 \cdot t) \quad or \quad b_1 \cdot exp(b_2 \cdot t) \tag{3.13}$$

$$V(t) = c_1 \cdot ln(t) + c_2 \cdot t \tag{3.14}$$

The linear model is commonly used in the literature to represent the fuel cell voltage drop during ageing through time, but it does not take into account what happens at the beginning and end of life. This can be solved by using either an exponential or a logarithmic function [96].

3.3.1.2/ BAYESIAN UPDATING APPROACH

From a Bayesian perspective, the tracking problem is to recursively estimate the probability distribution of the state $\mathbf{x}_k$ at time k by constructing the probability density function (PDF) $p(\mathbf{x}_k|\mathbf{z}_{1:k})$, given the available measurement $\mathbf{z}_{1:k}$ up to time k. It is assumed that the initial PDF $p(\mathbf{x}_0|\mathbf{z}_0) = p(\mathbf{x}_0)$ is available. Then, $p(\mathbf{x}_k|\mathbf{z}_{1:k})$ can be obtained by two stages : prediction and update.

Prediction Prediction stage uses the state model (3.7) to estimate the current state at time k with the prior PDF $p(\mathbf{x}_{k-1}|\mathbf{z}_{1:k-1})$ according to Chapman-Kolmogorov equation :

$$p(\mathbf{x}_k \mid \mathbf{z}_{1:k-1}) = \int p(\mathbf{x}_k \mid \mathbf{x}_{k-1}) p(\mathbf{x}_{k-1} \mid \mathbf{z}_{1:k-1}) d\mathbf{x}_{k-1} \tag{3.15}$$

Update At time k, a measurement $\mathbf{z}_k$ is available, which is used to update the prior PDF to obtain the posterior density of the current state via Bayes' rule :

$$p(\mathbf{x}_k \mid \mathbf{z}_{1:k}) = \frac{p(\mathbf{z}_k \mid \mathbf{x}_k) p(\mathbf{x}_k \mid \mathbf{z}_{1:k-1})}{p(\mathbf{z}_k \mid \mathbf{z}_{1:k-1})} \tag{3.16}$$

where the normalizing constant

$$p(\mathbf{z}_k \mid \mathbf{z}_{1:k-1}) = \int p(\mathbf{z}_k \mid \mathbf{x}_k) p(\mathbf{x}_k \mid \mathbf{z}_{1:k-1}) d\mathbf{x}_k \tag{3.17}$$

depends on the likelihood function defined by the measurement model (3.8) and the known statistics of $\mathbf{v}_k$. In the update stage (3.16), the measurement $\mathbf{z}_k$ is used to modify the prior density to obtain the required posterior density of the current state [13].

This forms the optimal Bayesian solution. However, it is only a conceptual solution : in general, it cannot be determined analytically [13]. For that purpose, a whole family of filtering tools exists ranging from the Kalman filter and its variations (extended Kalman filter or unscented Kalman filter), histograms and particle filters. The choice between these filters depends on the dynamics of the system and the shape of the noise distributions [155]. A non-exhaustive classification has been proposed in [55], as shown in Figure 3.6.

Among these Bayesian methods, Bayesian estimation with the particle filtering is found to be neither limited by either linearity nor Gaussian noise assumption. Particle filtering-based approaches are more and more employed for prognostics purposes and a thorough discussion of using this method for prognostics is found in [155].

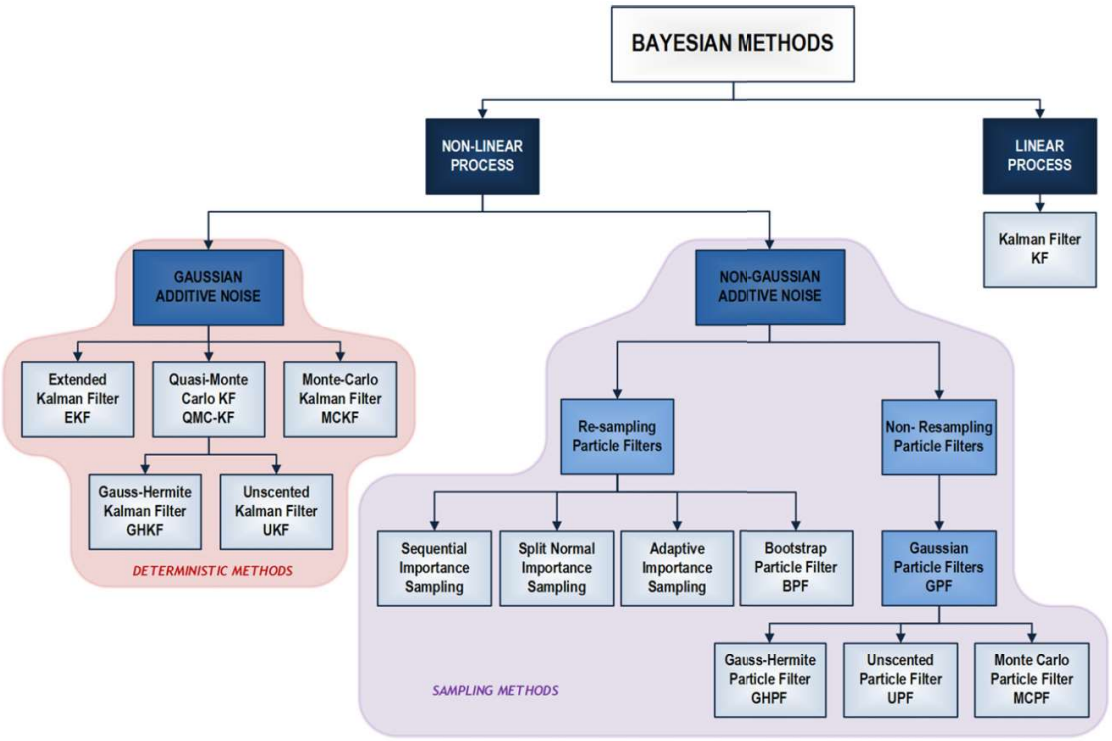

FIGURE 3.6 – A selection of methods for calculating a posteriori distribution [55]

3.3.2/ IMPLEMENTING PROGNOSTICS BY PARTICLE FILTERING

3.3.2.1/ SEQUENTIAL IMPORTANCE SAMPLING (SIS)

Sequential importance sampling (SIS) is the basis of implementing particle filtering. It is a Monte-Carlo method that approximates the probability distribution of the system state based on a set of samples and associated weights. The state estimates are calculated using these samples and their weights. As the number of the samples becomes very large, this Monte-Carlo characterization becomes an equivalent representation to the usual functional description of the posterior PDF $p(\mathbf{x}_k \mid \mathbf{z}_{1:k})$.

A discrete form of the state space given by the discrete weighted approximation is written as [13] :

$$p(\mathbf{x}_{0:k} \mid \mathbf{z}_{1:k}) \approx \sum_{i=1}^{N} \omega_k^i \delta(\mathbf{x}_{0:k} - \mathbf{x}_{0:k}^i) \tag{3.18}$$

The weights are normalized as $\sum \omega_k^i = 1$ and chosen according to the principle of importance sampling. Suppose $p(x) \propto \pi(x)$ is a probability density from which it is difficult to draw samples but for which $\pi(x)$ can be evaluated. $x^i \sim q(x), i = 1, 2, ..., N$ are the samples generated from a proposal $q(\cdot)$ called importance density [13]. The weighted approximation to $p(\cdot)$ is written as :

$$p(x) \approx \sum_{i=1}^{N} \omega^i \delta(x - x^i) \tag{3.19}$$

where $\omega^i \propto \frac{\pi(x^i)}{q(x^i)}$.

Therefore, at each iteration, the samples constitute an approximation to $p(\mathbf{x}_{0:k-1} \mid \mathbf{z}_{1:k-1})$ and will approximate $p(\mathbf{x}_{0:k} \mid \mathbf{z}_{1:k})$ with a new set of samples. According to

$$q(\mathbf{x}_{0:k} \mid \mathbf{z}_{1:k}) = q(\mathbf{x}_k \mid \mathbf{x}_{0:k-1}, \mathbf{z}_{1:k}) q(\mathbf{x}_{0:k-1} \mid \mathbf{z}_{1:k-1}) \tag{3.20}$$

one can derive the weight update equation :

$$\omega_k^i \propto \omega_{k-1}^i \frac{p(\mathbf{z}_k \mid \mathbf{x}_k^i) p(\mathbf{x}_k^i \mid \mathbf{x}_{k-1}^i)}{q(\mathbf{x}_k^i \mid \mathbf{x}_{k-1}^i, \mathbf{z}_k^i)} \tag{3.21}$$

and the posterior density [13] :

$$p(\mathbf{x}_k \mid \mathbf{z}_{1:k}) \approx \sum_{i=1}^{Ns} \omega_k^i \delta(\mathbf{x}_k - \mathbf{x}_k^i) \tag{3.22}$$

3.3.2.2/ PRINCIPLES OF PARTICLE FILTERING

Based on the above described SIS, the detailed steps of implementing SIS-type particle filtering are described as follows :

1. At the first stage ($k = 1$), the initial state x_0 is split into n samples, called particles, which represent the initial distribution PDF $p(x_0)$;
2. Propagate the n particles representing the system state PDF from x_{k-1} to x_k by the state model (3.7), and a new PDF is obtained ;
3. For each particle, estimate the associated weight by calculating its likelihood based on a newly available measurement $\mathbf{z}_k$:

$$\mathcal{L}(\mathbf{z}_k | \mathbf{x}_k, \sigma_{\mathbf{v}_k}) = \frac{1}{\sqrt{2\pi}\sigma_{\mathbf{v}_k}} exp(-\frac{(\mathbf{z}_k - \mathbf{x}_k)^2}{2\sigma_{\mathbf{v}_k}^2}) \tag{3.23}$$

   This calculation allows attributing weights at each particle according to the likelihood. Particles with higher weights represent the most probable states ;
4. After several iterations, the particles with low weights become too numerous, which influence the prediction step. Therefore, a resampling process is performed to remove the particles with small weights according to a given weight limit and replicated those with large weights ;
5. The posterior PDF built using resampling in the above step is used as the prior for the following iteration ;
6. The process is repeated until no measurement is available.

The entire process of implementing particle filtering is illustrated in Figure 3.7.

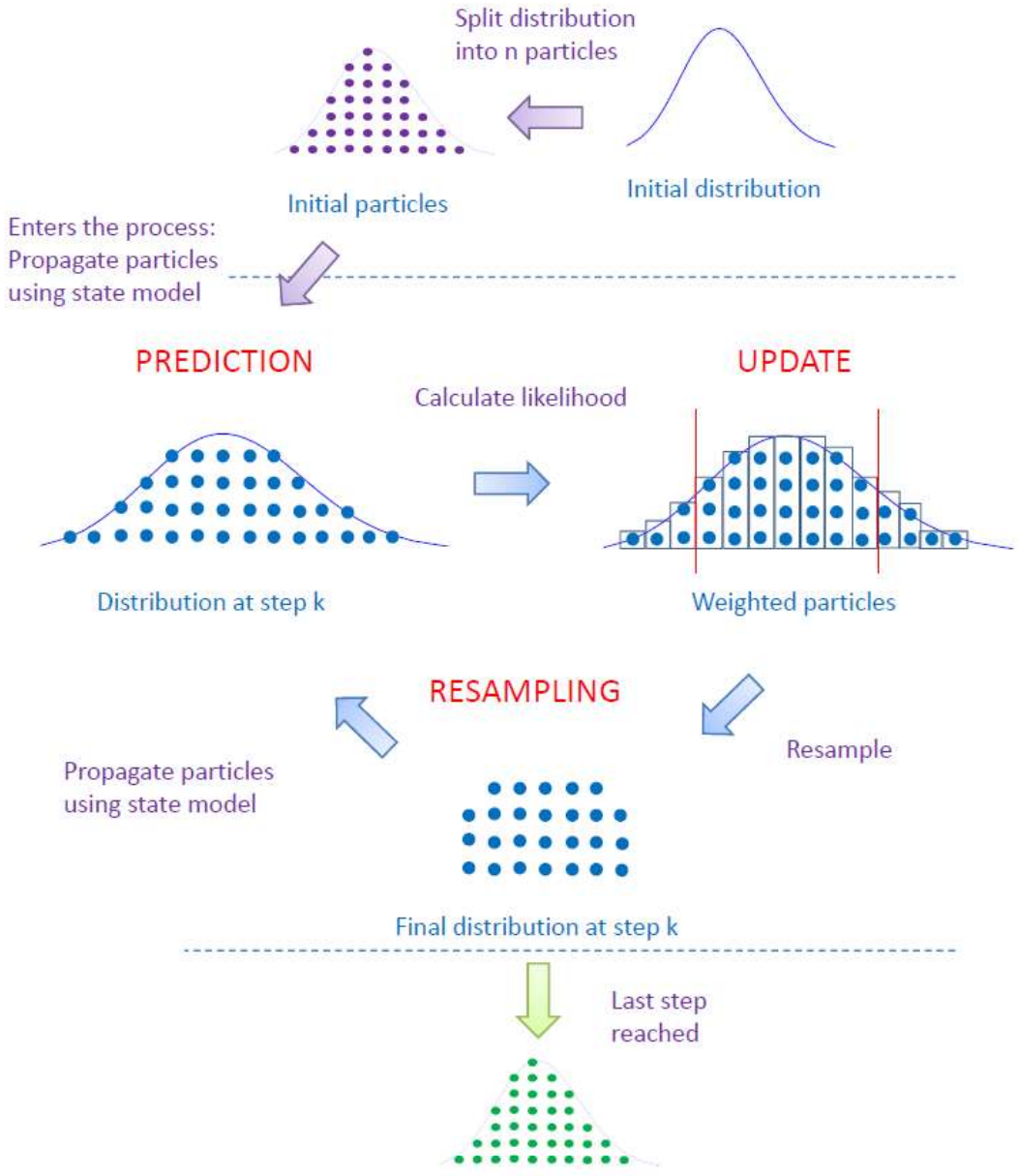

FIGURE 3.7 – Operation principle of particle filtering [96]

3.3.2.3/ PARTICLE FILTERING FOR PROGNOSTICS PURPOSE

For prognostics purpose, the states of the system are supposed to be learned by the available measurements and then be expected to predict the SOH and RUL without new measurements. Choosing particle filtering to perform prognostics, during the learning phase, it works as described above. The behaviour of the system is learned and the unknown coefficients in the state model are adjusted based on the measurements, as shown as the "LEARNING" phase in Figure 3.8. Once no measurement is available, only the state $\mathbf{x}_k$ is propagated from one to another and the likelihood is no longer calculated, as shown as the "PREDICTION" phase in Figure 3.8.

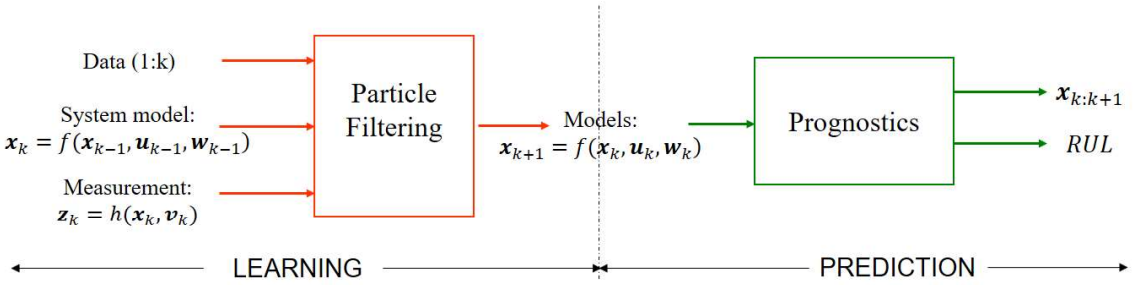

FIGURE 3.8 – Particle filtering process adapted for prognostics purpose

Supposing the state has a future path $\mathbf{x}_{k+1:k+l}, l = 1, ..., T-k$ and T is the entire horizon, the state $\mathbf{x}_{j-1}$ will pass to the state $\mathbf{x}_j$ with a transition PDF $p(\mathbf{x}_j \mid \mathbf{x}_{j-1})$. Thus, it is necessary to project $p(\mathbf{x}_k \mid \mathbf{z}_{0:k})$ among all possible future paths by a probability $\prod_{j=k+1}^{k+l} p(\mathbf{x}_j \mid \mathbf{x}_{j-1}) dx_{j-1}$ [59]. To calculate the l-step ahead posterior PDF, it is then combined with (3.7) and (3.16) :

$$p(\mathbf{x}_{k+l} \mid \mathbf{z}_{0:k}) = \int ... \int \prod_{j=k+1}^{k+l} p(\mathbf{x}_j \mid \mathbf{x}_{j-1}) p(\mathbf{x}_k \mid \mathbf{z}_{0:k}) \prod_{j=k}^{k+l-1} d\mathbf{x}_j \tag{3.24}$$

Based on Monte-Carlo PDF approximation, the upper equation could be approximated as [59] :

$$\hat{p}(\mathbf{x}_{k+l} \mid \mathbf{z}_{0:k}) = \sum_{i=1}^{N} \omega_{k+l-1}^{i} p(\mathbf{x}_{k+l} \mid \mathbf{x}_{k+l-1}^{i}) \tag{3.25}$$

In (3.25), $\hat{p}(\mathbf{x}_{k+l} \mid \mathbf{z}_{0:k})$ is a desired estimate that is obtained through an inverse transform resampling procedure : firstly, N values of a uniform random variable in the interval $[0, 1)$, $u^i \sim U[0, 1)$, then, the predicted state x_{k+l}^i is obtained through the interpolation of the cumulative state distribution :

$$F(\mathbf{X}_{k+l} \leq \mathbf{x}_{k+l}) = \int_{-\infty}^{\mathbf{X}_{k+l}} \hat{p}(\mathbf{x}_{k+l} \mid \mathbf{x}_{1:k+l-1}) d\mathbf{x}_{k+l} \tag{3.26}$$

Thus,

$$\mathbf{x}_{k+l}^i = \mathbf{F}^{-1}(u^i) \tag{3.27}$$

The weights of the resampled particles remain unchanged, i.e., $\omega_{k+l}^i = \omega_{k+l-1}^i$. This procedure is repeated until the time horizon is reached.

3.3.2.4/ RUL ESTIMATION

Since the RUL indicates how long the system could remain in use, it is calculated based on a pre-defined EOL threshold, noted as λ. The PDF of the estimated RUL is :

$$\hat{p}(RUL \leq l \mid \mathbf{z}_{0:k}) = \hat{p}(\mathbf{x}_{k+l} \geq \lambda \mid \mathbf{z}_{0:k}) \tag{3.28}$$

The estimate is updated based on new $\mathbf{z}_j, j = k+1, ..., k+l$. In fact, at each time step, the RUL distribution is the final particles distribution obtained when the failure threshold is reached [96]. A simpler solution is to use the particle distribution to calculate the PDF of the RUL estimates by fitting a mixture of Gaussian in a least square sense [31].

To implement particle filtering based prognostics in Matlab environment, the entire procedure is illustrated in **Algorithm 1.**

Algorithm 1 Particle filtering for prognostics purpose

Initialize $x_0^i, \sigma_{w_0}^i, \sigma_{v_0}^i, u_0^i$ with a uniform distribution ▷ System initialization
Time step $k = 1$
while $x_k^i > \lambda$ and $k \leq k_p$, **do**
  for $i = 1, ..., n$, **do** ▷ Importance sampling
    Draw particles $x_k^i \sim p(x_k^i \mid x_{k-1}^i, \sigma_{w_{k-1}}^i, u_{k-1}^i)$
    Assign weight $\omega_k^i = \mathcal{L}(z_k^i \mid x_k^i, \sigma_{v_k^i})$
  end for
  Normalize weight $\omega_k^i = \omega_k^i / \sum_{i=1}^n \omega_k^i$
  Calculate the cumulative sum of the normalized weights $Q_k^i|_{i=1}^n = Cumsum(\omega_k^i|_{i=1}^n)$
  for $i = 1, ..., n$, **do** ▷ Resampling
    $j = 1$
    Draw a random value $u^i \sim U[0, 1)$
    while $Q_k^i < u^i$, **do**
      $j = j + 1$
    end while
    Update state $x_k^j = x_k^j$
    Update noises $\sigma_{w_{k-1}}^j = \sigma_{w_{k-1}}^j$, $\sigma_{v_{k-1}}^j = \sigma_{v_{k-1}}^j$
    Update parameters $u_k^j = u_k^j$
  end for
  $k = k + 1$
end while
for $i = 1, ..., n$, **do** ▷ Prognostics from k_p
  while $x_k^i > \lambda$, **do**
    Propagate particles to the next time step $x_k^i = f(x_{k-1}^i, \sigma_{w_{k-1}}^i, u_{k-1}^i)$
    $k = k + 1$
  end while
  Estimate $\hat{R}UL_k^i = (k - k_p) \cdot \Delta t$
end for

3.4/ DEGRADATION DATA DESCRIPTION

3.4.1/ HYPOTHESES AND LIMITATIONS OF THE STUDY

Based on the literature review in Chapter 2, lithium-ion battery and PEM fuel cell are such complex systems that the internal state variables cannot be accessed by sensors or they can hardly be measured under operation conditions. Therefore, performing state estimation and prognostics on those power sources gives the possibility to develop a health-conscious EMS for fuel cell HEVs.

In the hybrid system, PEM fuel cell provides the most power demand while the lithium-ion battery deals with transient power need and regenerates the braking power. Due to the uncertain road driving conditions, the operation conditions of the power sources are variable and cannot be anticipated. To investigate the prognostics for the hybrid system, it is important that the following hypotheses must be made :

1. It is assumed that the available nonlinear historical failure data in this study can be used to explain past behaviour and can be used to predict the future.
2. It is assumed that the historical data obtained under variable experimental operation conditions can include the dynamics of random driving conditions of the hybrid vehicle.
3. It is assumed that ageing effects are the only considered cause for battery and fuel cell's performance degradation, while the sudden destruction on the components (open circuit, short-circuit faults, etc.) or some extreme operation conditions (extreme temperature, extreme humidity, etc.) are not taken into consideration. For the fuel cell, the fuel starvation is assumed to never happen.
4. It is assumed that the degradation phenomenon on each power source is independent of each other in the hybrid system, i.e., there is no added degraded effect to the power sources when they are hybridized in the system.
5. It is assumed that the predefined threshold is available for the end of serviceable system life.

In fact, prognostics for transport applications is rarely investigated due to the lack of experimental data and accelerated stress tests (ASTs). It remains as the limitation of our study. Further experiments on the degradation of the hybrid system are ongoing by our laboratory (FCLAB Federation). More results will be added once the experiments are done.

3.4.2/ PEM FUEL CELL DEGRADATION DATA

3.4.2.1/ DATA SOURCE AND PERFORMANCE DEGRADATION

The PEM fuel cell degradation dataset used for prognostics comes from the IEEE PHM 2014 Data Challenge launched by the IEEE Reliability Society, FCLAB research federation, FEMTO-ST Institute, and the Laboratory of excellence ACTION [95]. Experiments were carried out by FCLAB Research Federation (FR CNRS 3539, France, http ://eng.fclab.fr/) on test facilities that enable normal or accelerated ageing of FCS stacks under constant and variable operation conditions, while controlling and gathering

health monitoring data like power loads, temperatures, hydrogen and air stoichiometry rates, etc.

The test bench is adapted for the fuel cells with a power up to 1 kW and many physical parameters involved in the stack are measured and controlled in order to master the fuel cell operation conditions, summarized in Table 3.1.

TABLE 3.1 – Physical parameters controlled by the test bench

Parameter	Control range
Cooling temperature	20°C to 80°C
Cooling flow	0 to 10 l/min
Gas temperature	20°C to 80°C
Gas humidification	0 to 100% RH
Air flow	0 to 100 l/min
H_2 flow	0 to 30 l/min
Gas pressure	0 to 2 $bars$
Fuel cell current	0 to 300 A

The assembled fuel cell are 5-cell stacks. Each cell has an active area of 100 cm^2. The nominal current density of the cells is 0.70 A/cm^2. Their maximal current density is 1 A/cm^2. Two long-term tests were carried out : A first stack was operated in stationary regime at roughly nominal operating conditions (a current of 70 A was imposed) ; A second stack was operated under dynamic current testing conditions (a ripple current of 70 A with 7 A oscillations at a frequency of 5 kHz was imposed). For both tests, characterizations were carried out once per week (around every 160 hours) according to an identical protocol : polarization curve test (i.e. measuring the static I/V curve of the fuel cell stack), global historic curves (i.e. evaluating the evolution over time of voltage levels), and Electrochemical Impedance Spectroscopy (EIS) measurement (i.e. measuring the "Nyquist" plot of the fuel cell stack over a frequency range from 50 mHz to 10 kHz).

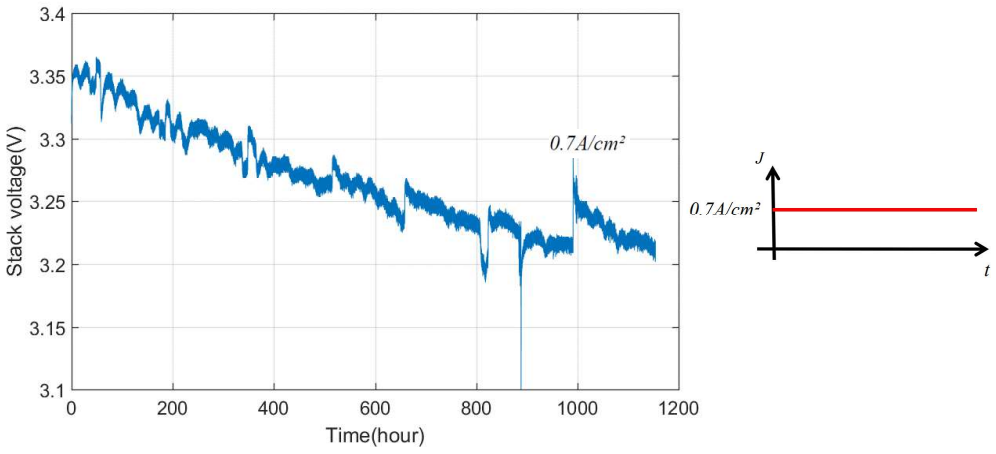

FIGURE 3.9 – Fuel cell stack voltage degradation under constant operation condition

Figure 3.9 shows the stack voltage drop signal over time in constant operation conditions with a current of 70 A, while Figure 3.10 shows the stack voltage drop signal in variable operation conditions with a ripple current. Several peaks at certain time instances can be

observed. In practice, characterization measurements lead to the observed sudden drops in power, and then the power jumps back getting recovered thanks to the reversibility of the stack.

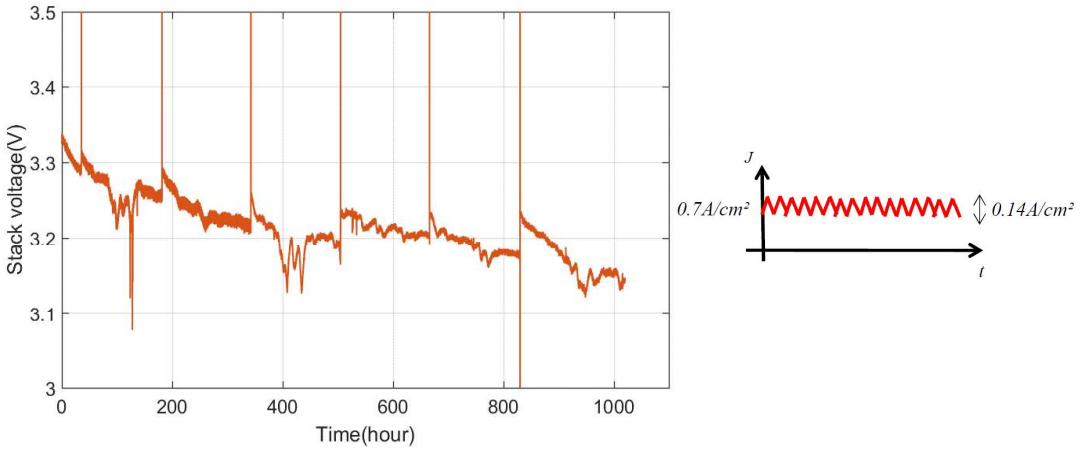

FIGURE 3.10 – Fuel cell stack voltage degradation under variable operation condition

As mentioned above, the utilization of fuel cells in a hybrid system is random and cannot be anticipated, and may be influenced by the operation of other power sources. Therefore, the historical dataset of the fuel cell operated under variable operation condition (with a ripple current) is chosen for the following prognostics study. It is a strong hypothesis due to the lack of real operation dataset of a hybrid system.

3.4.2.2/ DATA ANALYSIS AND PREPROCESSING

During the ageing experiments, voltage disturbances are inevitable. Besides, there are several visible peaks that are due to the characterizations carried out throughout its ageing process (polarization curve and EIS), as shown in Figure 3.10. Besides, the original signal is too noisy to implement prognostics. Thus, the data should be preprocessed to remove the peaks and filter the noises.

A kernel smoother could be used to filter the noisy data. Kernel smoother is a powerful smoothing tool since it is operated like the moving average, while the average is weighted [98]. The weights of the average depend on the kernel $K(t)$. Consider a signal $u(t)$ with n data points and let $u(t_j)$, $j = 1, 2, 3, ...n$ denote a sample point. The estimate of the filtered data point, $f(t_j)$ is given as follows :

$$f(t_j) = \frac{\sum_{i=1}^{n} s_i \cdot u(t_j)}{\sum_{i=1}^{n} s_i} \tag{3.29}$$

where

$$s = K(\frac{t_j - t}{h}) \tag{3.30}$$

h is the bandwidth and K is a Gaussian Kernel function given by

$$K(t) = \frac{e^{\frac{-t^2}{2}}}{\sqrt{2\pi}} \tag{3.31}$$

Figure 3.11 shows the data smoothing results with peak removed and noise filtered.

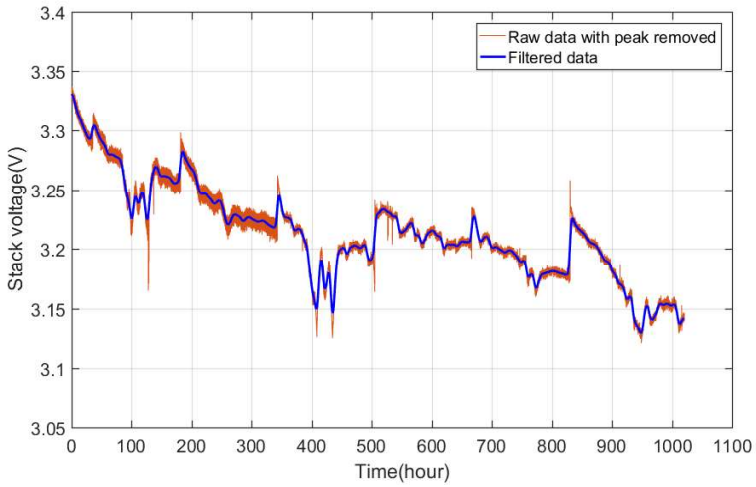

FIGURE 3.11 – Fuel cell data preprocessing result with peak removed and noise filtered

However, the dataset contains 131068 data points in total and using these data points to estimate the states requires huge storage memory, up to gigabytes to store the states, estimated parameters and particle weights. This would not be actually allowed in industrial application. Besides, too many points for state estimation will lead to overfitting problem, resulting in the divergence of the model [154]. Technically speaking, the dataset should be reduced.

Besides, due to the fact that among all the phenomena occurring within the fuel cell, the accumulation of ageing effects are the main factors that shorten its RUL and the degradation will not progress during an hour, time scales longer than an hour are considered [151]. This enables making mid-term and long-term predictions and consequent decisions.

To reduce the dataset, Jouin et al. have proposed two solutions : reduce the dataset by one point per hour, or reduce the dataset with respect to changes in the mission profile [32]. In this study, to learn the state of the system and to perform prognostics, the data is reduced using the first solution, at one point per hour by the cubic spline method, which is used to interpolate the data to obtain samples at a uniform time interval.

3.4.3/ LITHIUM-ION BATTERY DEGRADATION DATA

3.4.3.1/ DATA SOURCE AND CAPACITY DEGRADATION

For the application test, the lithium-ion battery dataset was obtained from the data repository of the National Aeronautic and Space Administration (NASA) Ames Prognostic Center of Excellence (PCoE) [187]. The test bench allows charging and discharging of the batteries until failure. When it comes to vehicle applications, randomized charge and discharge process should be considered due to uncertain driving conditions. Therefore, the datasets with batteries continuously cycled with randomly generated current profiles are chosen.

A set of four 18650 lithium-ion batteries (identified as RW9, RW10, RW11 and RW12) were continuously operated using a sequence of charging and discharging currents bet-

ween -4.5A and 4.5A, as shown in Figure 3.12. This type of charging and discharging operation is referred here as random walk (RW) operation in order to better represent practical battery usage.

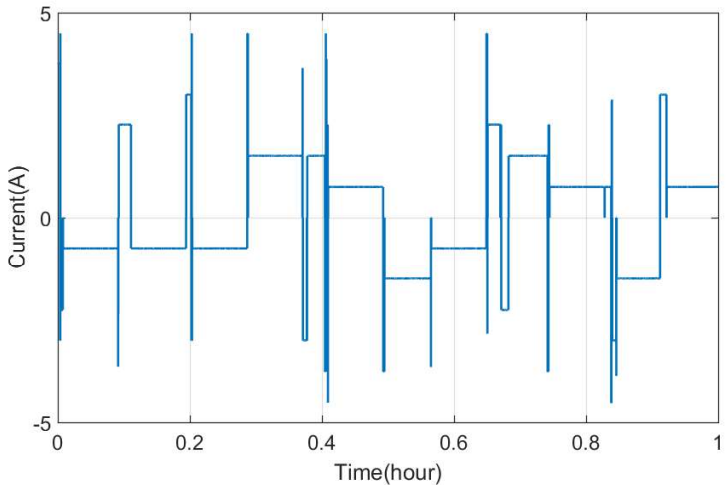

FIGURE 3.12 – Example of the battery random charging and discharging current

The procedure of the RW operation consists of :

1. Selecting a charging or discharging current at random from the set $\{$-4.5A, -3.75A, -3A, -2.25A, -1.5A, -0.75A, 0.75A, 1.5A, 2.25A, 3A, 3.75A, 4.5$A\}$. Negative currents are associated with charging and positive currents indicate discharging.
2. The selected current setpoint is applied until either the battery voltage goes outside the range (3.2$V \sim$ 4.2V) or 5 minutes has passed.
3. After each charging or discharging period, there will be a $<$1s period of rest while a new charging or discharging current setpoint is selected.
4. Steps 2 and 3 are repeated 1500 times, then characterization cycles are performed to benchmark battery state of health.

Characterization cycles are preformed once after 1500 periods (about 5 days). A reference charge and discharge cycle is used to observe the capacity : the batteries are first charged at 2A (constant current) until they reach 4.2V, at which time the charging switches to a constant voltage mode and continues charging the batteries until the charging current falls below 0.01A. Batteries are then discharged at 2A until the battery voltage crosses 3.2V. After each reference charge and discharge cycle, batteries are rested for a while with no current draw.

The differences in the voltage profiles observed in Figure 3.13 are due to the degradation of the battery's state of health over the experiment. As the battery ages, its charge storage capacity decreases, while its internal resistance increases, which result in a decrease in available Li-ions and therefore a faster discharge time for the given output current. Ageing-dependent changes are denoted with arrows in Figure 3.13.

The battery's capacity C can be benchmarked by integrating current over the reference cycles according to the ampere-hour counting ("Coulomb counting") method :

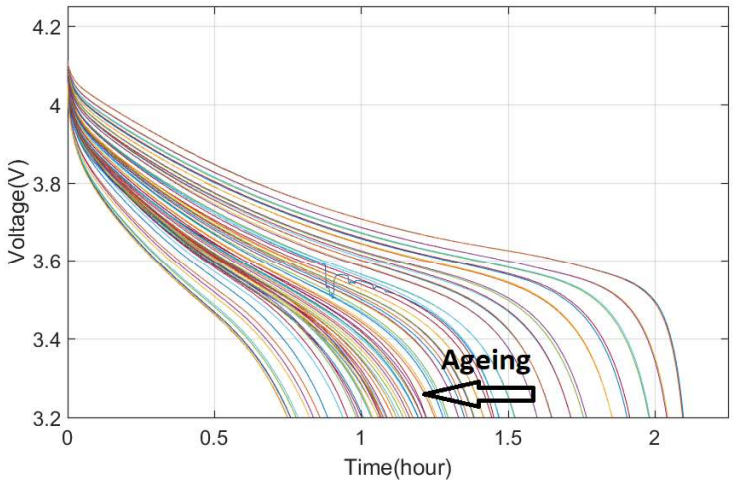

FIGURE 3.13 – Battery discharge voltage profiles in different characterization cycles

$$Maximum\ available\ capacity = \eta \int_{t0}^{t} \frac{i_{bat}(\tau)}{SOC_t - SOC_{t0}} d\tau \tag{3.32}$$

where η is the coulombic efficiency ($\eta < 1$ for charge and $\eta = 1$ for discharge). The benchmarked capacity integration results of the four tested batteries are plotted in Figure 3.14.

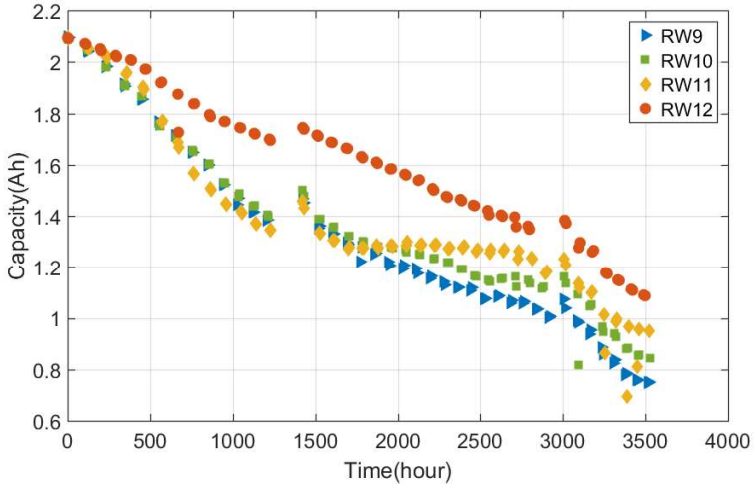

FIGURE 3.14 – Benchmarked battery capacity obtained by integrating current

The battery's state of health could be defined from the perspective of the battery's available capacity. It is expressed as

$$SOH = \frac{C_i}{C_0} \times 100\% \tag{3.33}$$

where C_i is the ith capacity value degenerated by the ith characterization cycle and C_0 is the initial capacity. In most studies, this definition of SOH is utilized to study the degrada-

tion performance of the battery and thus, prognostics could be performed based on the degraded capacity values.

3.4.3.2/ DATA ANALYSIS AND PREPROCESSING

The dataset RW12 was chosen to be the studied battery capacity degradation dataset. Since the capacity is calculated offline by integrating cycling current, there is no noisy signal, therefore, there is no need to perform filtering.

However, the dataset has a non-uniform time index and a relatively long time scale (5 days), which is adaptable for maintenance planning but not enough to fit a degradation model. In order to perform time-based prognostics, similarly to the data of PEM fuel cell, the capacity data are interpolated to obtain samples at a uniform time interval of 1 hour, as shown in Figure 3.15.

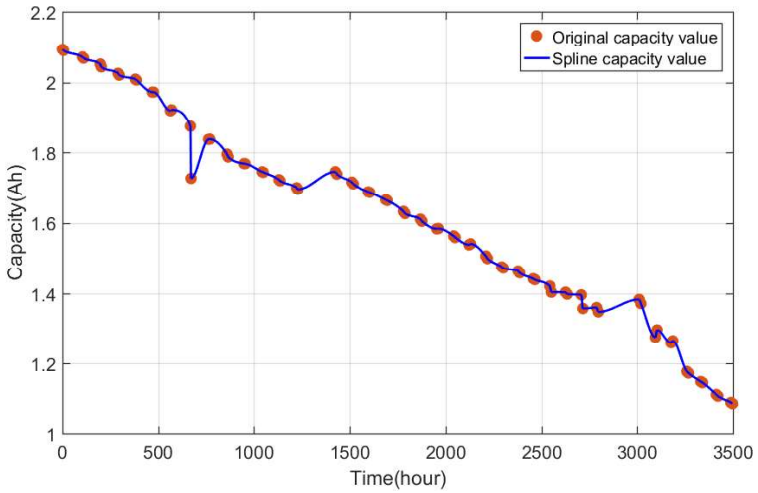

FIGURE 3.15 – Battery data preprocessing result by spline interpolation (dataset RW12)

3.5/ PARTICLE FILTERING PROGNOSTICS RESULTS AND EVALUATION

3.5.1/ RUL PROGNOSTICS FOR PEM FUEL CELL

3.5.1.1/ DEFINITION OF THE PEM FUEL CELL EOL THRESHOLD

Before implementing prognostics, an EOL threshold is defined at first to calculate the RULs and help to verify the prognostics results. The performance degradation of the studied PEM fuel cell's voltage is used as its health indicator and when defining its EOL threshold, it should be not located on particular voltage peaks that would be located out of the ageing trend [96]. Regarding the length of the experiment, the PEM fuel cell failure threshold under dynamic usage is fixed to 96% of the initial performance, calculated as,

$$EOL_{FC} = V_{init} \cdot 96\% = 3.13V \tag{3.34}$$

3.5.1.2/ ADAPTATION OF PARTICLE FILTERING TO FUEL CELL VOLTAGE DEGRADATION

The degradation trend of the degradation dataset described in Section 2.4 could be caught by various empirical models [70, 96, 97]. In order to include more possibilities of variation, the 2nd order exponential degradation model is chosen to track the fuel cell's performance and perform prognostics :

$$V(t) = b_1 \cdot exp(b_2 \cdot t) + b_3 \cdot exp(b_4 \cdot t) \tag{3.35}$$

where b_1, b_2, b_3 and b_4 are the model parameters, b_1 and b_3 determine the initial state and b_2 and b_4 define the degradation rate**.** Then, the state space model could be written from (3.35) :

$$\begin{aligned} x_{1,k} &= x_{1,k-1} \cdot exp(b_2) + \omega_{1,k}, \quad \omega_{1,k} \sim \mathcal{N}(0, \sigma^2_{\omega 1}) \\ x_{2,k} &= x_{2,k-1} \cdot exp(b_4) + \omega_{2,k}, \quad \omega_{2,k} \sim \mathcal{N}(0, \sigma^2_{\omega 2}) \end{aligned} \tag{3.36}$$

where $x_{1,k}$ and $x_{2,k}$ are two first-order independent Markov processes and the present voltage state can be obtained from $x_{1,k}$ and $x_{2,k}$:

$$x_k = b_1 \cdot x_{1,k} + b_3 \cdot x_{2,k} \tag{3.37}$$

where b_1, b_2, b_3 and b_4 are also states to be transited. The measurement model is then written as :

$$z_k = x_k + v_k, \quad v_k \sim \mathcal{N}(0, \sigma^2_v) \tag{3.38}$$

where v_k are supposed to be included in the measurement signal as the measurement noise. As no prior information on the initial distributions of the parameters is available, uniform distributions is applied [60]. The value for process noise variance is found through successive tuning as $\sigma^2_\omega = 10^{-4}$ and same process noise is assigned to the unknown parameters (b_1, b_2, b_3 and b_4). The measurement noise is assumed to be involved in the input signals. Besides, to ensure a better prediction, the number of $N = 3000$ particles is chosen in this implementation.

3.5.1.3/ FUEL CELL PROGNOSTICS RESULTS DEMONSTRATION AND EVALUATION

In order to save time for learning and memory for storage, a time scale of 10 hours is used. The model is trained by particle filtering with the measurement data until the prediction time t_λ**.** t_λ is set to different time instants along with the fuel cell performance degradation. To be adaptable to energy management, prognostics is performed every 50 hours from the 100th hour. Each prediction is calculated 100 times in order to avoid the dispersion of the results given by the particle filter**.**

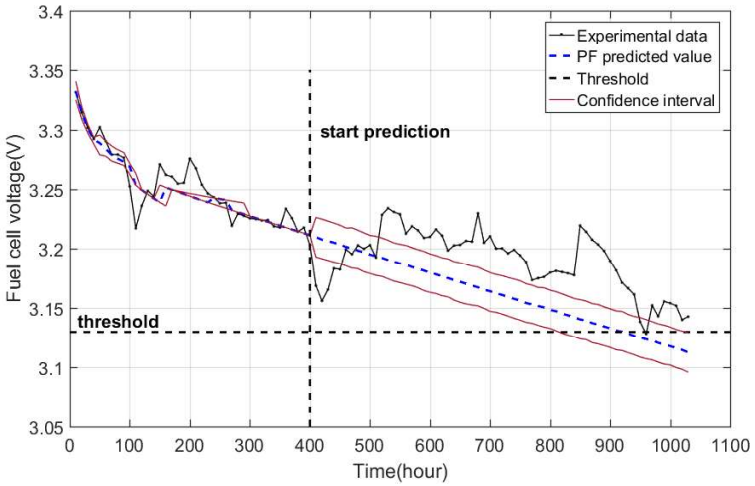

FIGURE 3.16 – Fuel cell voltage prognostics results (10-hours time scale)

Figure 3.16 shows the estimation and prognostics results of the fuel cell degradation at prediction time $t_\lambda = 400th$ hour. The predicted RUL is $[415\ 520\ 625]$ hours with a confidence interval (CI) of [5% 50% 95%] whereas the true RUL is 560 hours.

Indeed, when the particles are propagated at each time step, a new distribution of particles is created representing the last predicted state. However, all these distributions cannot be drawn in the same figure. The estimated voltage drawn in Figure 3.16 is the successive positions of the top of the particles distribution [96]. The RUL distribution is therefore represented by the final particles distribution obtained when the failure threshold is reached, as shown in Figure 3.17.

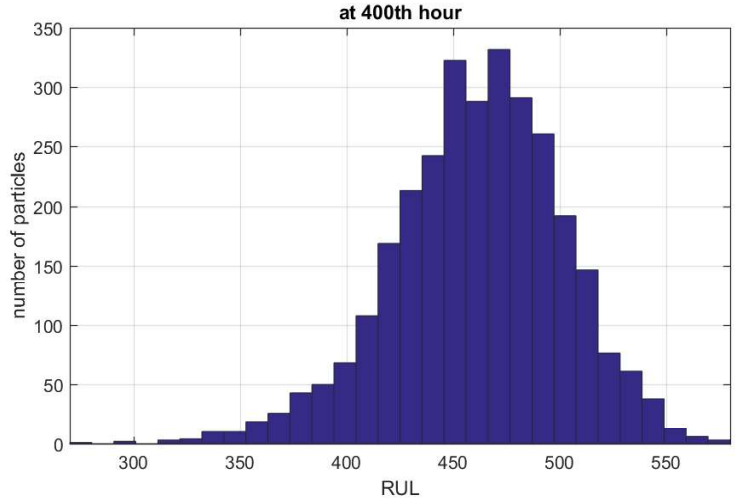

FIGURE 3.17 – Histogram of the fuel cell RUL predictions at 400th hour (10-hours time scale)

After implementing prognostics at different prediction time t_λ, based on (3.5) and (3.6), the predicted RULs, relative accuracy and precision of the predicted RULs at each prediction time step t_λ are evaluated in Table 3.2. As can be seen from the results, the particle

filtering prognostics with a time scale of 10 hours can reach an average relative accuracy of 0.9 and an average precision of 0.483.

TABLE 3.2 – Evaluation results of fuel cell prognostics (10-hours time scale)

t_λ	100	...	400	450	500	550	600	...	800	average
RUL^*_λ	860	...	560	510	460	410	360	...	160	-
$\hat{RUL}_\lambda$	660	...	530	460	490	380	380	...	180	-
$ReAcc$	0.765	...	0.946	0.902	0.935	0.927	0.944	...	0.875	0.9
Precision	0	...	0.375	0.412	0.5	0.488	0.528	...	1.125	0.483

To evaluate the reliability prognostics results, the acceptable error margin should be defined. According to Section 3.2, for early prediction, an error of 16% is allowable, while for late prediction, an error of 8% is allowable. The boxplot in Figure 3.18 shows the predicted RUL uncertainties (final distribution of particles) every 50 hours from the $100th$ hour with an error bound $[\alpha^-, \alpha^+] = [RUL^*_\lambda * (1 - 0.16), RUL^*_\lambda * (1 + 0.08)]$ and CI = 95%. As it is shown in Figure 3.18, the predictions in the first 300 hours are not accurate enough. After 300 hours, with more newly coming measurements, the predictions are improved and all included in the acceptable error bounds. Based on (3.5), the $\alpha - \lambda$ accuracy is listed in Table 3.3. Since all the predictions are included in the bounds, the $\alpha - \lambda$ accuracy reaches 1.

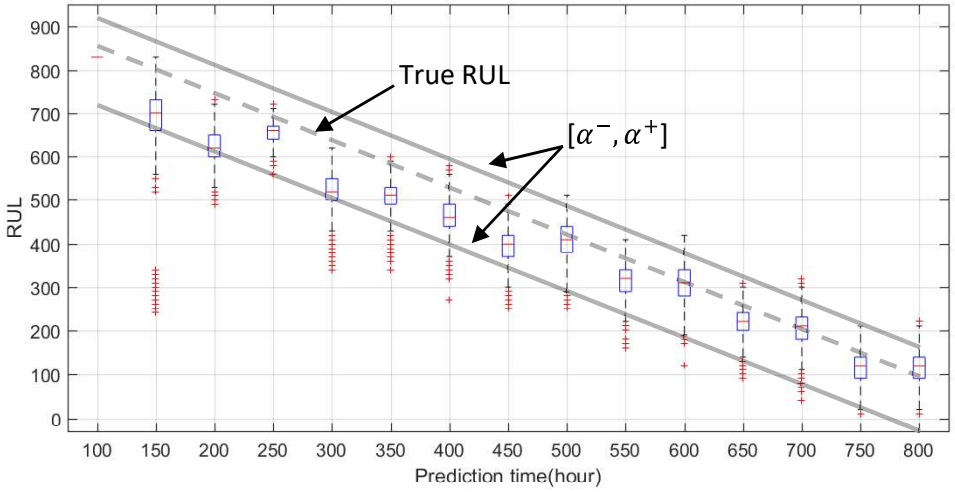

FIGURE 3.18 – Boxplot of fuel cell RUL predictions with error bounds (10-hours time scale)

TABLE 3.3 – $\alpha - \lambda$ accuracy of fuel cell prognostics results (10-hours time scale)

t_λ	100	...	400	450	500	550	600	...	800	average
$\alpha - \lambda$ accuracy	true	...	true	true	true	true	true	...	true	1

However, as shown in Figure 3.19, the precision shows a decreased tendency over the horizon. It indicates that the spread of the predicted RULs has a dependence on the distance to EOL. This could be explained by the large dynamics of the studied data.

As the degradation of the voltage recovered abnormally after 500 hours' operation, the predicted RULs spread severely.

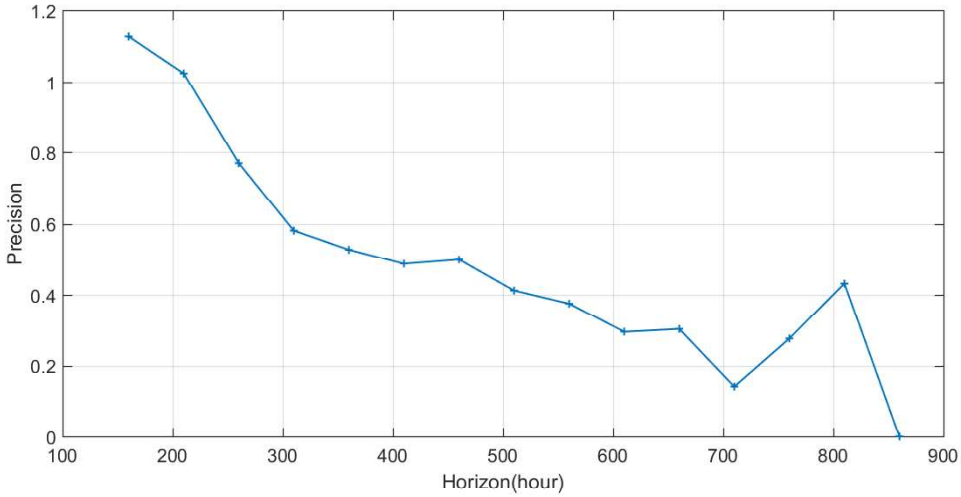

FIGURE 3.19 – Fuel cell RUL precision vs. horizon (10-hours time scale)

3.5.2/ RUL PROGNOSTICS FOR LITHIUM-ION BATTERY

3.5.2.1/ DEFINITION OF THE LITHIUM-ION BATTERY EOL THRESHOLD

The amount of energy that a battery can hold is measured in capacity (unit : Ah). Capacity is a significant health indicator that describes its ageing status and determines its runtime. The lithium-ion battery is regarded as to be failed when the remaining capacity drops below a certain percentage of its nominal capacity. However, different battery products have different EOL definitions in their warranty. For example, Tesla defines the EOL of its iconic Powerwall 1.0 and Powerwall 2.0 at 60% and 70% of original capacity, respectively [1]. In our study, a loss of 30% to its original capacity is defined as the battery EOL threshold since an accelerated capacity loss is observed when cycling is continued beyond 70-80% SOH according to the experimental results in [93]. The battery EOL threshold is written as :

$$EOL_{BAT} = C_{init} \cdot 70\% = 1.46Ah \tag{3.39}$$

3.5.2.2/ ADAPTATION OF PARTICLE FILTERING TO BATTERY CAPACITY DEGRADATION

To achieve a high global goodness-of-fit, an ensemble model fusing polynomial model and exponential model is used to describe the degradation trend of the battery, written as [87] :

$$Q(k) = \gamma_1 \cdot exp(\gamma_2 \cdot k) + \gamma_3 \cdot k^2 + \gamma_4 \tag{3.40}$$

Following state space model is used to solve the tracking problem using the nonlinear process function, x_k, and measurement function, z_k :

$$
\begin{aligned}
x_k &= f_k(x_{k-1}, \omega_{k-1}) = \begin{bmatrix} \gamma_{1,k-1} \\ \gamma_{2,k-1} \\ \gamma_{3,k-1} \\ \gamma_{4,k-1} \end{bmatrix} + \omega_{k-1}, \quad \omega_k \sim \mathcal{N}(0, \sigma_\omega^2) \\
z_k &= h_k(x_k, v_k), \quad v_k \sim \mathcal{N}(0, \sigma_v^2)
\end{aligned} \tag{3.41}
$$

where x_k is the current capacity value, γ_1, γ_2, γ_3 and γ_4 are the parameters to be estimated by the particle filter. ω_k and v_k are process noise and measurement noise, respectively. As explained before, the measurement noise is supposed to be included in the measurement signal so that there is no need to add v_k during the implementation of the algorithm. The process noise variance is tuned as $\sigma_\omega^2 = 10^{-4}$, while the number of 3000 particles is chosen with a uniform initial distribution.

3.5.2.3/ BATTERY PROGNOSTICS RESULTS DEMONSTRATION AND EVALUATION

Due to the fact that the studied battery doesn't gain obvious degradation in each hour, a time scale of 10 hours is chosen to implement the prognostics at the beginning. Figure 3.20 is an example showing the prognostics results with a 95% confidence interval at prediction time $t_\lambda = 500th$ hour. The predicted RUL is $[1672\ 1843\ 2000]$ hours with a confidence interval (CI) of [5% 50% 95%] whereas the true RUL is 1885 hours. The RUL distribution at $t_\lambda = 500th$ hour is shown in Figure 3.21.

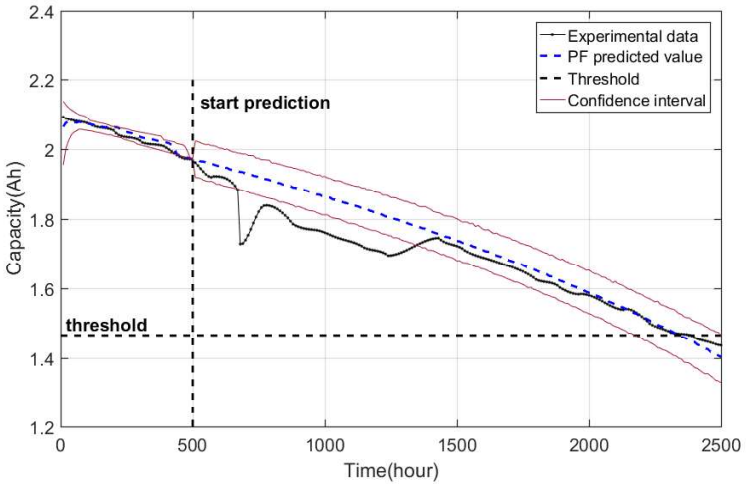

FIGURE 3.20 – Battery capacity prognostics results (10-hours time scale)

The prognostics is implemented every 100 hours from the $100th$ hour. Based on (3.5) and (3.6), the predicted RULs, relative accuracy and precision of the predicted RULs at each prediction time step t_λ are listed in Table 3.4. As it can be seen from the results, the particle filtering prognostics with a time scale of 10 hours can reach an average relative accuracy of 0.881 and an average precision of 0.406.

The acceptable error margins are defined as 16% (early prediction) and 8% (late prediction), as shown in Figure 3.22. The boxplot of prognostics results at different prediction time shows that the predictions before 400 hours are less accurate and less precise due

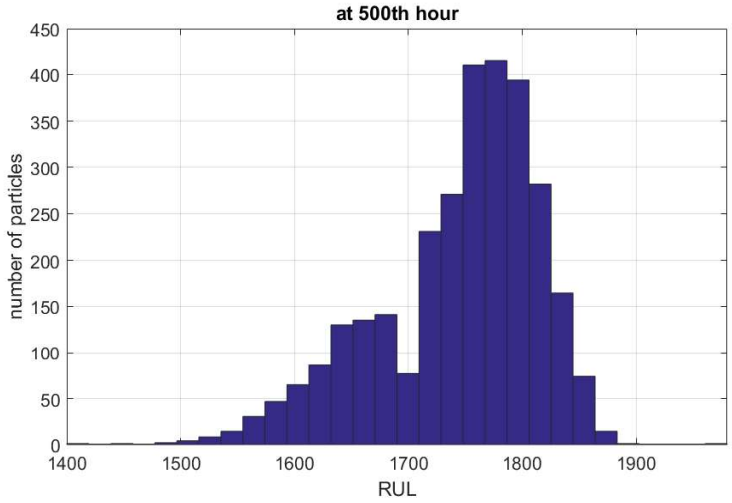

FIGURE 3.21 – Histogram of the battery RUL predictions at 500th hour (10-hours time scale)

to insufficient learning data. After 400 hours, the prediction results remain in the error margin region and most of them are early predictions. An average of 0.9 $\alpha - \lambda$ accuracy is reached as recorded in Table 3.5.

TABLE 3.4 – Evaluation results of battery prognostics (10-hours time scale)

t_λ	100	...	800	900	1000	1100	1200	...	2000	average
RUL^*_λ	2285	...	1585	1485	1385	1285	1185	...	385	-
$\hat{RUL}_\lambda$	2380	...	1430	1510	1150	1370	1130	...	250	-
$ReAcc$	0.958	...	0.902	0.983	0.83	0.934	0.954	...	0.649	0.881
Precision	0.678	...	0.177	0.195	0.188	0.21	0.203	...	0.623	0.406

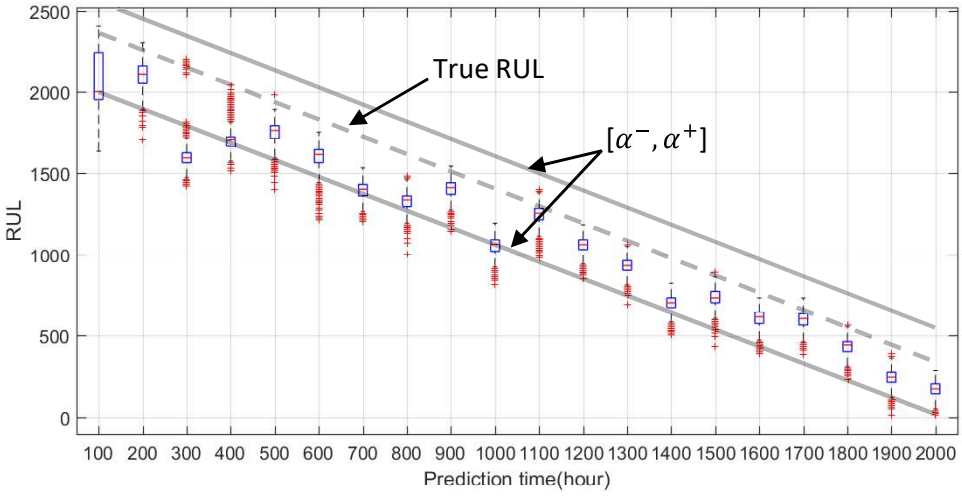

FIGURE 3.22 – Boxplot of battery RUL predictions with error bounds (10-hours time scale)

TABLE 3.5 – $\alpha - \lambda$ accuracy of battery prognostics (10-hours time scale)

t_λ	100	...	800	900	1000	1100	1200	...	2000	average
$\alpha - \lambda$ accuracy	true	...	true	true	true	true	true	...	true	0.9

In terms of prediction precision, an obvious decrease variation is shown Figure 3.23 as the prognostics horizon becomes larger. This is possibly due to the abnormal degradation trends in Figure 3.20 between 500 hours and 1500 hours. However, opposite to this decrease variation, the precision gets even worse when the prognostics horizon is large (at the beginning of the prediction). This is due to the insufficiency of input data.

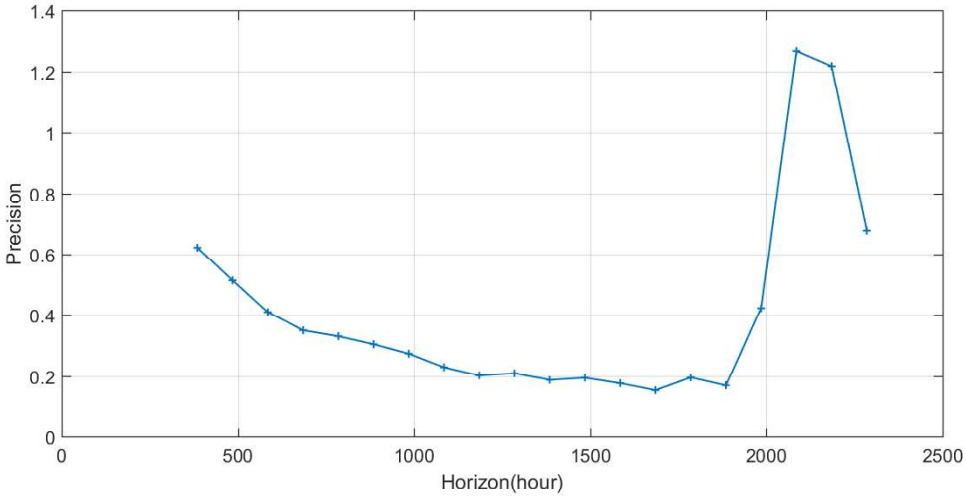

FIGURE 3.23 – Battery RUL precision vs. horizon

3.5.3/ MULTI-TIME SCALE ANALYSIS

The time scales used in the task of prediction or prognostics should be flexible according to specific applications [32]. The time scale of 10 hours used in the above section has achieved satisfying prediction results for both the prognostics of PEM fuel cell and lithium-ion battery. However, it is necessary to investigate how shorter and longer time scale could have an influence on the precision and accuracy of the prognostics results. As the battery capacity has been already sampled and it is meaningless to interpolate it any more, only the fuel cell is examined here in order to find out the possible relevance between data quality and prognostics performance.

First, prognostics on a shorter time scale of one hour is implemented. The same procedure is performed every 50 hours from the 100th hour. The predicted RULs, relative accuracy and precision at each prediction time step t_λ are listed in Table 3.6. A satisfied average accuracy of 0.924 is reached and the average precision is 0.181, which is improved by almost three times than the previously described 10-hours time scale prognostics.

The boxplot of RUL prediction uncertainties is shown in Figure 3.24 and the $\alpha-\lambda$ accuracy is listed in Table 3.7. As it is indicated in the figure, almost all predictions are included in the error bounds with high precision (thinner box). An $\alpha - \lambda$ accuracy of 0.933 is reached.

TABLE 3.6 – Evaluation results of fuel cell prognostics (1-hour time scale)

t_λ	100	...	400	450	500	550	600	...	800	average
RUL^*_λ	860	...	560	510	460	410	360	...	160	-
$\hat{RUL}_\lambda$	884	...	568	473	418	471	345	...	173	-
$ReAcc$	0.972	...	0.986	0.927	0.909	0.851	0.958	...	0.919	0.924
Precision	0.1	...	0.073	0.104	0.191	0.137	0.236	...	0.538	0.181

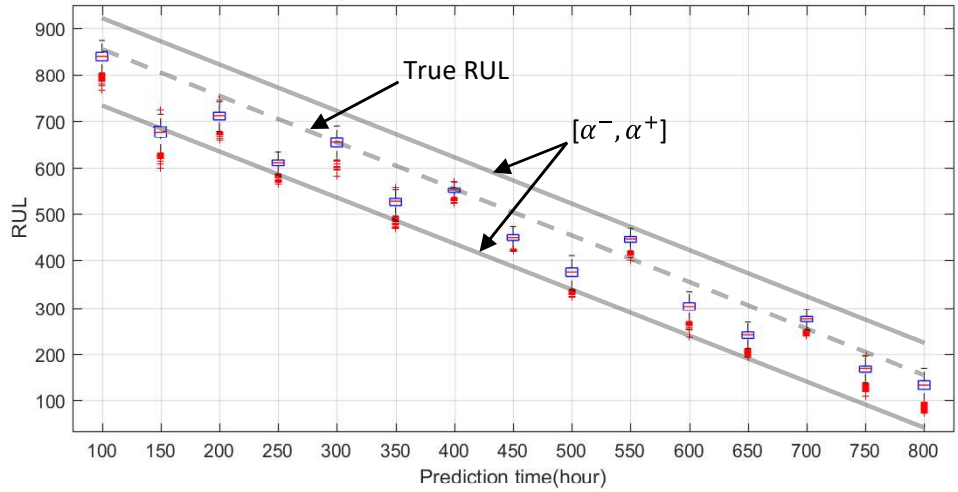

FIGURE 3.24 – Boxplot of fuel cell RUL predictions with error bounds (1-hour time scale)

TABLE 3.7 – $\alpha - \lambda$ accuracy of fuel cell prognostics (1-hour time scale)

t_λ	100	...	400	450	500	550	600	...	800	average
$\alpha - \lambda$ accuracy	true	...	true	true	true	true	true	...	true	0.933

However, if the time for running this procedure is considered, compared to the 10-hours time scale, it needs 10 times longer execution time. Therefore, there is no need to sacrifice the execution time while the prediction accuracy can hardly be further improved.

TABLE 3.8 – Evaluation results of fuel cell prognostics (20-hours time scale)

t_λ	100	...	400	460	500	560	600	...	800	average
RUL^*_λ	860	...	560	500	460	400	360	...	160	-
$\hat{RUL}_\lambda$	920	...	580	520	460	360	360	...	140	-
$ReAcc$	0.93	...	0.964	0.96	1	0.9	1	...	0.875	0.911
Precision	0.349	...	0.321	0.36	0.345	0.5	0.5	...	1.125	0.463

Next, larger time scales are examined. As a beginning, the time scale is lengthened to 20 hours and the prognostics result evaluation is recorded in Table 3.8. Results show that the predictions have reached an average accuracy of 0.911 and a precision index of 0.463, almost the same level to that of the 10-hours time scale implementation. The RUL

predictions with their uncertainties are plotted in Figure 3.25 and the $\alpha - \lambda$ accuracy is recorded in Table 3.9.

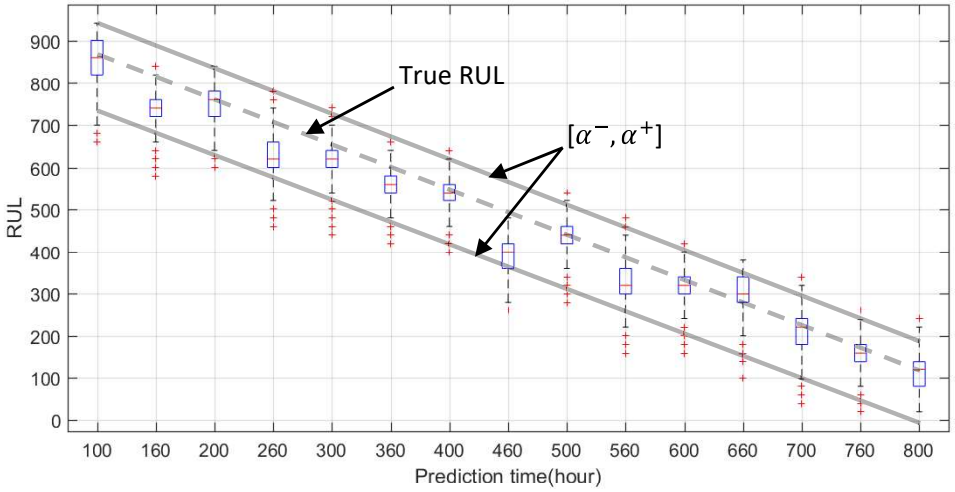

FIGURE 3.25 – Boxplot of fuel cell RUL predictions with error bounds (20-hours time scale)

TABLE 3.9 – $\alpha - \lambda$ accuracy of fuel cell prognostics (20-hours time scale)

t_λ	100	...	400	460	500	560	600	...	800	average
$\alpha - \lambda$ accuracy	true	...	true	true	true	true	true	...	true	1

The same procedure has been performed on two more different time scales of 30-hours and 40-hours. Results of accuracy and precision versus time plot are shown in Figure 3.26 and Figure 3.27.

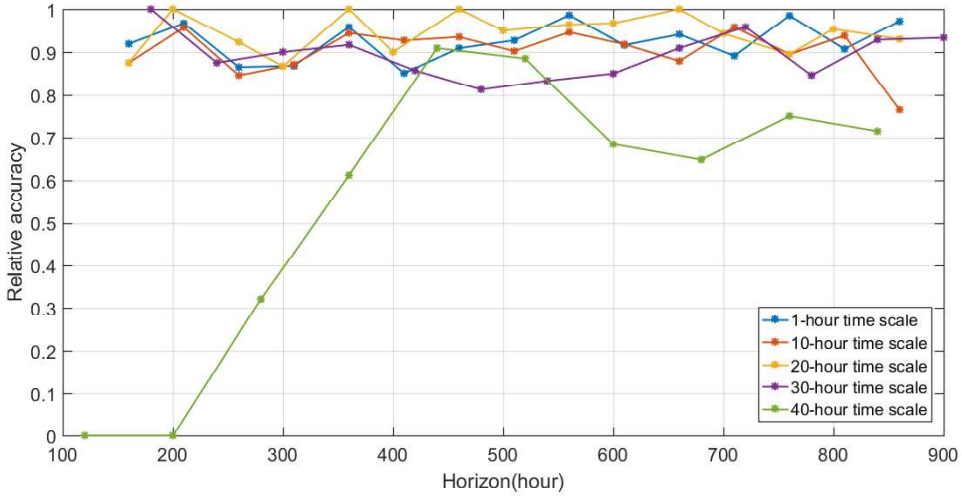

FIGURE 3.26 – Accuracy vs. time at different time scales

The accuracy of smaller time scales (1-hour, 10-hours and 20-hours) achieves a higher value, mostly around 0.9, while the accuracy of 30-hours time scale is not bad with only

some values closed to 0.8, as shown in Figure 3.26. However, the accuracy of the 40-hours time scale is the worst and can hardly fulfil the requirement of prognostics. The accuracy evolution doesn't see a clear dependence on the horizon. Regarding the evolution of precision of different time scale, the same tendency is observed at different time scales, as shown in Figure 3.27. As we have discussed above, worse precision values are caused by abnormal degraded voltages. Besides, 1-hour time scale prognostics has the best precision performance while 10-hours and 20-hours time scales have less good but acceptable precision performance. Precision goes worse when the time scale is enlarged to 30-hours and 40-hours. The predicted RUL are dispersed badly.

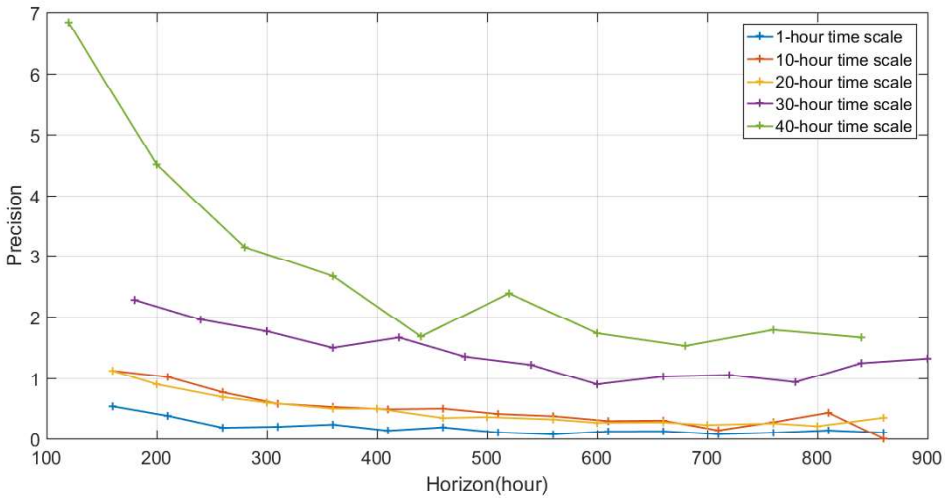

FIGURE 3.27 – Precision vs. time at different time scales

As a conclusion, prognostics on a time scale of 10 hours or 20 hours is reasonable to be used in our following study, considering the execution time and the completeness of the degradation information.

3.6/ SYNTHESIS

As prognostics is a key process in PHM cycle, this chapter has proposed to use the particle filtering based prognostics method to estimate and predict future health states of the fuel cell and the battery existing in a hybrid system. The aim of this chapter is to justify the effectiveness of the proposed prognostics method so that it could be combined with the energy management aspect in the fuel cell hybrid system. Post-prognostics decisions could be made based on the prognostics results, i.e., RUL estimates.

Based on a short review of prognostics requirements and prognostics methods, particle filtering is chosen as the prognostics tool to solve the prediction problem of fuel cell's and battery's ageing thanks to its adaptiveness to nonlinear and non-Gaussian problem. To justify the effectiveness of using particle filtering for RUL estimation of power sources in fuel cell HEVs, two historical datasets under dynamic operation conditions for battery and fuel cell are delicately selected, respectively. The fuel cell dataset is released by PHM challenge 2014, which is a 5-cell PEM stack operated under ripple current, while the battery dataset is the one obtained from NASA PCoE, which is a randomly used lithium-

ion battery charging and discharging by a random current profile. These datasets are chosen to meet the dynamic operation requirements in real driving conditions.

Particle filtering is used to track the power source performance degradation and the prediction of RULs is made. The results are evaluated by the offline evaluation metrics. On a 10-hours time scale, fuel cell prognostics results have reached an accuracy of 0.9, while battery prognostics results have reached an accuracy of 0.88. Besides, to investigate the influence of different time scale, same prognostics procedure has been executed on the fuel cell dataset with different time scales : short time-scale of 1 hour and long time-scale of 20, 30 and 40 hours. Results showed that shorter time scale needs 10 times more execution time while the accuracy cannot be improved. Longer time scales such as 10-hours and 20-hours have reached good accuracy while 30-hours and 40-hours time scales didn't obtain acceptable prognostics results. When one looks into depth the influence on result precision, it could be found that the shortest time-scale has the best precision while 10-hours and 20-hours time scales have similar and good enough precision results. Longer time-scale like 30-hours and 40-hours give the precision results far from satisfaction. Therefore, a moderate time-scale, like 10-hours and 20-hours, is suitable to be used for online health state prognostics.

However, the prognostics implemented in this chapter are based on existing experimental datasets and the dynamic operation conditions of the hybrid system are imitated by selecting datasets tested under dynamic conditions. It should be noticed that the interactions between the hybridizing power sources are not considered. The effectiveness of the prognostics method has been justified but it should be tested online and the results should be able to generate effective enough decision support. Online operation of hybrid system prognostics process is represented in Figure 3.28, where median RUL output is used as one of the inputs of the following EMS development.

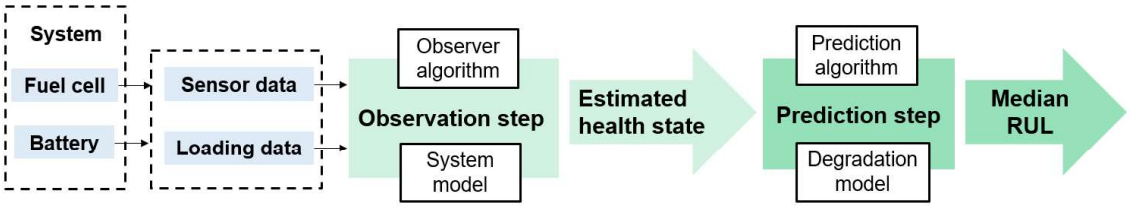

FIGURE 3.28 – Online operation of hybrid system prognostics process

In the next chapter, the developed prognostics method is used for the online health state prediction of the hybrid system to formulate a closed PHM cycle by developing a health-conscious EMS. The EMS is based on offline optimized fuzzy logic controller whose parameters are tuned by a classification and decision fusion process. It is going to be introduced and explained in details in the following chapter.

4

Online Health-Conscious EMS Development

4.1/ Introduction

Given the prognostics results obtained by prognostics methods, described in the last chapter, one can be aware of whether the future mission could be met and at what point can typical future mission could not be met. In this chapter, a decision-making process is proposed to complete the PHM cycle for the studied fuel cell system, which makes full use of the prognostics results to guide the design of EMSs for fuel cell HEVs.

A driving cycle defined by repeated WLTC class 2 driving cycles is used to run the fuel cell/battery hybrid system model built in Matlab/Simulink environment using energetic macroscopic representation (EMR). Due to the limit of lacking hybrid system degradation data, the degradation of the power sources is defined based on the degradation trend of historical data in a simulated way. Particle filtering is used online to performance state estimation and prognostics based on online operation data. The aim of this chapter is to develop a health-conscious EMS based on PHM knowledge, which is able to improve the durability of the power sources through the adjustments of the power distribution at different degradation levels. The brief scheme for demonstrating this process is shown in Figure 4.1.

In the context of this chapter, a baseline EMS is firstly developed using an optimized fuzzy logic controller. Fuzzy logic is a powerful tool for real-time control while it can only obtain an optimal solution with the help of intelligent methods. Genetic algorithm (GA) is selected here to optimize the membership functions first under the healthy state of the system and then at different degradation states. However, to perform actively corrective control, the parameters of fuzzy logic controllers need to be adjusted in real time and offline optimization is no longer effective during real driving conditions. Therefore, given the median RUL values obtained by online prognostics methods, a prognostics-based decision-making process is developed based on a classifier and a decision fusion procedure, which takes care about the current health state of the system and derives the proper parameters for the controller. In addition, as the degradation process of the power sources is a long-term procedure, there is no need to tune the controller at each time step. The occurrence of prognostics is based on the health state estimation and how to choose an effective criterion remains to be discussed and will be discussed in an early stage in this chapter.

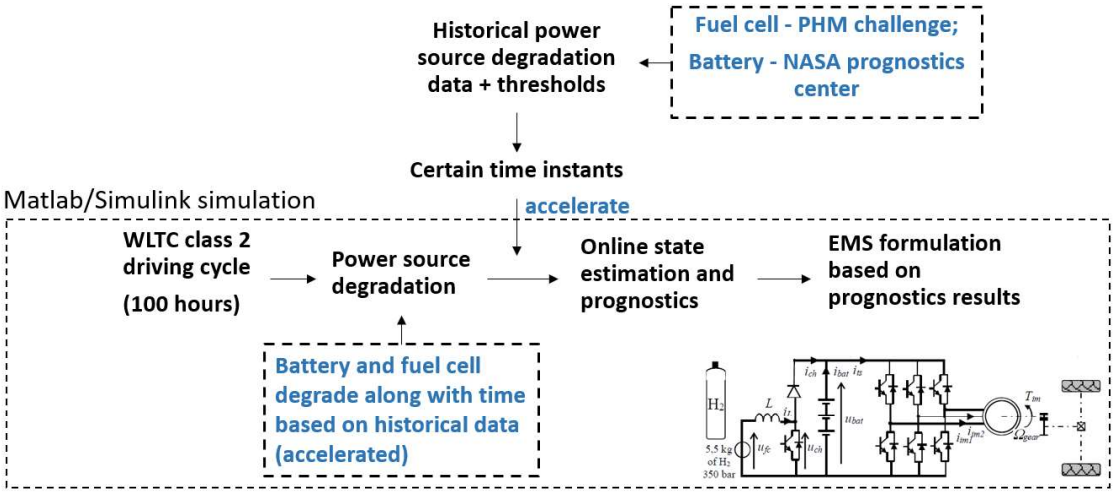

FIGURE 4.1 – Online prognostics-based EMS development in a simulated way

The contents of this chapter are arranged as follows : a simulation plant model of the studied fuel cell HEV is developed in Section 4.2, which is designed through EMR in a reduced topology. A baseline EMS is developed in Section 4.3 based on GA-optimized fuzzy logic controller. It is used to justify the effectiveness of the developed health-conscious EMS, which is described in Section 4.4. Simulation results are compared and analyzed, and a discussion on the occurrence frequency of prognostics is presented at the end of this chapter.

4.2/ SIMULATION PLANT MODEL OF FUEL CELL HEV

4.2.1/ FORWARD-FACING VEHICLE MODELLING

A fuel cell range extender HEV is considered in this study, where PEM fuel cells and a lithium-ion battery pack provide the power to the traction system. The considered architecture of the vehicle is based on the commercial Tazzari Zero electric vehicle with a modification in its energy storage system. For this thesis, a simple model of the vehicle is constructed using MATLAB®/Simulink® that is capable of being used for EMS optimization.

When considering about vehicle modelling, there are two modelling approaches : backward-facing modelling and forward-facing modelling. Backward facing modelling doesn't require a 'driver' model to control the speed, which means the speed profile is directly imposed to the vehicle model to calculate the power requirements, resulting in less simulation time. However, due to its 'quasi-static' nature, the backward model is non-casual and offers little information about drivability, and therefore meaningless for hardware-in-the-loop test system [81]. In the forward-facing model, a 'driver' model is used to obtain the demanded power based on the current speed and the reference speed, i.e. a speed controller. Therefore, it can accurately represent the causality observed in the real driving conditions and provide a better understanding of the dynamics and physical limits of the powertrain.

A forward-facing simulation plant model is constructed using a proportional-integral (PI) speed controller, see Figure 4.2. The plant model could be divided into two parts : the propulsion system and the power system. In the propulsion system, the electric motor is controlled by the speed controller which is designed based on the difference between the reference speed and the current speed calculated from the vehicle model. In the power system, there is a battery pack directly connected to the electric motor and a fuel cell connected to the battery using a DC/DC converter. Each of these components is connected by current and voltage signals in a feedback loop. An EMS is designed to control the DC/DC converter based on the speed of the vehicle, battery SOC and to be health-conscious, it is designed also depending on the current health states of the battery and the fuel cell.

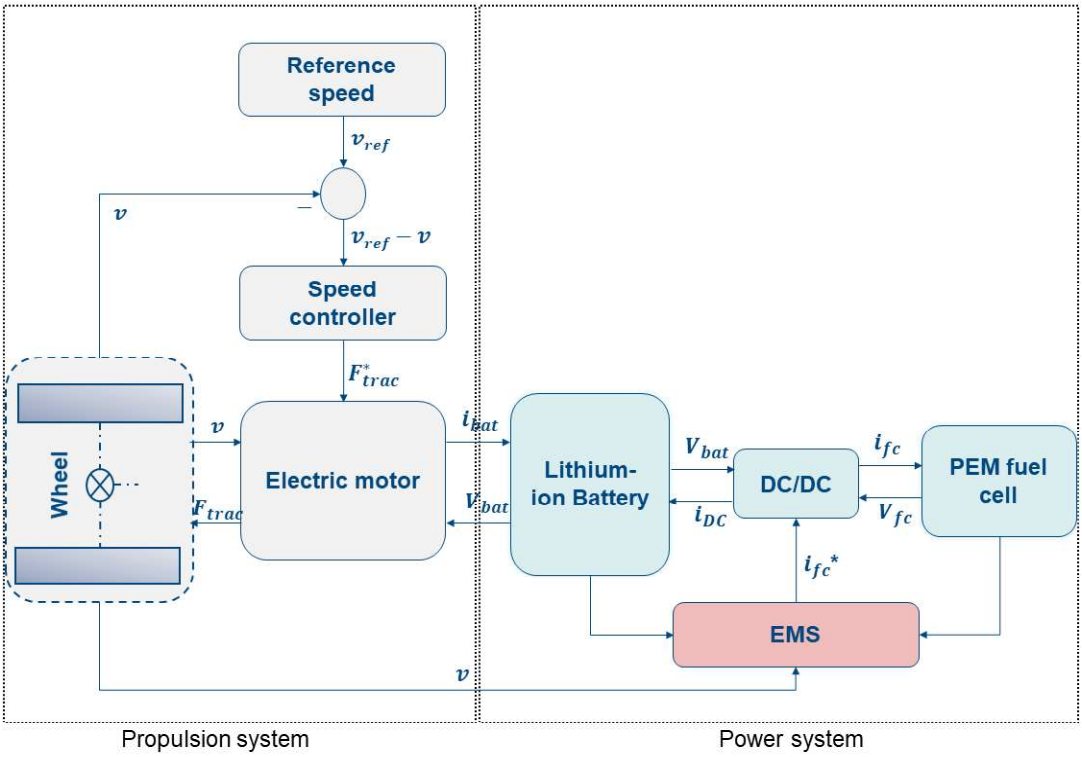

FIGURE 4.2 – Simulation plant model with forward-facing approach

4.2.2/ SPEED PROFILE

Three different driving cycles are defined to test the vehicle model. As shown in Figure 4.3, they are :

— An adapted NEDC (New European Driving Cycle) which is generally used to determined CO_2 emissions, energy consumption or vehicle range ;
— A class 2 WLTC (Worldwide harmonized Light vehicles Test Procedures). it is a widely used driving cycle in the performance examination of light-duty vehicles and can fulfil the urban driving conditions ;
— An urban driving cycle from a Tazzari Zero on-road test realized around the University of Lille 1 [95].

Considering the length of the test and the speed dynamics, WLTC class 2 driving cycle is

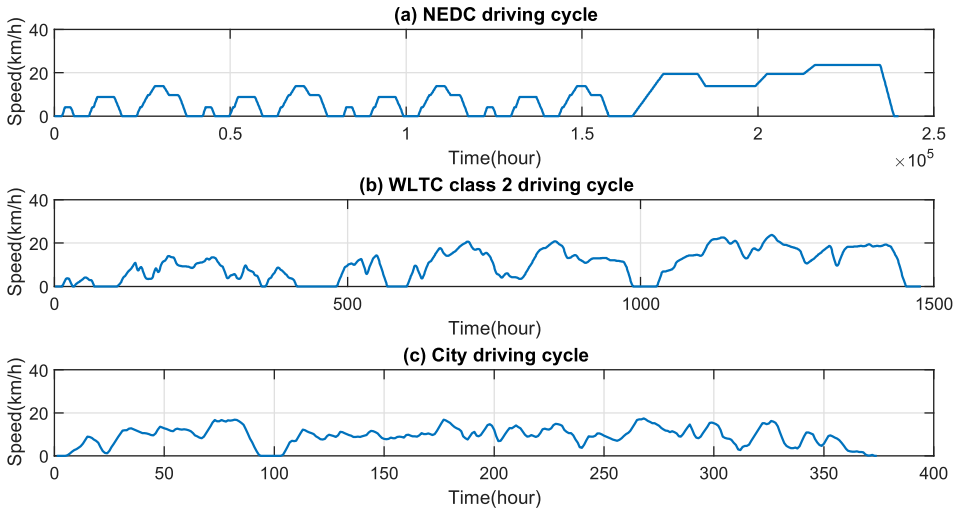

FIGURE 4.3 – Three different driving cycles : (a) NEDC driving cycle ; (b) WLTC class 2 driving cycle ; (c) City driving cycle

selected in the following study as the system speed input.

4.2.3/ VEHICLE MOTION MODELLING

The total traction force F_{tract} is calculated by the transmission force F_{trans} subtracting a braking force F_b.

$$F_{tract} = F_{trans} - F_b \tag{4.1}$$

The vehicle velocity v is obtained using Newton's second law of motion with the traction and resistive forces, F_{res} :

$$M_{tot}\frac{d}{dt}v = F_{tract} - F_{res} \tag{4.2}$$

where resistive forces, F_{res}, consists of the rolling resistance, the aerodynamic drag and the incline of the road, calculated by :

$$F_{res} = fM_{tot}g + \frac{1}{2}\rho c_x A(v + v_{wind})^2 + M_{tot}g\alpha \tag{4.3}$$

where f denotes the rolling resistance coefficient, M_{tot} is an equivalent total mass of the vehicle and the equivalent mass of the rotating parts, g the acceleration due to gravity, α the slope rate, ρ the air density, c_x the air drag coefficient and A the frontal area of the vehicle [140]. Specifications used to estimate the parameters used in the vehicle model is shown in Table 4.1.

TABLE 4.1 – Vehicle specifications

Parameter	Value
Vehicle mass (M_{tot})	698 kg
Coefficient of rolling resistance (f)	0.02
Standard aerodynamisme (c_xA)	0.7
Gravity constant (g)	9.81
Air density at 20°C (ρ)	1.223
Wind speed (v_{wind})	0
Slope (α)	0

4.2.4/ ELECTRIC MOTOR MODELLING

The electric motor model firstly calculates the required tractive force based on the reference speed and uses the mechanical load on the vehicle to calculate the electrical load on the battery and the fuel cell. In order to simplify the study, a static model is considered for the motor according to an efficiency map, see Figure 4.4. This efficiency map is included in the model as a lookup table as (4.4). It includes the inverter associated with the traction machine, the wheels, the gearbox, the mechanical transmission and the control algorithm [92].

$$\eta_{tract} = f(F_{trans}, v) \tag{4.4}$$

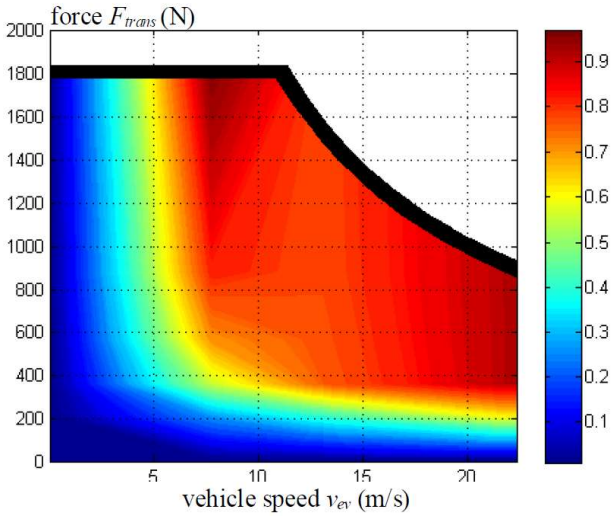

FIGURE 4.4 – Efficiency map deduced from an on-road test drive [92]

The traction system is directly controlled by a reference traction force $F_{trans-ref}$:

$$F_{trans} = F_{trans-ref} \tag{4.5}$$

where the tuning variable $F_{trans-ref}$ is linked to the controlled variable, vehicle speed. From the reference vehicle speed v_{ref}, the measured vehicle velocity and the estimated environment force F_{res}, the reference transmission force $F_{trans-ref}$ is obtained by :

$$F_{trans-ref} = C_v(t)(v_{ref} - v) + F_{res} \tag{4.6}$$

where $C_v(t)$ is a PI controller.

The current drawn by the motor, i_{ts} can be calculated as the transmission force of the motor, F_{trans}, divided by the traction system efficiency, and the motor supply voltage, which equals to the battery voltage :

$$i_{ts} = \frac{F_{trans} v}{u_{bat}(\eta_{tract})^k} \text{ with } k = \begin{cases} 1, & \text{if } P_{tract} > 0 \\ -1, & \text{if } P_{tract} < 0 \end{cases} \tag{4.7}$$

The specification of the electric motor could be found in Table 4.2. The peak power and peak force have been used as limits on the model to ensure that the motor is unlikely to ever exceed this time rating for all driving cycles. This control saturation is finally taken into account by the speed controller by using an anti-windup control loop [140].

TABLE 4.2 – Electric motor specifications

Parameter	**Value**
Maximal traction force ($F_{tract-max}$)	2000 N
Maximal traction power ($P_{tract-max}$)	15000 W

4.2.5/ BATTERY MODELLING

The traction battery pack used in this study is made up of four lithium-ion phosphate ($LiFePO_4$) battery modules and each module contains six battery cells connected in series, giving a total nominal voltage of 80 V and a total nominal capacity of 40 Ah.

An electrical equivalent circuit model is used to model the battery's behaviour, which describes the battery operating characteristics using a circuit network, i.e. a combination of voltage sources, resistors and capacitors, for co-design and co-simulation with other electrical circuits and systems. For electrical engineers, electrical models are more intuitive, useful, and easy to handle, especially when they can be used in circuit simulators and alongside application circuits. Here, the battery is modelled by an equivalent circuit including an open-circuit voltage u_0, a series resistance R_s, and a parallel combination of resistance capacitance $R_c C_c$, as shown in Figure 4.5.

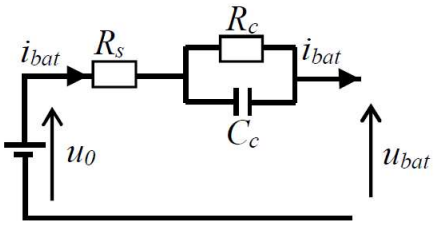

FIGURE 4.5 – Battery equivalent circuit model in the studied vehicle

The output battery voltage is calculated by (4.8) :

$$\begin{cases} \dot{u_{C_c}} = -\dfrac{u_{C_c}}{R_c C_c} + \dfrac{i_{bat}}{C_c} \\ u_{bat} = u_0 - u_{C_c} - i_{bat} R_s \end{cases} \tag{4.8}$$

where u_0, R_s, R_c and C_c are estimated from experimental tests. Battery parameters are specified in Table 4.3.

TABLE 4.3 – Parameters of the developed battery model

Parameter	**Value**
Storage capacity (Q_{bat})	40 Ah
Nominal cell voltage ($V_{cell-nom}$)	3.35 V
Minimal cell voltage ($V_{cell-min}$)	2.5 V
Maximal cell voltage ($V_{cell-max}$)	4.2 V
Internal resistance (R_s)	0.028 Ω
Parallel resistor (R_c)	0.1417 Ω
Parallel capacity (C_c)	3529.4 F

Since there is no sensor that could read SOC directly, SOC is estimated here by ampere-hour counting (Coulomb counting) method. According to this technique, SOC can be calculated by integrating the current with respect to time [108], expressed as :

$$SOC_t = SOC_{t_0} + \eta \int_{t_0}^{t} \frac{i_\tau}{Q_{max}} d\tau \tag{4.9}$$

where η is the coulombic efficiency ($\eta < 1$ for charge and $\eta = 1$ for discharge), i_τ is the battery current at time instant τ ($i_\tau > 0$ for charge and $i_\tau < 0$ for discharge), and Q_{max} is the maximum available capacity.

In real driving conditions, battery degradation is featured by capacity fade and impedance rise. However, in the simulated case, a degradation model is required to quantify its degradation. Based on the literature review, high C-rate, temperature, deep discharge, as well as SOC range of charge/discharge cycle would have an influence of the battery's degradation [65, 68, 158, 175, 177]. However, in HEV applications, only the battery current C-rate ranging higher than ±15C will contribute to significant severity of degradation, therefore, the C-rate effect on battery ageing can be neglected if the C-rate remains at relatively low levels. In fact, as the battery utilized in the fuel cell HEV is served as a energy storage system, the typical current C-rates normally range between ±4C. An example of the C-rate profile of the studied fuel cell HEV in WLTC class 2 driving cycle is shown in Figure 4.6 and the C-rate distribution is shown in Figure 4.7. It could be seen that the C-rates rarely exceed 3C so that the C-rate will not have an significant influence on battery's degradation [65, 68, 175].

Therefore, SOC ranges and depth-of-discharge have been considered for modelling the battery degradation trends in capacity fade (D_{bat}) during the vehicle cycling operation :

$$D_{bat} = f(t, \Delta SOC, DOD) \tag{4.10}$$

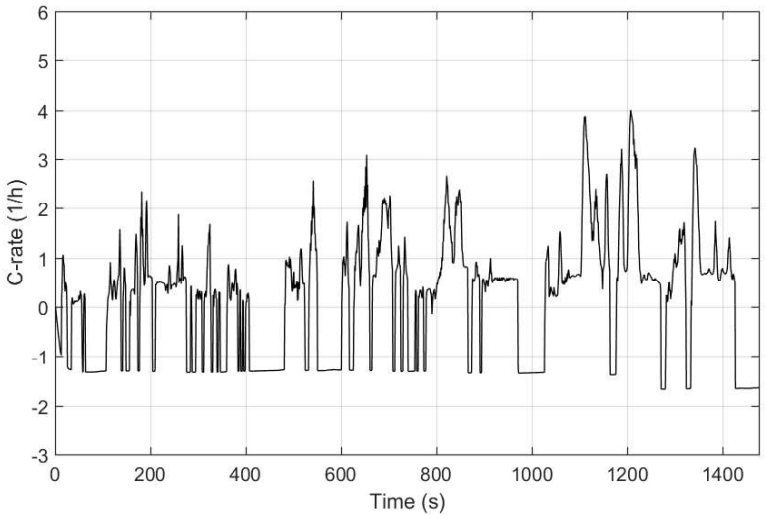

FIGURE 4.6 – C-rate profile of the studied fuel cell HEV in WLTC class 2 driving cycle

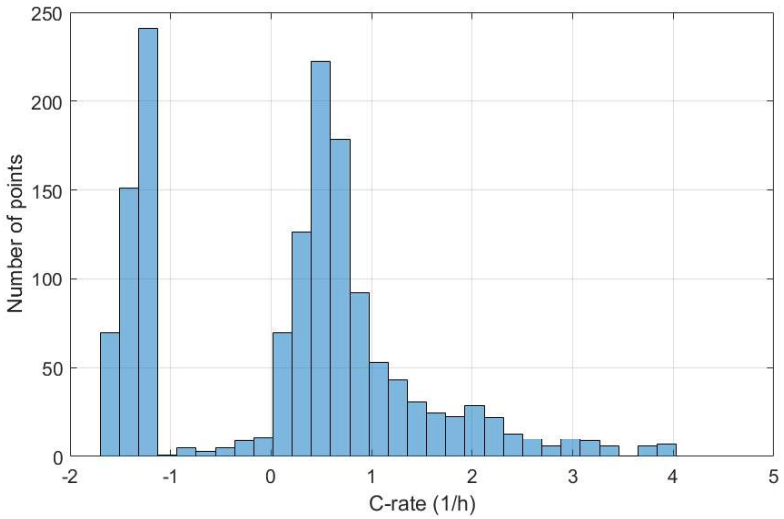

FIGURE 4.7 – C-rate distribution during WLTC class 2 driving cycle

4.2.6/ FUEL CELL SYSTEM MODELLING

The fuel cell system is composed of the PEM fuel cell, a smoothing inductor and a boost chopper for its current control. The function of the boost chopper is to step up the voltage generated by the fuel cell to the traction battery pack voltage. The smoothing inductor model and boost chopper model are represented by (4.11) and (4.12).

$$L\frac{d}{dt}i_{fc} = u_{fc} - u_{hfc} - r_L i_{fc} \tag{4.11}$$

$$\begin{cases} u_{hfc} = m_{hfc} u_{bat} \\ i_{hfc} = m_{hfc} i_{fc} \eta_{hfc} \end{cases} \tag{4.12}$$

where L and i_L are the inductance and resistance of the smoothing inductor, u_{hfc} and i_{hfc} are the chopper voltage and current, m_{hfc} is the modulation ratio of the fuel cell chopper and η_{hfc} is the efficiency of the chopper, $\eta_{hfc} = 0.95$.

To obtain the tuning variable m_{hfc}, (4.12) is written as :

$$m_{hfc} = \frac{u_{hfc-ref}}{u_{bat}} \tag{4.13}$$

where the reference chopper voltage is yielded by :

$$u_{hfc-ref} = -C_i(t)(i_{fc-ref} - i_{fc}) + u_{fc} \tag{4.14}$$

$C_i(t)$ is a PI controller.

Table 4.4 lists the specifications of the smoothing inductor and the boost chopper.

TABLE 4.4 – Smoothing inductor and boost chopper specifications

Parameter	**Value**
Inductance (L)	2.4375×10^{-4} H
Winding resistance (r_L)	0.0049 Ω
Boost chopper average input voltage (V_{in})	65 V
Boost chopper average output voltage (V_{out})	80 V
Boost chopper average efficiency (η)	95%

A fuel cell model is developed to calculate the voltage of the fuel cell stack dependent on its current. It can be considered as a voltage source deducing from its static polarization curve (see Figure 4.8) in order to maintain simplicity, written as :

$$u_{fc} = f(i_{fc}) \tag{4.15}$$

Besides, the fuel consumption is calculated by a static characteristic representing the H_2 mass flow versus current function (see Figure 4.9), written as :

$$\dot{m}_{H_2} = \int f(i_{fc})dt \tag{4.16}$$

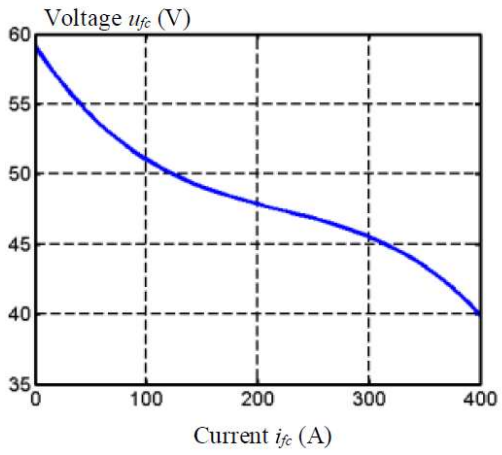

FIGURE 4.8 – Fuel cell polarization curve [140]

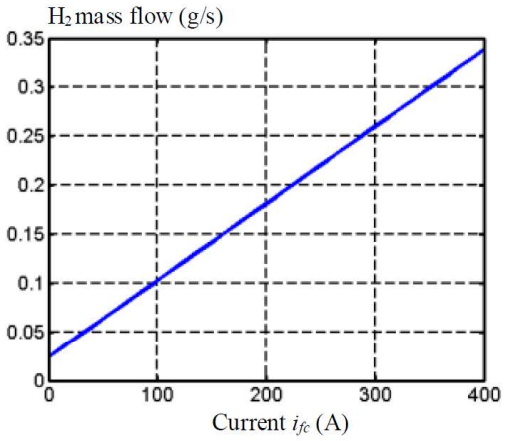

FIGURE 4.9 – H_2 mass flow vs. current curve [140]

The degradation of the fuel cell is made up of the degraded voltages due to the operation points and on/off switches [110, 142], written as :

$$V_{fc-degrade} = V_{ini} \cdot (1 - D_{fc} - D_{on/off}) \tag{4.17}$$

where

$$D_{fc} = \delta_0 \int f(1 + \frac{\alpha(P_{fc} - P_{nom})^2}{P_{nom}^2})dt \tag{4.18}$$

$$D_{on/off} = \begin{cases} \sum \Delta_{switch}, & \text{if } P_{fc,t} \geq 0 \wedge P_{fc,t-1} < 0 \\ 0, & \text{otherwise} \end{cases} \tag{4.19}$$

In (4.18) and (4.19), V_{ini} is the initial available fuel cell supplied voltage, P_{nom} is the nominal power of the fuel cell, α and δ_0 are the load coefficients and Δ_{switch} is the voltage loss coefficient for fuel cell's once switch. The specifications of the modelled fuel cell are listed in Table 4.5.

TABLE 4.5 – Fuel cell specifications

Parameter	Value
Fuel cell maximal power (P_{max})	16000 W
Fuel cell nominal power (P_{nom})	6000 W
Maximal fuel cell current (i_{fc-max})	400 A
Fuel cell voltage (u_{fc})	40-60 V
On/off degradation (Δ_{switch})	2.5×10^{-4}

4.2.7/ ENERGETIC MACROSCOPIC REPRESENTATION (EMR) OF THE VEHICLE

The hybrid electric vehicle is constructed in MATLAB®/Simulink® environment using Energetic Macroscopic Representation (EMR) toolbox, which is a graphical description for the definition of control schemes of complex energetic systems by considering their energetic exchanges between connected elements [67].

There are four basic elements to represent different energetic properties.

Source elements : The source elements are represented by green oval pictograms, which are the generators or receptors of the energy. In our system, there are battery and fuel cell using as source elements, whose input and output are current and voltage, respectively (see Figure 4.10).

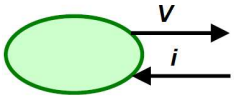

FIGURE 4.10 – EMR of energy source

Accumulation elements : The accumulation elements are represented by orange rectangles with an oblique bar. They accumulate internal energy (with or without loss), and therefore to fulfil the integral causality, their outputs are integral functions of their inputs. In our system, the smoothing inductor is an accumulator which can store energy and impose state variables (see Figure 4.11).

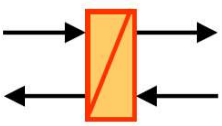

FIGURE 4.11 – EMR of accumulator

Conversion elements : The conversion elements are represented by orange squares (electrical or electromechanical conversion) in the pictograms (see Figure 4.12). They can convert energy without storage (with or without loss). For example, in our system, the boost chopper is an electrical conversion element which also possesses a tuning vector to manage the conversion of energy from the fuel cell to the bus. Besides, the traction

system is an electromechanical conversion element, which has converted the mechanical energy into electrical energy.

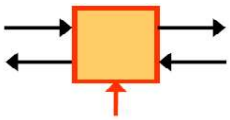

FIGURE 4.12 – EMR of conversion elements

Coupling elements : The coupling elements are represented by an overlapped orange pictogram, which distribute energy without accumulation (see Figure 4.13). In our system, the fuel cell is coupled to the battery by a boost chopper so that a coupling element is used to connect the boosted fuel cell voltage to the bus.

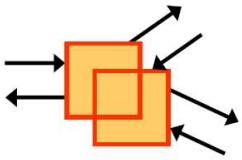

FIGURE 4.13 – EMR of coupling element

In addition to the elements, the EMR of the control scheme is depicted by blue parallelogram (see Figure 4.14), which can be defined using inversion rules. An accumulation element is inverted using closed-loop control, while the conversion elements can be directly inverted without control loop. Coupling elements are inverted using distribution inputs in order to define the distribution of energy within the system. Besides, an EMS is designed on a supervision level, which is used in order to define the local control references and the different distribution inputs to different energy sources.

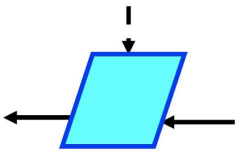

FIGURE 4.14 – EMR of control scheme

In order to reduce the complexity of the system, a reduced model has been constructed which dramatically reduces the computational burden required for the optimization process. In the reduced model, the reference velocity is calculated directly into reference demanded power so that it then becomes a backward-facing model where the feedback loop associated with the speed controller is removed. At last, the EMR of the studied vehicle is deduced from all the relationships presented in this section, as shown in Figure 4.15.

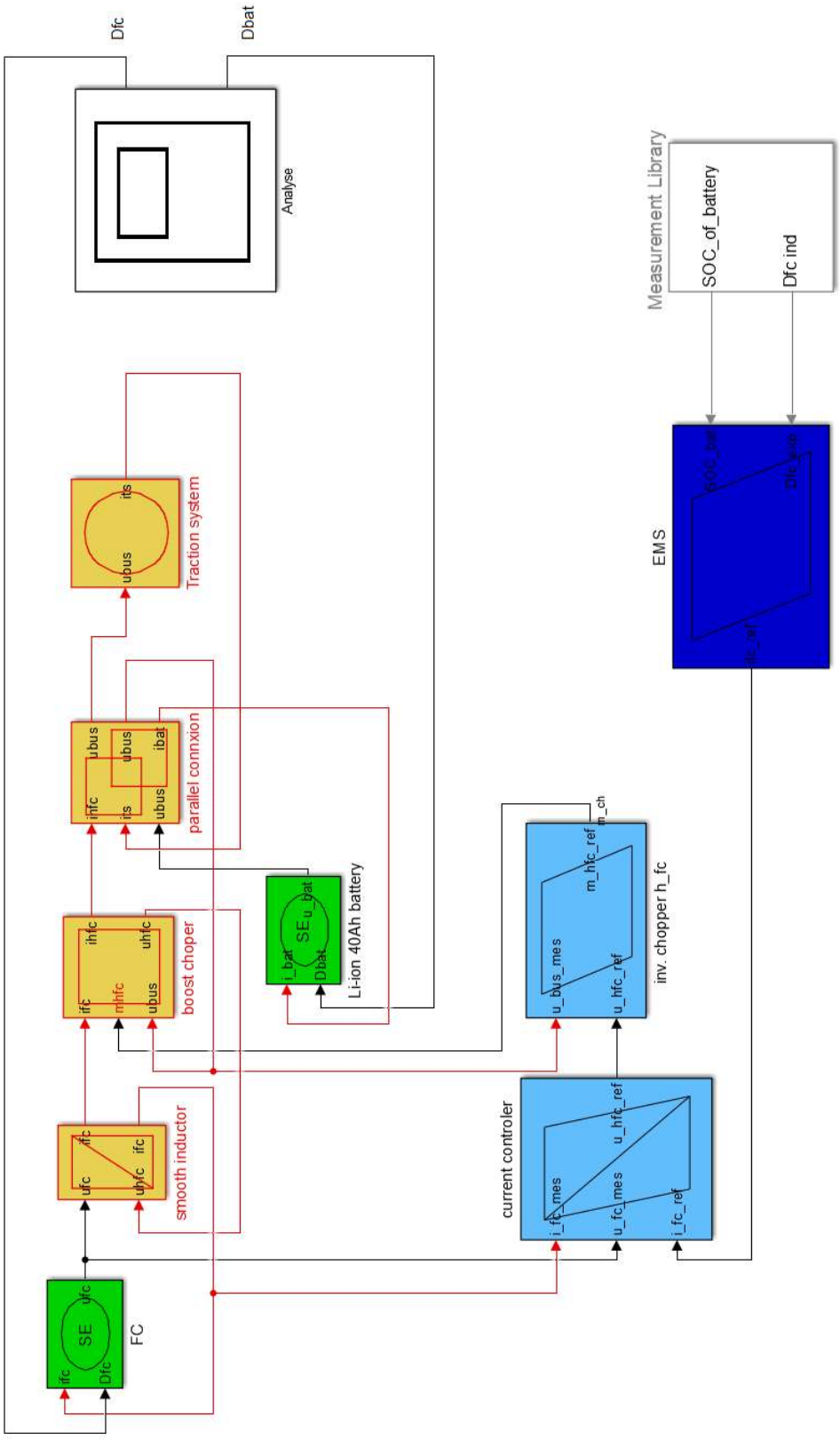

FIGURE 4.15 – EMR of the overall system

4.3/ BASELINE EMS DEVELOPMENT

EMS is a strategy to be designed in hybrid vehicles, which defines the amount of power that must be produced by the fuel cell and the battery. The objectives of EMS for electric vehicles could be consumption minimization, power source degradation mitigation, driving performance improvement, etc. In this thesis, it is the durability of the power sources, i.e. PEM fuel cells and lithium-ion battery pack, that is taken the dominant place. Therefore, the aim of the proposed controller is to increase power source lifetime and at the same time, save hydrogen consumption.

The EMS developed in this section is based on a fuzzy logic controller (FLC), which is a fuzzy rule-based strategy that could be implemented in real time without huge computation burden. To improve the optimality of the EMS, the membership functions of the FLC is tuned offline using genetic algorithm (GA).

4.3.1/ FUZZY LOGIC CONTROL STRATEGY

FLCs are intuitively easy to understand and allow the user to encapsulate the experience of experts in an efficient manner [10, 11]. In fact, fuzzy logic is a superset of conventional logic (Boolean), which was developed to address the concept of partially correct with respect to the value of true (1) and false (0) [10]. In FLC, the outputs are related to the inputs by IF-THEN rules which can be acquired by expert knowledge. Compared to other control strategies, fuzzy logic controller is favourable by [11] :

- Ability to translate imprecise/vague knowledge of human experts ;
- Simple, easy to implement technology ;
- Software design and hardware implementation support ;
- Results are easy to transfer from product to product ;
- Smooth controller behaviour ;
- Robust controller behaviour ;
- Ability to control unstable systems.

It should be noticed that, before designing the higher-level control loop corresponding to EMS, a first-order filter based controller (the smoothing inductor) is employed as the lower control loop to make sure the demanded power is followed and split the power between the battery and the fuel cell. That is to say, when sudden changes occur in the load power, the fuel cell still operates at its previous working point and the battery provides the difference [24, 39]. The fuel cell will take time to reach the desired power according to the current reference given by the EMS.

Therefore, the fuzzy logic controller used in our study is designed to meet the following durability objectives :

1. Maintaining the SOC of the lithium-ion battery in a reasonable range and limiting its cycling. The lower bound of the range is set to allow the battery to have adequate power for the traction system, while the higher bound of the range is set to allow the battery to recover the kinetic energy during the braking phase ;
2. Limiting the fuel cell operation dynamics to prolong its lifetime and making it work around the highest efficiency point to save hydrogen consumption ;

During implementation, the SOC of the battery is controlled to 75% as the optimal operation point, ensuring that the battery pack can both provide enough power for transient power demand and remain enough capability for regenerative braking. The efficiency of fuel cell usually reaches its highest in a range of 1/3 to 2/3 of its maximum power [178]. The output variable is the reference fuel cell current, which is normalized by its maximum current and described in the form of a triangle. The controller areas for the input and output are plot in Figure 4.16 and defined in Table 4.6 and 4.7.

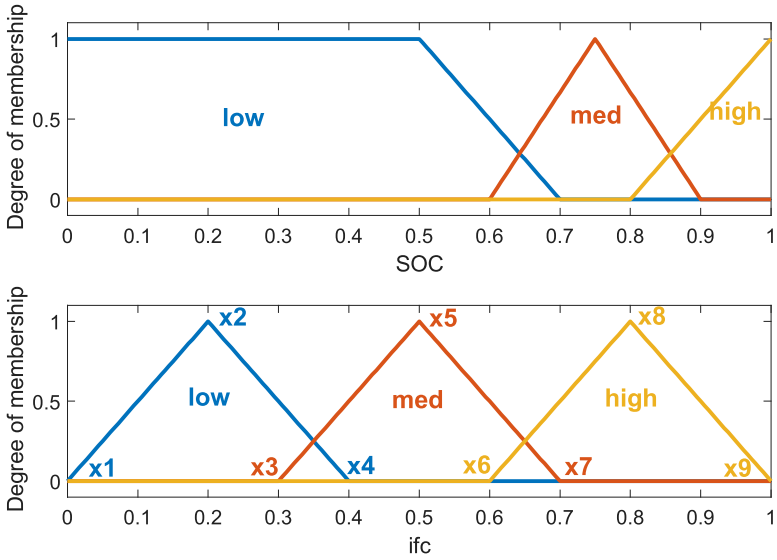

FIGURE 4.16 – Input and output control area of the FLC

The utilized rules are described as follows : when the SOC of the battery is low, fuel cell works at high current to recharge the battery ; when the SOC of the battery is good, fuel cell works at its optimal current to mitigate degradation ; and when the SOC of the battery is high, fuel cell works at low current to ensure the battery will not be overcharged. The sort of fuzzy system is Mamdani, while the inference mechanism is AND (minimum operator) and the diffuzication mode is centroid.

However, as discussed in the literature review, although the fuzzy logic controller is easy to implement in real time, it can hardly reach the optimal if the membership functions are designed without combining any optimization procedure [186]. Therefore, in this study, the parameters of the membership functions of the output fuel cell current ($[x_1,x_2,x_4]$, $[x_3,x_5,x_7]$, $[x_6,x_8,x_9]$) are going to be tuned by offline genetic algorithm optimization method described in the following section.

4.3.2/ GA OPTIMIZATION ADAPTED TO FLC

GA is an adaptive heuristic search algorithm based on the evolutionary ideas of natural selection and genetic processes where stronger individuals are likely the winners in a competing environment [22]. The basic principles of GA have first been proposed in [8] by Holland in 1975, which presumes that the potential solution of any problem is an individual and can be represented by a set of parameters. These parameters can be structured by a string of values in binary form and can be regarded as the genes of a chromosome [42].

TABLE 4.6 – Controller area of input SOC

Notation	Linguistic value	Fuzzy value
SOC_{lowmin}	SOC is considered to be low	0
SOC_{lowmax}		0.7
SOC_{medmin}	SOC is considered to be good	0.6
SOC_{medmax}		0.9
$SOC_{highmin}$	SOC is considered to be high	0.8
$SOC_{highmax}$		1

TABLE 4.7 – Controller area of output Ifc

Notation	Linguistic value	Fuzzy value
Ifc_{lowmin}	Fuel cell runs at low current	x_1
Ifc_{lowmax}		x_4
Ifc_{medmin}	Fuel cell runs at optimal current	x_3
Ifc_{medmax}		x_7
$Ifc_{highmin}$	Fuel cell runs at high current	x_6
$Ifc_{highmax}$		x_9

The potential of this chromosome is evaluated by a fitness function, which reflects how the goodness of the chromosome is related to the objectives. A set of selected chromosomes is called population and the population is subjected to generations (number of iterations). The population can be completed by a series of genetic operations : selection, crossover and mutation. After that, a new population called offspring with high fitness to the objective function is formed, which would give a better resolution than the previous generation [123]. After a number of generations, GA is expected to find a robust solution which is global optimal or close to the global optimal.

A general genetic algorithm works as follows [42] :

1. Initialize a randomly generated population of n chromosomes of binary form ;
2. Calculate the fitness of each chromosome according to the objective function ;
3. Select a pair of parent chromosomes from the current population while the probability of selection is an increasing function of fitness ;
4. Perform crossover to the pair with a crossover rate to form two offspring ;
5. Mutate the two offspring according to mutation rate and put the new chromosomes in the new population ;
6. Repeat 3, 4 and 5 until n offspring has been created ;
7. Replace the current population with the new one ;
8. Go to 2 and repeat the process until the generation limit is reached ;
9. Output the optimal solution ;

The advantage of GA is its potential of locating global optimum or near-global optimum solution without exhausted searching for all solution spaces. Besides, the processing time only increased as the square of the project size and not exponentially [123]. With its advantages, GA is widely used in the optimization problems in different fields of application :

design of adaptive systems, adaptive control, finite automation, determination of parameters for a series of neurons and fuzzy logic inferences [192].

GA could be well adaptive to the optimization of the fuzzy logic controller where all parameters of the membership functions are coded in one chromosome. In our case, the parameters of the membership functions of the output fuel cell current ($x1$-$x9$ in Figure 4.16) are offline optimized to satisfy a specified objective function on a given driving cycle. Here, the objective function aims to find a compromise between mitigating the fuel cell degradation and battery degradation. The objective function is written as (4.20).

$$ObjFun = w_1 \cdot D_{fc} + w_2 \cdot D_{bat} \tag{4.20}$$

where w_1 and w_2 are the weighting factors, D_{fc} and D_{bat} are the expressions of degradation defined in Section 4.2. The entire process of implementing GA optimization adapted to FLC is shown in Figure 4.17.

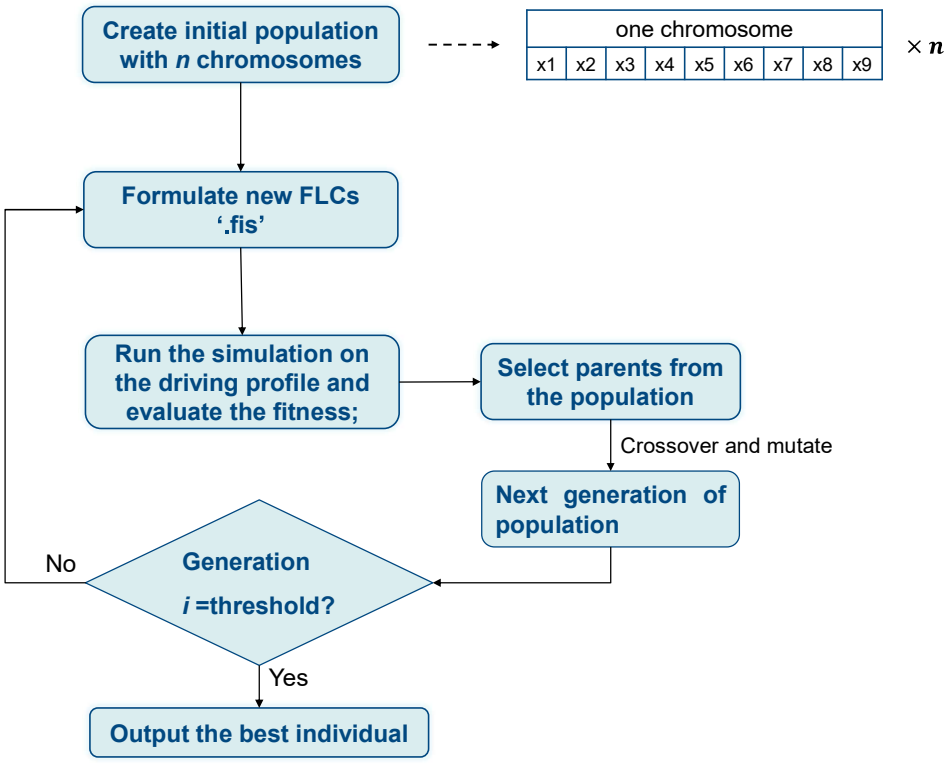

FIGURE 4.17 – FLC parameter optimization process based on GA

Genetic Algorithm Toolbox developed by University of Sheffield is used for our application, which is a MATLAB package within the framework of an existing CACSD package, especially capable in control systems engineering. It allows the retention of existing modelling and simulation tools for building objective functions and allows the user to make direct comparisons between genetic methods and traditional procedures [9]. The optimization results using this toolbox are presented in the next section.

4.3.3/ SIMULATION RESULTS DEMONSTRATION

The simulation is performed on a repeated driving profile WLTC class 2 described in Section 4.2. Its equivalent power demand is plot in Figure 4.18 (a) (the black dotted line). Through genetic algorithm, a new individual generation of membership function parameters for the FLC will output in each loop and the objective function values are compared to save the minimum one. This process is continued until reaching the specified generation numbers. The GA optimization results are compared with a non-optimized fuzzy logic controller in Figure 4.18. Figure 4.18 (a) is the power distribution result where it could be seen that the dynamics of the demanded power are mostly taken charge by the battery. Figure 4.18 (b) shows the optimization result by fuel cell power comparison. Compared to the non-optimized FLC, the optimized FLC has achieved more stable fuel cell operation and less variation to its nominal value. Battery SOC variation is compared in Figure 4.18 (c) where the optimized FLC controls the battery SOC to deviate less to its initial value. Figure 4.18 (d) and Figure 4.18 (e) calculate the accumulation of fuel cell degradation and battery degradation, respectively. It is indicated that the optimized FLC controls the system to cause less degradation of both the battery and the fuel cell. The fuel cell degradation has been mitigated to a large degree, by 97.4%, while battery degradation has been mitigated by 59.4%.

However, along with the degradation of the power sources, the optimized FLC will be no longer optimal to the degraded system. Although some real-time optimization-based strategies could calculate the optimal operation points along with the operation, the computation loads are huge and they cannot be easily compatible with the industrial use. Besides, the pre-defined degradation models in optimization-based strategies maybe not that accurate during the real operation and tend to result in inadequate operations. Therefore, in the next section, aiming at improving the durability of the power sources, a health-conscious EMS based on prognostics is proposed to catch the true degradation states of the power sources and make the corresponding corrective actions on the energy management in real time.

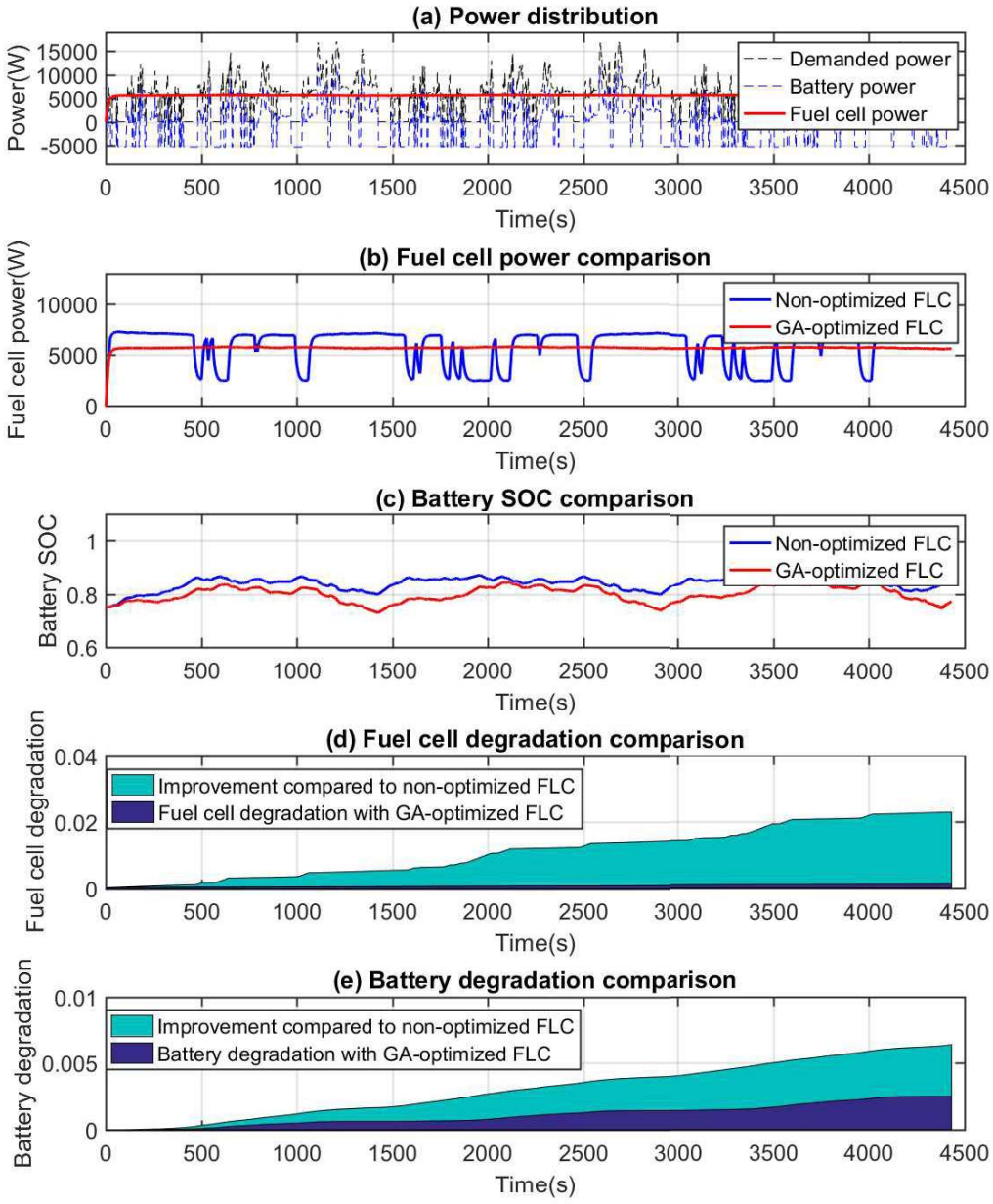

FIGURE 4.18 – GA-optimized FLC operation results compared to a non-optimized FLC : (a) Power distribution ; (b) Fuel cell power comparison ; (c) Battery SOC comparison ; (d) Fuel cell degradation comparison ; (e) Battery degradation comparison.

4.4/ HEALTH-CONSCIOUS EMS BASED ON PROGNOSTICS

The idea of the proposed health-conscious EMS is to find the optimal solutions under the different battery and fuel cell degradation cases indicated by prognostics. The optimization method introduced in the last section is a favourable way to find the optimal solution in control engineering, however, only a limited number of optimizations corresponding to different degradation cases could be performed offline. To solve this limitation, a decision-making process is developed to deal with the continuous degradation states in real time based on a series of classification and decision fusion methods.

4.4.1/ PROGNOSTICS-BASED DECISION-MAKING (PDM)

4.4.1.1/ LITERATURE BACKGROUND

As discussed in the literature review, PHM has been undergoing rapid development in recent years thanks to the sophisticated approaches in this field to estimate the system health information. Using prognostics information to extend the RUL of the system, improve reliability and increase the effectiveness can be referred as a prognostics-based decision-making (PDM) procedure [71]. However, researches on PDM and how to combine the prognostics health information to take actions haven't been completely investigated and are still in their early stages [61].

A few works on PDM developed for aeronautical and terrestrial vehicles have been proposed in the literature. Tang et al. have firstly proposed to use prognostics-enhanced control on the path planning of an unmanned ground vehicle [56]. RUL estimates are used as the constraints in the cost function of the path-planning algorithm and a PHM-enable automated contingency management (ACM) system is developed and tested, as shown in Figure 4.19. In order to perform PDM in a more general framework, mission planning case studies for an unmanned aerial vehicle for aeronautical applications have been implemented in [61, 71], in which the system model is a 'black box'. Afterwards, the demonstration of PDM algorithms on a hardware mobile robot platform has been done to deal with realistic fault scenarios in [106] and [72]. In addition to applying PDM in mission planning under electrical system faults, it can also be used to solve the routing problem. In [182], the prognostics algorithm is used to evaluate a set of feasible routes and the PDM procedure is applied to choose the route that consumes the least total travel cost.

4.4.1.2/ PDM STRUCTURE IN HEALTH-CONSCIOUS EMS DEVELOPMENT

As stated in [71], PDM can be defined as the process of selecting system actions based on the predictions of future system health states. While prognostics has been widely applied to the power sources, namely batteries and fuel cells, to estimate their current health state and estimate their future RULs, how to use the prognostics information in the procedure of designing EMS for HEVs has remained discussing. In order to take care of the power sources' durability, the structure of developing a health-conscious EMS is proposed in this section to give the basic ideas of how to combine PDM with energy management in vehicle control.

Based on the knowledge in Chapter 3, prognostics algorithm is able to estimate the future

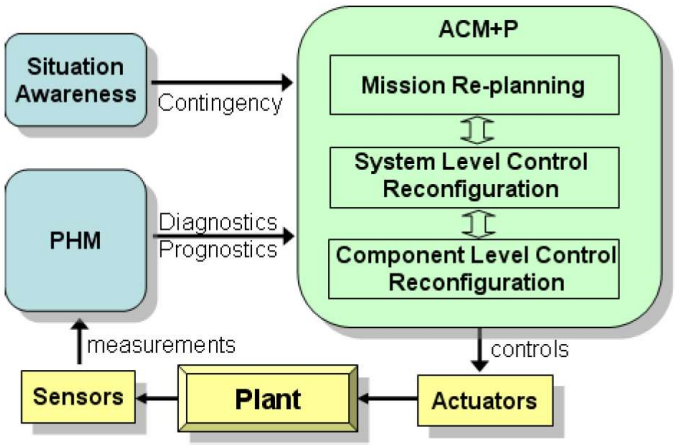

FIGURE 4.19 – PHM-enabled ACM system hierarchy [56]

states based on the previous degradation trend at each desired time instant. However, the degradation of power sources is a long-term procedure and there is no use to predict their RULs on short time scales, which will lead to huge computation burden and insufficient memory. Some researchers propose to define the time instants in order to indicate when to start performing the prognostics. According to [151], setting a threshold on the SOH to capture a performance drop may be one of the possible solutions. When it comes to implementing EMS, the key point is to select suitable action that is suitable for the current health state. Section 4.3 has described an effective health-conscious FLC that is tuned by offline GA optimization, however, the FLC cannot be tuned at each time instant and at each degradation state, which is not feasible and impossible to execute in real time. Therefore, a solution is proposed to optimize a limited number of FLCs under different degradation states offline and when RULs are obtained by the prognostics server, use a classifier to obtain the corresponding confidence factors to these degradation states. Then, a decision fusion method is applied to refine the online FLC parameters based on the classification results. A scheme of the structure of using PDM in the development of health-conscious EMS is demonstrated in Figure 4.20.

4.4.1.3/ HEALTH STATE CLASSIFICATION

In this study, three degradation states are defined for the fuel cell and the battery : no degradation, low degradation and high degradation. It is assumed that the battery reaches its EOL when the capacity degrades 30% [1, 93] and the fuel cell reaches its EOL when the power performance degrades 10% [190]. Therefore, ”No degradation” here refers that the performance of the battery and the fuel cell remains their original value, ”Low degradation” refers that the battery capacity degrades 12% and the fuel cell degrades 4% and ”High degradation” refers that the battery capacity degrades 24% and the fuel cell degrades 8%. It should be noted that the battery and the fuel cell may not degrade to the same degradation state since the battery usually has a longer lifetime than fuel cell, therefore, five degradation cases concurrently considering the degradation of both the battery and the fuel cell are listed in the following Table 4.8.

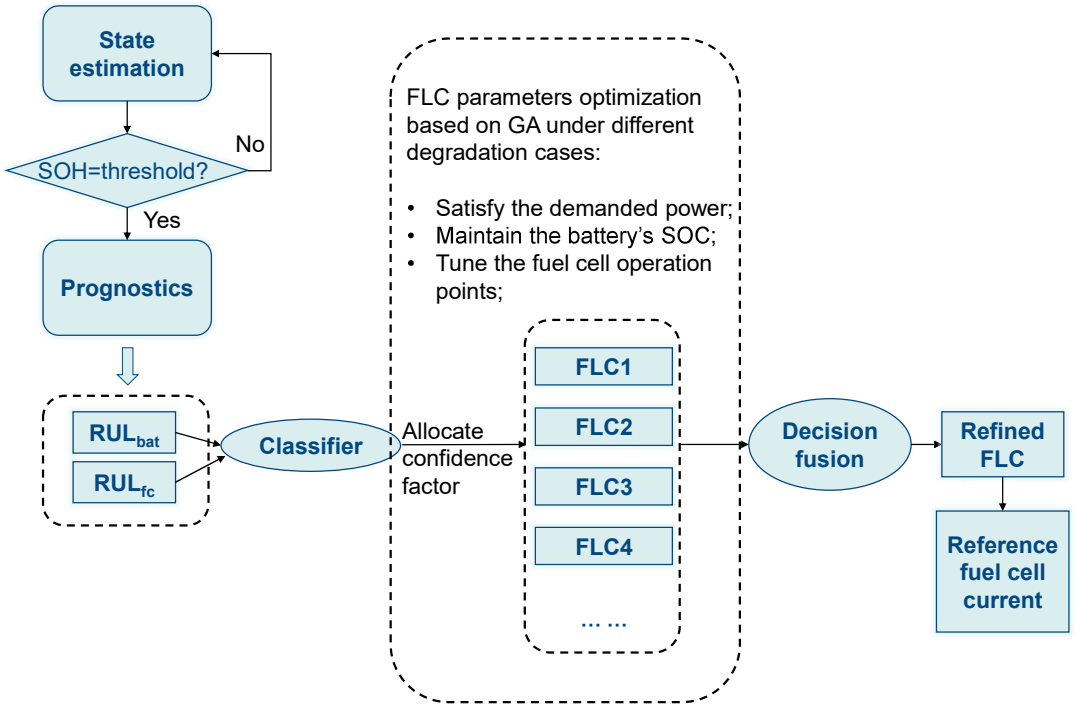

FIGURE 4.20 – Proposed structure of PDM for developing a health-conscious EMS

TABLE 4.8 – Five degradation cases of the hybrid system

Case No.	Fuel cell health state	Battery health state
1	No degradation	No degradation
2	Low degradation	No degradation
3	Low degradation	Low degradation
4	High degradation	Low degradation
5	High degradation	High degradation

After defining the five degradation cases, five GA-optimized FLCs are obtained offline under the corresponding cases. Despite the optimization done in the above section for the first no degradation case, the other four optimization results are plotted in Figure A.1 - Figure A.4 in Appendix A. The purpose of this offline optimization is to find the optimal solutions (i.e. the parameters of MFs) separately to different degradation states. However, the online operation is so complex and contains unprecedented changes that cannot be simply referred to a single degradation state as defined above for offline training. Therefore, to formulate the proper FLC that could be used for online operation, a fuzzy inference classifier is applied to obtain a probabilistic classification of the real-time degradation state. The degrees of resemblance are then fused by a decision fusion method based on Dempster-Shafer theory to elicit the best MF parameters for the online FLC. Details are given in the next section.

4.4.2/ FLC FORMULATION BASED ON DECISION FUSION

4.4.2.1/ FUZZY INFERENCE CLASSIFIER

Fuzzy inference classifiers have been widely applied in many fields, which have been proved promising tools that can offer high performance (classification rates) and computational efficiency [37]. The key point of a fuzzy inference classifier is to map the input space (the real-time estimated RULs) to an output space (five confidence factor values to the pre-defined degradation cases). To solve the problem that a certain value of RUL cannot unequivocally classify the degradation state in one case since the option to belong in the other cases should be possible. Thus, the set of RULs can be considered as a fuzzy set and fuzzy methods are appropriate to be applied to such a classification procedure.

The fuzzification of the inputs (RULs) is realized using three triangular-shaped and trapezoidal-shaped MFs, which corresponds to three degradation states : "No degradation", "Low degradation" and "High degradation". The vertices of the triangular and the trapezoidal are the approximated RUL values corresponding to the degradation state definition. On the other hand, there are five outputs and each consist of a Gaussian-shaped MF referred to the confidence factor value of the five degradation cases. The number and shape of the MFs were selected after an extensive set of preliminary tests that confirmed that the utilized MFs could present adequate qualitative results. For example, if the maximum RUL of the fuel cell is assumed as 1000 hours, the input MFs for the fuel cell degradation classifier are defined as follows :

High degradation :

$$MF_1(RUL) = \begin{cases} 1, & \text{if } 0 \leq RUL \leq 200 \\ 1 - \frac{RUL-200}{400}, & \text{if } 200 \leq RUL \leq 600 \\ 0, & \text{otherwise} \end{cases} \tag{4.21}$$

Low degradation :

$$MF_2(RUL) = \begin{cases} 1 - \frac{600-RUL}{400}, & \text{if } 200 \leq RUL \leq 600 \\ 1 - \frac{RUL-600}{400}, & \text{if } 600 \leq RUL \leq 1000 \\ 0, & \text{otherwise} \end{cases} \tag{4.22}$$

No degradation :

$$MF_3(RUL) = \begin{cases} 1 - \frac{1000-RUL}{400}, & \text{if } 600 \leq RUL \leq 1000 \\ 0, & \text{otherwise} \end{cases} \tag{4.23}$$

The MFs of the five outputs are Gaussian functions depending on two parameters, σ and c, which are given by :

$$MF_{output}(CF_n) = e^{\left(\frac{-(CF_n-c)^2}{2\sigma^2}\right)},\ n = 1, 2, 3, 4, 5 \tag{4.24}$$

where c and σ are the mean value and the variance, respectively. Here, the values c and σ are fixed at 1.

The control rules are defined according to Table 4.8 :

Rule1 : IF RUL is "No degradation", THEN CF_1 is calculated by MF_{output} ;
Rule2 : IF RUL is "Low degradation", THEN CF_2 is calculated by $MF_{output} \wedge CF_3$ is calculated by MF_{output} ;
Rule3 : IF RUL is "High degradation", THEN CF_4 is calculated by $MF_{output} \wedge CF_5$ is calculated by MF_{output}.

The structure of the proposed fuzzy inference classifier with the utilized MFs is represented in Figure 4.21. The classifier for the battery degradation is deduced with the same criteria as the fuel cell so that it will not be repeated here.

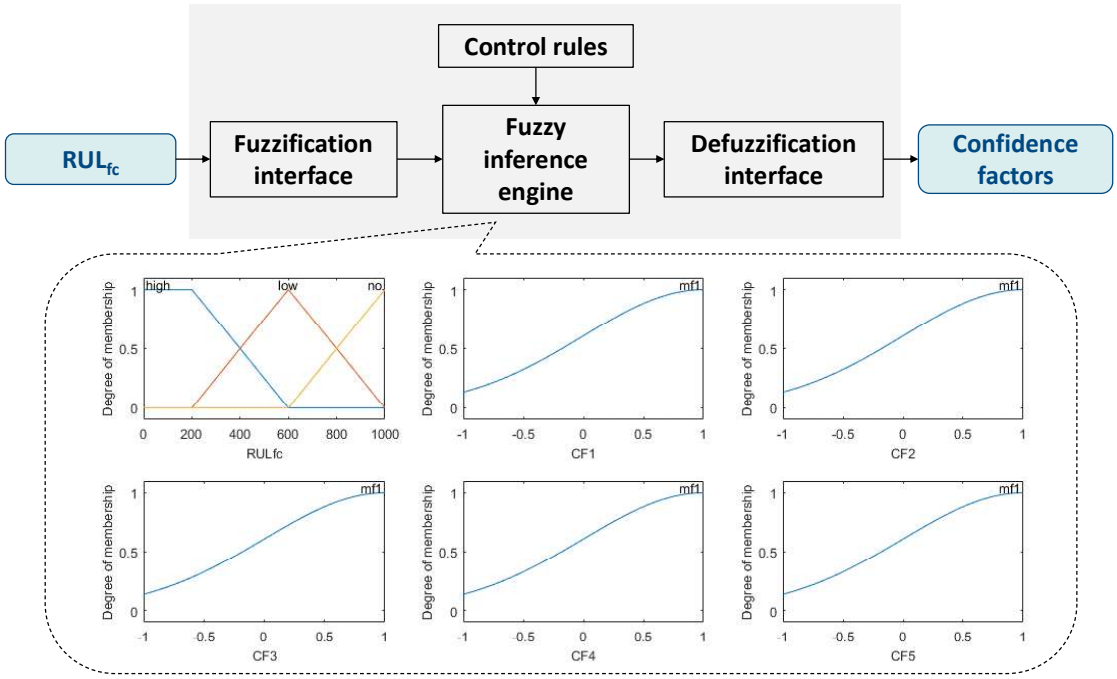

FIGURE 4.21 – Fuzzy inference classifier

Some of the classification results are demonstrated in Table 4.9.

TABLE 4.9 – Examples of classification results

$\hat{RUL}_{fc}$ (h)	CF1	CF2	CF3	CF4	CF5
884	0.59	0.22	0.22	0	0
568	0	0.8	0.8	0	0
418	0	0.45	0.45	0.38	0.38
345	0	0.29	0.29	0.53	0.53
173	0	0	0	1	1
...	...	...	...	...	...

Until now, for each input of prognostics result, i.e., RUL, five confidence factors are allocated to the pre-optimized FLCs under different degradation states. As explained above, in each FLC, there are three output MFs that have been optimized by GA. How to employ these confidence factors to the MFs is the next problem that will be solved by Dempster-Shafer decision fusion theory in the following sections.

4.4.2.2/ DECISION FUSION BASED ON DEMPSTER-SHAFER THEORY

Decision fusion is one of the three commonly used data fusion techniques whereas the other two are data association and state estimation [74]. It is a technique that fuses input decisions to obtain better or new decisions and aims to make a high-level inference about the events and activities that are produced from the previous detected targets [163]. There are two most common methods in decision fusion process : Bayesian method and Dempster-Shafer theory method. The Dempster-Shafer evidence theory is based on the mathematical theory introduced by Dempster and Shafer, which has generalized the Bayesian theory [6, 7]. The Dempster-Shafer evidence theory could be used to represent incomplete knowledge, updating beliefs, and a combination of evidence and allows to represent the uncertainty explicitly [74]. The main difference between Dempster-Shafer theory and other evidence theories is that the focal elements of a Dempster-Shafer structure can overlap each other, while the sum of the probability masses of the elements remains one [126].

The representation of the Dempster-Shafer theory is described as follows : a mutually exclusive and exhaustive element set is defined as $\Theta = \{\theta_1, \theta_2, ..., \theta_n\}$, which represents the all possible events. The elements of the set 2^Θ are called hypotheses. The basic probability assignment is given by a mass function $m : 2^\Theta \rightarrow [0, 1]$, which satisfies

$$m(\varnothing) = 0 \tag{4.25}$$

$$\sum_{A \in 2^\Theta} m(A) = 1 \tag{4.26}$$

where A is one of the hypotheses. A belief function $Bel : 2^\Theta \rightarrow [0, 1]$ defines the incomplete beliefs of one hypothesis :

$$Bel(A) = \sum_{B \subseteq A} m(B) \tag{4.27}$$

It is drawn from the sum of all the basic probability assignments of the subsets (B), belonging to the set of interest (A). When new evidence is available, a new mass function is obtained by a combination rule $m_1 \oplus m_2$, which combines the effects of two mass functions from different sources :

$$m(A) = m_1 \oplus m_2(A) = \frac{\sum_{B \cap C = A} m_1(B) m_2(C)}{1 - \sum_{B \cap C = \varnothing} m_1(B) m_2(C)} \tag{4.28}$$

4.4.2.3/ APPLYING DEMPSTER-SHAFER THEORY TO FLC FORMULATION

At first, the use of Dempster-Shafer theory to fuse offline optimization results is justified. The five optimized Ifc MFs under different degradation cases are shown in Figure 4.22. As described above, the first FLC has been optimized for case 1, however, one may not know if it works well with case 2. If the MF range of the first FLC contains the MF range of the second FLC, then one can say that the first FLC can also generate good results for the case 2. To take into account this situation, we consider the relationship between different FLCs with the help of Dempster-Shafer theory. It allows one to combine evidence from

different sources and arrive at a degree of belief that takes into account all the available evidences [126].

To apply Dempster-Shafer theory, it is necessary to determine the basic probability assignments ($m(A)$) and obviously, the above developed fuzzy inference classifier is a favourable method to get the degree of truth between 0 and 1. Therefore, using the basic probability assignments given by the classifier, one can combine the evidence from different degradation cases and calculate the belief measure value that takes into account all possible cases. It is done in a geometrical way. As seen in Figure 4.22, the shape of the five triangle MFs are geometrically different from each other. The ranges of the two sides (S1 and S2) of each triangle are compared in order to obtain the belief measures associated with each side.

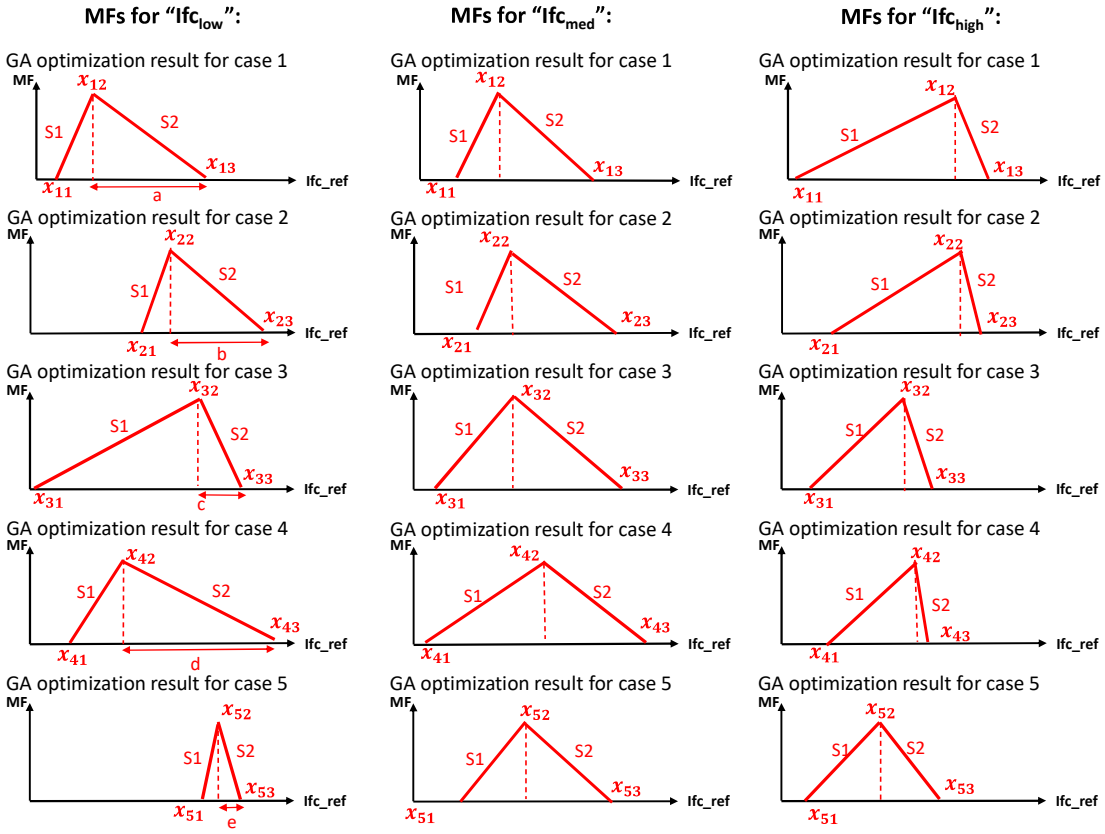

FIGURE 4.22 – Optimized Ifc MFs under different degradation cases

As indicated by (4.27), if the range of a side contains the range of other sides, the belief measure of this side should consider all the probabilities of the subsets. Using the MF of Ifc_{low} of case 2 as an example, in the first column of Figure 4.22, the range of S2 of the second MF (b) contains S2 of the third MF (c) and S2 of the fifth MF (e). However, It cannot cover the range of S2 of the first MF (a) and S2 of the fourth MF (d). As a result, the belief value of S2 of the first MF for case 2 is CF2+CF3+CF5. Other belief measure values are obtained using the same method and they are summarized in the third row of Table 4.10.

Then, to obtain the basic belief assignment m(A) for the MF of one case, a Möbius trans-

formation is used given the belief measure value of each side [28] :

$$m(A) = \sum_{B \subseteq A} (-1)^{|A-B|} Bel(B) \tag{4.29}$$

where $|A - B|$ represents the cardinality of $A - B$. Since the range of each side is defined by only two points, it is uncountable. Besides, in our case, the side ranges of the MFs are very small and the sizes of the ranges are relatively similar [178]. Therefore, (4.29) could be simplified as :

$$m(A) = \sum_{B \subseteq A} Bel(B) \tag{4.30}$$

Based on (4.30), the calculated basic probability assignments of confidence factors for the five degradation cases are listed in the fourth row of Table 4.10. The other two membership functions are calculated based on the refined confidence factors delicately defined in Table 4.11 and Table 4.12. Then, the dynamically adjusted parameters of the triangle MFs of the online FLCs are computed using a weighted arithmetic mean. To consider the health states of the fuel cell and the battery at the same time, the confidences to the two fuzzy logic MFs are considered by a weighted average method with different allocated weights. Therefore, the final MFs of the online used FLC are determined by the average weighted value of them.

TABLE 4.10 – Refined confidence factors of "Ifc_{low}" MFs

Degradation cases	**Case 1**		**Case 2**		**Case 3**		**Case 4**		**Case 5**	
Side	S1	S2	S1	S2	S1	S2	S1	S2	S1	S2
Belief measure value	CF1	CF1	CF2	CF2+CF3+CF5	CF3+CF1+CF2+CF4	CF3+CF5	CF4	CF4+CF2+CF3+CF5	CF5	CF5
Probability assignment	2CF1		2CF2+CF3+CF5		2CF3+CF1+CF2+CF4+CF5		2CF4+CF2+CF3+CF5		2CF5	

TABLE 4.11 – Refined confidence factors of "Ifc_{med}" MFs

Degradation cases	**Case 1**		**Case 2**		**Case 3**		**Case 4**		**Case 5**	
Side	S1	S2	S1	S2	S1	S2	S1	S2	S1	S2
Belief measure value	CF1	CF1	CF2	CF2+CF5	CF3+CF1+CF2	CF3+CF2+CF5	CF4+CF1+CF2+CF3+CF5	CF4+CF5	CF5+CF2	CF5
Probability assignment	2CF1		2CF2+CF5		2CF3+CF1+2CF2+CF5		2CF4+CF1+CF2+CF3+2CF5		2CF5+CF2	

TABLE 4.12 – Refined confidence factors of "Ifc_{high}" MFs

Degradation cases	**Case 1**		**Case 2**		**Case 3**		**Case 4**		**Case 5**	
Side	S1	S2	S1	S2	S1	S2	S1	S2	S1	S2
Belief measure value	CF1+CF3+CF4+CF5	CF1+CF2	CF2	CF2	CF3+CF4+CF5	CF3	CF4+CF5	CF4	CF5	CF5+CF4
Probability assignment	2CF1+CF2+CF3+CF4+CF5		2CF2		2CF3+CF4+CF5		2CF4+CF5		2CF5+CF4	

4.4.3/ SIMULATION RESULTS DEMONSTRATION

Simulations are carried out under MATLAB®/Simulink® environment. Due to memory limits, the simulation of the degradation process is accelerated based on the degradation trend obtained from the experiment results. The used WLTC class 2 driving cycle is repeated until 100 hours. Two simulations have been performed for the comparison. The first performed no prognostics and it operated with the baseline EMS all along the operation time regardless of the power source degradation. The other simulation implements the health-conscious EMS, which performed prognostics when the fuel cell drops 5% of its performance (10% loss of performance is regarded as fuel cell's EOL). According to the prognostics results, the real-time FLC was refined based on the above-described method and the simulation is stopped when the fuel cell reached its EOL.

The fuel cell power and battery SOC comparison results have been plotted in Figure 4.23 (a)-(d). Results showed that without considering degradation, the original FLC hasn't been tuned so it lost its optimality along with the system degradation and caused more fuel cell power dynamics and battery SOC decrease, as shown by the blue line in Figure 4.23. The health-conscious EMS tuned the FLC when the degradation of the fuel cell reaches 5% so that it lowered the power dynamics based on the current prognostics results and tried to maintain the battery SOC at a good level (red line in Figure 4.23). It could be seen in the zooming part when the prognostics happens that instead of operating with high dynamics, the fuel cell is tuned to find its good operation point again and the SOC of the battery is also starting to level up.

As it is assumed that the fuel cell reached its EOL when it lost 10% performance, the baseline EMS uses the fuel cell with too many dynamics so that it reached EOL much earlier than the health-conscious EMS. At the same time, the battery has degraded but can still be used when the fuel cell ends its life. By plotting the cumulative degradation of the fuel cell and the battery (Figure 4.24 (a)-(b)), it could be found that the health-conscious EMS has mitigated the degradation of the fuel cell prolonged the lifetime of the fuel cell by 42% approximately.

In real life, if the fuel cell degrades to its EOL in a hybrid system, there is no choice but to change the fuel cell to a new one. This will add extra cost. Now, it is assumed that the completed degraded fuel cell is replaced by a brand-new one while the battery could remain in use. The simulation is prolonged to calculate the economic cost by degradation. Results with fuel cell replaced are plotted in Figure 4.25.

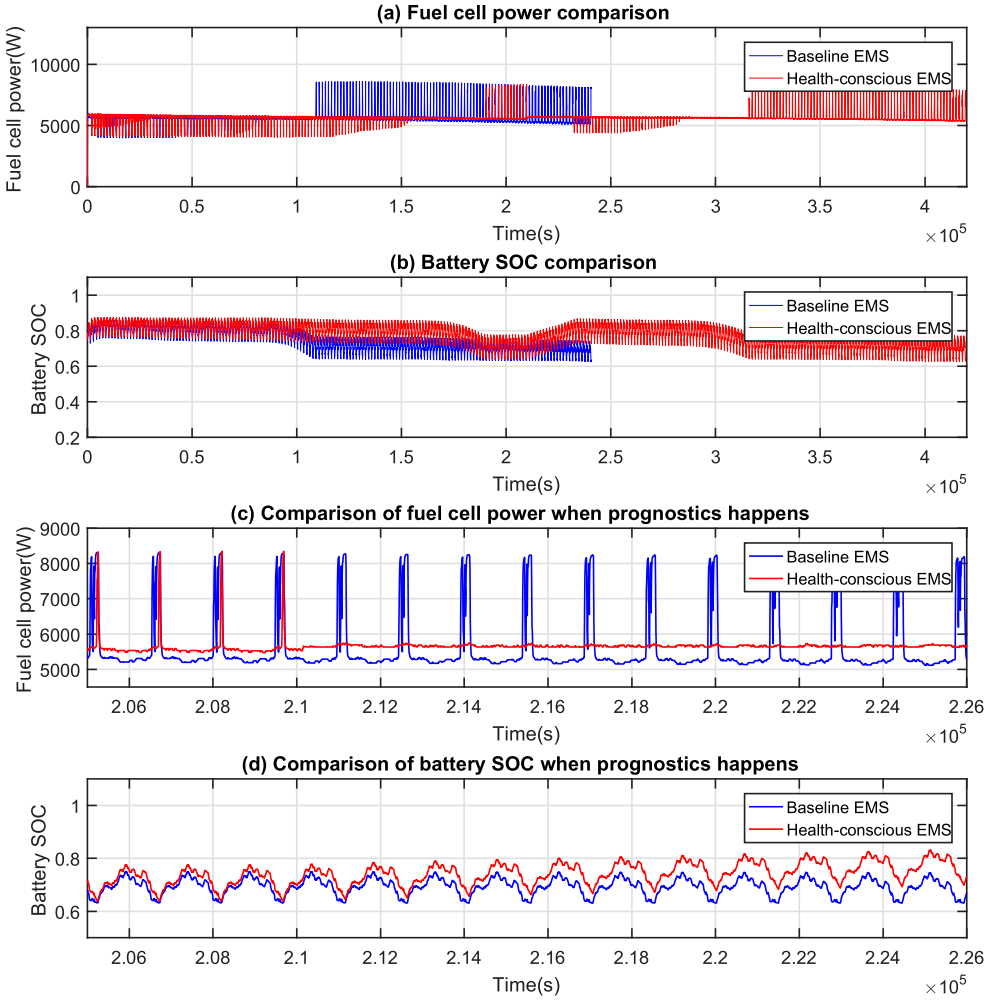

FIGURE 4.23 – Comparison results between baseline EMS and health-conscious EMS : (a) Fuel cell power comparison ; (b) Battery SOC comparison ; (c) Zooming part of the comparison of fuel cell power when prognostics happens ; (d) Zooming part of the comparison of battery SOC when prognostics happens.

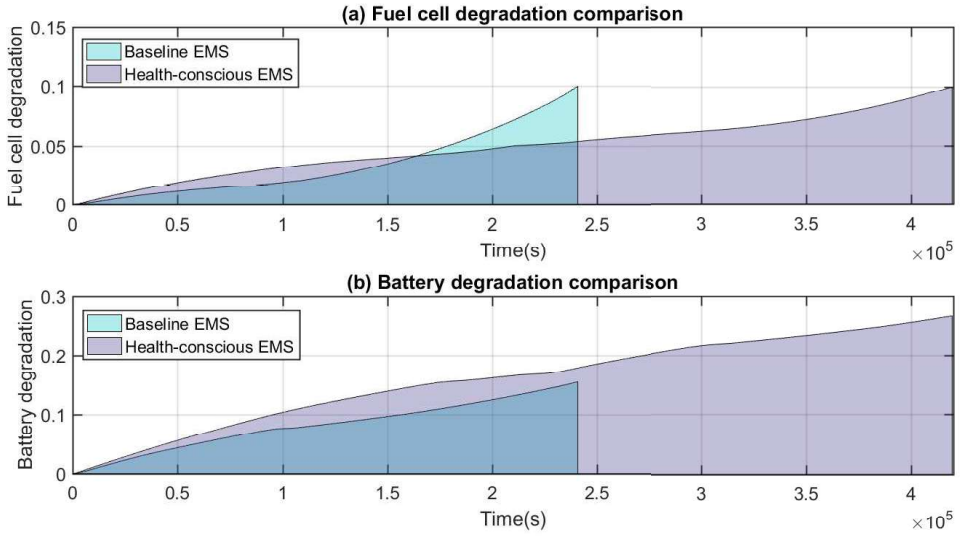

FIGURE 4.24 – Degradation comparison between baseline EMS and the proposed health-conscious EMS : (a) Comparison of fuel cell degradation ; (b) Comparison of battery degradation.

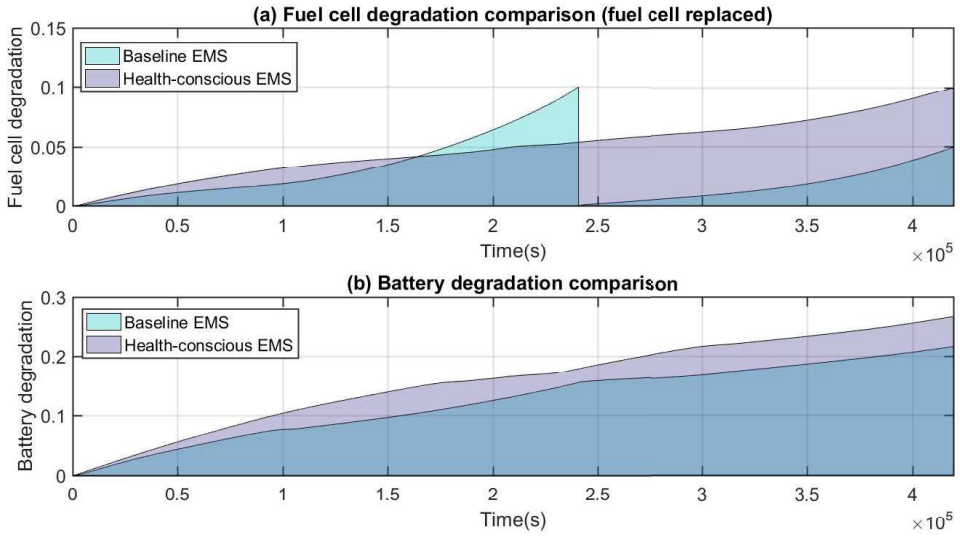

FIGURE 4.25 – Degradation comparison between baseline EMS and the proposed health-conscious EMS : (a) Comparison of fuel cell degradation (fuel cell replaced) ; (b) Comparison of battery degradation.

Based on 2020 automotive fuel cell system target defined by the US Department of Energy, the fuel cell costs 100 US dollars per kW [191]. The cost of the battery is fixed at 200 US dollars per kWh according to [128]. The second fuel cell with baseline EMS hasn't reached its EOL when the simulation stopped at the time point when the EOL of the fuel cell with health-conscious EMS is reached. Besides, both batteries in the two cases haven't reached their EOL. Therefore, the economic costs are calculated by compensating the unused part of fuel cell and battery (FC_{rest} and BAT_{rest}). They are compared in the following Table 4.13. Combining the degradation cost of both the fuel cell and the battery, the health-conscious EMS has effectively mitigated the degradation of the system and saves additionally the cost of maintenance caused by element replacements.

TABLE 4.13 – Comparison of the economic cost

Cost ($)	Fuel cells	Batteries	FC_{rest}	BAT_{rest}	Total
Baseline EMS	2*600	1*640	-303.6	-177.7	1358.7
Health-conscious EMS	1*600	1*640	0	-71.2	1168.8

4.4.4/ PROGNOSTICS OCCURRENCE DISCUSSION

In order to discover how prognostics occurrence will have an influence on mitigating the degradation, four more simulations have been performed with the prognostics happening at different frequencies. Except for the one defined above, another four simulations are executed where the prognostics is implemented whenever the fuel cell degrades by 1%, 2%, 3% and 4%, while the FLC is refined nine times, four times, three times and twice, respectively. The simulation is stopped whenever the fuel cell reached 10% degradation or the battery reached 30% degradation in order to compare the lifetime. This means that the battery and the fuel cell are not allowed to be replaced in these simulations and only one battery and one fuel cell are consumed ($600USD + 640USD = 1240USD$). The evolution of the measured fuel cell stack voltage is shown in Figure 4.26, which is smoothed and sampled and the evolution of the battery capacity degradation is shown in Figure 4.27.

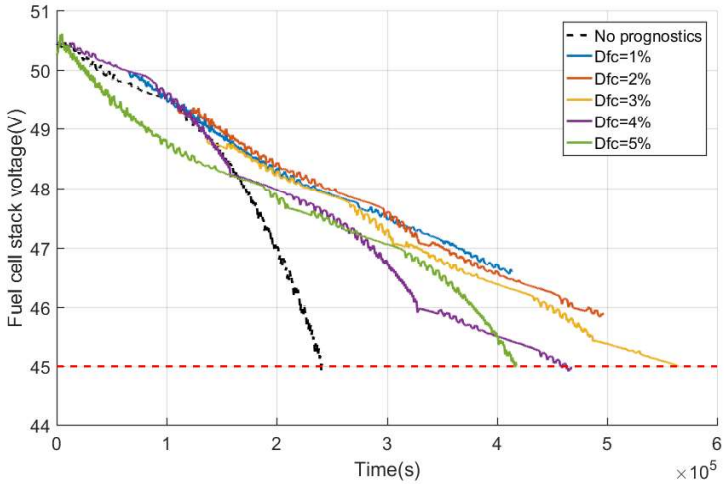

FIGURE 4.26 – Evolution of the measured fuel cell stack voltage

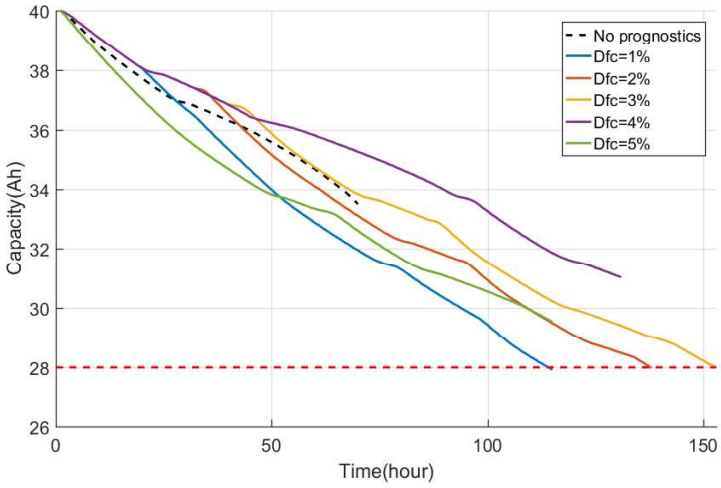

FIGURE 4.27 – Evolution of the measured battery capacity

As it could be seen from the results that the EMS without prognostics has reached the EOL of the fuel cell within 70 hours, while the other five EMSs with different prognostics occurrence frequencies have prolonged the lifetime of the system to different degrees. The EMSs with $\Delta D_{fc} = 1\%$, $\Delta D_{fc} = 2\%$ and $\Delta D_{fc} = 3\%$ have consumed the battery to its EOL before the EOL of the fuel cell, and the EMSs with $\Delta D_{fc} = 4\%$ and $\Delta D_{fc} = 5\%$ have reached the EOL of the fuel cell before the EOL of the battery. The comparison of the lifetime improvement is demonstrated in Figure 4.28. Compared to the baseline EMS, the proposed health-conscious EMSs with different prognostics occurrence frequencies can improve the lifetime of the hybrid system by at least 42.6% and the EMS3 with $\Delta D_{fc} = 3\%$ has reached the longest lifetime of the system, 56% longer than the baseline EMS.

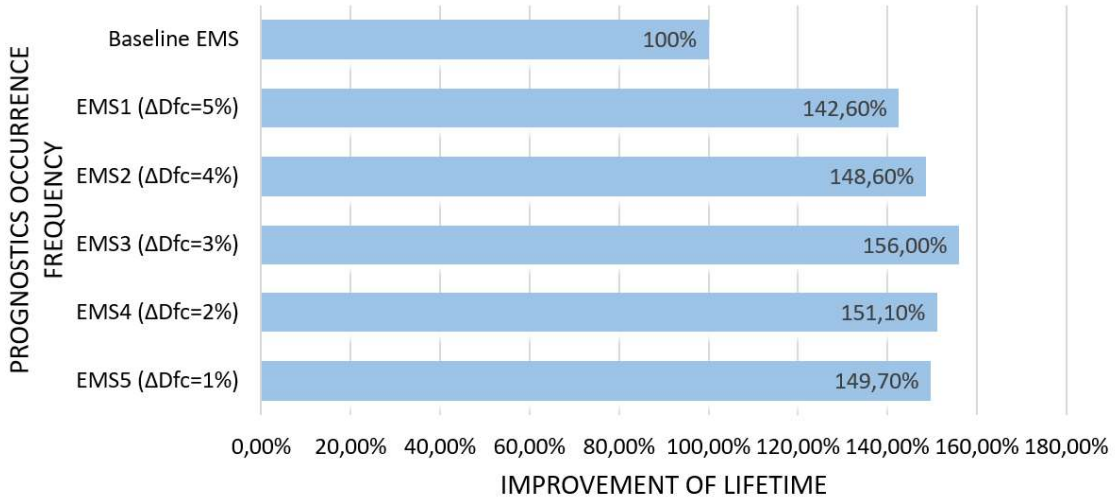

FIGURE 4.28 – Lifetime improvement comparison

However, it doesn't mean that frequent prognostics can lead to better performance of the hybrid system. As the battery and the fuel cell cannot degrade in the same manner, Table 4.14 quantified their degradation by cost and compared together with the lifetime improvement of different EMSs when the system reached its EOL.

TABLE 4.14 – Comparison of economic cost with different prognostics occurrence frequencies

	FC_{rest} ($)	BAT_{rest} ($)	Cost ($)	Lifetime improvement
Baseline EMS	0	-308.9	931.1	–
EMS 1 ($\Delta D_{fc} = 5\%$)	0	-71.2	1168.8	42.6%
EMS 2 ($\Delta D_{fc} = 4\%$)	0	-160.85	1079.1	48.6%
EMS 3 ($\Delta D_{fc} = 3\%$)	-19.8	0	1220.2	56.0%
EMS 4 ($\Delta D_{fc} = 2\%$)	-103.2	0	1136.8	51.1%
EMS 5 ($\Delta D_{fc} = 1\%$)	-183	0	1057	49.7%

Although the baseline EMS costs the least on the power source degradation, the fuel cell lost its functionality much earlier than the battery, which might cause extra maintenance or replacement cost, as discussed in the above section. EMSs with $\Delta D_{fc} = 5\%$ and $\Delta D_{fc} = 4\%$ consumes the fuel cell faster than the battery, while the EMS with $\Delta D_{fc} = 4\%$ saves more battery life and further improves the lifetime of the system, 48.6% compared to 42.6% when $\Delta D_{fc} = 5\%$. This is because the EMS with $\Delta D_{fc} = 4\%$ tuned the controller when the fuel cell degradation reached 4% and 8% while the EMS with $\Delta D_{fc} = 5\%$ tuned the controller only when the fuel cell degradation reached 5%. Therefore, it can be concluded that it is necessary to take into consideration the health state of the system when the fuel cell reaches high degradation so that the prognostics results could redirect the controller opportunely to avoid further degradation. EMSs with $\Delta D_{fc} = 3\%$, 2% and 1% tunes the controller more frequently according to the health state of the fuel cell and results show that the fuel cell degrades more slowly than the battery as the frequency of prognostics is getting higher. However, less cost on power source degradation doesn't mean longer system lifetime. The battery ends its life earlier when more consideration is taken on the fuel cell, which will lead to shorter system lifetime. Therefore, according to the results, too many times implementation of prognostics will not only add extra uncertainties to the health state prediction results but also shorten the entire system lifetime and add extra maintenance cost. Based on Table 4.14, the developed health-conscious EMS with $\Delta D_{fc} = 3\%$ is regarded to have the best performance with the highest lifetime improvement of 56%. Besides, further research emphasis could be placed on maintenance scheduling of the hybrid system based on health management.

The corresponding power distribution, battery SOC evolution and degradation evolution of both battery and fuel cell are plotted in Figure B.1 to Figure B.5 in Appendix B.

4.5/ SYNTHESIS

This chapter describes the contribution of developing an online health-conscious EMS for fuel cell HEVs, which is designed based on a prognostics-based decision-making process. Based on previous prognostics works, a simulation model of fuel cell HEV has been built in Matlab/Simulink environment. The power source degradation is simulated based on historical datasets. A prognostics-based decision-making process has been proposed, which refines the FLC through a health state classification and decision fusion approach. Results show that with an opportunely adjustable FLC, the degradation cost of the power sources has been mitigated and the lifetime of the system has been prolonged. Compared to existing health-conscious EMS, the proposed EMS has achieved online

auto-corrective control based on health state estimation and prediction. A comparison between the existing real-time optimization-based health-conscious EMSs that have been reviewed in Chapter 1 and the proposed health-conscious EMS is summarized in Table 4.15.

TABLE 4.15 – Comparison between the existing real-time optimization-based health-conscious EMSs and the proposed prognostics-based health-conscious EMSs

	Existing real-time optimization-based EMSs	Proposed prognostics-based EMS
Health state monitoring	Degradation knowledge is based on predefined models developed based on human expertise, which cannot react to the real driving conditions ;	Current health state and RULs are estimated online by prognostics based on prior observed monitored degradation data ;
decision-making process	The EMS is adjusted by solving the optimization problem at each step causing huge calculation burden ;	Decision is enabled by prognostics results by defining thresholds to reduce the redundancy of decisions ;
Optimality	Suboptimal due to the lack of global knowledge ;	Suboptimal due to error in decision-making process ;
Application	No long-term application yet ;	Long-term online operation capability ;

In fact, this study is a first trial of completing the PHM cycle for fuel cell HEV applications, which started from data collecting and data processing to online prognostics and complete the decision support at the end. However, this study is based on simulated data, real operation conditions haven't been considered. Besides, the optimality of the FLCs highly depends on the defined cost functions so that it can hardly reach the optimal point due to model limits. Further researches on hybrid system degradation observation and modelling and validations of the proposed EMS by experiments are expected in the future. Next chapter concludes all the previous chapters and limits and perspectives on the studied prognostics-based energy management are given at the end. Future works are expected in this field.

III

CONCLUSION

5

CONCLUSION AND PERSPECTIVES

This chapter concludes the research work by summarizing the issues addressed in this thesis. A discussion on the limits and possible future orientations is also laid out to go further on this subject.

5.1/ CONCLUSION

The works presented in this thesis are the contributions to the durability improvement of fuel cell/battery hybrid system. To do this, a cycle of PHM is realised in fuel cell HEV applications, i.e., not only the prognostics aspect but also the health management aspect, which is realised by developing an EMS based on prognostics results. To recapitulate, the main contributions are presented as follows :

The first chapter has provided a description of motivations and the general context of the subject of this research work. It has been pointed out that electric vehicles powered by the fuel cells are assumed to be a promising solution for the future's automotive market. The development of hybridizing fuel cell with other power sources, e.g., lithium-ion batteries, has been a polarizing topic for years. However, the unsatisfied lifetime of PEM fuel cell and batteries has been a common issue that impedes them from massive use in automobiles. To face this challenge, we have proposed to apply PHM in the health-conscious EMS design of HEVs. A framework of developing on-board prognostics-based health-conscious EMS, as well as the objectives and the methodology followed during the development of this work have been presented.

Then, in the second chapter, the possibility of hybridizing fuel cell with battery is justified and some generalities on PEM fuel cells and lithium-ion batteries are discussed. The operation principles and degradation mechanisms are presented, as well as their degradation modelling approaches that have existed in the literature of vehicle applications. Pros and cons are analyzed. As the PHM of fuel cell hybrid vehicles is still in a relatively early stage of development, prognostics methods based on state estimation are revealed to be the associated opportunities that can be combined with energy management to further improve the durability of the system.

The third chapter developed a particle filtering based prognostics algorithm for both PEM fuel cells and lithium-ion batteries. It is applied to historical datasets, which is a commonly used way in this field to interpret the power source degradation. As the prognostics results are expected to be used in the management aspect of PHM, we paid special attention to the evaluation of the prediction accuracy and precision. Besides, due to the fact that the

fuel cell health is indicated by its voltage drop, an investigation on different time scales is performed in order to see the possibility of saving online calculation cost and results have justified that a moderate time-scale has already satisfied performance and can be applied for online health state estimation and prognostics.

As a major contribution, the fourth chapter has presented the development of the proposed health-conscious EMS based on prognostics results, which is designed based on a decision-making process. It contributes to the improvement of the fuel cell hybrid system durability and has been validated on a simulated battery/fuel cell series hybrid system. Accelerated simulation has been implemented with repeated WLTC class 2 driving cycle for long-term operation. The key idea is to adjust the parameters of the fuzzy logic controller opportunely according to the current health state through classification and decision fusion approaches. An integrated PHM cycle has been realised in an early stage for the studied fuel cell HEV application. The process is shown in Figure 5.1. Results showed that the lifetime of the system has been considerably prolonged and the cost due to power source degradation has been mitigated.

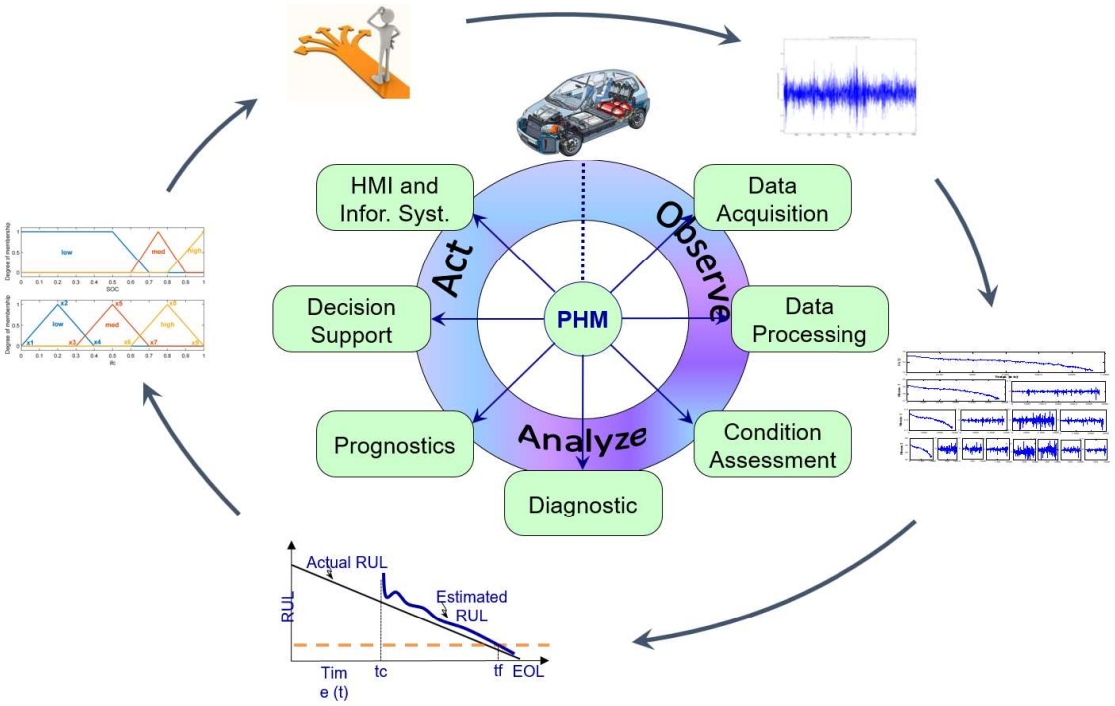

FIGURE 5.1 – PHM cycle realised in an early stage

5.2/ LIMITS OF THE CURRENT WORK

The work presented in this manuscript is oriented to formulate the entire PHM cycle and to make it work with energy management in fuel cell HEV applications. The results have shown an improvement on the system's durability and the mitigation of degradation cost. However, there are some limits that should be pointed out so that possible solutions could be come up.

— **Model dependence :** The particle filtering prognostics method developed in Chapter 3 is based on empirical models, however, the selection of models and the initia-

lization of model parameters can highly influence the prognostics results. As fuel cell is such a complex multi-physical system, fuel cell voltage can be a nonlinear function of current, stack temperature, the partial pressures of oxygen gas and the partial pressures of hydrogen gas inside the cell. The physical phenomenon involved in fuel cell ageing hasn't been well investigated for the moment and led to the difficulties in the selection of models. Besides, due to the uncertainties of on-board fuel cell operation, the degradation becomes more changeable and unpredictable. Improperly chosen models cannot well represent the degradation trend no matter how the parameters are calibrated.

— **RUL confidence :** The median RULs calculated according to the distribution of particles have been used online as the prognostics results to guide the following PDM process. However, the median RUL values cannot represent a hundred per cent confidence. RUL uncertainties have not been involved in the classification phase, instead, a classification method based on Gaussian-shaped fuzzy inference system is used.

— **Prognostics occurrence frequency :** The degradation states are roughly classified in the developed decision-making process and the frequency of prognostics occurrence is few tested (only five cases). However, in real operation conditions, more frequent actions should be taken and the result may be altered to the currently obtained one.

— **Optimality :** In Chapter 4, an offline optimization is realized by genetic algorithm. Due to the fact that the genetic algorithm is a global optimization approach, the driving cycle has to be known as prior knowledge. In this work, only one driving cycle is selected to obtain the optimized fuzzy logic controller under different degradation states. The influence of driving conditions is not taken into consideration.

— **Simulated data :** The obtained results of this work are based on simulation, where the degradation of the fuel cell and the battery are considered separately. Whether the interactions of the two power sources may have an influence on the degradation of each other hasn't been studied due to the lack of real hybrid system test data.

5.3/ PERSPECTIVES

Regarding the limits of this thesis, the following perspectives are proposed and worth considering to deepen the influence of this research.

1. Efforts should be made to enhance the results of prognostics that can be used to formulate the global PHM cycle. It should be independent of the operation conditions and predict the health state accurately and reliably. Studies have been done in the state of the art to develop the nonlinear physical models for the fuel cell system but the models are not general enough and the parameter characterization can always be an inevitable issue. To solve this problem, data-driven prognostics methods are increasingly considered in fuel cell PHM studies thanks to its model-free nature. Without any knowledge in physical or mechanical field, a data-driven prognostics method is expected to be developed to derive the behaviour model directly from the available data, while how to implement prognostics with limited datasets without sacrificing the robustness and reliability is still worth discussing. In fact, there are some data-driven methods existing in the literature that have been widely used in

fuel cell prognostics research [82, 104, 147, 148, 170, 180]. According to the author's recent results, a deep learning architecture has been proposed in recent works to implement fuel cell prognostics. The structure of the proposed method is shown in Figure 5.2, and the architecture used to train the data is based on stacked denoising autoencoder (SDA). However, more efforts are expected to integrate this method for the developed online PHM cycle.

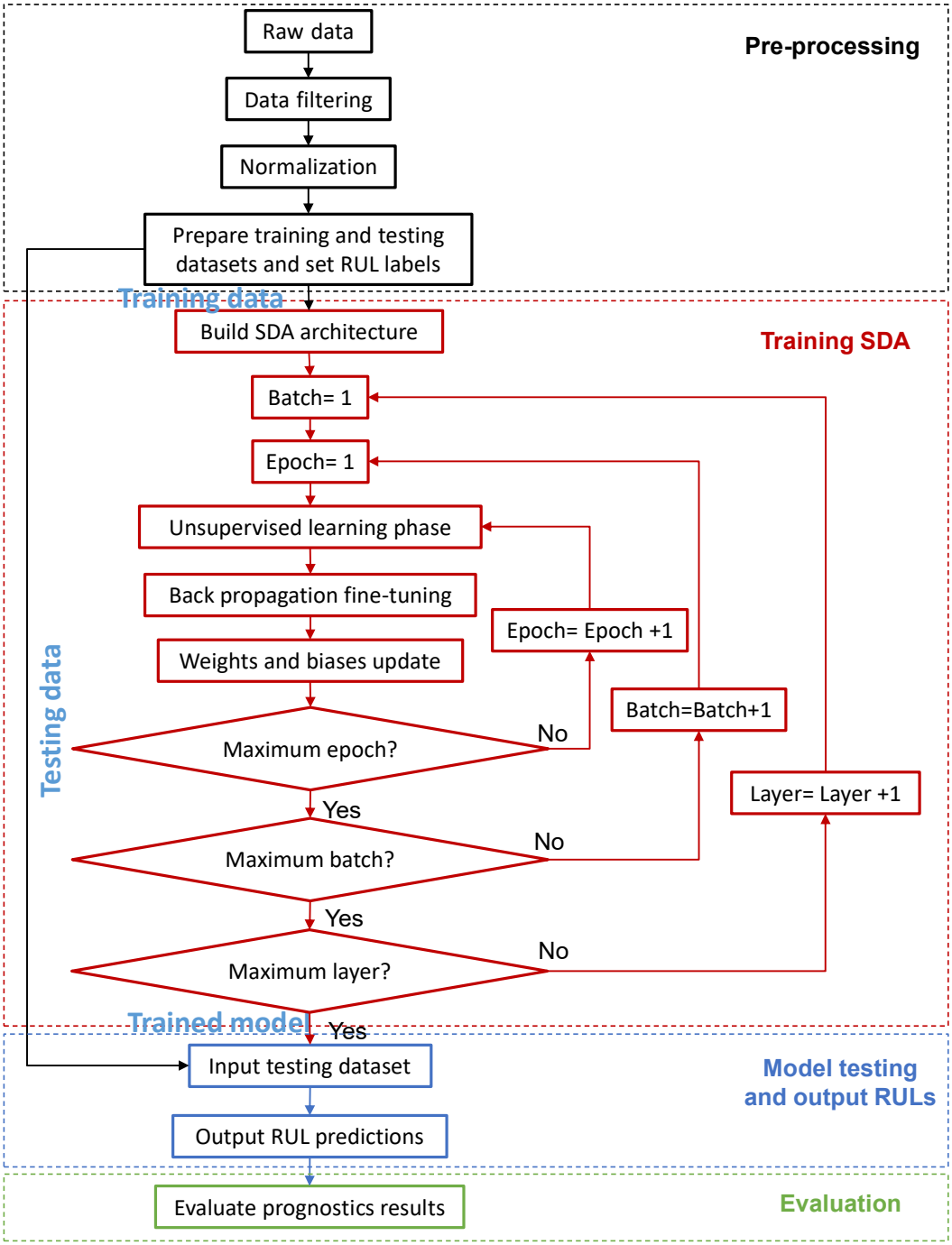

FIGURE 5.2 – Prognostics framework based on a deep learning architecture

2. Instead of modelling the prognostics uncertainties by fuzzy inference system in the

decision-making process, it is more reasonable to use the uncertainty of the RUL distribution to give the confidence factors to different degradation states, as shown in Figure 5.3, which can be easily obtained by the particle distribution when using particle filtering prognostics method. However, it requires high quality of prognostics performance, which is expected to be improved by the proposed deep learning prognostics method.

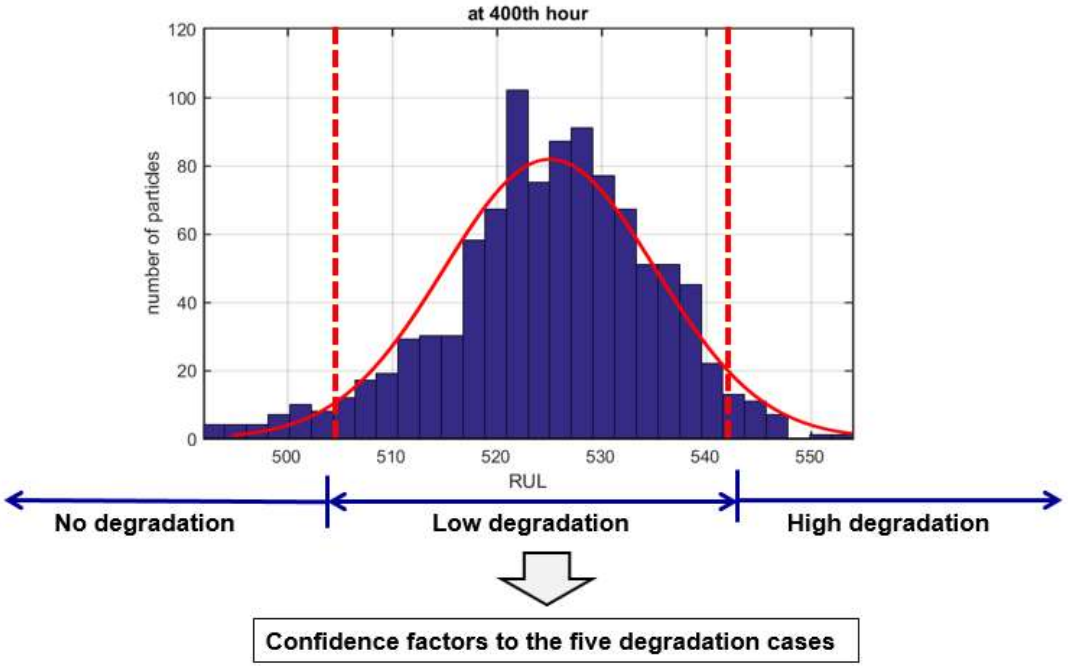

FIGURE 5.3 – Health state classification based on RUL uncertainty

3. A more detailed simulation with more variations on prognostics occurrence frequency is expected in future works using a more effective simulation tool or by simplifying the simulated model. As the focus of this thesis is to justify how to do immediate control towards the long-term degradation phenomenon, further investigations on decision support should be launched to enrich the developed framework.
4. More researches are expected to discover the variation of the results if the driving conditions are changed and to find a generalized solution that can help against this problem. Artificial intelligence methods, such as neural networks, model predictive control, etc. have been used in the literature to predict the driving conditions and can be promising methods to be combined in the optimization process.
5. The works implemented in this thesis are principally based on the simulated environment. A test campaign is expected to realize the results with real driving conditions and interactions in the hybrid system should be investigated. In fact, two field test platforms have been fabricated by our industrial partner H2SYS, the structures of which are demonstrated in Figure 5.4. Both of the two platforms are hybrid systems with a 600W fuel cell and a 24V battery connected in series by a DC/DC converter. The first hybrid system is fabricated with a simple battery management system (BMS) used for comparison and the second system is fabricated with an open supervisor, in which the developed prognostics-based health-conscious EMS could be coded and tested. Degradation of the power sources is going to be measured by their health indicators. Results are expected to be released in the author's

post-doctoral works and this kind of field tests is expected to allow much easier promotion of the developed technology into industry.

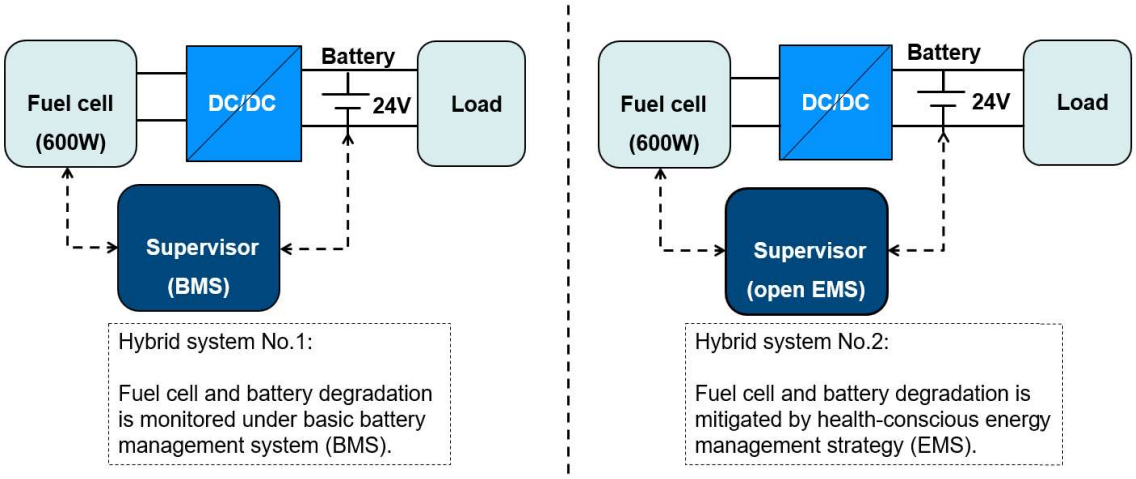

FIGURE 5.4 – Expected field test scenarios

6. Finally, it should be noticed that the EMS developed for the hybrid system, to its very nature, is an immediate control action. This thesis has tackled the problem that how to make immediate controls to avoid and to mitigate the degradation that appears as a long-term phenomenon. However, according to [151], to perform prognostics, phenomena with time constants greater than the hour are considered and the related maintenance scheduling and mission-replanning problem should be concerned in the decision support layer of PHM cycle. An illustration of decision policies is shown in Figure 5.5. To solve this problem, multi-criteria optimization, operational research techniques, combinatorial optimization (heuristics and meta-heuristics), case-based reasoning and knowledge-based reasoning are some promising methods that are worth studying. Besides, to implement control together with the scheduling and assignment problems is another underlying problem and should be considered to contribute to an integrated decision layer of PHM.

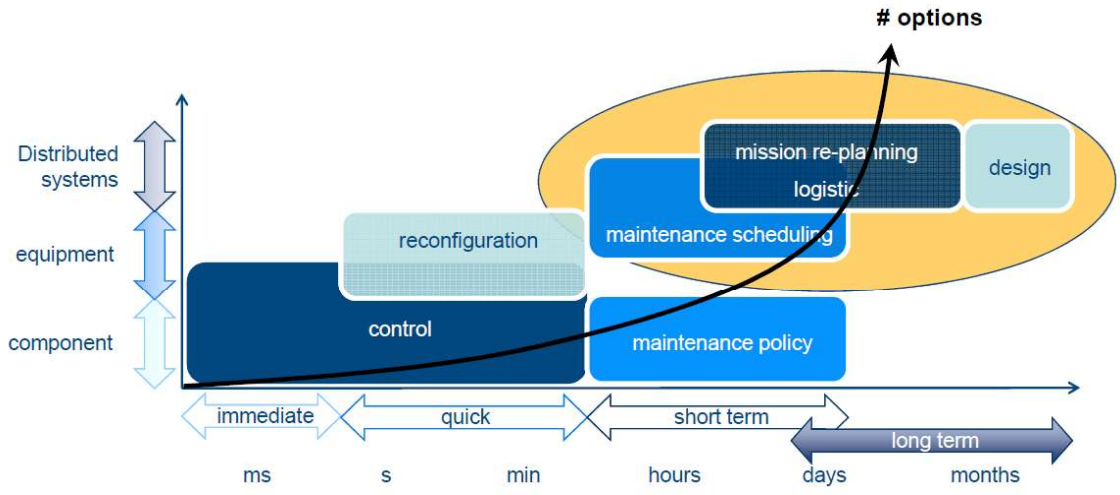

FIGURE 5.5 – Illustration of short/long-term decision policies [151]

BIBLIOGRAPHIE

[1] https://www.solarchoice.net.au/blog/tesla-powerwall-2-australia.

[2] **Development of high energy battery system with 300wh/kg (anl)**. https://www.energy.gov/eere/vehicles/annual-progress-reports.

[3] **Global energy & CO2 status report 2017**. https://www.iea.org/geco/.

[4] **Hydrogen roadmap europe : A sustainable pathway for the european energy transition**. https://www.fch.europa.eu/publications.

[5] **Mechanical properties at the protected lithium interface (ornl)**. https://www.energy.gov/eere/vehicles/annual-progress-reports.

[6] DEMPSTER, A. P. **A generalization of bayesian inference**. *Journal of the Royal Statistical Society : Series B (Methodological) 30*, 2 (1968), 205–232.

[7] SHAFER, G. **A mathematical theory of evidence**, vol. 42. Princeton university press, 1976.

[8] HOLLAND, J. H., AND OTHERS. **Adaptation in natural and artificial systems : an introductory analysis with applications to biology, control, and artificial intelligence**. MIT press, 1992.

[9] CHIPPERFIELD, A., FLEMING, P., AND M. FONSECA, C. **Genetic algorithm tools for control systems engineering**. *Proceedings of Adaptive Computing in Engineering Design and Control 23* (01 1994).

[10] COX, E. **The Fuzzy Systems Handbook : A Practitioner's Guide to Building, Using, and Maintaining Fuzzy Systems**. Academic Press Professional, Inc., San Diego, CA, USA, 1994.

[11] REZNIK, L. **Fuzzy controllers handbook : how to design them, how they work**. Elsevier, 1997.

[12] CHRISTEN, T., AND CARLEN, M. W. **Theory of ragone plots**. *Journal of Power Sources 91*, 2 (2000), 210 – 216.

[13] ARULAMPALAM, M. S., MASKELL, S., GORDON, N., AND CLAPP, T. **A tutorial on particle filters for online nonlinear/non-gaussian bayesian tracking**. *IEEE Transactions on Signal Processing 50*, 2 (Feb 2002), 174–188.

[14] PISANI, L., MURGIA, G., VALENTINI, M., AND D'AGUANNO, B. **A new semi-empirical approach to performance curves of polymer electrolyte fuel cells**. *Journal of Power Sources 108* (06 2002), 192–203.

[15] ISO13381-1. **Condition monitoring and diagnostics of machines e prognostics e part1 : general guidelines**. *International Organization for Standardization* (2004).

[16] PLETT, G. **Extended kalman filtering for battery management systems of lipb-based hev battery packs : Part 1. background**. *Journal of Power Sources 134* (06 2004), 252–261.

[17] PLETT, G. L. **Extended kalman filtering for battery management systems of lipb-based hev battery packs : Part 2. modeling and identification**. *Journal of Power Sources 134*, 2 (2004), 262 – 276.

[18] PLETT, G. L. **Extended kalman filtering for battery management systems of lipb-based hev battery packs : Part 3. state and parameter estimation**. *Journal of Power Sources 134*, 2 (2004), 277 – 292.

[19] VETTER, J., NOVÁK, P., WAGNER, M., VEIT, C., MÖLLER, K.-C., BESENHARD, J., WINTER, M., WOHLFAHRT-MEHRENS, M., VOGLER, C., AND HAMMOUCHE, A. **Ageing mechanisms in lithium-ion batteries**. *Journal of Power Sources 147*, 1 (2005), 269 – 281.

[20] CHEN, M., AND RINCON-MORA, G. A. **Accurate electrical battery model capable of predicting runtime and iv performance**. *IEEE transactions on energy conversion 21*, 2 (2006), 504–511.

[21] WANG, A., AND YANG, W. **Design of energy management strategy in hybrid vehicles by evolutionary fuzzy system part i : Fuzzy logic controller development**. In *2006 6th World Congress on Intelligent Control and Automation* (June 2006), vol. 2, pp. 8324–8328.

[22] ALCALA, R., ALCALA-FDEZ, J., AND HERRERA, F. **A proposal for the genetic lateral tuning of linguistic fuzzy systems and its interaction with rule selection**. *IEEE Transactions on Fuzzy Systems 15*, 4 (Aug 2007), 616–635.

[23] HISSEL, D., CANDUSSO, D., AND HAREL, F. **Fuzzy-clustering durability diagnosis of polymer electrolyte fuel cells dedicated to transportation applications**. *IEEE Transactions on Vehicular Technology, 56* (10 2007), 2414 – 2420.

[24] BOUQUAIN, D., BLUNIER, B., AND MIRAOUI, A. **A hybrid fuel cell/battery wheelchair — modeling, simulation and experimentation**. In *2008 IEEE Vehicle Power and Propulsion Conference* (Sep. 2008), pp. 1–6.

[25] CHANDRASEKARAN, R., BI, W., AND F. FULLER, T. **Robust design of battery/fuel cell hybrid systems—methodology for surrogate models of pt stability and mitigation through system controls**. *Journal of Power Sources 182* (08 2008), 546–557.

[26] DI DOMENICO, D., FIENGO, G., AND STEFANOPOULOU, A. **Lithium-ion battery state of charge estimation with a kalman filter based on a electrochemical model**. In *Control Applications, 2008. CCA 2008. IEEE International Conference on* (2008), Ieee, pp. 702–707.

[27] GOEBEL, K., SAHA, B., SAXENA, A., CELAYA, J., AND CHRISTOPHERSEN, J. **Prognostics in battery health management**. *Instrumentation and Measurement Magazine, IEEE 11* (09 2008), 33 – 40.

[28] LIU, L., AND YAGER, R. R. **Classic Works of the Dempster-Shafer Theory of Belief Functions : An Introduction**. Springer Berlin Heidelberg, Berlin, Heidelberg, 2008, pp. 1–34.

[29] MEINTZ, A., AND FERDOWSI, M. **Control strategy optimization for a parallel hybrid electric vehicle**. In *Vehicle Power and Propulsion Conference, 2008. VPPC'08. IEEE* (2008), pp. 1–5.

[30] PEI, P., CHANG, Q., AND TANG, T. **A quick evaluating method for automotive fuel cell lifetime**. *International Journal of Hydrogen Energy 33* (07 2008), 3829–3836.

[31] SAHA, B., AND GOEBEL, K. **Uncertainty management for diagnostics and prognostics of batteries using bayesian techniques**. In *2008 IEEE Aerospace Conference* (March 2008), pp. 1–8.

[32] SAXENA, A., CELAYA, J., BALABAN, E., GOEBEL, K., SAHA, B., SAHA, S., AND SCHWABACHER, M. **Metrics for evaluating performance of prognostic techniques**. In *2008 International Conference on Prognostics and Health Management* (Oct 2008), pp. 1–17.

[33] WU, J., YUAN, X.-Z., MARTIN, J., WANG, H., ZHANG, J., SHEN, J., WU, S., AND MÉRIDA, W. **A review of pem fuel cell durability : Degradation mechanisms and mitigation strategies**. *Journal of Power Sources 184* (09 2008), 104–119.

[34] ARCE, A., J. DEL REAL, A., AND BORDONS, C. **Mpc for battery/fuel cell hybrid vehicles including fuel cell dynamics and battery performance improvement**. *Journal of Process Control 19* (09 2009), 1289–1304.

[35] SAHA, B., AND GOEBEL, K. **Modeling li-ion battery capacity depletion in a particle filtering framework**. In *Proceedings of the Annual Conference of the Prognostics and Health Mngt Society* (01 2009), pp. 1–10.

[36] SAXENA, A., CELAYA, J., SAHA, B., SAHA, S., AND GOEBEL, K. **On applying the prognostic performance metrics**. In *Annual Conference of the Prognostics and Health Management Society (PHM09), San Diego, CA* (2009).

[37] ALVANITOPOULOS, P., ANDREADIS, I., AND ELENAS, A. **Fuzzy inference systems for automatic classification of earthquake damages**. vol. 339, pp. 368–375.

[38] BASHASH, S., MOURA, S., AND FATHY, H. **Charge trajectory optimization of plug-in hybrid electric vehicles for energy cost reduction and battery health enhancement**. In *Proceedings of the 2010 American Control Conference, ACC 2010* (08 2010), pp. 5824 – 5831.

[39] BLUNIER, B., SIMÕES, M. G., AND MIRAOUI, A. **Fuzzy logic controller development of a hybrid fuel cell-battery auxiliary power unit for remote applications**. In *2010 9th IEEE/IAS International Conference on Industry Applications - INDUSCON 2010* (Nov 2010), pp. 1–6.

[40] BUBNA, P., BRUNNER, D., GANGLOFF, J., ADVANI, S., AND PRASAD, A. **Analysis, operation and maintenance of a fuel cell/battery series-hybrid bus for urban transit applications**. *Journal of Power Sources 195* (06 2010), 3939–3949.

[41] FORMAN, J., BASHASH, S., STEIN, J., AND FATHY, H. **Reduction of an electrochemistry-based li-ion battery health degradation model via constraint linearization and padé approximation**. In *ASME 2010 Dynamic Systems and Control Conference, DSCC2010* (2010), vol. 2, pp. 173–183.

[42] MARTINEZ-SOTO, R., CASTILLO, O., AGUILAR, L. T., AND MELIN, P. **Fuzzy logic controllers optimization using genetic algorithms and particle swarm optimization**. In *Advances in Soft Computing* (Berlin, Heidelberg, 2010), G. Sidorov, A. Hernández Aguirre, and C. A. Reyes García, Eds., Springer Berlin Heidelberg, pp. 475–486.

[43] SAXENA, A., CELAYA, J., SAHA, B., SAHA, S., AND GOEBEL, K. **Metrics for offline evaluation of prognostic performance**. *International Journal of Prognostics and Health Management 1*, 1 (2010), 4–23.

[44] ZHAO, H., AND BURKE, A. **Effects of different powertrain configurations and control strategies on fuel economy of fuel cell vehicles**. In *The 25th World Battery, Hybrid and Fuel Cell Electric Vehicle Symposium and Exhibition* (2010).

[45] BASHASH, S., MOURA, S., C. FORMAN, J., AND K. FATHY, H. **Plug-in hybrid electric vehicle charge pattern optimization for energy cost and battery longevity**. *Journal of Power Sources 196* (01 2011), 541–549.

[46] BAYINDIR, K., ALI GÖZÜKÜÇÜK, M., AND TEKE, A. **A comprehensive overview of hybrid electric vehicle : Powertrain configurations, powertrain control techniques and electronic control units**. *Energy Conversion and Management 52* (02 2011), 1305–1313.

[47] CAPIZZI, G., BONANNO, F., AND NAPOLI, C. **Recurrent neural network-based control strategy for battery energy storage in generation systems with intermittent renewable energy sources**. In *Clean Electrical Power (ICCEP), 2011 International Conference on* (2011), IEEE, pp. 336–340.

[48] CELAYA, J., SAXENA, A., SAHA, S., AND GOEBEL, K. **Prognostics of power mosfets under thermal stress accelerated aging using data-driven and model-based methodologies**. *Proceedings of International Conference on Prognostics and Health Management, Montreal 2* (01 2011).

[49] FERNÁNDEZ-RAMÍREZ, L., GARCIA-TRIVIÑO, P., GARCIA, C., AND JURADO, F. **Hybrid electric system based on fuel cell and battery and integrating a single dc/dc converter for a tramway**. *Energy Conversion and Management 52* (05 2011), 2183–2192.

[50] HE, W., WILLIARD, N., OSTERMAN, M., AND PECHT, M. **Prognostics of lithium-ion batteries based on dempster–shafer theory and the bayesian monte carlo method**. *Journal of Power Sources 196* (12 2011), 10314–10321.

[51] HOKE, A., BRISSETTE, A., MAKSIMOVIC, D., PRATT, A., AND SMITH, K. **Electric vehicle charge optimization including effects of lithium-ion battery degradation**. In *IEEE Vehicle Power and Propulsion Conference* (10 2011), pp. 1 – 8.

[52] MICEA, M. V., UNGUREAN, L., CARSTOIU, G. N., AND GROZA, V. **Online state-of-health assessment for battery management systems**. *IEEE Transactions on Instrumentation and Measurement 60*, 6 (June 2011), 1997–2006.

[53] ONANENA, R., OUKHELLOU, L., CANDUSSO, D., HAREL, F., HISSEL, D., AND AKNIN, P. **Fuel cells static and dynamic characterizations as tools for the estimation of their ageing time**. *International Journal of Hydrogen Energy 36* (01 2011), 1730–1739.

[54] REMMLINGER, J., BUCHHOLZ, M., MEILER, M., BERNREUTER, P., AND DIETMAYER, K. **State-of-health monitoring of lithium-ion batteries in electric vehicles by on-board internal resistance estimation**. *Journal of Power Sources 196* (06 2011), 5357–5363.

[55] SIKORSKA, J., HODKIEWICZ, M., AND MA, L. **Prognostic modelling options for remaining useful life estimation by industry**. *Mechanical Systems and Signal Processing 25*, 5 (2011), 1803 – 1836.

[56] TANG, L., HETTLER, E., ZHANG, B., AND DECASTRO, J. **A testbed for real-time autonomous vehicle phm and contingency management applications**. In *Annual conference of the prognostics and health management society* (2011), pp. 1–11.

[57] VENERI, O., MIGLIARDINI, F., CAPASSO, C., AND CORBO, P. **Dynamic behaviour of li batteries in hydrogen fuel cell power trains**. *Journal of Power Sources 196*, 21 (2011), 9081 – 9086.

[58] WANG, J., LIU, P., HICKS-GARNER, J., SHERMAN, E., SOUKIAZIAN, S., VERBRUGGE, M., TATARIA, H., MUSSER, J., AND FINAMORE, P. **Cycle-life model for graphite-lifepo 4 cells**. *Journal of Power Sources 196* (04 2011), 3942–3948.

[59] ZIO, E., AND PELONI, G. **Particle filtering prognostic estimation of the remaining useful life of nonlinear components**. *Reliability Engineering & System Safety 96*, 3 (2011), 403 – 409.

[60] AN, D., CHOI, J.-H., AND KIM, N. **A tutorial for model-based prognostics algorithms based on matlab code**. *Proceedings of the Annual Conference of the Prognostics and Health Management Society 2012, PHM 2012* (01 2012), 224–232.

[61] BALABAN, E., AND ALONSO, J. **An approach to prognostic decision making in the aerospace domain**. *Proceedings of the Annual Conference of the Prognostics and Health Management Society 2012, PHM 2012* (01 2012), 396–415.

[62] EBBESEN, S., ELBERT, P., AND GUZZELLA, L. **Battery state-of-health perceptive energy management for hybrid electric vehicles**. *Vehicular Technology, IEEE Transactions on 61* (09 2012), 2893–2900.

[63] GITTLEMAN, C. S., COMS, F. D., AND LAI, Y.-H. **Chapter 2 - membrane durability : Physical and chemical degradation**. In *Polymer Electrolyte Fuel Cell Degradation*, M. M. Mench, E. C. Kumbur, and T. N. Veziroglu, Eds. Academic Press, Boston, 2012, pp. 15 – 88.

[64] MARTÍNEZ, J. S., JOHN, R. I., HISSEL, D., AND PÉRA, M.-C. **A survey-based type-2 fuzzy logic system for energy management in hybrid electrical vehicles**. *Information Sciences 190* (2012), 192 – 207.

[65] ONORI, S., SPAGNOL, P., MARANO, V., GUEZENNEC, Y., AND RIZZONI, G. **A new life estimation method for lithium-ion batteries in plug-in hybrid electric vehicles applications**. *Int. J. of Power Electronics 4* (01 2012), 302 – 319.

[66] PYTEL, K. **The fuzzy genetic system for multiobjective optimization**. In *2012 Federated Conference on Computer Science and Information Systems (FedCSIS)* (Sept 2012), pp. 137–140.

[67] ROBOAM, X. **Systemic design methodologies for electrical energy systems : analysis, synthesis and management**. John Wiley & Sons, 2012.

[68] TODESCHINI, F., ONORI, S., AND RIZZONI, G. **An experimentally validated capacity degradation model for li-ion batteries in phevs applications**. *IFAC Proceedings Volumes 45*, 20 (2012), 456 – 461. 8th IFAC Symposium on Fault Detection, Supervision and Safety of Technical Processes.

[69] XING, Y., W. M. MA, E., TSUI, K.-L., AND PECHT, M. **A case study on battery life prediction using particle filtering**. In *Proceedings of IEEE 2012 Prognostics and System Health Management Conference, PHM-2012* (05 2012), pp. 1–6.

[70] ZHANG, X., AND PISU, P. **An unscented kalman filter based approach for the health-monitoring and prognostics of a polymer electrolyte membrane fuel cell**. In *Annual conference of the prognostics and health management society* (2012), pp. 1–9.

[71] BALABAN, E., AND ALONSO, J. J. **A modeling framework for prognostic decision making and its application to uav mission planning**.

[72] BALABAN, E., NARASIMHAN, S., DAIGLE, M., ROYCHOUDHURY, I., SWEET, A., BOND, C., AND GOROSPE, G. **Development of a mobile robot test platform and methods for validation of prognostics-enabled decision making algorithms**. *International Journal of Prognostics and Health Management 4*, 1 (2013), 87.

[73] BARRE, A., DEGUILHEM, B., GROLLEAU, S., GERARD, M., SUARD, F., AND RIU, D. **A review on lithium-ion battery ageing mechanisms and estimations for automotive applications**. *Journal of Power Sources 241* (2013), 680 – 689.

[74] CASTANEDO, F. **A review of data fusion techniques**. *The Scientific World Journal 2013* (2013).

[75] FERNANDEZ, I., CALVILLO, C., SÁNCHEZ-MIRALLES, A., AND BOAL, J. **Capacity fade and aging models for electric batteries and optimal charging strategy for electric vehicles**. *Energy 60* (10 2013), 35–43.

[76] HERB, F., RAO AKULA, P., TRIVEDI, K., JANDHYALA, L., NARAYANA, A., AND WOHR, M. **Theoretical analysis of energy management strategies for fuel cell electric vehicle with respect to fuel cell and battery aging**. In *2013 World Electric Vehicle Symposium and Exhibition, EVS 2014* (11 2013), pp. 1–9.

[77] JOUIN, M., GOURIVEAU, R., HISSEL, D., MARION-PÉRA, M.-C., AND ZERHOUNI, N. **Prognostics and health management of pemfc - state of the art and remaining challenges**. *International Journal of Hydrogen Energy 38* (11 2013), 15307–15317.

[78] KELOUWANI, S., AGBOSSOU, K., AND DUBÉ, Y. **Impacts of blended mode and charge-sustaining mode on the battery efficiency for a serial fc-phev**. In *IEEE International Symposium on Industrial Electronics* (05 2013), pp. 1–5.

[79] MARTÍNEZ, J. S., MULOT, J., HAREL, F., HISSEL, D., PÉRA, M.-C., JOHN, R. I., AND AMIET, M. **Experimental validation of a type-2 fuzzy logic controller for energy management in hybrid electrical vehicles**. *Engineering Applications of Artificial Intelligence 26*, 7 (2013), 1772 – 1779.

[80] MIAO, Q., XIE, L., CUI, H., LIANG, W., AND PECHT, M. **Remaining useful life prediction of lithium-ion battery with unscented particle filter technique**. *Microelectronics Reliability 53*, 6 (2013), 805–810.

[81] MOHAN, G., ASSADIAN, F., AND LONGO, S. **Comparative analysis of forward-facing models vs backward-facing models in powertrain component sizing**. vol. 2013.

[82] MORANDO, S., JEMEI, S., GOURIVEAU, R., ZERHOUNI, N., AND HISSEL, D. **Fuel cells prognostics using echo state network**. In *IECON Proceedings (Industrial Electronics Conference)* (11 2013), pp. 1632–1637.

[83] MOURA, S., STEIN, J., AND K. FATHY, H. **Battery-health conscious power management in plug-in hybrid electric vehicles via electrochemical modeling and stochastic control**. *Control Systems Technology, IEEE Transactions on 21* (05 2013), 679–694.

[84] NUHIC, A., TERZIMEHIC, T., SOCZKA-GUTH, T., BUCHHOLZ, M., AND DIETMAYER, K. **Health diagnosis and remaining useful life prognostics of lithium-ion batteries using data-driven methods**. *Journal of Power Sources 239* (2013), 680–688.

[85] RAFFAELE, P., ZHENG, Z., HISSEL, D., MARION-PÉRA, M.-C., PIANESE, C., SORRENTINO, M., BECHERIF, M., AND YOUSFI-STEINER, N. **A review on model-based diagnosis methodologies for pemfcs**. *International Journal of Hydrogen Energy 38* (06 2013), 7077–7091.

[86] WENG, C., CUI, Y., SUN, J., AND PENG, H. **On-board state of health monitoring of lithium-ion batteries using incremental capacity analysis with support vector regression**. *Journal of Power Sources 235* (08 2013), 36–44.

[87] XING, Y., W.M. MA, E., TSUI, K.-L., AND PECHT, M. **An ensemble model for predicting the remaining useful performance of lithium-ion batteries**. *Microelectronics Reliability 53* (06 2013), 811–820.

[88] ANDREASEN, S., ASHWORTH, L., SAHLIN, S., JENSEN, H.-C., AND KÆR, S. **Test of hybrid power system for electrical vehicles using a lithium-ion battery pack and a reformed methanol fuel cell range extender**. *International Journal of Hydrogen Energy 39* (01 2014), 1856–1863.

[89] CADET, C., JEMEI, S., DRUART, F., AND HISSEL, D. **Diagnostic tools for pemfcs : From conception to implementation**. *International Journal of Hydrogen Energy 39* (07 2014), 10613–10626.

[90] CHEN, Z., MI, C., XU, J., GONG, X., AND YOU, C. **Energy management for a power-split plug-in hybrid electric vehicle based on dynamic programming and neural networks**. *IEEE Transactions on Vehicular Technology 63* (05 2014), 1567–1580.

[91] COLIN, G., CHAMAILLARD, Y., CHARLET, A., AND NELSON-GRUEL, D. **Towards a friendly energy management strategy for hybrid electric vehicles with respect to pollution, battery and drivability**. *Energies 7* (09 2014), 6013–6030.

[92] DEPATURE, C., LHOMME, W., BOUSCAYROL, A., SICARD, P., AND BOULON, L. **Efficiency map of the traction system of an electric vehicle from an on-road test drive**. In *2014 IEEE Vehicle Power and Propulsion Conference (VPPC)* (Oct 2014), pp. 1–6.

[93] ECKER, M., NIETO, N., KÄBITZ, S., SCHMALSTIEG, J., BLANKE, H., WARNECKE, A., AND SAUER, D. U. **Calendar and cycle life study of li(nimnco)o2-based 18650 lithium-ion batteries**. *Journal of Power Sources 248* (2014), 839 – 851.

[94] GIMENEZ, A., MORENO, J.-L., GONZALEZ, R., AND LÓPEZ, J. **Energy management strategy for plug-in hybrid electric vehicles. a comparative study**. *Applied Energy 113* (01 2014), 816–824.

[95] GOURIVEAU, R., HILAIRET, M., HISSEL, D., JEMEI, S., JOUIN, M., LECHARTIER, E., MORANDO, S., PAHON, E., PERA, M., AND ZERHOUNI, N. **Ieee phm 2014 data challenge : Outline, experiments, scoring of results, winners**. *IEEE 2014 PHM Challenge, Tech. Rep.* (2014).

[96] JOUIN, M., GOURIVEAU, R., HISSEL, D., PÉRA, M.-C., AND ZERHOUNI, N. **Prognostics of pem fuel cell in a particle filtering framework**. *International Journal of Hydrogen Energy 39*, 1 (2014), 481–494.

[97] JOUIN, M., GOURIVEAU, R., HISSEL, D., ZERHOUNI, N., AND MARION-PÉRA, M.-C. **Prognostics of proton exchange membrane fuel cell stack in a particle filtering framework including characterization disturbances and voltage recovery**. In *2014 International Conference on Prognostics and Health Management, PHM 2014* (06 2014).

[98] KIMOTHO, J. K., MEYER, T., AND SEXTRO, W. **Pem fuel cell prognostics using particle filter with model parameter adaptation**. In *2014 International Conference on Prognostics and Health Management* (June 2014), pp. 1–6.

[99] LIAO, L., AND KÖTTIG, F. **Review of hybrid prognostics approaches for remaining useful life prediction of engineered systems, and an application to battery life prediction**. *IEEE Transactions on Reliability 63*, 1 (March 2014), 191–207.

[100] REZVANIZANIANI, S. M., LIU, Z., CHEN, Y., AND LEE, J. **Review and recent advances in battery health monitoring and prognostics technologies for electric vehicle (ev) safety and mobility**. *Journal of Power Sources 256* (06 2014), 110–124.

[101] SANTUCCI, A., SORNIOTTI, A., AND LEKAKOU, C. **Power split strategies for hybrid energy storage systems for vehicular applications**. *Journal of Power Sources 258* (07 2014), 395–407.

[102] SARASKETA-ZABALA, E., GANDIAGA, I., RODRIGUEZ-MARTINEZ, L., AND VILLARREAL, I. **Calendar ageing analysis of a lifepo 4/graphite cell with dynamic model validations : Towards realistic lifetime predictions**. *Journal of Power Sources 272* (2014), 45–57.

[103] SCHMALSTIEG, J., KÄBITZ, S., ECKER, M., AND SAUER, D. **A holistic aging model for li(nimnco)o2 based 18650 lithium-ion batteries**. *Journal of Power Sources 257* (07 2014), 325–334.

[104] SILVA, R., GOURIVEAU, R., JEMEI, S., HISSEL, D., BOULON, L., AGBOSSOU, K., AND YOUSFI-STEINER, N. **Proton exchange membrane fuel cell degradation prediction based on adaptive neuro-fuzzy inference systems**. *International Journal of Hydrogen Energy 39* (07 2014), 11128–11144.

[105] SONG, Z., HOFMANN, H., JIANQIU, L., HOU, J., HAN, X., AND OUYANG, M. **Energy management strategies comparison for electric vehicles with hybrid energy storage system**. *Applied Energy 134* (12 2014), 321–331.

[106] SWEET, A., GOROSPE, G., DAIGLE, M., CELAYA, J., BALABAN, E., ROYCHOUDHURY, I., AND NARASIMHAN, S. **Demonstration of prognostics-enabled decision making algorithms on a hardware mobile robot test platform**.

[107] XU, L., JIANQIU, L., OUYANG, M., HUA, J., AND YANG, G. **Multi-mode control strategy for fuel cell electric vehicles regarding fuel economy and durability**. *International Journal of Hydrogen Energy 39* (02 2014), 2374–2389.

[108] BAI, G., WANG, P., AND HU, C. **A self-cognizant dynamic system approach for prognostics and health management**. *Journal of Power Sources 278* (2015), 163 – 174.

[109] BERECIBAR, M., GANDIAGA, I., VILLARREAL, I., OMAR, N., VAN MIERLO, J., AND VAN DEN BOSSCHE, P. **Critical review of state of health estimation methods of li-ion batteries for real applications**. *Renewable and Sustainable Energy Reviews 56* (12 2015), 572–587.

[110] CHEN, H., PEI, P., AND SONG, M. **Lifetime prediction and the economic lifetime of proton exchange membrane fuel cells**. *Applied Energy 142* (03 2015), 154–163.

[111] CHEN, Z., XIA, B., YOU, C., AND MI, C. C. **A novel energy management method for series plug-in hybrid electric vehicles**. *Applied Energy 145* (2015), 172 – 179.

[112] CHRENKO, D., GAN, S., GUTENKUNST, C., KRIESTEN, R., AND MOYNE, L. L. **Novel classification of control strategies for hybrid electric vehicles**. In *2015 IEEE Vehicle Power and Propulsion Conference (VPPC)* (Oct 2015), pp. 1–6.

[113] CORDOBA-ARENAS, A., ONORI, S., GUEZENNEC, Y., AND RIZZONI, G. **Capacity and power fade cycle-life model for plug-in hybrid electric vehicle lithium-ion battery cells containing blended spinel and layered-oxide positive electrodes**. *Journal of Power Sources 278* (2015), 473 – 483.

[114] GUO, J., LI, Z., AND PECHT, M. **A bayesian approach for li-ion battery capacity fade modeling and cycles to failure prognostics**. *Journal of Power Sources 281* (2015), 173–184.

[115] HU, X., JIANG, J., CAO, D., AND EGARDT, B. **Battery health prognosis for electric vehicles using sample entropy and sparse bayesian predictive modeling**. *IEEE Transactions on Industrial Electronics 63* (01 2015), 1–1.

[116] IBRAHIM, M., WIMMER, G., JEMEI, S., AND HISSEL, D. **Energy management for a fuel cell hybrid electrical vehicle**. In *Proceedings, IECON 2014 - 40th Annual Conference of the IEEE Industrial Electronics Society* (02 2015), pp. 3955–3961.

[117] JAVED, K., GOURIVEAU, R., ZERHOUNI, N., AND HISSEL, D. **Improving accuracy of long-term prognostics of pemfc stack to estimate remaining useful life**. In *2015 IEEE International Conference on Industrial Technology (ICIT)* (March 2015), pp. 1047–1052.

[118] JIANG, J., AND ZHANG, C. **Fundamentals and application of lithium-ion batteries in electric drive vehicles**. 01 2015.

[119] LECHARTIER, E., LAFFLY, E., PÉRA, M.-C., GOURIVEAU, R., HISSEL, D., AND ZERHOUNI, N. **Proton exchange membrane fuel cell behavioral model suitable for prognostics**. *International Journal of Hydrogen Energy 40*, 26 (2015), 8384 – 8397.

[120] LIN, C., TANG, A., MU, H., WANG, W., AND WANG, C. **Aging mechanisms of electrode materials in lithium-ion batteries for electric vehicles**. *Journal of Chemistry 2015* (06 2015).

[121] LIU, C., AND LIU, L. **Optimal power source sizing of fuel cell hybrid vehicles based on pontryagin's minimum principle**. *International Journal of Hydrogen Energy 40* (07 2015), 8454–8464.

[122] LIU, D., ZHOU, J., PAN, D., PENG, Y., AND PENG, X. **Lithium-ion battery remaining useful life estimation with an optimized relevance vector machine algorithm with incremental learning**. *Measurement 63* (2015), 143 – 151.

[123] MARIAJAYAPRAKASH, A., SENTHILVELAN, T., AND GNANADASS, R. **Optimization of process parameters through fuzzy logic and genetic algorithm – a case study in a process industry**. *Applied Soft Computing 30* (2015), 94 – 103.

[124] MARTEL, F., DUBE, Y., KELOUWANI, S., AND AGBOSSOU, K. **Economy-focused phev battery lifetime management through optimal fuel cell load sharing**. In *2015 IEEE Vehicle Power and Propulsion Conference (VPPC)* (Oct 2015), pp. 1–9.

[125] MARTEL, F., KELOUWANI, S., DUBÉ, Y., AND AGBOSSOU, K. **Optimal economy-based battery degradation management dynamics for fuel-cell plug-in hybrid electric vehicles**. *Journal of Power Sources 274* (2015), 367 – 381.

[126] MASELENO, A., HASAN, M. M., AND TUAH, N. J. **Combining fuzzy logic and dempster-shafer theory**. *Indonesian Journal of Electrical Engineering and Computer Science 16*, 3 (12 2015), 583–590.

[127] MAYUR, M., STRAHL, S., HUSAR, A., AND BESSLER, W. G. **A multi-timescale modeling methodology for pemfc performance and durability in a virtual fuel cell car**. *International Journal of Hydrogen Energy 40*, 46 (2015), 16466 – 16476.

[128] NYKVIST, B., AND NILSSON, M. **Rapidly falling costs of battery packs for electric vehicles**. *Nature Climate Change 5* (03 2015), 329–332.

[129] RAVEY, A., MOHAMMADI, A., AND BOUQUAIN, D. **Control strategy of fuel cell electric vehicle including degradation process**. In *IECON 2015 - 41st Annual Conference of the IEEE Industrial Electronics Society* (11 2015), pp. 003508–003513.

[130] SARASKETA-ZABALA, E., GANDIAGA, I., MARTINEZ-LASERNA, E., RODRIGUEZ-MARTINEZ, L., AND VILLARREAL, I. **Cycle ageing analysis of a lifepo 4/graphite cell with dynamic model validations : Towards realistic lifetime predictions**. *Journal of Power Sources 275* (2015), 573–587.

[131] SULAIMAN, N., HANNAN, M., MOHAMED, A., MAJLAN, E., AND DAUD, W. W. **A review on energy management system for fuel cell hybrid electric vehicle : Issues and challenges**. *Renewable and Sustainable Energy Reviews 52* (2015), 802 – 814.

[132] WHITELEY, M., FLY, A., LEIGH, J., DUNNETT, S., AND JACKSON, L. **Advanced reliability analysis of polymer electrolyte membrane fuel cells using petri-net analysis and fuel cell modelling techniques**. *International Journal of Hydrogen Energy 40*, 35 (2015), 11550 – 11558.

[133] ZHANG, P., YAN, F., AND DU, C. **A comprehensive analysis of energy management strategies for hybrid electric vehicles based on bibliometrics**. *Renewable and Sustainable Energy Reviews 48* (2015), 88 – 104.

[134] ZHENG, X., AND FANG, H. **An integrated unscented kalman filter and relevance vector regression approach for lithium-ion battery remaining useful life and short-term capacity prediction**. *Reliability Engineering & System Safety 144* (2015), 74–82.

[135] ZHENG, X., AND FANG, H. **An integrated unscented kalman filter and relevance vector regression approach for lithium-ion battery remaining useful life and short-term capacity prediction**. *Reliability Engineering & System Safety 144* (2015), 74 – 82.

[136] BAGHDADI, I., BRIAT, O., DELÉTAGE, J.-Y., GYAN, P., AND VINASSA, J.-M. **Lithium battery aging model based on dakin's degradation approach**. *Journal of Power Sources 325* (09 2016), 273–285.

[137] BRESSEL, M., HILAIRET, M., HISSEL, D., AND BOUAMAMA, B. O. **Extended kalman filter for prognostic of proton exchange membrane fuel cell**. *Applied Energy 164* (2016), 220 – 227.

[138] CAI, Y., YANG, F., AND OUYANG, M. **Impact of control strategy on battery degradation for a plug-in hybrid electric city bus in china**. *Energy 116* (2016), 1020 – 1030.

[139] CAPROS, P., VITA, A. D., TASIOS, N., SISKOS, P., KANNAVOU, M., PETROPOULOS, A., EVANGELOPOULOU, S., ZAMPARA, M., PAPADOPOULOS, D., NAKOS, C., PAROUSSOS, L., FRAGIADAKIS, K., TSANI, S., KARKATSOULIS, P., FRAGKOS, P., KOUVARITAKIS, N., ISAKSSON, L. H., WINIWARTER, W., PUROHIT, P., SANABRIA, A. G., FRANK, S., FORSELL, N., GUSTI, M., HAVLIK, P., OBERSTEINER, M., WITZKE, H., AND KESTING, M. **Eu reference scenario 2016 - energy, transport and ghg emissions trends to 2050.**, July 2016.

[140] DEPATURE, C., JEMEI, S., BOULON, L., BOUSCAYROL, A., MARX, N., MORANDO, S., AND CASTAINGS, A. **Ieee vts motor vehicles challenge 2017 - energy management of a fuel cell/battery vehicle**. In *2016 IEEE Vehicle Power and Propulsion Conference (VPPC)* (Oct 2016), pp. 1–6.

[141] ETTIHIR, K., BOULON, L., AND AGBOSSOU, K. **Optimization-based energy management strategy for a fuel cell/battery hybrid power system**. *Applied Energy 163* (02 2016), 142–153.

[142] FLETCHER, T., THRING, R., AND WATKINSON, M. **An energy management strategy to concurrently optimise fuel consumption and pem fuel cell lifetime in a hybrid vehicle**. *International Journal of Hydrogen Energy 41* (09 2016), 21503–21515.

[143] FLETCHER, T., THRING, R., WATKINSON, M., AND STAFFELL, I. **Comparison of fuel consumption and fuel cell degradation using an optimised controller**. *ECS Transactions 71* (02 2016), 85–97.

[144] GARCIA-TRIVIÑO, P., FERNÁNDEZ-RAMÍREZ, L., GIL-MENA, A., LLORENS, F., GARCIA, C., AND JURADO, F. **Optimized operation combining costs, efficiency and lifetime of a hybrid renewable energy system with energy storage by battery and hydrogen in grid-connected applications**. *International Journal of Hydrogen Energy 41* (11 2016), 23132–23144.

[145] HERRERA, V. I., MILO, A., GAZTANAGA, H., AND CAMBLONG, H. **Multi-objective optimization of energy management and sizing for a hybrid bus with dual energy storage system**. In *2016 IEEE Vehicle Power and Propulsion Conference (VPPC)* (Oct 2016), pp. 1–6.

[146] HERRERA PÉREZ, V., GAZTAÑAGA, H., MILO, A., SAEZ-DE IBARRA, A., ETXEBERRIA-OTADUI, I., AND NIEVA, T. **Optimal energy management and sizing of a battery supercapacitor based light rail vehicle with multi-objective approach**. *IEEE Transactions on Industry Applications 52* (08 2016), 3367–3377.

[147] IBRAHIM, M., STEINER, N. Y., JEMEI, S., AND HISSEL, D. **Wavelet-based approach for online fuel cell remaining useful lifetime prediction**. *IEEE Transactions on Industrial Electronics 63*, 8 (Aug 2016), 5057–5068.

[148] JAVED, K., GOURIVEAU, R., ZERHOUNI, N., AND HISSEL, D. **Prognostics of proton exchange membrane fuel cells stack using an ensemble of constraints based connectionist networks**. *Journal of Power Sources 324* (2016), 745 – 757.

[149] JIANQIU, L., HU, Z., XU, L., OUYANG, M., FANG, C., HU, J., CHENG, S., PO, H., ZHANG, W., AND JIANG, H. **Fuel cell system degradation analysis of a chinese plug-in hybrid fuel cell city bus**. *International Journal of Hydrogen Energy 41* (07 2016), 15295–15310.

[150] JIN, F., WANG, M., AND HU, C. **A fuzzy logic based power management strategy for hybrid energy storage system in hybrid electric vehicles considering battery degradation**. In *2016 IEEE Transportation Electrification Conference and Expo (ITEC)* (June 2016), pp. 1–7.

[151] JOUIN, M., BRESSEL, M., MORANDO, S., GOURIVEAU, R., HISSEL, D., PÉRA, M.-C., ZERHOUNI, N., JEMEI, S., HILAIRET, M., AND BOUAMAMA, B. O. **Estimating the end-of-life of pem fuel cells : Guidelines and metrics**. *Applied Energy 177* (2016), 87 – 97.

[152] JOUIN, M., GOURIVEAU, R., HISSEL, D., MARION-PÉRA, M.-C., AND ZERHOUNI, N. **Degradations analysis and aging modeling for health assessment and prognostics of pemfc**. *Reliability Engineering and System Safety 148* (2016), 78 – 95.

[153] JOUIN, M., GOURIVEAU, R., HISSEL, D., PÉRA, M.-C., AND ZERHOUNI, N. **Joint particle filters prognostics for proton exchange membrane fuel cell power prediction at constant current solicitation**. *IEEE Transactions on reliability 65*, 1 (2016), 336–349.

[154] JOUIN, M., GOURIVEAU, R., HISSEL, D., PÉRA, M. C., AND ZERHOUNI, N. **Combined predictions for prognostics and predictive control of transportation pemfc**the authors would like to thank the anr project propice (anr-12-prge-0001) and the labex action project (contract "anr-11-labx-01-01") both funded by the french national re-search agency for their support.** *IFAC-PapersOnLine 49*, 28 (2016), 244 – 249. 3rd IFAC Workshop on Advanced Maintenance Engineering, Services and Technology AMEST 2016.

[155] JOUIN, M., GOURIVEAU, R., HISSEL, D., PÉRA, M.-C., AND ZERHOUNI, N. **Particle filter-based prognostics : Review, discussion and perspectives**. *Mechanical Systems and Signal Processing 72-73* (2016), 2 – 31.

[156] MARTEL, F., DUB, Y., KELOUWANI, S., JAGUEMONT, J., AND AGBOSSOU, K. **Long-term assessment of economic plug-in hybrid electric vehicle battery lifetime degradation management through near optimal fuel cell load sharing**. *Journal of Power Sources 318* (06 2016), 270–282.

[157] MARX, N., HISSEL, D., GUSTIN, F., BOULON, L., AND AGBOSSOU, K. **On the sizing and energy management of an hybrid multistack fuel cell – battery system for automotive applications**. *International Journal of Hydrogen Energy 42* (07 2016), 1518–1526.

[158] SAXENA, S., HENDRICKS, C., AND PECHT, M. **Cycle life testing and modeling of graphite/licoo 2 cells under different state of charge ranges**. *Journal of Power Sources 327* (2016), 394–400.

[159] SHEN, J., AND KHALIGH, A. **Design and real-time controller implementation for a battery-ultracapacitor hybrid energy storage system**. *IEEE Transactions on Industrial Informatics 12* (10 2016), 1–1.

[160] SURI, G., AND ONORI, S. **A control-oriented cycle-life model for hybrid electric vehicle lithium-ion batteries**. *Energy 96* (02 2016), 644–653.

[161] WU, L., FU, X., AND GUAN, Y. **Review of the remaining useful life prognostics of vehicle lithium-ion batteries using data-driven methodologies**. *Applied Sciences 6*, 6 (2016), 166.

[162] XU, F., JIAO, X., SASAKI, M., AND WANG, Y. **Energy management optimization in consideration of battery deterioration for commuter plug-in hybrid electric vehicle**. In *2016 55th Annual Conference of the Society of Instrument and Control Engineers of Japan (SICE)* (Sept 2016), pp. 218–222.

[163] ALOFI, A., ALGHAMDI, A., ALAHMADI, R., ALJUAID, N., AND HEMALATHA, M. **A review of data fusion techniques**. *International Journal of Computer Applications 167*, 7 (2017).

[164] BANERJEE, A., SHILINA, Y., ZIV, B., ZIEGELBAUER, J. M., LUSKI, S., AURBACH, D., AND HALALAY, I. C. **Review—multifunctional materials for enhanced li-ion batteries durability : A brief review of practical options**. *Journal of The Electrochemical Society 164*, 1 (2017), A6315–A6323.

[165] DAS, H., TAN, C. W., AND YATIM, A. H. **Fuel cell hybrid electric vehicles : A review on power conditioning units and topologies**. *Renewable and Sustainable Energy Reviews 76* (09 2017), 268–291.

[166] HU, X., MARTINEZ, C. M., AND YANG, Y. **Charging, power management, and battery degradation mitigation in plug-in hybrid electric vehicles : A unified cost-optimal approach**. *Mechanical Systems and Signal Processing 87* (2017), 4 – 16. Signal Processing and Control challenges for Smart Vehicles.

[167] LI, H., RAVEY, A., N'DIAYE, A., AND DJERDIR, A. **Equivalent consumption minimization strategy for fuel cell hybrid electric vehicle considering fuel cell degradation**. In *2017 IEEE Transportation Electrification Conference and Expo (ITEC)* (06 2017), pp. 540–544.

[168] MA, X., ZHANG, Y., YIN, C., AND YUAN, S. **Multi-objective optimization considering battery degradation for a multi-mode power-split electric vehicle**. *Energies 10* (07 2017), 975.

[169] MAJED, C., H. KARAKI, S., AND JABR, R. **Neural network technique for hybrid electric vehicle optimization**. In *Journal of Civil Engineering* (03 2017), vol. 1, pp. 11–23.

[170] MORANDO, S., JEMEI, S., HISSEL, D., GOURIVEAU, R., AND ZERHOUNI, N. **Proton exchange membrane fuel cell ageing forecasting algorithm based on echo state network**. *International Journal of Hydrogen Energy 42*, 2 (2017), 1472 – 1480.

[171] OPILA, D. F. **Equivalent degradation minimization strategy for balancing battery and capacitor usage in hybrid energy storage systems for electric vehicles**. In *2017 American Control Conference (ACC)* (May 2017), pp. 315–321.

[172] PELLETIER, S., JABALI, O., LAPORTE, G., AND VENERONI, M. **Battery degradation and behaviour for electric vehicles : Review and numerical analyses of several models**. *Transportation Research Part B : Methodological 103* (2017), 158 – 187. Green Urban Transportation.

[173] STROE, D., SWIERCZYNSKI, M., STROE, A., KAER, S. K., AND TEODORESCU, R. **Lithium-ion battery power degradation modelling by electrochemical impedance spectroscopy**. *IET Renewable Power Generation 11*, 9 (2017), 1136–1141.

[174] SUTHARSSAN, T., MONTALVAO, D., CHEN, Y. K., WANG, W.-C., PISAC, C., AND ELEMARA, H. **A review on prognostics and health monitoring of proton exchange membrane fuel cell**. *Renewable and Sustainable Energy Reviews 75* (2017), 440 – 450.

[175] WU, Y., KEIL, P., SCHUSTER, S. F., AND JOSSEN, A. **Impact of temperature and discharge rate on the aging of a licoo2/lini0.8co0.15al0.05o2 lithium-ion pouch cell.** *Journal of The Electrochemical Society 164*, 7 (2017), A1438–A1445.

[176] XU, L., FANG, C., HU, J., CHENG, S., LI, J., OUYANG, M., AND LEHNERT, W. **Parameter extraction and uncertainty analysis of a proton exchange membrane fuel cell system based on monte carlo simulation.** *International Journal of Hydrogen Energy 42*, 4 (2017), 2309 – 2326.

[177] YUE, M., JEMEI, S., ZERHOUNI, N., AND GOURIVEAU, R. **Towards the energy management of a fuel cell/battery vehicle considering degradation**. In *2017 IEEE Vehicle Power and Propulsion Conference (VPPC)* (Belfort, France, dec 2017), IEEE, p. 6.

[178] ZHOU, D., AL-DURRA, A., GAO, F., RAVEY, A., MATRAJI, I., AND SIMÕES, M. G. **Online energy management strategy of fuel cell hybrid electric vehicles based on data fusion approach.** *Journal of Power Sources 366* (2017), 278 – 291.

[179] GIELEN, D. **Global energy transformation - a roadmap to 2050**, 04 2018.

[180] MA, R., YANG, T., BREAZ, E., LI, Z., BRIOIS, P., AND GAO, F. **Data-driven proton exchange membrane fuel cell degradation predication through deep learning method.** *Applied Energy 231* (2018), 102 – 115.

[181] PALACÍN, M. R. **Understanding ageing in li-ion batteries : a chemical issue.** *Chem. Soc. Rev. 47* (2018), 4924–4933.

[182] ROZAS, H., MUNOZ-CARPINTERO, D., PEREZ, A., MEDJAHER, K., AND ORCHARD, M. **An approach to prognosis-decision-making for route calculation of an electric vehicle considering stochastic traffic information**. In *Fourth european conference of the prognostics and health management society 2018* (Utrecht, NL, July 2018).

[183] XU, B., OUDALOV, A., ULBIG, A., ANDERSSON, G., AND KIRSCHEN, D. S. **Modeling of lithium-ion battery degradation for cell life assessment.** *IEEE Transactions on Smart Grid 9*, 2 (March 2018), 1131–1140.

[184] YUE, M., JEMEI, S., GOURIVEAU, R., AND ZERHOUNI, N. **Developing a health-conscious energy management strategy based on prognostics for a battery/fuel cell hybrid electric vehicle**. In *VPPC 2018* (Chicago, Il, USA, aug 2018), p. 6.

[185] ZHAN, C., WU, T., LU, J., AND AMINE, K. **Dissolution, migration, and deposition of transition metal ions in li-ion batteries exemplified by mn-based cathodes – a critical review.** *Energy & Environmental Science 11*, 2 (2018), 243–257.

[186] YUE, M., JEMEI, S., GOURIVEAU, R., AND ZERHOUNI, N. **Review on health-conscious energy management strategies for fuel cell hybrid electric vehicles : Degradation models and strategies.** *International Journal of Hydrogen Energy 44*, 13 (2019), 6844 – 6861.

[187] BOLE, B., KULKARNI, C., AND DAIGLE, M. **Randomized battery usage data set.** http://ti.arc.nasa.gov/project/prognostic-data-repository. NASA Ames Prognostics Data Repository, NASA Ames Research Center, Moffett Field, CA.

[188] KURTZ, J., DINH, H., AND SAUR, G. **National renewable energy laboratory : Fuel cell technology status : Degradation**. https://www.hydrogen.energy.gov/annual_progress.html.

[189] KURTZ, J., SPRIK, S., AINSCOUGH, C., AND SAUR, G. **National renewable energy laboratory : Fuel cell electric vehicle evaluation**. https://www.hydrogen.energy.gov/annual_progress.html.

[190] OF ENERGY, U. D. **The department of energy hydrogen and fuel cells program plan ; 2011**. http://www.hydrogen.energy.gov/roadmaps_vision.html.

[191] OF ENERGY, U. D. **The department of energy hydrogen and fuel cells program plan ; 2011**. https://www.energy.gov/eere/vehicles/downloads/us-drive-fuel-cell-technical-team-roadmap.html.

[192] PRIYONO, A., SOFWAN, A., DAMAYANTI, S., AND PINARDI, S. **Optimization of fuzzy logic using genetic algorithm and clonal system in traffic control system.**

[193] WILSON, A., MARCINKOSKI, J., AND PAPAGEORGOPOULOS, D. **On-road fuel cell stack durability – 2016**. https://www.hydrogen.energy.gov/program_records.html.

TABLE DES FIGURES

LISTE DES TABLES

IV

APPENDIX

A

GA OPTIMIZATION RESULTS UNDER DIFFERENT DEGRADATION STATES

Simulation results are demonstrated in Figure A.1 to Figure A.4 corresponding to the degradation cases 2 to 5 defined in Table 4.8. As the parameters of the FLC are optimized under different degradation cases, they are varying from each other. However, it should be noticed that GA optimization is limited by the generation number so that the optimization results could only be sub-optimal ones and the larger the generation number, the better the results could be. In our simulation, the generation is determined as 400 and, in each generation, 50 individuals are generated. As it could be seen in the results, the optimization results are good enough to achieve smooth fuel cell operation and good SOC maintenance.

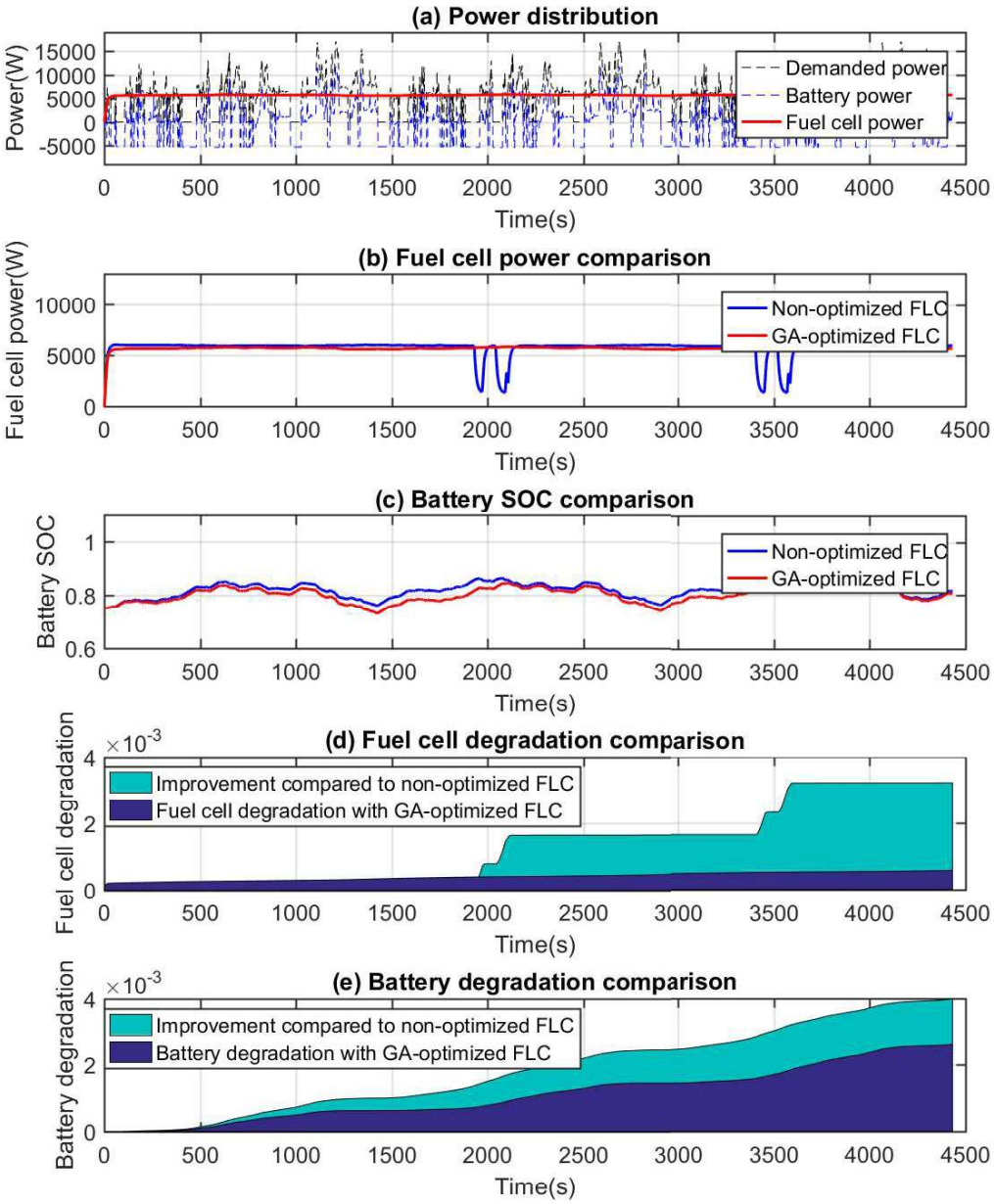

FIGURE A.1 – Fuzzy logic controller results after GA optimization (degradation case 2) : (a) Power distribution ; (b) Fuel cell power comparison ; (c) Battery SOC comparison ; (d) Fuel cell degradation comparison ; (e) Battery degradation comparison.

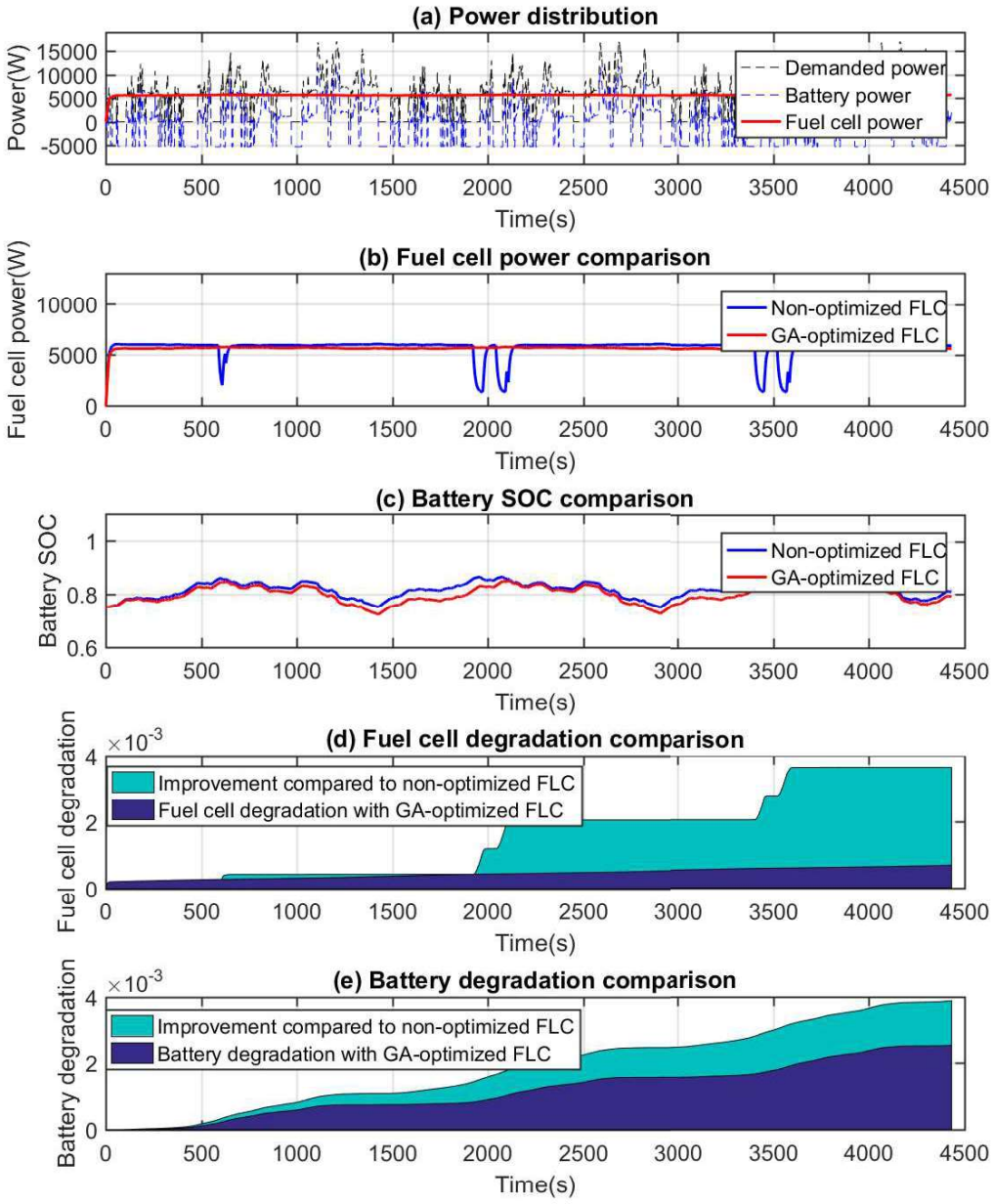

FIGURE A.2 – Fuzzy logic controller results after GA optimization (degradation case 3) : (a) Power distribution ; (b) Fuel cell power comparison ; (c) Battery SOC comparison ; (d) Fuel cell degradation comparison ; (e) Battery degradation comparison.

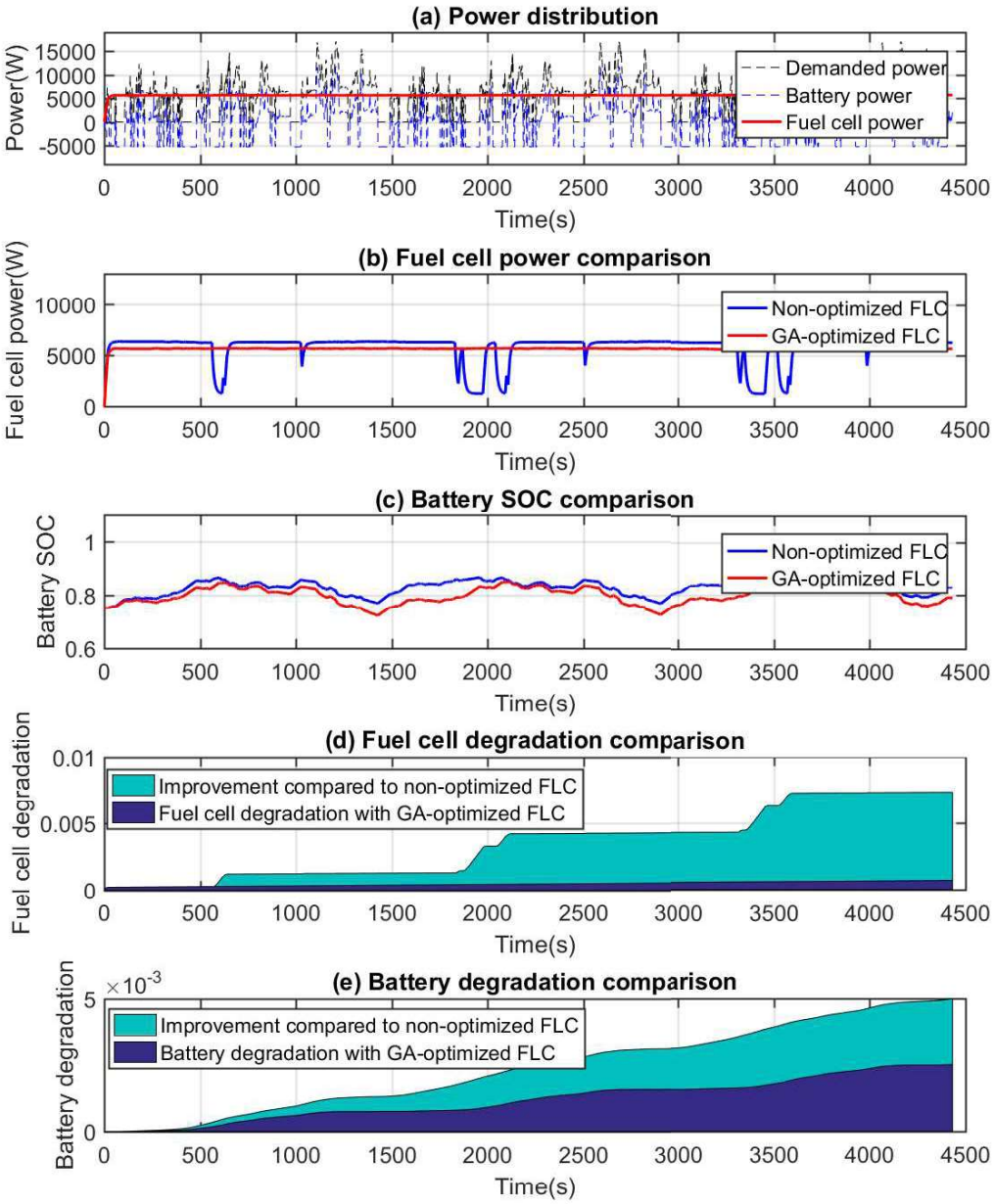

FIGURE A.3 – Fuzzy logic controller results after GA optimization (degradation case 4) : (a) Power distribution ; (b) Fuel cell power comparison ; (c) Battery SOC comparison ; (d) Fuel cell degradation comparison ; (e) Battery degradation comparison.

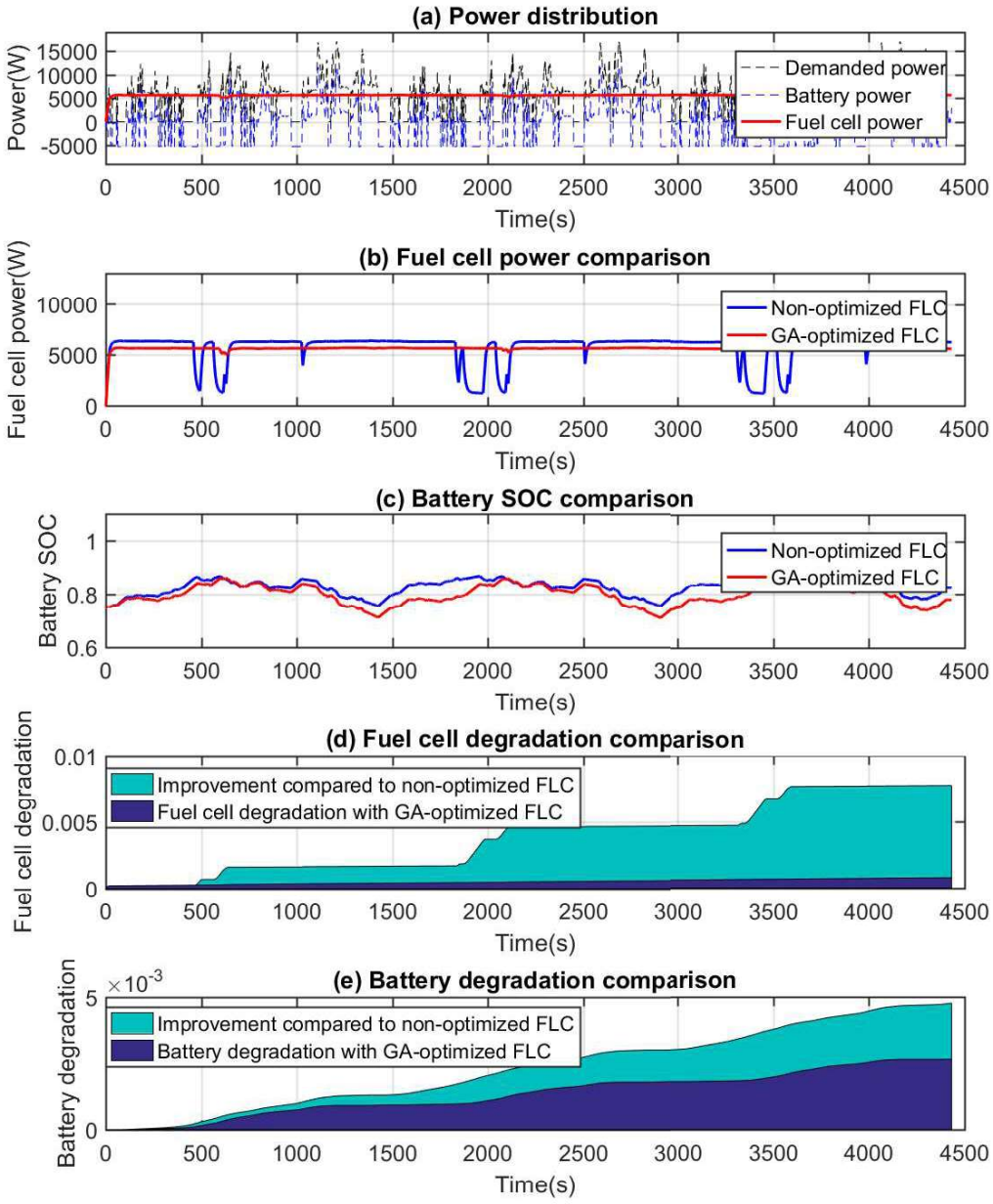

FIGURE A.4 – Fuzzy logic controller results after GA optimization (degradation case 5) : (a) Power distribution ; (b) Fuel cell power comparison ; (c) Battery SOC comparison ; (d) Fuel cell degradation comparison ; (e) Battery degradation comparison.

B

SIMULATION RESULTS WITH DIFFERENT PROGNOSTICS OCCURRENCE

In order to discover if the prognostics occurrence could have an influence on mitigating the degradation, five simulations have been performed with the prognostics happening at different frequencies. They are executed by having the prognostics implemented whenever the fuel cell degrades by 1%, 2%, 3%, 4% and 5%, while the FLC is refined nine times, four times, three times, twice and once, respectively. The simulation is stopped whenever the fuel cell reached 10% degradation or the battery reached 30% degradation in order to compare the lifetime. Table 4.14 in Chapter 4 compared the cost and the lifetime improvement of different EMSs when the system reached its EOL. The corresponding power distribution, battery SOC evolution and degradation evolution of both battery and fuel cell are plotted as follows :

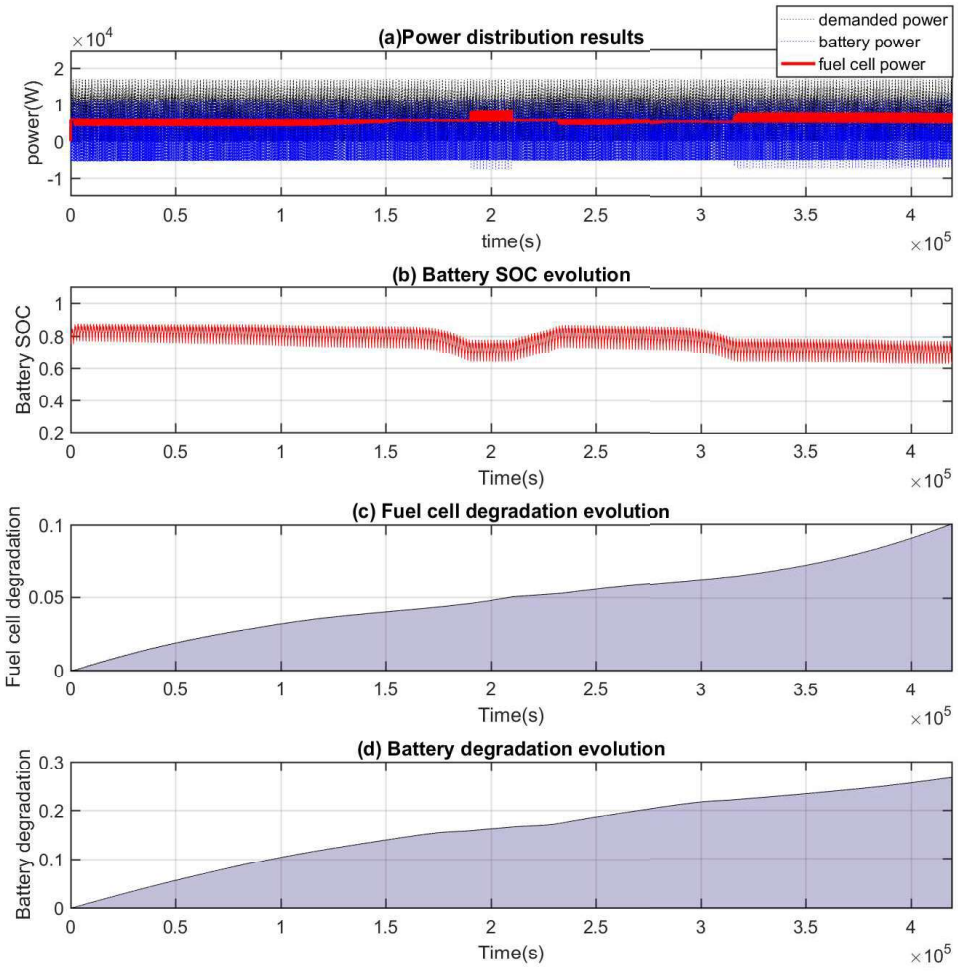

FIGURE B.1 – Simulation results with $\Delta D_{fc} = 0.5$: (a) Power distribution ; (b) Battery SOC evolution ; (c) Fuel cell degradation evolution ; (d) Battery degradation revolution.

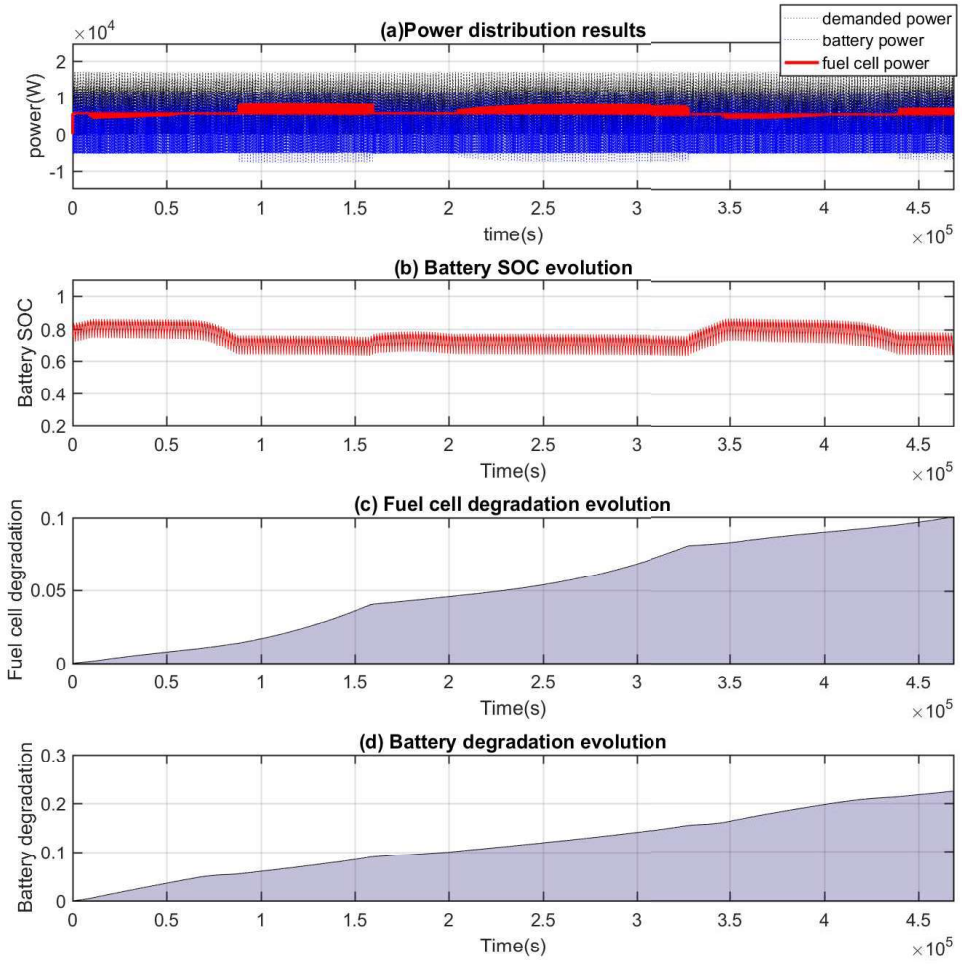

FIGURE B.2 – Simulation results with $\Delta D_{fc} = 0.4$: (a) Power distribution ; (b) Battery SOC evolution ; (c) Fuel cell degradation evolution ; (d) Battery degradation revolution.

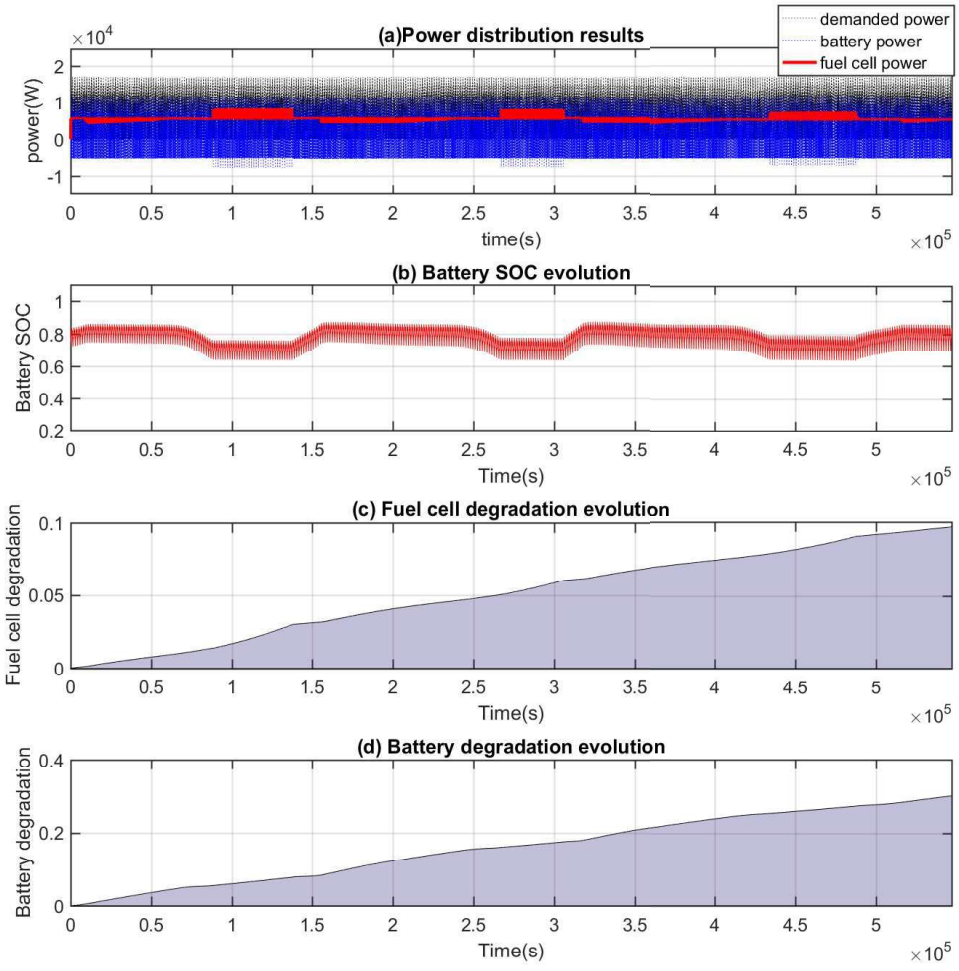

FIGURE B.3 – Simulation results with $\Delta D_{fc} = 0.3$: (a) Power distribution ; (b) Battery SOC evolution ; (c) Fuel cell degradation evolution ; (d) Battery degradation revolution.

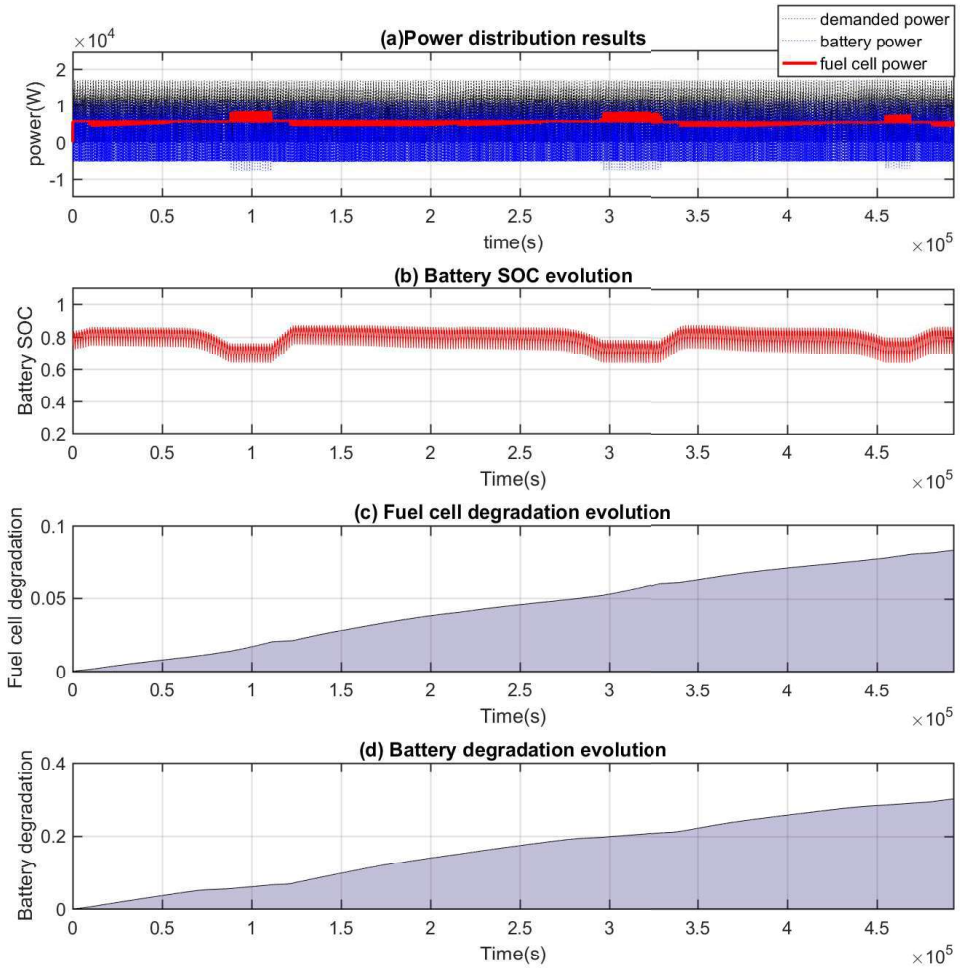

FIGURE B.4 – Simulation results with $\Delta D_{fc} = 0.2$: (a) Power distribution ; (b) Battery SOC evolution ; (c) Fuel cell degradation evolution ; (d) Battery degradation revolution.

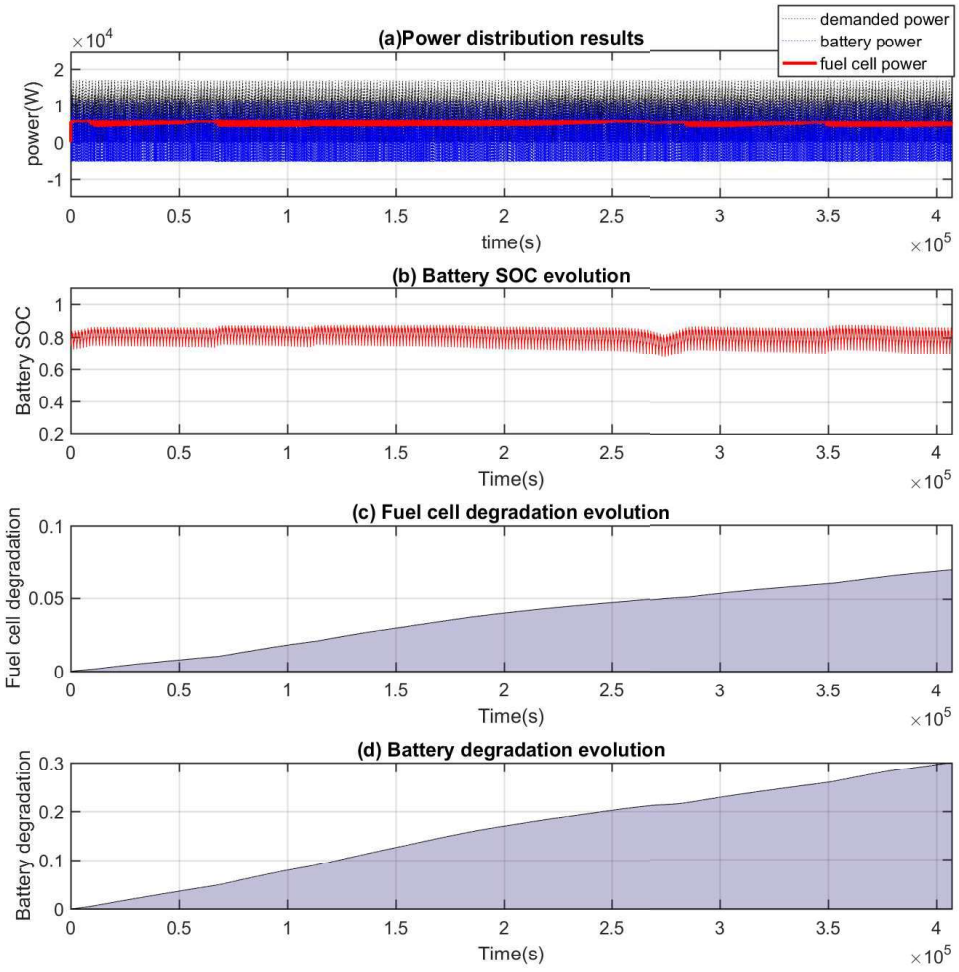

FIGURE B.5 – Simulation results with $\Delta D_{fc} = 0.1$: (a) Power distribution ; (b) Battery SOC evolution ; (c) Fuel cell degradation evolution ; (d) Battery degradation revolution.

C

List of publications

Journals :

1. Meiling Yue, Samir Jemei, Rafael Gouriveau, Noureddine Zerhouni, ”Review on health-conscious energy management strategies for fuel cell hybrid electric vehicles : Degradation models and strategies,” *International Journal of Hydrogen Energy*, Volume 44, Issue 13, 2019, Pages 6844-6861, ISSN 0360-3199, https ://doi.org/10.1016/j.ijhydene.2019.01.190.
2. Meiling Yue, Samir Jemei, Noureddine Zerhouni, ”Health-Conscious Energy Management for Fuel Cell Hybrid Electric Vehicles based on Prognostics-Enabled Decision-Making,” *IEEE Transactions on Vehicular Technology*, Early Access.

Conferences :

1. M. Yue, S. Jemei and N. Zerhouni, ”Energy management strategy based on prognostics-enabled decision-making for fuel cell hybrid electric vehicles,” *2019 GdR Hydrogène, Systèmes et Piles à Combustible*, Le Croisic, France, 2019.
2. M. Yue, S. Jemei and N. Zerhouni, ”Developing a Health-Conscious Energy Management Strategy based on Prognostics for a Fuel cell Hybrid Electric Vehicle,” *8th International Conference on Fundamentals & Development of Fuel Cells (FDFC)*, Nantes, 2019.
3. M. Yue, S. Jemei, R. Gouriveau and N. Zerhouni, ”Developing a Health-Conscious Energy Management Strategy Based on Prognostics for a Battery/Fuel Cell Hybrid Electric Vehicle,” *2018 IEEE Vehicle Power and Propulsion Conference (VPPC)*, Chicago, IL, 2018, pp. 1-6. doi : 10.1109/VPPC.2018.8604987
4. M. Yue, S. Jemei, R. Gouriveau and N. Zerhouni, ”Developing a Prognostics-based Energy Management Strategy for Battery/Fuel cell Hybrid Electric Vehicles,” *2018 GdR Hydrogène, Systèmes et Piles à Combustible*, Grenoble, France, 2018.
5. M. Yue, S. Jemei, N. Zerhouni and R. Gouriveau, ”Towards the Energy Management of a Fuel Cell/Battery Vehicle Considering Degradation,” *2017 IEEE Vehicle Power and Propulsion Conference (VPPC)*, Belfort, 2017, pp. 1-6. doi : 10.1109/VPPC.2017.8330983

Document réalisé avec LaTeX et :
le style LaTeX pour Thèse de Doctorat créé par S. Galland — http://www.multiagent.fr/ThesisStyle
la collection de paquets `tex-upmethodology` — http://www.arakhne.org/tex-upmethodology/